Heat conduction in two and three dimensions : computer modelling of building physics applications

Blomberg, Thomas

1996

Total number of authors:
1

HEAT CONDUCTION
IN TWO AND THREE DIMENSIONS

Computer Modelling of

Building Physics Applications

Thomas Blomberg

The Cover

The front cover figure shows the surface temperatures for a corner, see
Section 6.9. The temperatures are calculated by HEAT3 and displayed
using MATLAB. The calculation took less than a minute on a PC.

The back cover figures show the input, the numerical mesh, and the
calculated temperatures for a window frame with 20 cavities. The tem-
peratures are calculated by HEAT2 and displayed using MATLAB. Ra-
diation inside the cavities is taken into account. This calculation took a
few minutes on a PC.

Natural laws have no pity

Robert A. Heinlein ("Time enough for love")

Preface

This work has been made within the research tradition of the *Lund Group for Computational Building Physics*. The mathematical part of Chapter 7 concerning radiation coupled to heat conduction has been formulated by my supervisor Docent Johan Claesson.

To Sanja and Julia, I owe a debt of gratitude for all the hours stolen from them. It is always encouraging to know that they are around.

Contents

Summary

Computer programs for transient and steady-state heat conduction in two and three dimensions have been developed. The programs are part of a library, developed by *Lund Group for Computational Building Physics*, dealing with building physics and ground heat. The PC-programs HEAT2 and HEAT3 can be used for analyses of thermal bridge effects, heat transfer through the corners of a window, heat loss from a house to the ground, to mention but a few applications. These programs are now used by researchers and consultant engineers in more than twenty countries. HEAT2R (Blomberg, 1994c) is a newly developed program for transient and steady-state heat conduction in cylindrical coordinates r and z.

The robust method of explicit finite differences is used. This method closely follows the physical equations. The mathematical equations for two- and three-dimensional heat conduction and the numerical formulation are presented. The numerical error for different meshes is studied and compared with analytical solutions. The effectiveness of the method of successive over-relaxation is demonstrated, while the gain using "successive subdivision" is modest. Results from calculations with two or three different meshes may be used to estimate more accurate results. The gain using this technique can be quite substantial.

With our numerical technique and computer programs, it is quite easy to solve a wide range of heat conduction problems. A problem using 15000 computational nodes may require a few minutes of CPU-time on a modern PC. The difficult case of steel girders in thermal insulation, using one million computational cells, was solved in about five hours on a Pentium (90 MHz).

The programs have been used to solve many thermal problems. A number of examples are reported in order to provide the user with help and guidelines concerning choice of numerical mesh, accuracy, etc. One example deals with certain low-conductivity panels placed in foam. This problem with its intricate geometry is solved without difficulty with the three-dimensional program HEAT3. Another example deals with the thermal bridge of a wall with steel girders in mineral wool. The thermal conductivity of steel is about 1700 times higher than that of mineral wool, which may cause problems with the numerical accuracy. The use of one million computational cells made it possible to establish a numerical error of less than 0.1%.

The problem of thermal radiation in a cavity coupled to heat conduction and ventilation is analyzed in detail. The presented equations are well suited for an iterative

computer solution procedure, which turns out to be robust and very rapid. The back cover figures show the input, the numerical mesh, and the calculated temperatures for a window frame with 20 cavities.

The definition of the U-value for a foundation with floor heating is analyzed. The proposed formula, obtained by superposition, requires two independent simulations. The analysis is illustrated by a few examples.

Nomenclature

Note that a few symbols do not follow the ISO standard. For example, the ISO standard uses Θ for the temperature in degree Celsius. Chapter 7, dealing with radiation, has its own list of symbols.

Symbol	Quantity, (Units)
A	area, (m^2)
A_j	thermal response coefficient, $(\mathrm{W/(m^2K)})$
B_j	thermal response coefficient, $(\mathrm{W/(m^2K)})$
C	volumetric heat capacity, $(\mathrm{J/(m^3K)})$
c_p	specific heat capacity, $(\mathrm{J/(kg{\cdot}K)})$
E	energy, quantity of heat, $(\mathrm{J/m})$ or (J)
H	energy, quantity of heat, (J)
I	rate of internal heat generation per unit volume, $(\mathrm{W/m^3})$
K	thermal conductance, $(\mathrm{W/(m{\cdot}K)})$ or $(\mathrm{W/K})$
L	length, (m)
N	number of computational cells
n	ventilation rate, $(\mathrm{h^{-1}})$
Q	heat flow, $(\mathrm{W/m})$ or (W)
q	heat flow, $(\mathrm{W/m^2})$
q_c	convective heat transfer, $(\mathrm{W/m^2})$
q_r	radiative heat transfer, $(\mathrm{W/m^2})$
R	thermal resistance, $(\mathrm{m^2K/W})$
R_e	equivalent thermal resistance, $(\mathrm{m^2K/W})$
R_j	thermal response reduction factor, (-)
T	temperature, $(^\circ\mathrm{C})$ or (K)
T_m	average temperature of surfaces, (K)
t	time, (s)
U	"U-value", $(\mathrm{W/(m^2K)})$
V	volume, $(\mathrm{m^3})$

Greek letters	
α_c	convective heat transfer coefficient, $(\mathrm{W/(m^2K)})$
α_r	radiative heat transfer coefficient, $(\mathrm{W/(m^2K)})$
ΔT	temperature difference, $(^\circ\mathrm{C})$ or (K)
Δt	time-step, (s)

Δx	cell width, (m)
δ	coefficient for steady-state criterion, (-)
ϵ	emissivity, (-)
λ	thermal conductivity, (W/(m·K))
ω	successive over-relaxation coefficient, (-)
ρ	density, (kg/m^3)
σ_s	Stefan-Boltzmann constant, (5.67·10^{-8} W/(m^{2}K^4))
τ	time, (s)
ε	relative error, (-)

Chapter 1

Introduction

1.1   Purpose of the thesis

For many practical heat transfer problems it is not possible to obtain a solution by means of analytical techniques. Instead, solving them requires the use of numerical methods, which in many cases allow such problems to be solved quickly. Often, an engineer can easily see the effect of changes in parameters when modelling a problem numerically. To work in this way is much faster and tends to be more inexpensive, than assembling and working with the actual experimental apparatus.

The rate of progress concerning computer capacity and facilities has been, and is, considerable. Many problems that a decade ago required a large main-frame computer can now be solved on a personal computer. The first aim of this doctoral work has been to develop a new generation of computer programs for transient and steady-state heat conduction in two and three dimensions.

A large range of heat transfer problems within the field of buildings physics can be analyzed using these tools. There are, however, many things to keep in mind when modelling a problem, such as how to choose the numerical mesh, the proper boundary conditions, numerical accuracy, numerical stability, etc. The second aim of the thesis is to provide advice and guidelines how to deal with various problems that occur in building physics applications. To this aim, a large part is devoted to specific problems (Chapter 6).

The third aim of the thesis is to address a number of particular topics and problems: Numerical accuracy, successive over-relaxation, methods to increase accuracy by combining results from calculations using different numerical meshes, solution of large three-dimensional problems, solution of problems with large difference in thermal conductivity (steel versus insulation), heat conduction coupled to radiation in cavities, and how to obtain a proper U-value for a foundation with floor heating.

Many computer models are poorly documented regarding assumptions, used mathematical and physical equations, and manuals. The author has tried to avoid this.

A limitation of this work is that it is not a thesis about numerical techniques. The focus is set on applications in building physics using discrete approximations of physical

balances and other relations. Various numerical techniques presented in the standard literature are not discussed.

1.2 Background and prospects

There has been a remarkable development in personal computers during the last decades. Computational speed has increased 1000-fold. In the same time, the cost of a PC has been reduced to less than 1/10th of what it was. A PC has a very competitive performance/price ratio compared with other types of computers.

Improvements in software design tools have also been dramatic. In 1987, when I began to write computer programs for applications within building physics, there were large limitations regarding the size of code and data that could be managed compared with today. A few years later software for managing so-called user-friendly data input with pull-down menus started to appear. The program HEAT2 has about 45000 lines of source code, of which about 35000-40000 lines contain subroutines for dealing with input and output of data.

The most time-consuming work in computer programming is obviously the part aimed at making an application "easy to use". In the future, a technique called object-oriented programming is likely to become prevalent in developing all types of computer programs. This is a very efficient way to produce better computer programs in less time with low software defect rates. During the last few years this technique has been adapted to the PC environment, although it has existed for decades in other operating systems. Powerful and very affordable tools are now available. A couple of examples are Borland's Delphi (Borland, 1995), and the ObjectWindows library (Borland, 1993), for the Microsoft Windows environment. The program HEAT2W (Blomberg, 1994b) is implemented using this technique.

There is a great variety of computer codes for solving heat conduction problems. Appendix B shows a list of a few common computer programs available today.

1.3 Numerical method

The numerical techniques used in the present study are based on explicit finite differences. An advantage of this method is that it provides a good physical understanding and allows for simple incorporation of modifications, such as heat sources or phase change. A limitation in this work is that only Cartesian coordinates and cylindrical coordinates are used. This means that the considered problem must be described using a rectangular grid. This limitation is, however, quite reasonable in building physics. The main advantage is that the input often becomes much simpler than that of more general geometries.

A major work in the development and formulation of this explicit method is the doctoral thesis of Bengt Eftring entitled *Numerical Calculations of Thermal Processes*, see (Eftring, 1990). Much of the mathematical and numerical results in this thesis is a con-

tinuation of that work, especially in three dimensions.

1.4   Survey of the thesis

The mathematical equations for heat conduction in two and three dimensions, and in cylindrical coordinates, are described in Chapter 2. Boundary conditions and complications such as internal regions containing liquid fluid or air are discussed.

The numerical formulation of the mathematical equations is described in Chapter 3. Computational mesh and thermal conductances are dealt with. Formulas are given for how to calculate heat flows, temperatures and the stable time-step. The method of successive over-relaxation in the steady-state case is described.

Numerical studies are presented in Chapter 4. The first topic involves accuracy considerations for different computational meshes. The second topic deals with how calculations for different meshes can be used to estimate more accurate results. The third section deals with the effect of successive over-relaxation on the computer simulation time. A method called subdivision is also described.

Computer programs for transient and steady-state heat conduction in two and three dimensions, and in cylindrical coordinates, have been developed. These are called HEAT2 (Blomberg, 1990, 1991), HEAT3 (Blomberg, 1993a, 1994a), and HEAT2R (Blomberg, 1994c). They are discussed briefly in Chapter 5. The programs are part of a library (Arfvidsson et al, 1993), developed by *Lund Group for Computational Building Physics*. The library contains about 30 programs dealing with building physics and ground heat.

Chapter 6 presents some applications within the fields of building physics and ground heat. The following topics are studied:

Metal thermal bridges in insulation	*(Section 6.2)*
Glass-encapsulated evacuated powder panels	*(Section 6.3)*
Rock caverns used for heat storage	*(Section 6.4)*
Thermal shielding of rock caverns	*(Section 6.5)*
U-value for a window accounting for the wall	*(Section 6.6)*
Temperature and moisture conditions in attics	*(Section 6.7)*
Insulated wall with slotted steel U-girders	*(Section 6.8)*
Heat flow through a corner	*(Section 6.9)*
Slab on the ground	*(Section 6.10)*
House with a floor heating system	*(Section 6.11)*
Construction block filled with insulation	*(Section 6.12)*
Heat flow through a wall with metal studs	*(Section 6.13)*

The examples deal with quite different topics. This shows the versatility of the developed programs. A major concern has been how to choose the numerical mesh and how to

assess the accuracy. The calculation time on a PC is often shown in the examples. Even though these numbers very soon will be "out of date", they will hopefully tell a future reader how fast a particular problem can be solved.

The problem of thermal radiation in a cavity coupled to heat conduction and ventilation is analyzed in detail in Chapter 7. The presented equations are well suited for an iterative computer solution procedure, which turns out to be robust and very rapid.

Chapter 2

Mathematical description

2.1   Governing differential equations

The governing partial differential heat conduction equation in two dimensions for the temperature $T(x, y, t)$ is

$$\frac{\partial}{\partial x}(\lambda_x \frac{\partial T}{\partial x}) + \frac{\partial}{\partial y}(\lambda_y \frac{\partial T}{\partial y}) + I(x, y, t) = C\frac{\partial T}{\partial t} \qquad (2.1)$$

Here I, (W/m^3), is the rate of internal heat generation. The thermal conductivities in the x, y-directions are denoted by λ_x and λ_y, (W/(m·K)), respectively. The volumetric heat capacity is denoted by C, (J/(m^{3}K)), which is the density times the specific heat capacity ($C = \rho \cdot c_p$). The thermal conductivities in the two directions are usually the same ($\lambda_x = \lambda_y$). The internal heat generation is often zero. In the steady-state case, the right-hand side of Eq. (2.1) is zero. In the case of three dimensions, we have

$$\frac{\partial}{\partial x}(\lambda_x \frac{\partial T}{\partial x}) + \frac{\partial}{\partial y}(\lambda_y \frac{\partial T}{\partial y}) + \frac{\partial}{\partial z}(\lambda_z \frac{\partial T}{\partial z}) + I(x, y, z, t) = C\frac{\partial T}{\partial t} \qquad (2.2)$$

A third case concerns rotationally symmetric heat flow with cylindrical coordinates r and z, see Fig. 2.1. The heat conduction equation to be solved is

$$\frac{1}{r}\frac{\partial}{\partial r}\left(\lambda \cdot r\frac{\partial T}{\partial r}\right) + \frac{\partial}{\partial z}\left(\lambda\frac{\partial T}{\partial z}\right) = C\frac{\partial T}{\partial t} \qquad (2.3)$$
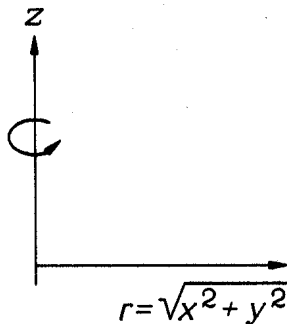
Figure 2.1: Rotationally symmetric heat flow in cylindrical coordinates r and z.

2.2 Boundary conditions

There are two main types of boundary conditions which can be applied to the boundary segments ($b.s.$). The first type gives a prescribed temperature of the surrounding region, $T_{b.s.}(t)$, and a given surface resistance R, (m^2K/W):

$$T_{b.s.}(t) - T|_{surf} = R \cdot (-\lambda)\frac{\partial T}{\partial n}\bigg|_{surf} \qquad (°C) \tag{2.4}$$

Here, $\partial T/\partial n$ is the derivative in the normal direction. The second type gives a prescribed heat flow into the region:

$$(-\lambda)\frac{\partial T}{\partial n}\bigg|_{b.s.} = f(t) \quad (W/m^2) \tag{2.5}$$

Figure 2.2 shows an internal boundary separating two different materials of thermal conductivities λ_1 and λ_2. The temperature is of course continuous at the boundary. The normal to the boundary is denoted by $\hat{n}$. There is a continuity of the heat flow across the boundary. The condition of continuous heat flow perpendicular to the boundary is

$$\lambda_1\frac{\partial T}{\partial n}\bigg|_1 = \lambda_2\frac{\partial T}{\partial n}\bigg|_2 \tag{2.6}$$
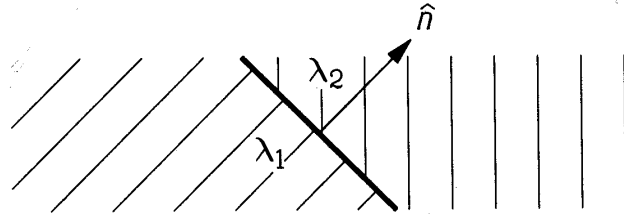
Figure 2.2: The normal $\hat{n}$ at an internal boundary.

There may be a contact resistance R_{ins}, (m^2K/W), between two regions, see Fig. 2.3. In this case, the temperature is different on the two sides of the contact resistance. The condition for continuous heat flow at this internal insulation is

$$\lambda_2\frac{\partial T}{\partial n}\bigg|_2 = \frac{T|_2 - T|_1}{R_{ins}} = \lambda_1\frac{\partial T}{\partial n}\bigg|_1 \tag{2.7}$$
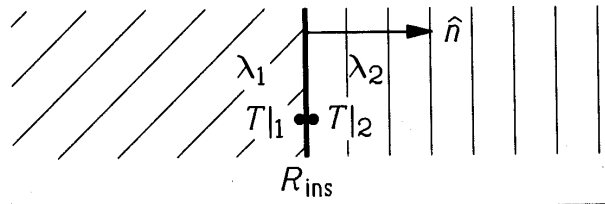
Figure 2.3: Case involving internal insulation.

2.3 Initial conditions

The initial temperature distribution at time $t=t_{\text{start}}$ is denoted in two dimensions by $T(x,y,t_{\text{start}})$, in three dimensions by $T(x,y,z,t_{\text{start}})$, and in cylindrical coordinates by $T(r,z,t_{\text{start}})$. In the steady-state case, the initial temperatures are irrelevant to the solution.

2.4 Fluid regions

Consider Fig. 2.4, in which S denotes the boundary surface of an internal region containing a fluid with a volumetric heat capacity C_{fluid}, $(\text{J}/(\text{m}^3\text{K}))$. The inward normal for the region is denoted by $\hat{n}$, and the volume of the fluid by V_{fluid}, (m^3). The heat flow into the area Q_{in}, (W), is obtained by an integral over the boundary surface S. The flow equals the rate of increase of the heat content in the fluid:

$$Q_{in} = \oint -\lambda \frac{\partial T}{\partial n}dS = C_{fluid} \cdot V_{fluid}\frac{\partial T_{fluid}}{\partial t} \qquad (W) \tag{2.8}$$

In the case involving a cavity filled with air, the heat capacity may be put to zero and the right-hand side of (2.8) becomes zero.
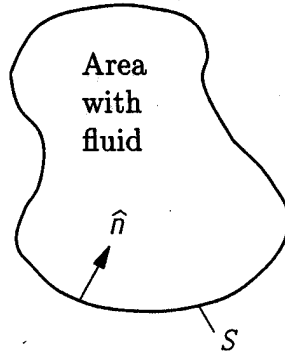
Figure 2.4: A fluid region enclosed by the boundary surface S.

2.5 Heat conduction coupled to radiation in a cavity

Heat conduction in solid building parts coupled to long-wave thermal radiation in air cavities is a frequently occurring and studied type of process in building physics. The numerical simulation of this coupling poses particular problems. Figure 7.1, right, shows a typical example. An equation system for the radiative exchange coupled to convective heat transfer in the cavity and heat conduction to the nodes in the numerical mesh must be solved at each time.

A systematic analysis of this problem is presented in Chapter 7. The number of original $(2N+1)$ equations is reduced as much as possible (to N equations). The final

formulas, and in particular the iterative process to account for the nonlinearity due to the forth-power radiation law, are formulated to suit computer modelling.

Chapter 3

Numerical formulation

In the numerical formulation, the partial differential equation is replaced by a discrete approximation. The temperature field is approximated by values at discrete points. This gives a computational mesh. The field is considered at consecutive time-steps with a time increment Δt.

In this study, only Cartesian (and cylindrical) meshes will be used. The increments in x-, y-, and z-directions are denoted by Δx_i, Δy_j, and Δz_k, respectively. The smaller these increments are, the better is the agreement with the "true" temperature distribution.

3.1   Heat conduction in two dimensions

3.1.1   Computational mesh

Consider a two-dimensional body that is divided into increments in the x- and y-directions as shown in Fig. 3.1. This rectangular mesh may have computational cells of different sizes. The width and height of cell (i, j) are denoted by Δx_i and Δy_j, respectively. The temperature in the midpoint of cell (i, j) at the considered time-step is denoted by $T_{i,j}$.
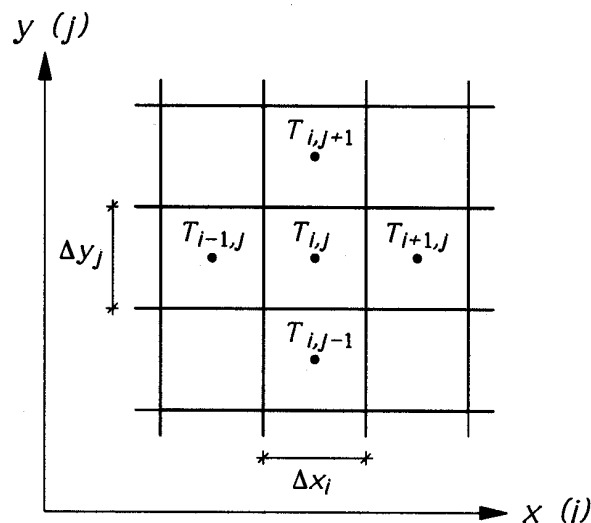
Figure 3.1: Choice of indices for the cells in the computational mesh.

3.1.2 Thermal conductances

The thermal coupling between the cells in the numerical mesh is described by thermal conductances. Figure 3.2 shows the notation of indices for the conductances.
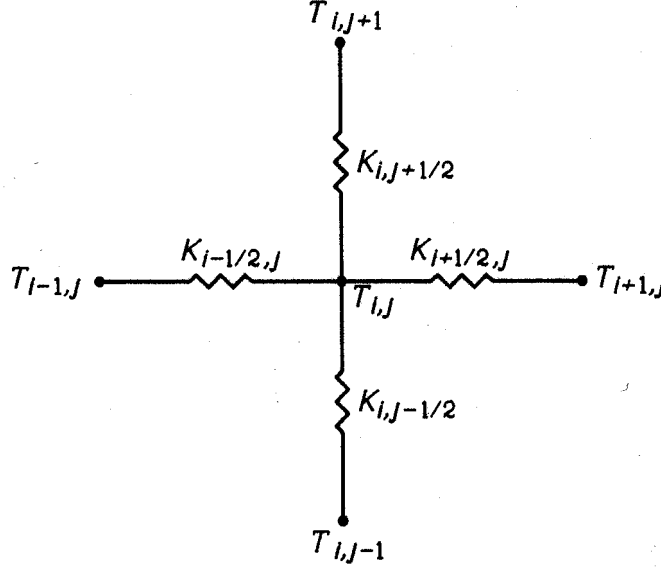
Figure 3.2: The thermal conductances between cell (i, j) and its neighboring cells.

The conductance per unit length perpendicular to the (x, y)-plane between the two cells $(i\text{-}1,j)$ and (i, j) is denoted by $K_{i-\frac{1}{2},j}$, $(\text{W}/(\text{m·K}))$. It is calculated as

$$K_{i-\frac{1}{2},j} = \frac{\Delta y_j}{\Delta x_{i-1}/(2\lambda_{x\,i-1,j}) + \Delta x_i/(2\lambda_{x\,i,j}) + R_{i-\frac{1}{2},j}} \qquad (\text{W}/(\text{m·K})) \qquad (3.1)$$

Here $\lambda_{x\,i,j}$ is the thermal conductivity in the x-direction for cell (i, j). The conductance refers to the total heat flow through the side Δy_j per unit length. The first term in the denominator is the thermal resistance in the x-direction for half of the cell $(i\text{-}1,j)$, the second term being the resistance for half of the cell (i, j). The third term $R_{i-\frac{1}{2},j}$, $(\text{m}^2\text{K}/\text{W})$, is an optional additional thermal resistance at the interface between the two cells $(i\text{-}1,j)$ and (i, j) as shown in Fig. 3.3.

For the cell $(1, j)$ lying at the boundary as shown in Fig. 3.5, the conductance $K_{\frac{1}{2},j}$ is calculated as

$$K_{\frac{1}{2},j} = \frac{\Delta y_j}{\Delta x_1/(2\lambda_{x\,1,j}) + R_{\frac{1}{2},j}} \qquad (3.2)$$

Here $R_{\frac{1}{2},j}$, $(\text{m}^2\text{K}/\text{W})$, is the boundary surface resistance.
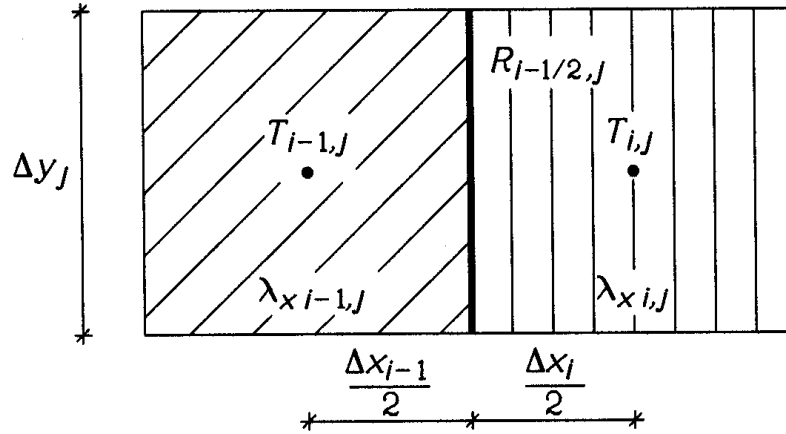
Figure 3.3: Thermal resistance between cell $(i\text{-}1,j)$ and cell (i,j).

3.1.3 Heat flows

Figure 3.4 shows the four heat flows associated with an internal cell.
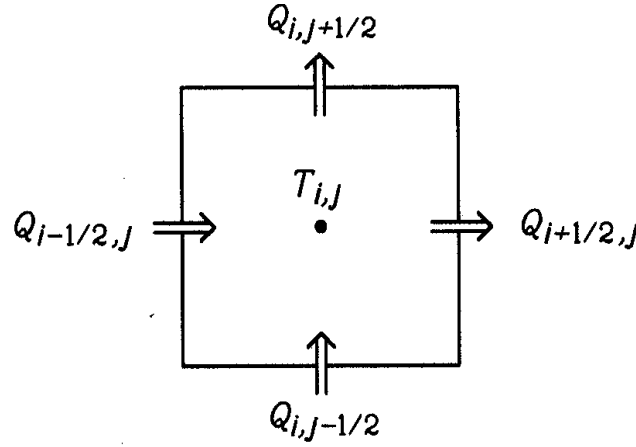
Figure 3.4: The four heat flows of cell (i,j).

The heat flow through the left boundary $Q_{i-\frac{1}{2},j}$, (W/m), is

$$Q_{i-\frac{1}{2},j} = K_{i-\frac{1}{2},j} \cdot (T_{i-1,j} - T_{i,j}) \qquad \text{(W/m)} \tag{3.3}$$

The heat flow through the lower boundary $Q_{i,j-\frac{1}{2}}$ is

$$Q_{i,j-\frac{1}{2}} = K_{i,j-\frac{1}{2}} \cdot (T_{i,j-1} - T_{i,j}) \qquad \text{(W/m)} \tag{3.4}$$

The heat flow through a boundary cell is determined by the boundary condition. Consider, for example, the outer boundary cell $(1,j)$ in Fig. 3.5. If a temperature is given, Eq. (3.3) is modified to

$$Q_{\frac{1}{2},j} = K_{\frac{1}{2},j} \cdot (T_{\text{b.s.}}(t) - T_{1,j}) \qquad \text{(W/m)} \tag{3.5}$$

11
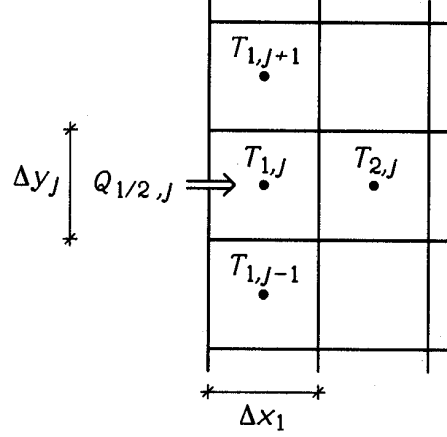
Figure 3.5: Heat flow $Q_{\frac{1}{2},j}$ through the outer boundary of boundary cell $(1,j)$.

If a boundary heat flow $q_{\text{b.s.}}$, (W/m^2), is given, the heat flow per unit length perpendicular to the (x, y)-plane is

$$Q_{\frac{1}{2},j} = q_{\text{b.s.}}(t) \cdot \Delta y_j \qquad (\text{W/m}) \tag{3.6}$$

The accumulated heat flow during a time-step Δt for the left boundary segment to which cell $(1, j)$ belongs is

$$E_{\text{b.s.}}^{new} = E_{\text{b.s.}} + \Delta t \cdot \sum_j Q_{\frac{1}{2},j} \qquad (\text{J/m}) \tag{3.7}$$

where the summation involves all cells that belong to the boundary segment.

3.1.4 New temperatures

The heat capacity of cell (i, j) becomes $C_{i,j} \Delta x_i \Delta y_j$ per unit length perpendicular to the (x, y)-plane. Here $C_{i,j}$, $(\text{J}/(\text{m}^3\text{K}))$, is the volumetric heat capacity for cell (i, j).

The increase of the energy for an internal cell during time-step Δt is given by the energy balance below. In the formula, $T_{i,j}$ is the old temperature of cell (i, j), and $T_{i,j}^{new}$ the new one. The development in time is incremented by Δt, and the new time becomes $t^{new} = t + \Delta t$. The heat generation in cell (i, j) is denoted by $I_{i,j}$, (W/m^3). A negative value indicates a heat sink. The heat generation is often zero.

$$C_{i,j} \cdot \Delta x_i \cdot \Delta y_j \cdot (T_{i,j}^{new} - T_{i,j}) =$$

$$(Q_{i-\frac{1}{2},j} - Q_{i+\frac{1}{2},j} + Q_{i,j-\frac{1}{2}} - Q_{i,j+\frac{1}{2}} + I_{i,j} \cdot \Delta x_i \cdot \Delta y_j) \cdot \Delta t \tag{3.8}$$

The final equation for the new temperature becomes

$$T_{i,j}^{new} = T_{i,j} + \frac{\Delta t}{C_{i,j} \Delta x_i \Delta y_j} \left(Q_{i-\frac{1}{2},j} - Q_{i+\frac{1}{2},j} + Q_{i,j-\frac{1}{2}} - Q_{i,j+\frac{1}{2}} + I_{i,j} \Delta x_i \Delta y_j \right) \tag{3.9}$$

3.1.5 Choice of time-step

The stable time-step Δt for cell (i,j) is determined from the following stability criterion:

$$\Delta t < \frac{C_{i,j}\Delta x_i \Delta y_j}{K_{i-\frac{1}{2},j} + K_{i+\frac{1}{2},j} + K_{i,j-\frac{1}{2}} + K_{i,j+\frac{1}{2}}} \qquad \text{for all } i \text{ and } j \qquad (3.10)$$

This criterion must be satisfied for all cells (i,j). The smallest stable time-step obtained is used for all cells to guarantee stability. The analysis leading to this criterion is not given here. The reader is referred to (Eftring, 1990).

3.1.6 Iterative calculation

Equation (3.9) gives the new temperature based on the change in energy during the time-step Δt. This calculation is made for all cells. The updated temperatures give the new heat flows between the cells according to Eqs (3.3)-(3.6), which in turn change the temperatures again, and so on.

3.1.7 Steady-state case

Transient problems are solved with the above method of explicit forward differences. This means that the old temperatures are used to calculate the heat flows. The new temperatures $T_{i,j}^{new}$ are calculated by Eq. (3.9).

The successive over-relaxation method is used in the steady-state case, see (Hirsch, 1992). Here, the temperatures are calculated in the same way as with explicit forward difference, but new temperatures are used in the formulas as they arise. The temperatures are calculated using an over-relaxation factor ω that lies in the range 1.0-2.0. An optimized ω may give calculation times between 1/50th and 1/10th of that required for a calculation not using over-relaxation (ω=1.0), see Section 4.3. The optimized ω typically lies in the range 1.8-2. In HEAT2, HEAT2R, and HEAT3, this factor is initially set to 1.95. Equation (3.9) is modified to

$$T_{i,j}^{new} = T_{i,j} + \frac{\Delta t \cdot \omega}{C_{i,j}\Delta x_i \Delta y_j} \left(Q_{i-\frac{1}{2},j} - Q_{i+\frac{1}{2},j} + Q_{i,j-\frac{1}{2}} - Q_{i,j+\frac{1}{2}} + I_{i,j}\Delta x_i \Delta y_j \right) \quad (3.11)$$

The heat capacities of the cells do not matter in the steady-state solution. The stable time-step for each cell determines the time-scale for temperature changes within the cell. It is better if all cells have the same stable time-step, which means the thermal response time for each cell is the same. Accordingly, the heat capacities $C_{i,j}$ are chosen to give the same time-step for all cells. The heat capacities are determined by putting Δt equal to the right-hand side in (3.10). The chosen capacities are then

$$C_{i,j} = \Delta t \cdot \frac{K_{i-\frac{1}{2},j} + K_{i+\frac{1}{2},j} + K_{i,j-\frac{1}{2}} + K_{i,j+\frac{1}{2}}}{\Delta x_i \Delta y_j} \qquad (3.12)$$

Actually, the choice of Δt does not matter since it cancels in Eq. (3.11).

3.1.8 Internal regions containing fluid

In some cases there is a need to model an internal area containing liquid fluid or air. An example of this is rock cavities with water used for heat storage.

Two cases are considered when modelling an internal region with a fluid: the fluid has heat capacity, or the fluid has negligible heat capacity, see Section 2.4.

For the given fluid volume V_{fluid} with the volumetric heat capacity C_{fluid}, the temperature of the fluid T_{fluid} is calculated from the energy balance involving the surrounding cells. Equation (2.8) becomes in a discrete approximation

$$C_{fluid} \cdot V_{fluid} \cdot (T_{fluid}^{new} - T_{fluid}) = \sum_{n=1}^{N} K_n \cdot (T_n - T_{fluid}) \cdot \Delta t \qquad (3.13)$$

The temperatures in the cells adjacent to the fluid region are denoted by T_n. The thermal conductance between the center of the cell in question and the fluid is denoted by K_n. The total number of cells, N, enclosing the fluid volume is taken into account in calculating the new fluid temperature, T_{fluid}^{new}.

Air may be approximated as a fluid with negligible heat capacity. The air temperature T_a inside an internal region becomes an average of the temperatures in the surrounding cells:

$$T_a = \frac{\sum_{n=1}^{N}(K_n \cdot T_n)}{\sum_{n=1}^{N} K_n} \qquad (3.14)$$

3.2 Heat conduction in three dimensions

3.2.1 Thermal conductances

Figure 3.6 shows a cell (i, j, k) with the side lengths Δx_i, Δy_j, and Δz_k. There are six adjacent cells. The figure also shows the cell $(i, j, k+1)$ located directly above.

The heat flow $Q_{i,j,k+\frac{1}{2}}$, (W), from cell (i, j, k) to cell $(i, j, k+1)$ is given by the thermal conductance multiplied by the temperature difference between these two cells:

$$Q_{i,j,k+\frac{1}{2}} = K_{i,j,k+\frac{1}{2}} \cdot (T_{i,j,k} - T_{i,j,k+1}) \qquad \text{(W)} \qquad (3.15)$$

where $K_{i,j,k+\frac{1}{2}}$, (W/K), is the conductance between the two cells (i, j, k) and $(i, j, k+1)$. The other five heat flows pertaining to cell (i, j, k) are calculated in the same way.

Fig. 3.7 shows the six thermal conductances of cell (i, j, k). The conductance $K_{i,j,k+\frac{1}{2}}$, (W/K), between the two cells (i, j, k) and $(i, j, k+1)$ is calculated as

$$K_{i,j,k+\frac{1}{2}} = \frac{\Delta x_i \Delta y_j}{\Delta z_k/(2\lambda_{i,j,k}) + \Delta z_{k+1}/(2\lambda_{i,j,k+1}) + R_{i,j,k+\frac{1}{2}}} \qquad \text{(W/K)} \qquad (3.16)$$
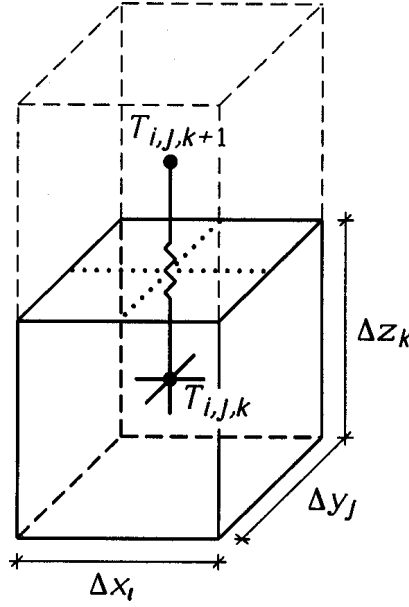
Figure 3.6: Computational cells (i, j, k) and $(i, j, k+1)$.
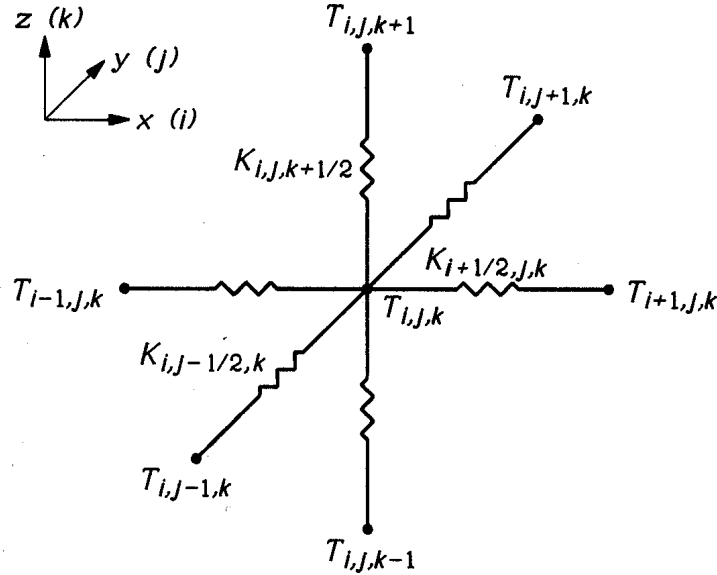
Figure 3.7: Thermal conductances connected to cell (i, j, k).

Here $\lambda_{i,j,k}$, $(\mathrm{W/(m \cdot K)})$, is the thermal conductivity in cell (i, j, k). The conductance refers to the total heat flow through the area $\Delta x_i \Delta y_j$. The first term in the denominator is the thermal resistance in the z-direction for half of the cell (i, j, k), the second term being the resistance for half of the cell $(i, j, k+1)$. The third term, $R_{i,j,k+\frac{1}{2}}$, is an optional additional thermal resistance at the interface between the two cells (i, j, k) and $(i, j, k+1)$.

Equation (3.16) is valid for all internal cells (an internal cell has at least one cell on each side). For boundary cells, the equation is modified in the following way. Consider

15

cell $(1, j, k)$ that lies at the boundary in the same way as cell $(1, j)$ in Fig. 3.5. The conductance which couples the temperature $T_{1,j,k}$ with a boundary temperature is

$$K_{\frac{1}{2},j,k} = \frac{\Delta y_j \Delta z_k}{\Delta x_1/(2\lambda_{1,j,k}) + R_{\frac{1}{2},j,k}} \qquad (\text{W/K}) \tag{3.17}$$

Here, $R_{\frac{1}{2},j,k}$, $(\text{m}^2\text{K/W})$, is the boundary surface resistance.

3.2.2 Heat flows

An energy balance is calculated for each cell. The total heat flow to cell (i, j, k) from the six adjacent cells is put in the variable $H_{i,j,k}$ (W):

$$H_{i,j,k} = K_{i-\frac{1}{2},j,k} \cdot (T_{i-1,j,k} - T_{i,j,k}) + K_{i+\frac{1}{2},j,k} \cdot (T_{i+1,j,k} - T_{i,j,k}) + \tag{3.18}$$

$$K_{i,j-\frac{1}{2},k} \cdot (T_{i,j-1,k} - T_{i,j,k}) + K_{i,j+\frac{1}{2},k} \cdot (T_{i,j+1,k} - T_{i,j,k}) +$$

$$K_{i,j,k-\frac{1}{2}} \cdot (T_{i,j,k-1} - T_{i,j,k}) + K_{i,j,k+\frac{1}{2}} \cdot (T_{i,j,k+1} - T_{i,j,k}) \qquad (\text{W})$$

Changes in the energy of a cell due to such modifications as heat sources/sinks are directly made by adding or subtracting the values to the variable $H_{i,j,k}$ as $I_{i,j,k} \cdot \Delta x_i \Delta y_j \Delta z_k$. This method simplifies the calculation procedure.

Another advantage of the introduction of $H_{i,j,k}$ is that less data need to be allocated in computer memory. Consider first the two-dimensional case where we have the following six arrays:

$$T_{i,j} \quad C_{i,j} \quad K_{i+\frac{1}{2},j} \quad K_{i,j+\frac{1}{2}} \quad Q_{i+\frac{1}{2},j} \quad Q_{i,j+\frac{1}{2}}$$

The arrays that are needed in the three-dimensional case are normally eight:

$$T_{i,j,k} \quad C_{i,j,k} \quad K_{i+\frac{1}{2},j,k} \quad K_{i,j+\frac{1}{2},k} \quad K_{i,j,k+\frac{1}{2}} \quad Q_{i+\frac{1}{2},j,k} \quad Q_{i,j+\frac{1}{2},k} \quad Q_{i,j,k+\frac{1}{2}}$$

Introducing the $H_{i,j,k}$-variable gives instead six three-dimensional arrays:

$$T_{i,j,k} \quad C_{i,j,k} \quad K_{i+\frac{1}{2},j,k} \quad K_{i,j+\frac{1}{2},k} \quad K_{i,j,k+\frac{1}{2}} \quad H_{i,j,k}$$

Note that only three of the products (conductance multiplied by temperature difference in Eq. (3.18)) have to be calculated at each time-step. This may save almost half the computer time compared with a direct use of Eq. (3.18). The following procedure, which is used for all internal cells (i,j,k), illustrates this. Three local variables, Q_x, Q_y, and Q_z, are introduced in order to decrease the number of arithmetic operations. The heat flows from the three cells "upstream" $(i{+}1,j,k)$, $(i,j{+}1,k)$, and $(i,j,k{+}1)$ to cell (i,j,k) are put in the variables:

$$Q_x = K_{i+\frac{1}{2},j,k} \cdot (T_{i+1,j,k} - T_{i,j,k})$$

$$Q_y = K_{i,j+\frac{1}{2},k} \cdot (T_{i,j+1,k} - T_{i,j,k})$$

$$Q_z = K_{i,j,k+\frac{1}{2}} \cdot (T_{i,j,k+1} - T_{i,j,k})$$

The change in heat for the cells "upstream" is directly made as

$$H^{new}_{i+1,j,k} = H_{i+1,j,k} - Q_x$$

$$H^{new}_{i,j+1,k} = H_{i,j+1,k} - Q_y$$

$$H^{new}_{i,j,k+1} = H_{i,j,k+1} - Q_z$$

At the same time-step, the energy is increased in cell (i,j,k) as

$$H^{new}_{i,j,k} = H_{i,j,k} + Q_x + Q_y + Q_z$$

3.2.3   New temperatures

The net heat flow during a time-step Δt results in an increase or a decrease in temperature. The temperature at the next time-step becomes

$$T^{new}_{i,j,k} = T_{i,j,k} + \frac{\Delta t}{C_{i,j,k}\Delta x_i \Delta y_j \Delta z_k} \cdot H_{i,j,k} \tag{3.19}$$

where $C_{i,j,k}$, $(\mathrm{J/(m^3 K)})$, is the volumetric heat capacity. Equations (3.18) and (3.19) are used iteratively. Temperatures are updated and new flows are calculated using these new temperatures, and so forth, see Section 3.1.6.

The successive over-relaxation method is used for the steady-state case. The over-relaxation factor ω lies in the range 1.0-2.0. See Sections 3.1.7 and 4.3 for further discussions of ω. Equation (3.19) is modified to

$$T^{new}_{i,j,k} = T_{i,j,k} + \frac{\Delta t \cdot \omega}{C_{i,j,k}\Delta x_i \Delta y_j \Delta z_k} \cdot H_{i,j,k} \tag{3.20}$$

The heat capacities $C_{i,j,k}$ are chosen to give the same time-step for all cells:

$$C_{i,j,k} = \Delta t \cdot \frac{\sum K}{\Delta x_i \Delta y_j \Delta z_k} \tag{3.21}$$

where $\sum K$ is given in Eq. (3.23).

3.2.4   Choice of time-step

The stable time-step Δt for cell (i, j, k) is determined using the following stability criterion:

$$\Delta t < \frac{C_{i,j,k}\Delta x_i \Delta y_j \Delta z_k}{\sum K} \qquad \text{for all } i,\ j,\ \text{and } k \tag{3.22}$$

where

$$\sum K = K_{i-\frac{1}{2},j,k} + K_{i+\frac{1}{2},j,k} + K_{i,j-\frac{1}{2},k} + K_{i,j+\frac{1}{2},k} + K_{i,j,k-\frac{1}{2}} + K_{i,j,k+\frac{1}{2}} \tag{3.23}$$

This criterion must be satisfied for all cells (i, j, k). The smallest stable time-step obtained is used for all cells to guarantee stability, see (Eftring, 1990).

3.3 Heat conduction in cylindrical coordinates

The temperature along the radius r and at the vertical distance z at time t is denoted by $T = T(r, z, t)$. We consider a radial and a vertical thermal process, rotationally symmetric around the z-axis. The interval along r is divided into a numerical mesh with the cell widths Δr_i, $i = 1, ... N$. See Figure 3.8. The midpoint of cell i lies at $r = r_i$. The inner boundary lies at $r = r_-$, and the outer boundary lies at $r = r_+$. Note that r_- may be zero, i.e. at the z-axis. We have:

$$r_1 = r_- + \frac{\Delta r_1}{2} \qquad r_i = r_{i-1} + \frac{\Delta r_{i-1}}{2} + \frac{\Delta r_i}{2} \qquad i = 2, ..., N \qquad (3.24)$$

The sum of the cell widths equals the total width of the annulus:

$$\sum_{i=1}^{N} \Delta r_i = r_+ - r_- \qquad (3.25)$$
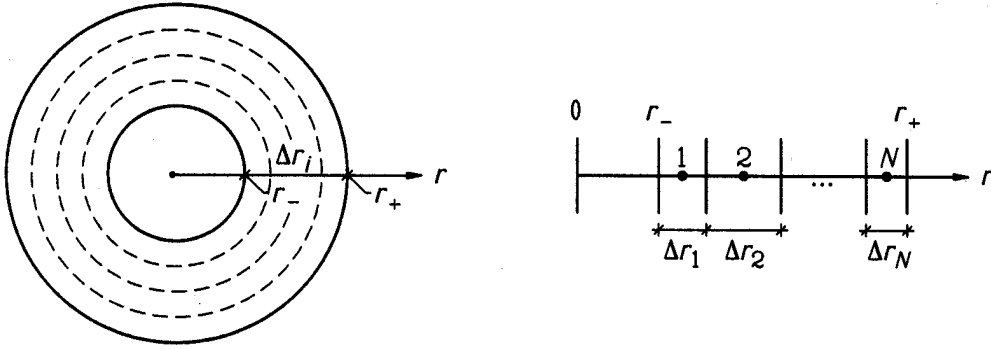
Figure 3.8: Mesh in the radial direction.

In the z-direction, the cell widths are denoted by Δz_j. See Figure 3.9. The temperature at the midpoint of cell (i, j) at time step n is denoted $T_{i,j}$:

$$T_{i,j} = T(r_i, z_j, n\Delta t) \qquad (3.26)$$
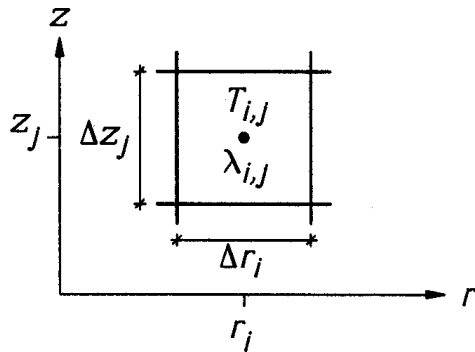
Figure 3.9: Mesh in cylindrical coordinates.

The cell (i, j) is an annular ring of cylindrical shape:

$$\text{cell } (i, j): \quad r_i - \Delta r_i/2 \leq r \leq r_i + \Delta r_i/2 \quad z_j - \Delta z_j/2 \leq z \leq z_j + \Delta z_j/2 \qquad (3.27)$$

The volume becomes:

$$\left[\pi(r_i + \Delta r_i/2)^2 - \pi(r_i - \Delta r_i/2)^2\right]\Delta z_j = 2\pi r_i \Delta r_i \Delta z_j \tag{3.28}$$

The conductance between cell $(i\text{-}1,j)$ and (i,j) is:

$$K_{i-0.5,j} = \frac{\Delta z_j}{\frac{1}{2\pi\lambda_{i-1,j}}\ln\left(\frac{r_{i-0.5}}{r_{i-1}}\right) + \frac{1}{2\pi\lambda_{i,j}}\ln\left(\frac{r_i}{r_{i-0.5}}\right) + \frac{R_{i-0.5,j}}{2\pi r_{i-0.5}}} \quad \text{(W/K)} \tag{3.29}$$

Here, the first of the three terms in the denominator is the thermal resistance (per unit height) of the annulus $r_{i-1} < r < r_{i-0.5}$. There may be an internal resistance $R_{i-0.5,j}$, $(\text{m}^2\text{K/W})$, at the interface between the cells.

The conductance in the z-direction is equal to the one-dimensional conductance multiplied by the area of the cell perpendicular to z, i.e. $2\pi r_i \Delta r_i$:

$$K_{i,j-0.5} = \frac{2\pi r_i \Delta r_i}{0.5\Delta z_{j-1}/\lambda_{i,j-1} + 0.5\Delta z_j/\lambda_{i,j} + R_{i,j-0.5}} \quad \text{(W/K)} \tag{3.30}$$
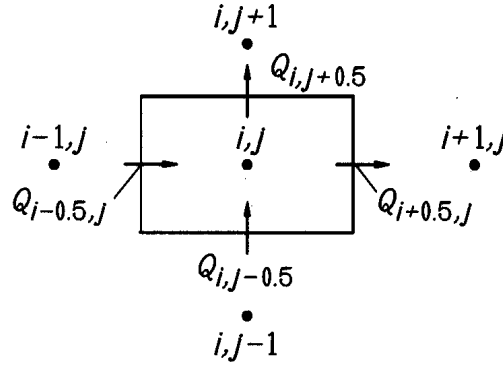
Figure 3.10: Definition of flows (W) to and from cell (i,j).

The heat flows, see Fig. 3.10, are given by a conductance times the temperature difference. The flows become for all i and j:

$$Q_{i-0.5,j} = K_{i-0.5,j}(T_{i-1,j} - T_{i,j}) \qquad \text{all } i \text{ and } j \tag{3.31}$$

$$Q_{i,j-0.5} = K_{i,j-0.5}(T_{i,j-1} - T_{i,j}) \qquad \text{all } i \text{ and } j \tag{3.32}$$

The heat balance equation becomes:

$$C_{i,j}2\pi r_i \Delta r_i \Delta z_j(T_{i,j}^{new} - T_{i,j}) = \tag{3.33}$$

$$\left[Q_{i-0.5,j} - Q_{i+0.5,j} + Q_{i,j-0.5} - Q_{i,j+0.5}\right]\Delta t$$

The criterion for numerical stability is, (Eftring, 1990):

$$\Delta t < \frac{C_{i,j}2\pi r_i \Delta r_i \Delta z_j}{K_{i-0.5,j} + K_{i+0.5,j} + K_{i,j-0.5} + K_{i,j+0.5}} \qquad \text{for all } i \text{ and } j \tag{3.34}$$

19

Chapter 4

Numerical studies

A few numerical studies are reported here for steady-state cases. The first topic involves accuracy considerations for different computational meshes. Generally, the smaller the computational cells are, the better is the agreement with the "true" temperature distribution. The second topic deals with how calculations for different meshes can be used to estimate more accurate results. The third topic shows the effect of successive over-relaxation on the computer simulation time. A method called subdivision is also described.

4.1   Heat flow through a cube

The accuracy of the numerical solution is higher with a finer mesh. Different equidistant meshes are studied here for the cube shown in Fig. 4.1. The total number of cells ranges from one to one million (100^3). The following steady-state problem is considered. The temperature on the surface $z=L_z$ is 1, and zero on the other five sides. The thermal conductivity is 1.0, and the side lengths are $L_x=1$, $L_y=1$ and $L_z=1$. A relative error ε is calculated by comparing the heat flows through the bottom side obtained from the numerical and the analytical solutions. The analytical solution to this problem is given in Appendix A, see Eq. (A.3). The heat flow through the bottom side is

$$Q^{exact} = \frac{64}{\pi^3} \sum_{m=0}^{\infty} \sum_{n=0}^{\infty} \frac{1}{(2m+1)^2} \frac{1}{(2n+1)^2} \frac{\sqrt{(2m+1)^2 + (2n+1)^2}}{\sinh\left[\pi\sqrt{(2m+1)^2 + (2n+1)^2}\right]} \qquad (4.1)$$

This double sum is easily computed and becomes using the first ten terms of m and n

$$Q^{exact} = 0.0688189 \quad \text{W}$$

The following criterion for when to stop a steady-state calculation is recommended as a European standard (CEN, 1995). The sum of all heat flows (positive and negative) entering the boundaries, divided by the sum of the absolute values of all these heat flows, must be less than 0.001. However, since we are interested in the numerical accuracy, this value is put to $1 \cdot 10^{-6}$ instead. Figure 4.2 and Table 4.1 show the error as a function of number of computational cells $N_x=N_y=N_z$. The flow obtained in the numerical

calculations is denoted by Q, (W). The relative error is expressed as $\varepsilon=(Q-Q^{exact})/Q^{exact}$.
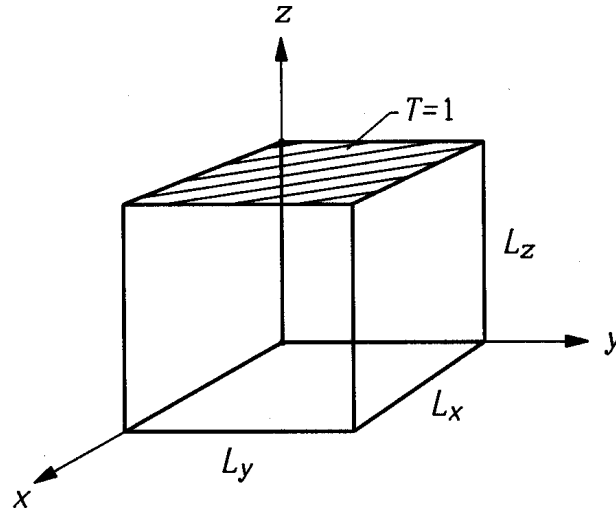
Figure 4.1: Cube $(L_x=L_y=L_z)$ with $T=1$ on one side and $T=0$ on the other five sides.

N_x	$N=N_x^3$	Q (W)	ε (%)
1	1	1/3	384
2	8	1/6	142
10	1000	0.071889	4.5
20	8000	0.069576	1.1
30	27000	0.069154	0.49
40	64000	0.069007	0.27
50	125000	0.068939	0.17
60	216000	0.068903	0.12
70	343000	0.068880	0.09
80	512000	0.068866	0.07
90	729000	0.068856	0.05
100	1000000	0.068849	0.04

Table 4.1: Heat flow and relative error as a function of number of computational cells.

The error becomes 1.1% for 20^3 (8000) computational cells, and the CPU-time is a few seconds on a Pentium/90. With 100^3 (1000000) cells, the error is 0.04%, and the calculation takes 29 minutes. Note that it is a symmetric problem. The cube may be divided in the middle along the x, y-directions. Thus, the calculations are actually performed with $(N_x/2) \cdot (N_y/2) \cdot N_z$ cells.
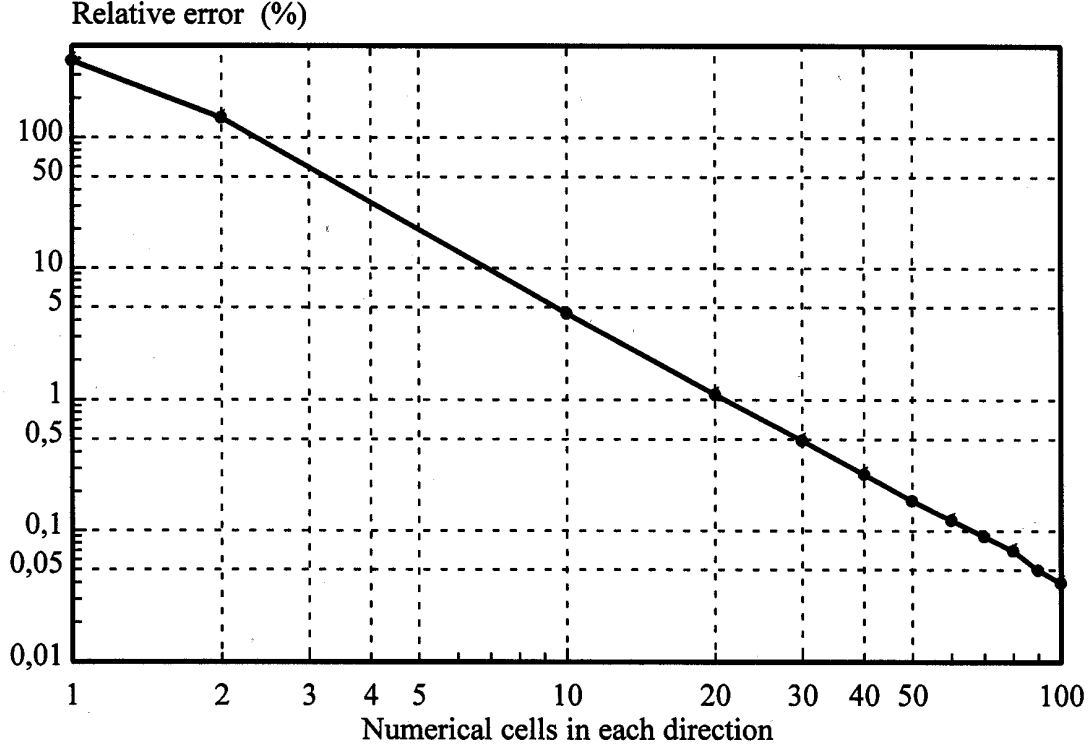
Figure 4.2: The relative error as a function of number of computational cells.

4.2 Improving results by combining simulations

4.2.1 Using two simulations for equidistant meshes

For an equidistant mesh, the finite-difference approximation of $\partial^2 T/\partial x^2$ has a truncation (or discretization) error of magnitude Δx^2 or $1/N_x^2$, see (Kakaç et al, 1985). This is shown in Fig. 4.2, which indicates $\ln(\varepsilon)$ as a function of $\ln(N_x)$ to be a straight line with very good agreement for $N_x \geq 2$. The absolute error can then be written approximately as

$$\varepsilon = \frac{\alpha}{N_x^{\beta}} \tag{4.2}$$

where α is a coefficient independent upon the numerical mesh. The coefficient β is the slope of the curve on a logarithmic scale:

$$\ln(\varepsilon) = \ln(\alpha) - \beta \cdot \ln(N_x) \tag{4.3}$$

Values for $N_x=10$ and $N_x=60$ according to Table 4.1 give

$$\beta = \frac{\ln(4.5) - \ln(0.12)}{\ln(60) - \ln(10)} = 2.023 \tag{4.4}$$

which is very close to 2. Thus, for an *equidistant* mesh β equals 2. The relationship between the error ε for the total number of cells denoted $N=N_x \cdot N_y \cdot N_z$, where $N_x=N_y=N_z$,

can be written as

$$\varepsilon = \frac{\alpha}{N_x^2} = \frac{\alpha}{N^{2/3}} \tag{4.5}$$

The numerically calculated heat flow Q has the error $\varepsilon = (Q - Q^{exact})/Q^{exact}$. This gives with Eq. (4.5):

$$Q = Q^{exact} + \frac{\alpha}{N^{2/3}} \cdot Q^{exact} \quad (W) \tag{4.6}$$

Since $\alpha \cdot Q^{exact}$ is constant, $\alpha' = \alpha \cdot Q^{exact}$ will be used from now on:

$$Q = Q^{exact} + \frac{\alpha'}{N^{2/3}} \quad (W) \tag{4.7}$$

The coefficient α' should be approximately constant, regardless of the number of cells. The two unknown variables Q^{exact} and α' can be calculated using two numerical simulations involving different number of cells N_1 and N_2. Let Q^* denote our estimation of the exact value Q^{exact}. The two flows Q_1 and Q_2 become

$$Q_1 = Q^* + \frac{\alpha'}{N_1^{2/3}} \tag{4.8}$$

$$Q_2 = Q^* + \frac{\alpha'}{N_2^{2/3}} \tag{4.9}$$

Solving for α' gives

$$\alpha' = (Q_1 - Q^*) \cdot N_1^{2/3} = (Q_2 - Q^*) \cdot N_2^{2/3} \tag{4.10}$$

The estimated heat flow Q^* becomes

$$Q^* = \frac{Q_2 \cdot N_2^{2/3} - Q_1 \cdot N_1^{2/3}}{N_2^{2/3} - N_1^{2/3}} \tag{4.11}$$

Consider the problem described in the previous section. The results for three pairs N_1 and N_2 are given in Table 4.2. The second row with $N_1=1000$ and $N_2=8000$ cells, respectively, shows that the error decreases from 1.1% to 0.02%. This error is less than the error obtained from the simulation with 1000000 cells (0.04%), see Table 4.1.

N_1	Q_1 (W)	ε (%)		N_2	Q_2 (W)	ε (%)		Q^* (W)	ε (%)
8	1/6	142	+	1000	0.071889	4.5	→	0.067940	1.3
1000	0.071889	4.5	+	8000	0.069576	1.1	→	0.068805	0.02
8000	0.069576	1.1	+	27000	0.069154	0.49	→	0.068816	0.004

Table 4.2: Estimated heat flows Q^* based on results from two simulations involving different meshes for the cube problem, see Eq. (4.11).

It is clear that combining results according to Eq. (4.11) can increase the accuracy considerably.

Another test is made for the example presented in Section 6.4 (*Rock caverns used for heat storage*). Table 6.8 shows results for different meshes in the two-dimensional case. Equation (4.11) is now used for the two first cases with equidistant meshes containing 48 and 614 cells, respectively. According to Table 4.3, the error is decreased from 10% to 3.9%. Here, the error is relative the heat flow obtained in the case with 15025 cells placed in an expansive mesh, (6.021 W/m).

N_1	Q_1 (W/m)	ε (%)		N_2	Q_2 (W/m)	ε (%)		Q^* (W/m)	ε (%)
48	3.692	39	+	614	5.402	10	→	5.785	3.9

Table 4.3: Estimated heat flows Q^* based on results from two simulations involving different equidistant meshes for the two-dimensional problem presented in Section 6.4.

4.2.2 Using two simulations for expansive meshes

The numerical mesh of a practical heat transfer problem is often irregular. What happens if Eq. (4.11) is used in such a case? Consider the example presented in Section 6.2 entitled *Metal thermal bridges in thermal insulation*, see Table 6.4 (also shown below as Table 4.6). By combining results for 2736 and 11616 cells, the error can be decreased from 1.8% to 0.5%, see Table 4.4. The CPU-time required for these two simulations is about a minute (Pentium/90). A single numerical simulation requires about 60000 cells to give an error of 0.5%. The CPU-time in this case is about 8 minutes.

N_1	Q_1 (W)	ε (%)		N_2	Q_2 (W)	ε (%)		Q^* (W)	ε (%)
128	0.02819	17.6	+	1215	0.03223	5.8	→	0.03339	2.4
1215	0.03223	5.8	+	2736	0.03290	3.8	→	0.03383	1.1
2736	0.03290	3.8	+	11616	0.03360	1.8	→	0.03403	0.5

Table 4.4: Estimated heat flows Q^* for the three-dimensional problem in Section 6.2.

The result for the example presented in Section 6.4 (*Rock caverns used for heat storage*) is as follows. Equation (4.11) is used for the two first cases with expansive meshes containing 48 and 608 cells, respectively, see Table 6.8. According to Table 4.5, the error is decreased from 2.4% to 0.8%.

N_1	Q_1 (W/m)	ε (%)		N_2	Q_2 (W/m)	ε (%)		Q^* (W/m)	ε (%)
48	5.025	17	+	608	5.875	2.4	→	6.067	0.8

Table 4.5: Estimated heat flows Q^* based on results from two simulations involving different expansive meshes for the two-dimensional problem presented in Section 6.4.

Again, combining results according to Eq. (4.11) increases the accuracy considerably.

4.2.3   Using three simulations for arbitrary meshes

As shown in Eq. (4.4), β equals 2 for equidistant meshes. In the case of expansive meshes, β is unknown and Eq. (4.7) is modified to $Q=Q^{exact}+\alpha'/N^{\beta/3}$. The three unknown variables Q^*, α', and β can be calculated by carrying out three numerical simulations with different number of cells N_1, N_2 and N_3:

$$Q_1 = Q^* + \frac{\alpha'}{N_1^{\beta/3}} \tag{4.12}$$

$$Q_2 = Q^* + \frac{\alpha'}{N_2^{\beta/3}} \tag{4.13}$$

$$Q_3 = Q^* + \frac{\alpha'}{N_3^{\beta/3}} \tag{4.14}$$

Subtracting Q_2 from Q_1 gives

$$Q_1 - Q_2 = \alpha' \left(\frac{1}{N_1^{\beta/3}} - \frac{1}{N_2^{\beta/3}} \right) \tag{4.15}$$

and subtracting Q_3 from Q_1 gives

$$Q_1 - Q_3 = \alpha' \left(\frac{1}{N_1^{\beta/3}} - \frac{1}{N_3^{\beta/3}} \right) \tag{4.16}$$

Combining (4.15) and (4.16) gives

$$\frac{Q_1 - Q_2}{Q_1 - Q_3} = \frac{1 - (N_1/N_2)^{\beta/3}}{1 - (N_1/N_3)^{\beta/3}} \tag{4.17}$$

from which β can be obtained from an iterative calculation, using e.g. the Wijngaarden-Dekker-Brent method, (Chapra et al, 1985). Subsequently, α' is given by (4.15) or (4.16).

Let us first test this formula for the cube problem with its *equidistant* mesh. The results for N_1=1000, N_2=8000, and N_3=27000 are, using Eq. (4.17):

$$\frac{0.071889 - 0.069576}{0.071889 - 0.069154} = \frac{1 - (1000/8000)^{\beta/3}}{1 - (1000/27000)^{\beta/3}} \tag{4.18}$$

An iterative calculation gives β=2.025. This is very close to β=2, which is to be expected for an equidistant mesh. Equation (4.15) gives α'=0.325 and Eq. (4.12) gives the estimated value Q^*:

$$Q^* = Q_1 - \frac{\alpha'}{N_1^{\beta/3}} = 0.071889 - \frac{0.325}{1000^{2.025/3}} = 0.068821 \, \text{W} \tag{4.19}$$

which has a relative error of 0.003% compared with the analytically calculated heat flow Q^{exact}=0.0688189, see Eq. (4.1). This error is again smaller than that obtained in the three-dimensional calculation with N=1000000 cells (0.04%), see Tab 4.1.

In order to test Eqs (4.12)-(4.17) in a case with expansive mesh, consider once again the example in Section 6.2 entitled *Metal thermal bridges in thermal insulation*. Table 4.6 shows the flows obtained for different numerical meshes and the required computation time for two PC:s and a workstation from Silicon Graphics. See Section 6.2 for more details.

Number of cells	Q (W)	error	CPU-time 486/33	CPU-time Pentium/90	CPU-time Silicon Graphics
128	0.02819	17.6%	-	2s	-
1215	0.03223	5.8%	-	6s	-
2736	0.03290	3.8%	-	10s	-
11616	0.03360	1.8%	220s	46s	27s
193492	0.03411	0.2%	1h 40m	22m	-
270400	0.03415	0.1%	2h 56m	36m	13m
1000000	0.03421	-	-	5h	1h 50m

Table 4.6: Calculated flows and CPU-time for the problem described in Section 6.2.

The heat flows calculated for N_1=128, N_2=1215, and N_3=2736 give with Eq. (4.17):

$$\frac{0.02819 - 0.03223}{0.02819 - 0.03290} = \frac{1 - (128/1215)^{\beta/3}}{1 - (128/2736)^{\beta/3}} \tag{4.20}$$

This gives β=1.440 which should be compared with 2 for a problem with uniform mesh. Equation (4.15) gives $\alpha' = -0.0628$, and Eq. (4.12) gives the estimated value Q^*:

$$Q^* = Q_1 - \frac{\alpha'}{N_1^{\beta/3}} = 0.02819 - \frac{-0.0628}{128^{1.440/3}} = 0.03431 \, \text{W} \tag{4.21}$$

which has a relative error of 0.3% compared with the case with 1000000 cells (Q=0.03421), see Table 4.6. This should be compared with the results from the three calculations for which the smallest error obtained was 3.8% for N=2736 cells. A single numerical simulation requires 110000 cells for the error to be 0.3%. According to Table 4.6, the three first calculations take less than half a minute, while the calculation with 110000 cells takes 15 minutes on the Pentium. Thus, it takes for this case about 30 times longer time to use a calculation with 110000 cells, than to combine the results for 128, 1215, and 2736 cells, to obtain an error of 0.3%.

4.2.4 Conclusions

Two methods for estimating more accurate heat flows by using the results of two or of three numerical calculations were described. Table 4.2 shows the estimated heat flow for the cube problem, see Section 4.1, with an *equidistant* mesh. Two simulations with N_1=1000 and N_2=8000 cells decreased the error from 1.1% to 0.02%. The computation time for these two simulations is a few seconds. The estimated error is less than the error obtained from a single simulation with 1000000 cells (0.04%), see Table 4.1. The CPU-time for this simulation is half an hour.

Consider the example in Section 6.2 entitled *Metal thermal bridges in thermal insulation*. This is a problem with a quite irregular mesh (*expansive*). The error was lowered from 3.8% to 0.3% by combining results from three calculations with 128, 1215, and 2736 cells, respectively. These three calculations take less than half a minute. A single numerical simulation requires 110000 cells to give an error of 0.3%. This calculation will take about 15 minutes. The method of combining results from two calculations with 1215 and 2736 cells lowered the error from 3.8% to 1.1%.

The number of cells required to obtain satisfactory numerical accuracy depends on various parameters such as geometry and materials. The following criterion is recommended as a European standard (CEN, 1995). The sum of the absolute values of all the heat flows entering the object is calculated twice, once for n cells and once for $2n$ cells. The relative difference between the flows must be smaller than 2%. If not, further mesh division is required. At least two numerical calculations are needed to check the above criterion. It is therefore simple to use one of the methods described above using two or three simulations to obtain more accurate heat flows for problems that are analyzed in two or three dimensions.

Estimations of more accurate temperatures can be done in the same way as with heat flows by substituting the heat flows in the equations with temperatures.

4.3   Successive over-relaxation

4.3.1   Introduction

Different numerical techniques can be used to decrease the CPU-time. One example is the successive over-relaxation method (Hirsch, 1992) for steady-state analyses, see Section 3.2.3. It is shown below that the CPU-time may be decreased significantly when this technique is used.

4.3.2   Optimized over-relaxation coefficient

Consider the five heat conduction problems in three dimensions in Sections 6.2, 6.4, 6.8, 6.9, and 6.10. Table 4.7 shows the calculation time in minutes on a Pentium/90 as a function of the relaxation coefficient ω. The number of computational cells and the stop criterion δ, see Eq. (6.1) in Section 6.2.4, are also shown.

The minimum CPU-time is underlined in the table. As shown, the method of over-relaxation is very efficient. An optimized ω gives calculation times between 1/50th and 1/10th of that required for a calculation not using over-relaxation (ω=1.0). Consider the example in Section 6.9 (*Heat flow through a corner*). The optimized ω in the case with 7600 cells is 1.85 (0.37 minutes). In the case with 246000 cells, the optimized ω is 1.95 (13 minutes). Using 721000 cells (not shown in the table), the optimized ω becomes 1.96 (44 minutes). If the optimized value of ω is unknown, the recommended value to use is 1.95. This is the default value in the programs.

ω	Metal U-girders Section 6.2 $N=11616$ $\delta=1\cdot10^{-5}$	Slotted steel Section 6.8 $N=28560$ $\delta=1\cdot10^{-5}$	Corner Section 6.9 $N=246000$ $\delta=1\cdot10^{-5}$	Corner Section 6.9 $N=7600$ $\delta=1\cdot10^{-5}$	Slab Section 6.10 $N=25221$ $\delta=1\cdot10^{-4}$	Cavern Section 6.4 $N=15968$ $\delta=1\cdot10^{-4}$
1.00	24 min.	59 min.	596 min.	4.2 min.	78 min.	33 min.
1.50	24	57	192	1.4	78	12
1.55	24	46	164	1.2	78	11
1.60	14	37	139	1.1	78	9.7
1.65	11	31	118	0.88	78	8.5
1.70	9.5	27	97	0.73	38	7.4
1.75	7.4	22	79	0.58	28	6.4
1.80	5.7	19	60	0.40	22	5.4
1.85	4.2	15	44	_0.37_	16	4.5
1.90	2.6	13	27	0.52	11	3.6
1.91	2.3	12	24	0.53	10	3.4
1.92	2.1	11	20	0.57	8.9	3.2
1.93	1.8	11	15	0.63	7.9	3.1
1.94	1.5	10	13	0.70	6.9	2.9
1.95	1.2	10	_13_	0.80	5.9	2.7
1.96	0.88	9.2	17	1.0	4.9	2.6
1.97	_0.82_	8.7	21	1.3	3.9	2.4
1.98	1.0	8.2	29	1.7	_2.6_	2.3
1.99	1.6	7.6	50	3.2	3.4	2.1
2.00	1.6	_6.5_	507	33	27	_1.8_

Table 4.7: CPU-time in minutes as a function of the over-relaxation coefficient.

4.3.3 Conclusions

It has been shown that the successive over-relaxation method is simple to use and that it is very efficient. The optimized ω lies typically in the range 1.8-2. In HEAT2, HEAT2R, and HEAT3, this factor is initially set to 1.95.

4.4 Subdivision

There is an option in HEAT3 for letting the mesh be automatically gradually refined. Figure 4.3 shows the principle of subdivision, involving the mesh being refined twice in two dimensions. In the first calculation, the computational area has only one computational cell. The calculated temperature T_A for this cell becomes stable after a few iterations. At this point a new numerical mesh is generated with 2·2 cells, all with the initial temperature T_A. The conductances are calculated according to Section 3.1.2. A new iteration is performed, and the steady-state temperatures in these cells are denoted by T_B, T_C, T_D, and T_E. A more refined grid is generated containing 4·4 cells with these temperatures. Thus, in the refinement each cell is divided into four new cells. In three dimensions, each

cell is divided into eight new cells.
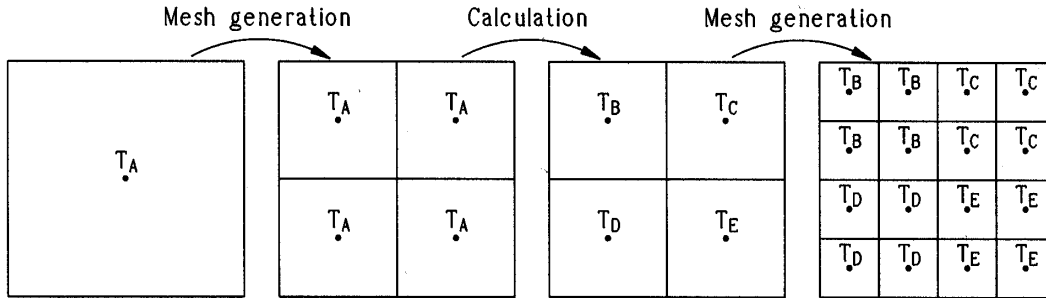
Figure 4.3: Principle of subdivision.

The following study shows the rate of convergence, with and without subdivision, for a particular case. Consider the cube in Fig. 4.1 having a temperature of $T=1$ on the upper side $z=L_z$ and of $T=0$ on the other five sides. Using the option for subdivision, the computation starts with one cell. The following levels are then simulated with $2 \cdot 2 \cdot 2$, $4 \cdot 4 \cdot 4$, $8 \cdot 8 \cdot 8$, $16 \cdot 16 \cdot 16$, and $32 \cdot 32 \cdot 32$ cells. The final mesh for the symmetric problem is specified in advance to contain $32 \cdot 32 \cdot 64$ (65536) computational cells. The criterion for when to stop the calculation for the final mesh is when $\delta=1 \cdot 10^{-4}$, see Sec. 6.2.4. The criterion for changing to a level with a finer mesh is the same. Figure 4.4 and Table 4.8 show the results from simulations with various relaxation coefficients, with and without subdivision. The minimum CPU-time (underlined in the table) is 0.92 minutes when subdivision is used, and 2.1 minutes without subdivision. This means that it takes more than twice as long if subdivision is not used, for optimum relaxation coefficients.

Figure 4.4: CPU-time in minutes with and without subdivision for the cube problem.

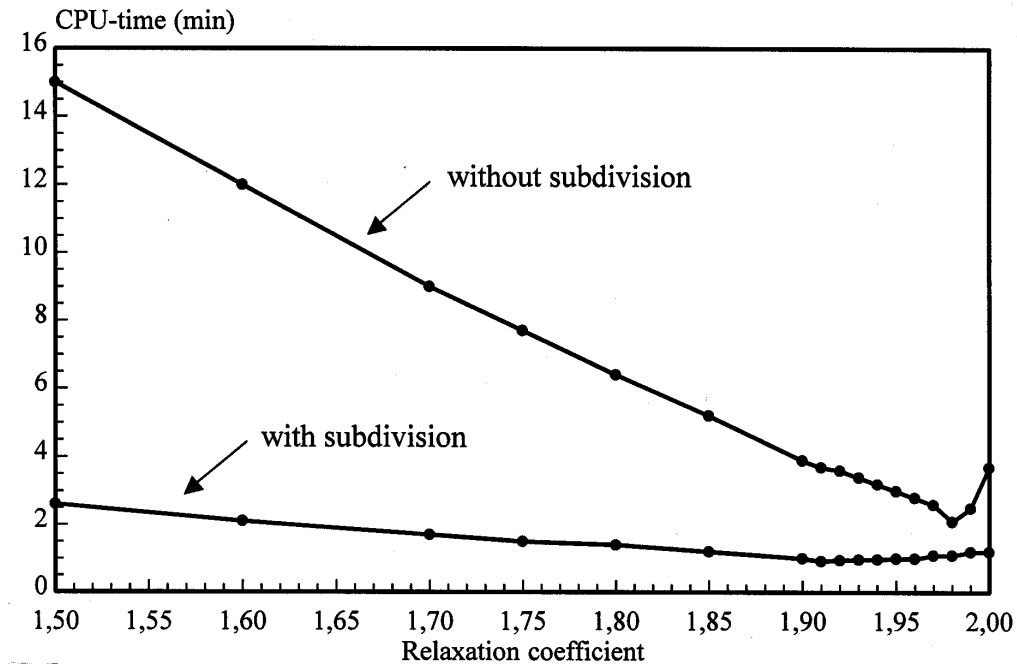| ω	without subdivision	with subdivision
1.00	42 min.	6.3 min.
1.50	15	2.6
1.60	12	2.1
1.70	9	1.7
1.75	7.7	1.5
1.80	6.4	1.4
1.85	5.2	1.2
1.90	3.9	1.0
1.91	3.8	*0.92*
1.92	3.6	0.95
1.93	3.4	0.97
1.94	3.2	0.98
1.95	3.0	1.0
1.96	2.8	1.0
1.97	2.6	1.1
1.98	*2.1*	1.1
1.99	2.5	1.2
2.0	3.7	1.2

Table 4.8: CPU-time in minutes with and without subdivision for the cube.

For a given problem, the optimized ω is often unknown. A good guess of the relaxation coefficient in a problem might be one close to the optimized ω. The choice of an optimized ω is less important in the case with subdivision.

In the example above, the initial temperature was put to zero. Guessing initial temperatures close to the steady-state temperatures in cases without subdivision will give decreased CPU-time. However, when ω approaches the optimum over-relaxation coefficient the gain becomes smaller and the guessed initial temperatures less important. The initial temperature is of no importance when subdivision is used, since the average temperature is quickly calculated for a small number of cells.

The more complex example presented in Section 6.9 (*Heat flow through a corner*) with a quite irregular mesh, has also been studied. For an optimized ω, the CPU-time is 32 seconds with subdivision, and 22 seconds without subdivision on a Pentium/90 ($\delta = 1 \cdot 10^{-5}$). Actually, for all ω between 1.0 and 2.0, using subdivision turned out to be between 10% and 50% slower.

4.4.1   Conclusions

It is clear that the method of subdivision does decrease the CPU-time in some cases. The cube that was considered in the example was well adapted to being subdivided due to its simple geometric structure. The CPU-time was decreased to half for optimum relaxation coefficients. In more complex cases, the gain in CPU-time will be smaller or none. A great deal of effort is required to handle the mesh generation into finer grids. Subdivision is probably of minor importance for practical purposes.

4.5   Circular disc with transverse heat loss

Consider a circular disc with transverse heat loss. The height of the disc is H, and there is a transverse loss upwards and downwards with a heat transfer coefficient α_0, (W/(m²K)). See Fig. 4.5.
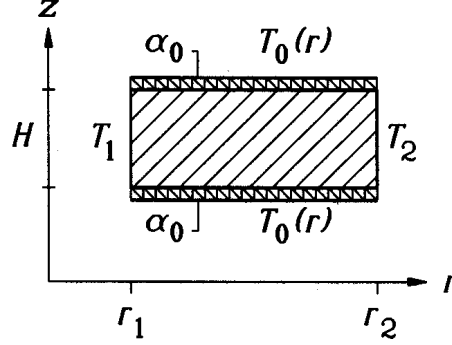

Figure 4.5: Circular disc with transverse heat loss.

The heat balance equation involving the radial heat flow $Q(r)$, (W), becomes:

$$-\frac{d}{dr}\left[Q(r)\right] + 2 \cdot 2\pi r \cdot \alpha_0 (T_0 - T) = 0 \tag{4.22}$$

or

$$\frac{d}{dr}\left(2\pi\lambda H r \frac{dT}{dr}\right) = 4\pi\alpha_0 r (T - T_0) \tag{4.23}$$

In the case of constant coefficients we have, (Claesson et al, 1994):

$$\frac{1}{r}\frac{d}{dr}\left(r\frac{dT}{dr}\right) = \frac{1}{\ell^2}(T - T_0) \tag{4.24}$$

The characteristic length ℓ (m) is defined by

$$\ell = \sqrt{\frac{H\lambda}{2\alpha_0}} \tag{4.25}$$

With the substitution $T(r) = T_0 + f(r')$, $r' = r/\ell$, we get the equation

$$\frac{d^2 f}{d(r')^2} + \frac{1}{r'} \cdot \frac{df}{dr'} - f(r') = 0 \tag{4.26}$$

The solutions are modified Bessel functions of order zero:

$$f(r') = \beta_1 \cdot I_0(r') + \beta_2 \cdot K_0(r') \tag{4.27}$$

The constants β_1 and β_2 are determined by the boundary temperatures T_1 and T_2. The solution becomes

$$T(r) - T_0 = (T_1 - T_0)\frac{K_0(r_2/\ell)I_0(r/\ell) - I_0(r_2/\ell)K_0(r/\ell)}{K_0(r_2/\ell)I_0(r_1/\ell) - I_0(r_2/\ell)K_0(r_1/\ell)} +$$

$$+(T_2 - T_0)\frac{K_0(r_1/\ell)I_0(r/\ell) - I_0(r_1/\ell)K_0(r/\ell)}{K_0(r_1/\ell)I_0(r_2/\ell) - I_0(r_1/\ell)K_0(r_2/\ell)} \tag{4.28}$$

Numerical calculations have been made for the following data:

$$
\begin{array}{ll}
\lambda=1 & H=2 \\
r_1=0.1 & r_2=1.1 \\
T_1=0 & T_2=1 \\
T_0=0 & \alpha_0=1
\end{array}
$$

This gives $\ell=1$. The analytical solution for $r=0.6$ becomes

$$T(0.6) - 0 = 0 \cdot \frac{K_0(r_2/\ell)I_0(r/\ell) - I_0(r_2/\ell)K_0(r/\ell)}{K_0(r_2/\ell)I_0(r_1/\ell) - I_0(r_2/\ell)K_0(r_1/\ell)} +$$

$$+(1 - 0)\frac{2.4271 \cdot 1.0920 - 1.0025 \cdot 0.7775}{2.4271 \cdot 1.3262 - 1.0025 \cdot 0.3656} = 0.65594 \tag{4.29}$$

Table 4.9 shows the calculated temperatures $T(r=0.6)$ and the relative error ε compared with the analytical solution as a function of numerical cells in the r-direction. The relative error becomes 0.13% using 9 cells.

Number of cells	calculated value	ε (%)
1	0.58755	10.4
3	0.64772	1.25
5	0.65299	0.45
7	0.65446	0.23
9	0.65506	0.13
11	0.65537	0.09
21	0.65582	0.02
31	0.65591	0.005
41	0.65594	0

Table 4.9: Calculated temperatures and relative errors.

4.6   Plane radial case

Consider a *plane, radial* case, where the temperature $T(r)$ depends on the radial distance r. Figure 4.6 shows an annulus $r_1 \leq r \leq r_2$. The temperature on the inner circle is T_1 and on the outer one T_2.
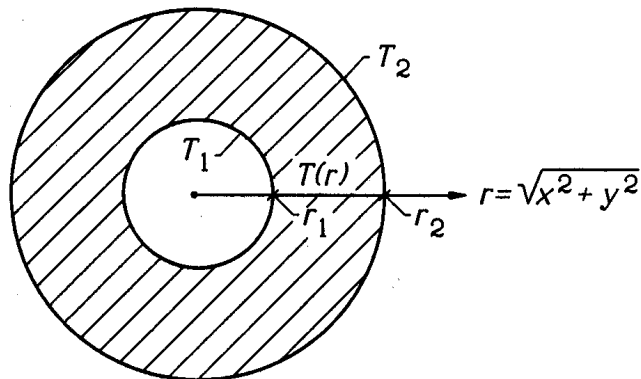

Figure 4.6: Radial heat flow in an annulus.

We consider a height H perpendicular to the (x, y)-plane. The cylindrical area becomes $2\pi r H$. The total radial heat flow $Q(r)$ becomes

$$Q(r) = -\lambda \cdot 2\pi r H \cdot \frac{dT}{dr} \quad \text{(W)} \tag{4.30}$$

In the basic case of constant λ and no further complications, the heat flow Q is independent of r. The temperature becomes by integration of $1/r$

$$T(r) = T_1 + (T_2 - T_1) \cdot \frac{\ln(r/r_1)}{\ln(r_2/r_1)} \qquad r_1 \leq r \leq r_2 \tag{4.31}$$

The heat flow is

$$Q = \frac{2\pi\lambda H}{\ln(r_2/r_1)} \cdot (T_1 - T_2) \tag{4.32}$$

This means that the thermal conductance of the annulus is:

$$K_{\text{annulus}} = \frac{2\pi\lambda H}{\ln(r_2/r_1)} \tag{4.33}$$

The thermal resistance is the inverse:

$$R_{\text{annulus}} = \frac{1}{2\pi\lambda H} \cdot \ln\left(\frac{r_2}{r_1}\right) \tag{4.34}$$

Numerical calculations have been made for the following data:

$$\begin{array}{ll} \lambda=1 & H=1 \\ r_1=0.1 & r_2=1.1 \end{array}$$

$$T_1=0 \qquad\qquad T_2=1$$

The calculated heat flow becomes 2.620292. The same result is obtained from Eq. (4.32). The temperature at the distance $r=0.6$ becomes $T(r=0.6)=0.74722$, which is the same as the analytically calculated temperature using Eq. (4.31). These exact results are due to the fact that we use exact logarithmic resistances for the radial flow, see Eq. (4.34). This is only a test that the computer program is without errors.

4.7   Conclusions

A few numerical studies are reported. One study involves accuracy considerations for different computational meshes. Generally, the smaller the computational cells are, the better is the agreement with the "true" temperature distribution. The accuracy using an expansive mesh is often considerably higher than that using an equidistant mesh with the same number of cells.

Different numerical techniques can be used to decrease CPU-time. It has been shown that the successive over-relaxation method in the steady-state case is simple to use and that it is very efficient. An optimized over-relaxation coefficient ω may give calculation times between 1/50th and 1/10th of that required for a calculation not using over-relaxation ($\omega=1.0$). The optimized ω lies typically in the range 1.8-2.

Another technique is the method of subdivision, which means that the mesh is gradually refined. The analyses show that this method decreases CPU-time in some cases. However, if one succeeds in finding an optimized relaxation factor ω, either by use of analytical equations or by numerical tests, subdivision should be of minor importance.

Results from two or three calculations using different meshes may be used to estimate more accurate results. Consider the example in Section 6.2 entitled *Metal thermal bridges in thermal insulation*. This is a problem in three dimensions with a quite irregular mesh. The error was lowered from 3.8% to 0.3% by combining results from three calculations with 128, 1215, and 2736 cells, respectively. These three calculations take together less than half a minute. A single numerical simulation requires 110000 cells to give an error of 0.3%. This calculation will take about 15 minutes. The method of combining results from two calculations with 1215 and 2736 cells lowered the error from 3.8% to 1.1%. The gain using this technique can be quite substantial.

Chapter 5

Description of computer programs

5.1   HEAT2 - Two-dimensional heat conduction

HEAT2 (Blomberg, 1990, 1991) is a PC-program for two-dimensional transient and steady-state heat conduction within objects that can be described in a rectangular grid. It belongs to the latest generation of computer models from the *Lund Group for Computational Building Physics*, and is based on 25 years of experience. It is well adapted to the following applications within building physics:

> *Analysis of thermal bridges*
> *Calculation of U-values for building construction parts*
> *Estimation of surface temperatures used e.g. for surface condensation risks*
> *Calculation of heat losses to the ground from a house*
> *Optimization of insulation fitting*
> *Analysis of floor heating systems*

Great efforts have been made to develop a user-friendly interface. Input data is given via an integrated menu system. The user works with an input mesh that facilitates and minimizes the input procedure. The time to generate the complete input for a reasonably complicated case, after a few hours' experience of the program, is less than 10 minutes. It is possible to enlarge various graphical pictures to show details of, for example, the computational mesh or the isotherms.

Arbitrary thermal properties and initial temperatures can be specified. Boundary conditions can vary over time as being periodic, step-wise constant, or step-wise linear. HEAT2 can handle such internal modifications as heat sources, internal boundaries of prescribed temperature, and internal regions containing air or fluid of a given temperature. Internal resistances can be specified at cell interfaces.

HEAT2 solves the heat conduction equation by the method of explicit finite differences, as described in Chapter 3. The computational mesh is chosen by the user, and the stable time-step is calculated automatically. In the steady-state case, fast computation is achieved by over-relaxation. The time required to solve a reasonably complicated steady-state problem with 10000 computational nodes is usually less than a minute.

There is support for hard copy printing. The user may print isotherms, temperature field, and numerical mesh. It is possible to export output data files from HEAT2 to MATLAB (MathWorks Inc., 1992) where different plots such as isotherm plots and surface plots may be drawn.

Newer versions of HEAT2 may account for thermal radiation in cavities, see Chapter 7. Figure 5.1 shows calculated isotherms for a window frame with 20 cavities. See also the figures on the back cover. This calculation took a few minutes on a PC.
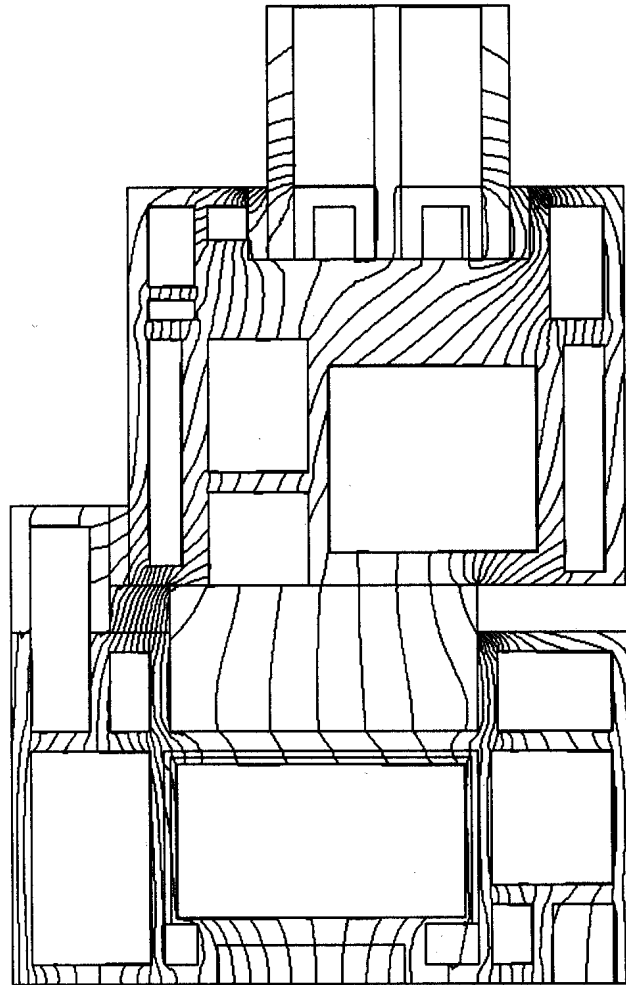
Figure 5.1: Calculated isotherms for a window frame with radiation inside 20 cavities.

5.2   HEAT2W - Preprocessor to HEAT2

HEAT2W (Blomberg, 1994b) is a drawing program that makes it simple to describe a large range of heat transfer problems. The user builds up the geometry by using rectangles of different materials. The rectangles may overlap each other. Figures 5.2 and 5.3 show the input of a slab on the ground, and the numerical mesh, respectively.
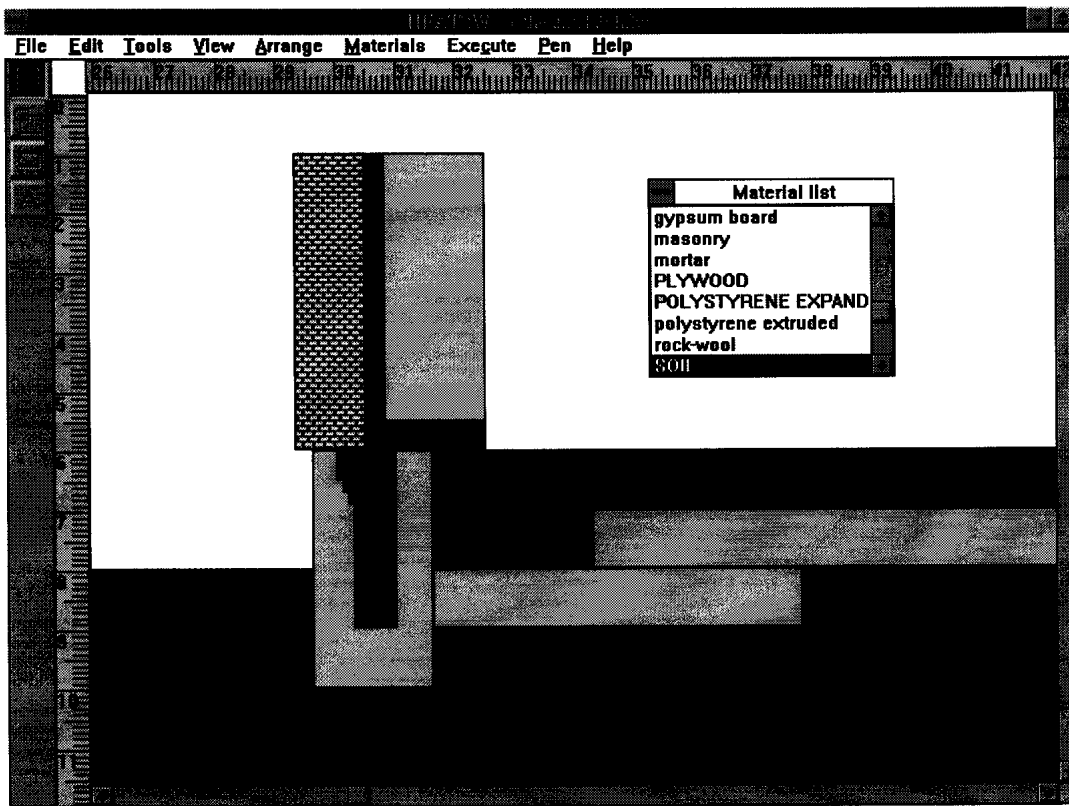
Figure 5.2: A screen-view of the program HEAT2W showing a slab on the ground.
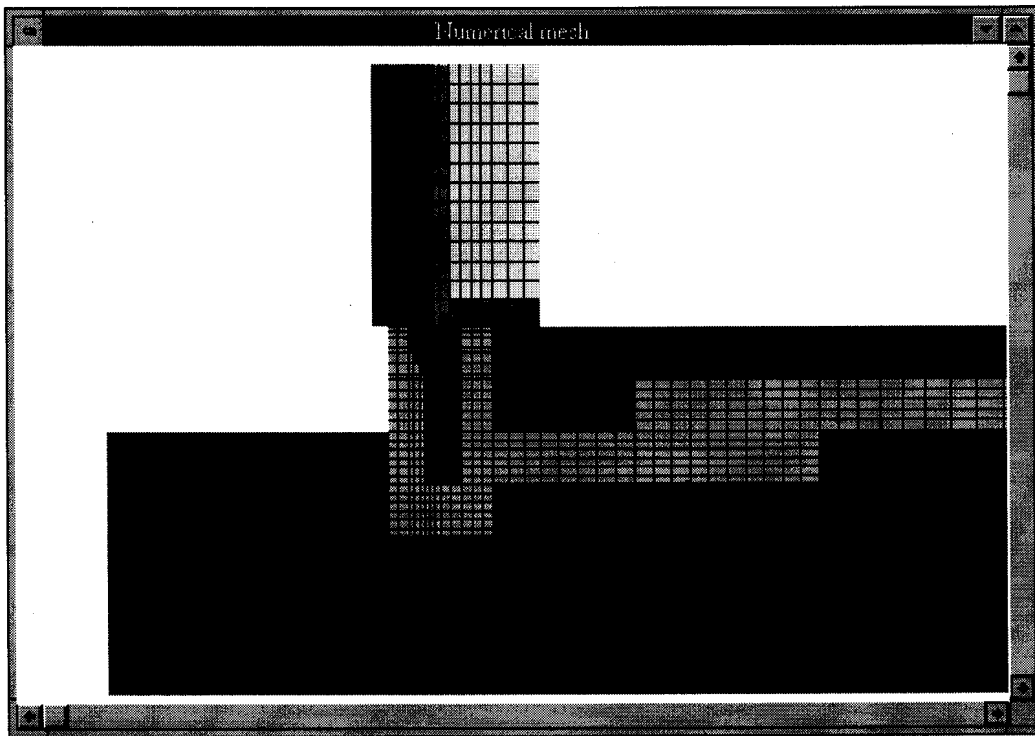

Figure 5.3: Part of the numerical mesh for a slab on the ground.

The current version of HEAT2W serves as a preprocessor to the DOS-version HEAT2.

A generated input file is read into HEAT2 where boundary conditions have to be specified before the problem can be simulated. The numerical mesh is automatically generated, but can easily be changed.

HEAT2W provides many advantages being a program under the Microsoft Windows environment, such as exporting (or importing) objects (e.g. pictures or text) via the clipboard to other programs for drawing or editing. It is also possible to scan a building design drawing and import it via the clipboard into HEAT2W. The actual heat transfer problem could easily be described just by drawing rectangles "on" the imported design drawing.

5.3   HEAT3 - Three-dimensional heat conduction

HEAT3 (Blomberg, 1993a, 1994a) is a computer program for three-dimensional transient and steady-state heat conduction. The heat equation is solved with explicit forward finite differences. The successive over-relaxation technique is used in the steady-state case.

The program can be used for analyses of thermal bridges, heat transfer through corners of a window, heat loss from a house to the ground, to mention but a few applications. One important restriction is that the problem has to be described in a parallelepipedical mesh, i.e. all boundary surfaces are parallel to one of the Cartesian coordinate planes. For a reasonably complicated case, 10-15 minutes work is sufficient for an experienced user to describe the geometry, the numerical mesh, and the boundary conditions. The steady-state problem shown on the front cover took less than a minute to solve on a Pentium/90.

The output temperature field can be imported into MATLAB (MathWorks Inc., 1992). This program has powerful options concerning plots in two and three dimensions. The front cover figure shows the surface temperatures for a corner, see Section 6.9. The temperatures are calculated by HEAT3 and displayed using MATLAB.

There are many similarities between HEAT2 and HEAT3. These two programs are based on the same numerical method, they automatically calculate the maximum stable time-step, and they use the successive over-relaxation technique for the steady-state case, to mention but a few of the similarities. Both of them use an *input mesh* to describe the geometry, the numerical mesh, and the boundary conditions.

One example of an application is a wall with thermal insulation and with cross-laid steel girders. The ratio of the thermal conductivity between the steel and the insulation material is about 1700. With 270000 computational cells, the calculations took 36 minutes on an Intel Pentium/90, and 13 minutes on a Silicon Graphics workstation (the Crimson model). With 1000000 computational cells, the calculations took 5 hours on the Pentium, and less than 2 hours on the Crimson. This example is discussed further in Section 6.2 (*Metal thermal bridges in thermal insulation*).

The used compiler MicroWay NDP Pascal (MicroWay, 1991) produces optimized 32-bit

protected mode code. This gives high calculation speed and allows for memory allocation for large three-dimensional problems. The maximum number of computational cells depends on the amount of memory available (extended or expanded RAM), see Table 5.1. Up to one million numerical cells may be used on a PC with 32 Mb RAM. About 420000 cells can be addressed with 16 Mb, and 64000 with 4 Mb. Versions for other memory configurations are available upon request.

PC memory configuration	number of maximum computational cells	required memory (RAM) (extended or expanded)
4 Mb RAM	40·40·40=64000	2.4 Mb RAM
6 Mb RAM	50·50·50=125000	4.0 Mb RAM
16 Mb RAM	75·75·75=421875	12.5 Mb RAM
32 Mb RAM	100·100·100=1000000	31 Mb RAM

Table 5.1: Versions of HEAT3 and maximum number of computational cells.

H3VIEW is a separate program that allows the user to check the input data for HEAT3. The program reads the input data file and draws the problem in a three-dimensional perspective. Details of particular interest may be enlarged or rotated in space.

5.4 HEAT2R - Heat conduction in cylindrical coordinates r and z.

HEAT2R (Blomberg, 1994c) is a computer program for transient and steady-state heat conduction in cylindrical coordinates r and z. It may be used for problems that can be described in a mesh where the boundaries follow the coordinates r and z. The heat equation is solved using explicit forward finite differences.

There are many similarities between HEAT2 and HEAT2R. These two programs are based on the same numerical method, they automatically calculate the maximum stable time-step, and they use the successive over-relaxation technique for the steady-state case, to mention but a few of the similarities. Both use an *input mesh* to describe geometry, numerical mesh, and boundary conditions. Internal resistances may be specified at cell interfaces.

5.5 TR2 - Calculation of thermal response factors

Thermal response factors may be used to calculate heat flows through the components of a building in order to be able to design for the heating or cooling load. Each component, such as a wall, roof, window, etc., has a heat capacity that affects the heat flows. The thermal response factor method is a relatively quick and simple way to calculate the transient flows through the external and internal surfaces.

The thermal response factor method was introduced by G.P. Mitalas and D.G. Stephenson about 25 years ago (Stephenson et al, 1967a, 1967b, 1971). Computers made it easy to

evaluate transient heat flow through one-dimensional building components such as walls, roofs and the like. This method is widely used by the American Society of Heating, Refrigeration, and Airconditioning Engineers, Inc. (ASHRAE).

TR2 (Blomberg, 1992) is a PC-program for calculation of surface heat flows in one and two dimensions for building components under transient conditions according to the thermal response factor method. The program was developed in collaboration with Prof. Lorenzo Agnoletto, Istituto di Fisica Tecnica di Udine, and Dott. Piercarlo Romagnoni, Istituto di Fisica Tecnica di Padova, Italy. A paper was presented at the conference *CLIMA 2000* in London (Agnoletto, 1993). One application for thermal response factors is described in Section 6.7 (*Temperature and moisture conditions in attics*).

TR2 uses the numerical technique described in Chapter 3 to calculate the response factors for a given triangular, or step-wise constant, unit step. The procedure in TR2 may be summarized in two steps:

1. Calculation of conduction thermal response factors in one and two dimensions.

2. Calculation of heat flows, due to internal and external temperature excitations, through the surfaces of the component considered, using the calculated response factors.

Chapter 6

Studies of particular heat conduction problems

6.1 Introduction

The following studies deal with quite different topics to show the versatility of the developed computer programs. The examples are also chosen with the intent to illustrate how to deal with various problems that arise in numerical simulation of heat conduction processes. A major concern has been how to choose the numerical mesh and how to assess the accuracy. Most of the examples have been published earlier nearly in the same version. The following is a brief introduction to each example.

6.1.1 Metal thermal bridges in thermal insulation

This paper presents a calculation in three dimensions for a wall with cross-laid U-girders of steel. A few recipes on how to choose an appropriate mesh are given. Up to 1000000 nodal points are used. The paper was presented at the 3rd conference on *Building Physics in the Nordic Countries* in Copenhagen in 1993, (Blomberg, 1993b). See page 47.

6.1.2 Glass-encapsulated evacuated powder panels

This paper involves simulations in three dimensions for the heat transmitted through a "wall" containing glass-encapsulated evacuated panels placed in foam. The work was done in collaboration with Prof. Leon R. Glicksman, Depts of Building Technology and Mechanical Engineering, Massachusetts Institute of Technology, Cambridge, USA. See page 55.

6.1.3 Rock caverns used for heat storage

Rock caverns could be used for heat storage. This is exemplified by the underground storage in Skarvik, Sweden (Claesson et al, 1989a). These caverns, used earlier as oil depots, could be filled with water and used as a heat store. The heat loss from one such cavity is examined here. Of particular interest is the accuracy obtained for different equidistant and expansive numerical meshes using calculations in two and three dimensions. See page 61.

6.1.4 Thermal shielding of rock caverns

When liquid natural gas, LNG, is stored in a rock cavern, proper insulation to protect the surrounding rock against the cold medium is needed. The paper (Claesson et al, 1989b) presents results from calculations in two dimensions with HEAT2 where heating pipes are modelled as internal heat sources. The results are based on the principle of superposition. This report was carried out in cooperation with Johan Claesson, Lund Group for Ground Heat. See page 71.

6.1.5 U-value for a window accounting for the wall

When a window is mounted in a wall, additional heat losses occur due to thermal bridge effects around the window. Numerical calculations in two dimensions were carried out to estimate this effect. This work was initiated by Prof. F. de Ponte, Istituto di Fisica Tecnica di Padova, Italy. The paper was presented at the 3rd conference on *Building Physics in the Nordic Countries* in Copenhagen in 1993, (Blomberg, 1993c). See page 81.

6.1.6 Temperature and moisture conditions in attics

Calculations for temperature and moisture conditions in different kinds of attics are compared with experimental data in this study. The program TR2 has been used to calculate thermal response factors, see Section 5.5, for different types of roofs. This study was made in collaboration with Dr. Ingemar Samuelsson, Swedish National Testing and Research Institute, and presented at the 3rd conference on *Building Physics in the Nordic Countries* in Copenhagen in 1993, (Blomberg et al, 1993d). See page 89.

6.1.7 Insulated wall with slotted steel U-girders

An insulated wall can be supported internally by thin steel girders. Calculation of the heat transmittance is a difficult numerical problem due to the high ratio of thermal conductivity between the insulation and the steel. The study presents results of calculations in three dimensions. The proper choice of the numerical mesh is discussed. The dependence of the U-value on a number of different parameters is dealt with. This paper was presented at *Stålbyggnadsdagen 1995*, see (Blomberg, 1995b). See page 103.

6.1.8 Heat flow through a corner

This example deals with heat flow through a corner. This three-dimensional heat conduction problem is a test reference case in the European standards (CEN, 1995). Heat flows and surface temperatures are given for different numerical meshes. See page 113.

6.1.9 Slab on the ground

This example concerns a slab on the ground. A three-dimensional simulation of the heat loss to the ground is shown. A few calculation recipes are given. See page 119.

6.1.10 House with a floor heating system

This section deals with houses partially heated by a floor heating system. Formulas are given for the heat loss to the ground and for the effective U-value for the floor. The more of the total heating demand that is supplied by the floor heating system, the more does the heat loss to the ground (and the effective U-value for the floor) increase. See page 125.

6.1.11 Construction block filled with insulation

This study presents calculations in three dimensions of the heat flow through a wall built by construction blocks filled with insulation. The proper choice of the numerical mesh is discussed. The dependence of the obtained U-value on a few parameters is dealt with. A few parametric variations are made. See page 135.

6.1.12 Heat flow through a wall with metal studs

Heat conduction in constructions with both insulation and metal parts often causes particular computational problems because of the wide difference in thermal conductivities. The ratio of the maximum and minimum thermal conductivity is almost 8000 in this example. This is a test reference case in the European standards (CEN, 1995) for heat conduction in two dimensions. Heat flows and temperatures are given for different numerical meshes. See page 143.

6.2 Metal thermal bridges in thermal insulation

6.2.1 Introduction

Girders and crossbars of steel or aluminium may be used to support the thermal insulation in walls. The thin metal parts create thermal bridges, since the thermal conductivity of the metal may be several thousand times higher than that of the insulation material. This results in particular problems for the numerical calculations of the heat flow processes involved.

This paper presents an analysis of these numerical complications. A few recipes on how to choose an appropriate mesh are given. Up to 1000000 nodal points are used. It is shown that genuinely three-dimensional numerical calculations must be used in order to calculate a proper U-value. A wall with cross-laid girders is shown in Fig. 6.1. The thermal conductivity of the steel is about 1700 times greater than that of the insulation material.

Three computers were used for the numerical calculations. The first two are ordinary PC:s with Intel 486/33 and Pentium/90 processors, respectively. The third is a Silicon Graphics workstation (the Crimson model). The three-dimensional program HEAT3 (Blomberg, 1993a, 1994a) has been used. The code was optimized for high calculation speed for all computers. In the PC case, a compiler (MicroWay, 1991) that produces 32-bit code was used. It may be mentioned that the Silicon Graphics computer was about 3 times faster than the Pentium. The help from Anders Follin and Peter Jonsson, Dept. of Geotechnology, Lund University, for their assistance with the Crimson Computer is gratefully acknowledge.

6.2.2 Wall with crossed U-girders

Figure 6.1 shows a sketch of the wall. The wall is build by two gypsum wallboards, mineral wool, and two crossed U-girders. The U-girders are separated by a distance of 300 mm. This distance was given as a prerequisite when this study was commissioned. A more practical center-to-center distance is 0.6 m. This is discussed later. Other dimensions (mm) are shown in the figure.

The calculations are made for a unit temperature difference. The air temperature is put to 1 °C on one side of the wall and 0 °C on the other side. The indoor and outdoor surface resistances are 0.13 and 0.04 m²K/W, respectively. Table 6.1 shows the thermal conductivity λ, (W/(m·K)), of the materials.

material	λ (W/(m·K))
insulation	0.036
steel	60
gypsum	0.22

Table 6.1: Thermal conductivities used in the calculations.
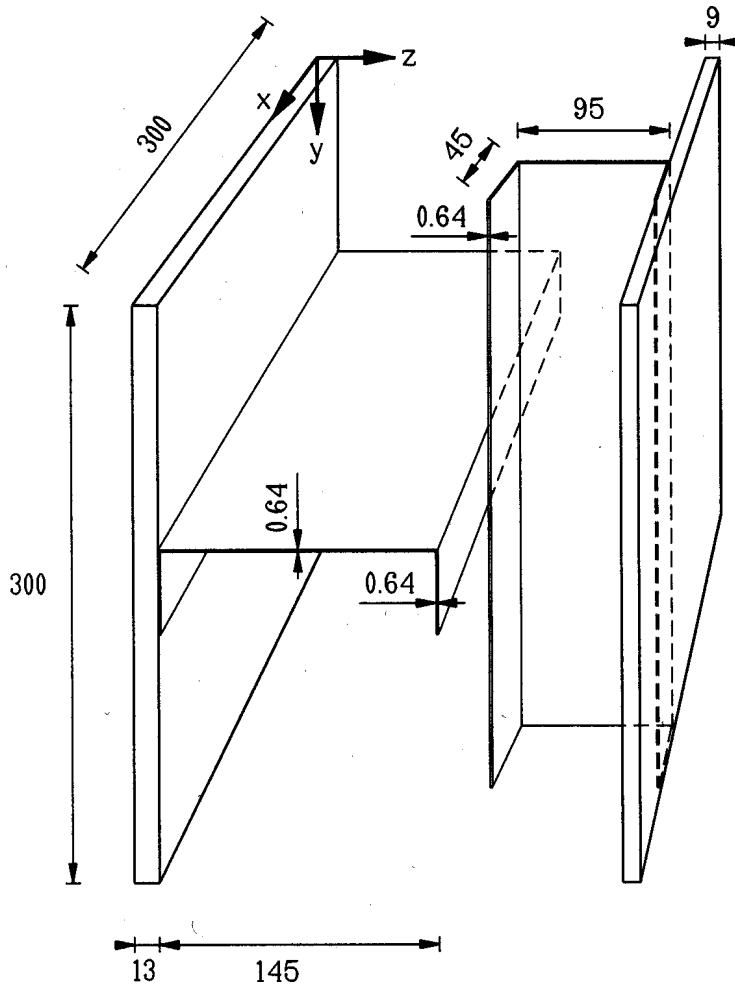
Figure 6.1: Schematic figure of a wall with cross-laid U-girders.

The part of the wall that is cut out is considered to be representative of the whole wall, even though there is no perfect symmetry. The boundaries of the other four sides through the wall (the boundary areas in the (x, z)- and (y, z)-planes in Fig. 6.1) are adiabatic.

6.2.3   Computational mesh

A number of segments is specified for each direction in order to define the problem and generate the computational mesh. For the wall considered there are four segments in the x-direction, four in the y-direction, and eight in the z-direction, see Figs 6.2 and 6.3. The computational mesh is shown for the case with 11616 computational cells, see Table 6.3.

The length of each segment is given in Table 6.2. Due to symmetry, the data for the y-direction are the same as that for the x-direction. The total number of computational cells is generated by specifying the number of cells in the segments in each of the three directions. An expansive mesh is used. An expansion coefficient ξ is given for each input segment in each direction. The lengths of the computational cells in the segment increase or decrease by this factor.

48
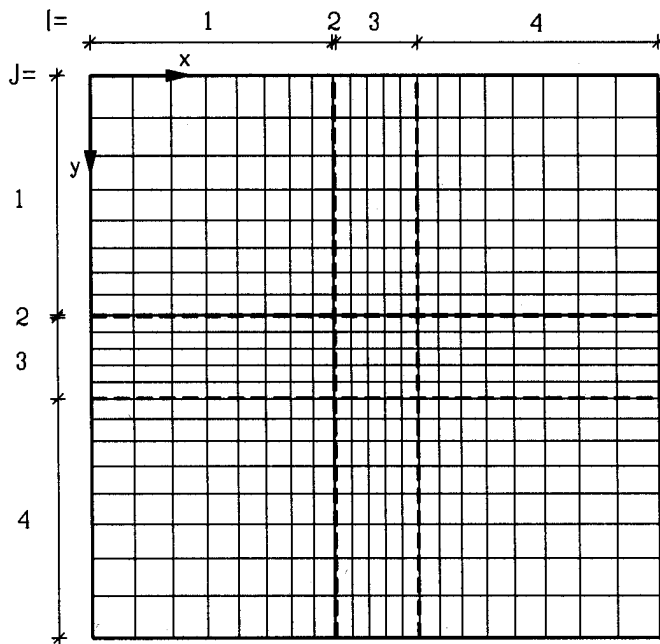
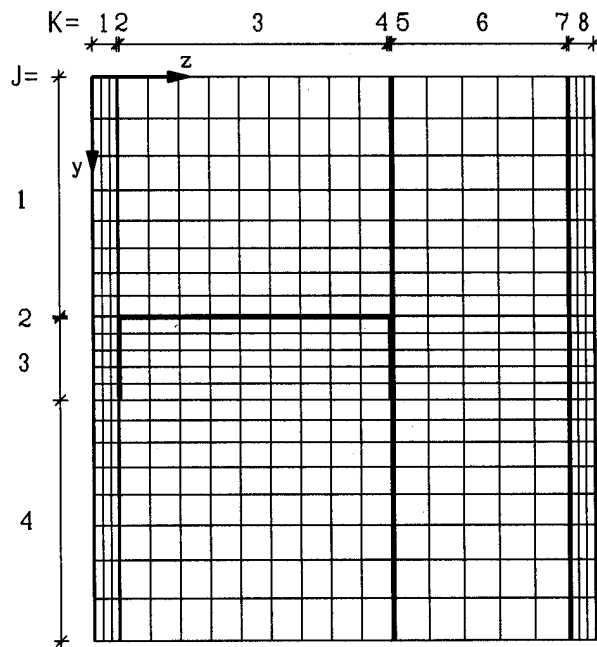Figure 6.2: Input segments and a computational mesh in the x, y-direction.

Figure 6.3: Input segments and a computational mesh in the y, z-direction.

The calculations for the wall are made using a gradually refined mesh. The total number of cells ranges from 128 to 1000000. Since each segment has at least one cell, the minimum number of cells is 128 $(4 \cdot 4 \cdot 8)$. Table 6.3 gives the mesh division for all the

49

segment	thickness (mm)	expansion coeff.
$I=1$	$\Delta x_1=127.5$	$\xi_{x1}=0.9$
$I=2$	$\Delta x_2=0.64$	$\xi_{x2}=1$
$I=3$	$\Delta x_3=44.36$	$\xi_{x3}=1$
$I=4$	$\Delta x_4=127.5$	$\xi_{x4}=1.1$
$K=1$	$\Delta z_1=13$	$\xi_{z1}=0.8$
$K=2$	$\Delta z_2=0.64$	$\xi_{z2}=1$
$K=3$	$\Delta z_3=143.72$	$\xi_{z3}=1$
$K=4$	$\Delta z_4=0.64$	$\xi_{z4}=1$
$K=5$	$\Delta z_5=0.64$	$\xi_{z5}=1$
$K=6$	$\Delta z_6=93.72$	$\xi_{z6}=1$
$K=7$	$\Delta z_7=0.64$	$\xi_{z7}=1$
$K=8$	$\Delta z_8=9$	$\xi_{z8}=1.2$

Table 6.2: Thickness and expansion coefficients for the input segments.

cases considered. Figures 6.2 and 6.3 show as mentioned before the case with 11616 cells.

cells	Nx_1	Nx_2	Nx_3	Nx_4	Nz_1	Nz_2	Nz_3	Nz_4	Nz_5	Nz_6	Nz_7	Nz_8
128	1	1	1	1	1	1	1	1	1	1	1	1
1215	3	1	2	3	2	1	4	1	1	3	1	2
2736	4	1	3	4	3	1	5	1	1	4	1	3
11616	8	1	5	8	3	1	9	1	1	5	1	3
193492	24	1	12	24	8	1	19	1	1	13	1	8
270400	25	1	14	25	10	1	22	1	1	18	1	10
1000000	37	1	25	37	17	1	34	1	1	28	1	17

Table 6.3: Number of computational cells in each segment.

6.2.4 Criterion for steady-state

Since the solution technique is iterative, a criterion for when to stop the iterations must be employed. The following stop criterion, which is recommended as a European standard (CEN, 1995), is used: the sum of all heat flows (positive and negative) entering the boundaries, divided by the sum of the absolute values of all these heat flows, must be equal to or less than 0.001, see Eq. (6.1). In the present case, this means the flow into the wall on the warm side minus the flow out through the cold side, divided by the sum of these two absolute values, is less than 0.001.

$$\delta = \frac{\sum_{i=1}^{N} Q_i}{\sum_{i=1}^{N} |Q_i|} \leq 0.001 \tag{6.1}$$

6.2.5 Results

The calculated heat flows through the wall section Q, (W), are shown in Table 6.4 (stop criterion $\delta=1\cdot10^{-3}$). For an increasing number of cells, the solution converges to the stable flow 0.03421 W. The relative errors compared to the last case with one million cells are given in the third column. The error for the case with 11616 cells is 1.8%. The required run-time, labeled as CPU-time, is also shown. The calculations indicate the Silicon Graphics computer to be about 3 times faster than the Pentium/90.

The number of cells required to obtain satisfactory accuracy depends on the problem considered. The following criterion is recommended as a European standard (CEN, 1995). The sum of the absolute values of all the heat flows entering the object is calculated twice, once for n cells and once for $2n$ cells. The relative difference between the flows must be smaller than 2%. If not, further mesh division is required. Comparing the second and third case, the third case having 2.3 times as many cells as the second, the difference is about 1-0.03290/0.03223=2.1%. Thus, according to the standard, it should be sufficient with about 2700 cells. This is, however, an underestimation of the real flow of at least 4%. From this it is clear that the above rule should be used with caution.

Number of cells	Q (W)	error	CPU-time 486/33	CPU-time Pentium/90	CPU-time Silicon Graphics
128	0.02819	17.6%	-	2s	-
1215	0.03223	5.8%	-	6s	-
2736	0.03290	3.8%	-	10s	-
11616	0.03360	1.8%	220s	46s	27s
193492	0.03411	0.2%	1h 40m	22m	-
270400	0.03415	0.1%	2h 56m	36m	13m
1000000	0.03421	-	-	5h	1h 50m

Table 6.4: Results for seven different numerical meshes ($\delta=1\cdot10^{-3}$).

The U-value of the wall becomes $0.03421/(0.300\cdot0.300)=0.380$ W/(m²K). The corresponding wall without steel has the thermal resistance:

$$R_{1-D} = 0.04 + 0.13 + \frac{0.013 + 0.009}{0.22} + \frac{0.240}{0.036} = 6.937 \quad \text{m}^2\text{K/W} \tag{6.2}$$

The U-value without steel becomes 1/6.937=0.144 W/(m²K). Thus, the wall with U-girders of steel has about 2.6 (0.380/0.144) times larger U-value than a wall without such girders. If the thickness of the steel is doubled from 0.64 mm to 1.28 mm, the U-value becomes 0.513 W/(m²K), i.e. it increases an additional 35%.

Table 6.5 shows that the heat flows are almost the same when using the stop criterion $\delta=1\cdot10^{-5}$. The CPU-time is almost doubled compared to using $\delta=1\cdot10^{-3}$.

Number of cells	Q (W)	error	CPU-time 486/33	CPU-time Pentium/90
128	0.02821	17.6%	6s	3s
1215	0.03223	5.8%	34s	9s
2736	0.03290	3.8%	75s	17s
11616	0.03360	1.8%	361s	72s
193492	0.03411	0.2%	3h 13m	39m
270400	0.03415	0.1%	5h 13m	1h 4m
1000000	0.03421	-	-	9h 36m

Table 6.5: Results for seven different numerical meshes (δ=1·10^{-5}).

6.2.6 Calculations for the steel without insulation

The thermal conductivity of the steel is about 1700 times larger than that of the insulation material. The heat flow between the steel and the insulation should therefore be relatively small compared with the flow along the steel. It turns out to be a rather good approximation to separate the problem into two cases and add the two flows.

In the first case, the steel is not taken into account. This gives a one-dimensional problem. The flow through the considered part of the wall, with a temperature difference of 1 °C, and a thermal resistance of 6.937, Eq. (6.2), becomes

$$Q_{1dim} = \frac{0.300 \cdot 0.300}{6.9367} = 0.01297 \quad W \tag{6.3}$$

The second case considers only the flow in the steel. There is no flow in the insulation. The boundary condition between steel and insulation is an adiabatic one. A first simulation is made with 2816 computational cells. This case has the same numerical grid as the case with 11616 cells when the insulation was part of the computational region. The second simulation uses 64660 cells, which corresponds to the case with 193492 cells.

The heat flow through the steel wall is added to the one-dimensional solution (6.3), see Table 6.6. The relative error of the flows, $1 - (Q_{steel} + Q_{1dim})/Q$, becomes 0.5%. Note that the cases are compared with the corresponding cases, not with the case with 1000000 cells. The run-time is about half compared with the case when the insulation is considered (δ=1·10^{-3}).

cells	corresp. case	Q_{steel} (W)	CPU-time (486/33)	$Q_{steel} + Q_{1dim}$ (W)	error
2816	11616	0.02043	80s	0.03340	0.5%
64660	193492	0.02097	51m	0.03394	0.5%

Table 6.6: Calculated flows without insulation (δ=1·10^{-3}).

6.2.7 Conclusions

Girders and crossbar support of metal create truly three-dimensional thermal bridge effects in a well insulated wall. The thermal bridge effects due to the metal increased the U-value by a factor 2.6 to 0.380 W/(m^{2}K) with a center-to-center distance of 0.3 m between the girders. A more practical distance is 0.6 m, and the U-value becomes in this case 0.203 W/(m^{2}K), i.e. a factor 1.4 compared to a wall without girders (0.144 W/(m^{2}K)).

The paper presents calculations with HEAT3. The numerical error of the U-value becomes 2% using about 10000 cells in an expansive mesh. The CPU-time on a Pentium/90 is about one minute. An error below 0.2% requires about 200000 cells and a CPU-time of about half an hour.

6.3 Glass-encapsulated evacuated powder panels

6.3.1 Introduction

Figure 6.4 shows a glass-encapsulated evacuated panel lying on a glass plate of 2 mm thickness. The panel is filled with a powder called Perlite that has very low thermal conductivity in vacuum. According to (McElroy et al, 1984) and (Solomou, 1993) the conductivity of the powder remains nearly constant at vacuum levels below 133 N/m^2. When the vacuum level rises above that, the conductivity rises significantly, from 0.006 W/(m·K) to 0.07 W/(m·K) at normal pressure. The panel has been developed and tested at the Building Technology Division, Massachusetts Institute of Technology, Cambridge, USA.

Evacuated insulation panels have a larger thermal resistance compared with ordinary foam insulation materials of the same thickness. This gives advantages in applications where the insulation must be put in thin walls, e.g. insulation of refrigerators. An example is shown in Fig. 6.5, where four panels are imbedded in foam insulation. The vacuum insulation panels can suffer a reduction in the overall thermal resistance by more than a factor of two (Glicksman, 1991) due to the heat transfer in the envelope material around the circumference of the panel. Use of wider panels reduces the heat transfer, but the width is limited by practical design constraints. A possibility to reduce the heat flow is to place the panels in alternative configurations in the wall.

6.3.2 Calculations

A heat flow calculation in three dimensions is made to determine the heat transmitted through the wall shown in Fig. 6.5. The figure shows the plane section and the cross-section, respectively. The wall is 0.042 m thick and has a total width and height of 0.233 m. The enclosing glass is 0.15 mm thick and the glass plate is 2 mm thick. Panels 1 and 4 lie upside down.
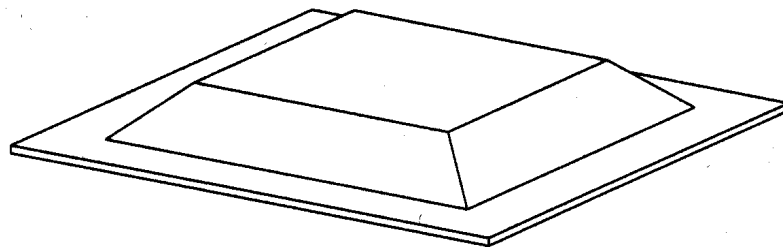
Figure 6.4: Glass-encapsulated evacuated powder panel.

An equivalent thermal conductivity λ_e is introduced for the wall:

$$Q = \lambda_e \cdot \frac{\Delta T}{\Delta z} \cdot A \quad (\text{W})$$

where Q, (W), is the total heat flow through the wall, ΔT the temperature difference, Δz the thickness of the wall, and A the area of the wall. Measurements done by (Solomou, 1993) gave λ_e=0.0166 W/(m·K).
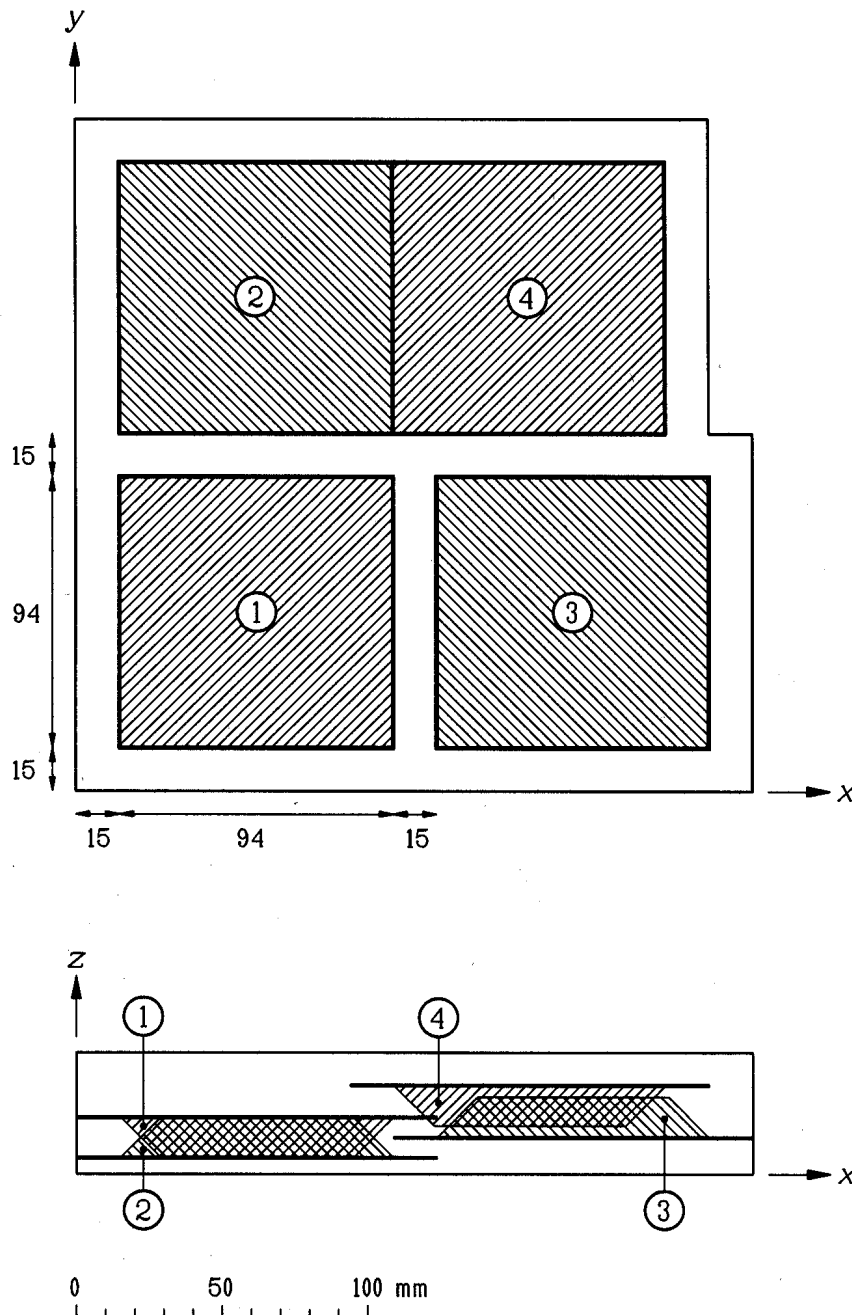
Figure 6.5: "Wall" with four glass-encapsulated evacuated powder panels imbedded in foam. Panels 1 and 4 lie upside down.

56

6.3.3 Assumptions

A few assumptions are made in the calculations. Heat transfer inside the panels by radiation and by convection is neglected. The surface thermal resistance is taken to be zero, and the boundary condition around the specimen to be adiabatic. The temperature at the top side in Fig. 6.5 is put to 1 °C and at the bottom side to 0 °C. The following thermal conductivities have been used:

<div style="text-align:center">

Glass   1.4 W/(m·K)
Powder 0.006 W/(m·K)
Foam   0.020 W/(m·K)

</div>

There is a relatively large thermal bridge effect due to the 0.15 mm thick glass that surrounds the panels. The vertical heat flow is mainly along the parts of the glass that have a slope of 1:2. This is modelled by thinner vertical glass of thickness 0.134 mm, calculated as $0.15 \cdot \sin(\arctan(2))$, since HEAT3 requires the problem to be described in Cartesian coordinates.

The calculations were carried out on a PC (486DX/33) using HEAT3. It took about five minutes to solve the problem using 43000 cells, and about two hours using 253000 cells. The distribution of the computational cells in the three directions x, y, z, see Fig. 6.5, is as follows. There are 33, 29, and 47 cells, respectively, in each direction in the case with 43000 cells. In the case with 253000 cells, there are 65 cells in each direction. The smallest cells are those lying along the enclosing glass. This means that they are 0.15 mm wide. The difference between the heat flow obtained with 43000 cells compared with 253000 cells was about 0.5%. It should be quite sufficient to use 43000 cells in this case.

6.3.4 Calculations

The calculations gave an equivalent thermal conductivity larger than the measured one. Table 6.7 shows the calculated equivalent thermal conductivities λ_e. With 253000 computational cells, λ_e was calculated to be 0.0195 W/(m·K), i.e. 17% larger than the measured value 0.0166 W/(m·K), see case 2.

Estimations of the minimum and maximum equivalent thermal conductivity gave 0.0169 W/(m·K) and 0.0213 W/(m·K), respectively. These estimates were based on calculations carried out by hand.

The glass has a certain influence on the heat flow. In case 3 in Table 6.7, the enclosing 0.15 mm thick glass is replaced by foam, the 2 mm thick glass plate remaining. The equivalent thermal conductivity is decreased to 0.0173 W/(m·K). When all the glass is replaced by foam, λ_e becomes 0.0160 W/(m·K), see case 4.
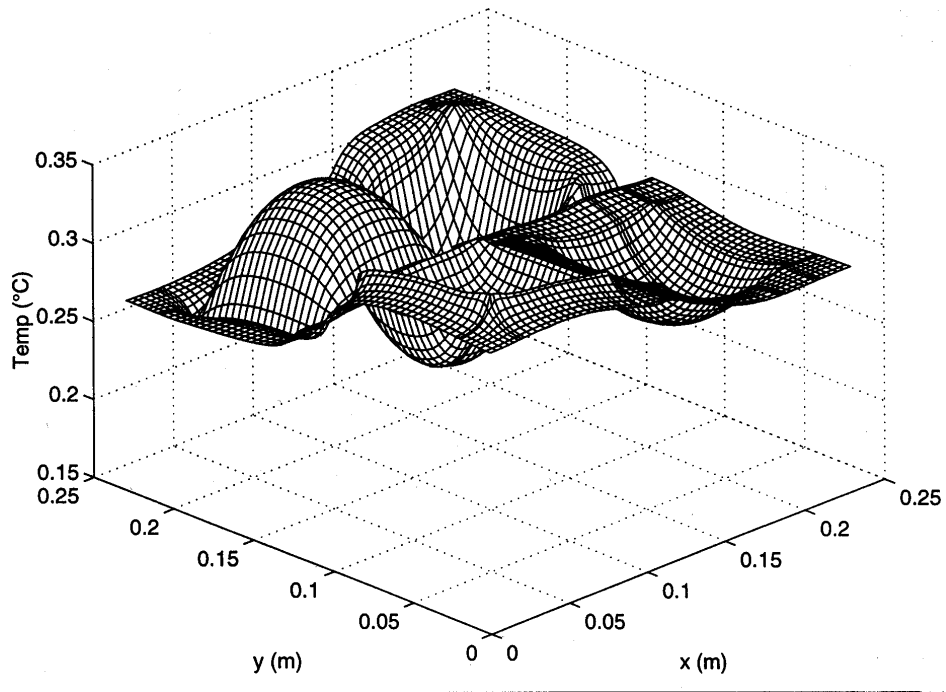
Figure 6.6: Calculated temperatures for the cross-section at the cut shown in Fig. 6.7.
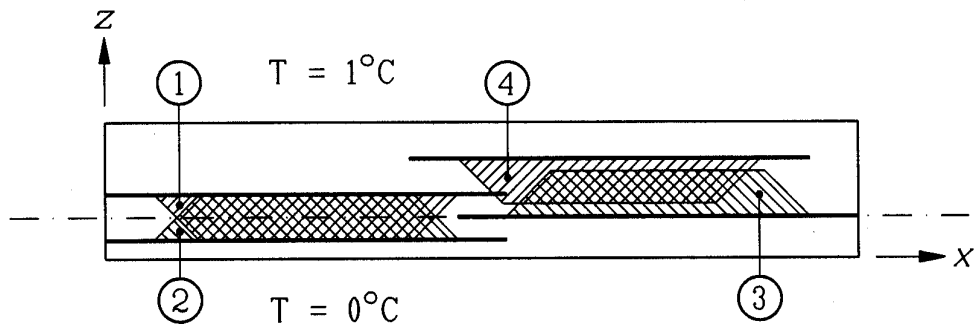
Figure 6.7: Cross-section for Fig. 6.6.

case	number of cells	Q, (W)	λ_e, (W/(m·K))	comments
1	43000	0.0240	0.0194	
2	253000	0.0241	0.0195	
3	43000	0.0214	0.0173	enclosing glass of 0.15 mm thickness replaced by foam
4	43000	0.0198	0.0160	all glass replaced by foam

Table 6.7: Calculated equivalent thermal conductivities.

Figure 6.6 shows the calculated temperatures for the cross-section marked in Fig. 6.7 at the level of the bottom plate of the 3rd panel. The grid in the figure gives an idea of the mesh in the case with 65 cells in each direction.

Consider first panel 3. The cross-section is along the glass plate. The glass tends to even out the temperature along the plate. The dip in the middle is caused by the insulation effect of the powder inside the panel.

Panel 4 lies upside down slightly above the cross-section. There is a temperature dip in the middle of the panel on the underside. The temperature around the dip is higher in the corner compared with the inner part.

The panels 1 and 2 are divided in the middle by the cross-section. Panel 1 lies upside down, the plate on top yielding a higher temperature in the surrounding 0.15 mm thick glass. Panel 2 has a higher temperature in the middle than in the area outside the powder. This is due to the temperature being lower and more evenly distributed along the bottom of the plate. This in turn produces a higher temperature in the middle of the panel.

6.3.5 Conclusions

The calculations gave an equivalent thermal conductivity larger than the measured one. Table 6.7 shows the calculated equivalent thermal conductivities λ_e. With 253000 computational cells, λ_e was calculated to be 0.0195 W/(m·K), i.e. 17% larger than the measured value 0.0166 W/(m·K). The calculated value does not include surface resistances of the wall. This may be one explanation to the discrepancy. Another explanation could be that the geometry of the problem was not exactly the same in the measurements as in the calculations. There also may be uncertainties regarding the thermal conductivities.

Various modifications are quite straightforward to model, such as decreasing the thermal bridge effects due to the glass, changing the position of the panels, using a greater number of panels and the like.

6.4 Rock caverns used for heat storage

6.4.1 Introduction

Rock caverns could be used for heat storage, here exemplified by the underground storage in Skarvik, Sweden. A comprehensive analysis is presented in (Claesson, 1989a). The caverns, used earlier as oil depots, could be filled with water and used as a heat store. The heat loss from one such cavern is examined here. The aim of the present study is to illustrate the accuracy for various choices of numerical mesh, using calculations in two and three dimensions.

6.4.2 Data for analysis

Figure 6.8 shows the cavern. The length, height and width of the cavern are L=180 m, H=30 m, and B=18 m, respectively. The distance from the upper surface to the ground surface is 30 m. The thermal conductivity and the thermal volumetric heat capacity of the ground are λ=3.5 W/(m·K) and C=2.19 MJ/(m³K), respectively.

There are two symmetry planes in the three-dimensional case, the (x, z)-plane, and the (y, z)-plane, see Fig. 6.8. The calculations are made for one quarter of the entire area that extends 500 m outwards and 500 m downwards from the cavern. The temperature on the surfaces that lie inside the cavern is put to 1 °C, and the temperature at the ground surface is put to 0 °C. This gives the heat loss per unit excess temperature, which can be used to calculate the heat loss for the annual average temperature, see (Claesson et al, 1985).
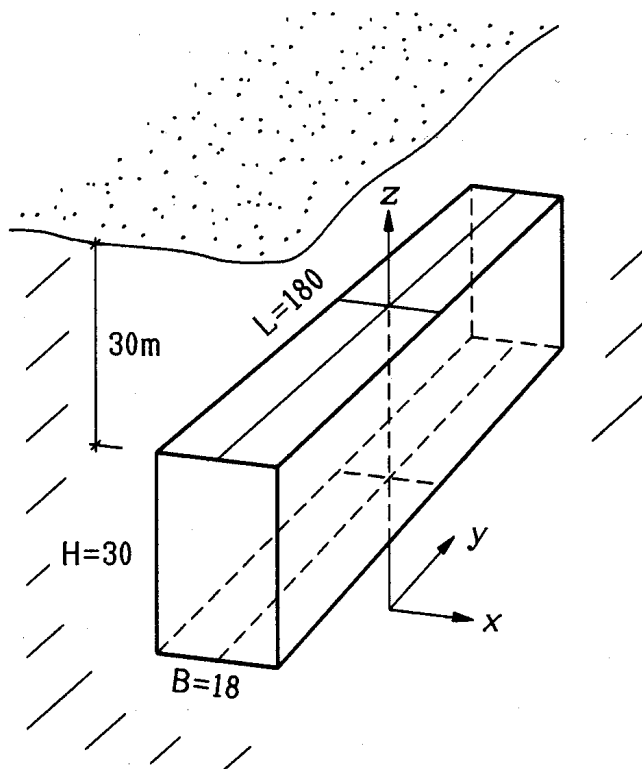
Figure 6.8: Underground cavern used for heat storage.

6.4.3 Steady-state calculations in two dimensions

Table 6.8 shows the steady-state heat loss from the cavern obtained with HEAT2. The heat loss from the cavern is the same as the heat flow upwards through the ground denoted by Q_{ground}, (W/m). The calculations consider heat flow per unit length perpendicular to the (x, z)-plane according to Fig. 6.8.

Twelve cases involving different numerical meshes are shown. The number of computational cells ranges from 48 to 15607. Equidistant and expansive meshes have been used. Figure 6.9 shows the expansive mesh around the cavern in the case with 1565 computational cells. The smallest cell outside the corners of the cavern is $0.9 \cdot 3.0$ m^2. In the cases with equidistant meshes, all cells have the same size as far as possible.

There is symmetry in the (y, z)-plane, see Fig. 6.8, and only one half of the problem is considered. The values for Q_{ground} in Table 6.8 should therefore be doubled. The error for Q_{ground} is calculated relative to the last case using 15025 ($125 \cdot 125$) cells in an expansive mesh. The approximate CPU-time for a Pentium/90 is shown in the last column. The successive over-relaxation coefficient ω is here 1.95, see Section 3.1.7.

number of cells	type of mesh	Q_{ground} (W/m)	error	CPU-time
48 ($7 \cdot 7$)	equidistant	3.692	39%	1 sec.
48 ($7 \cdot 7$)	expansive	5.025	17%	1 sec.
614 ($22 \cdot 28$)	equidistant	5.402	10%	5 sec.
608 ($22 \cdot 28$)	expansive	5.875	2.4%	10 sec.
1598 ($40 \cdot 40$)	equidistant	5.616	6.7%	15 sec.
1565 ($40 \cdot 40$)	expansive	5.969	0.9%	30 sec.
4221 ($65 \cdot 65$)	equidistant	5.826	3.2%	1 min.
4175 ($65 \cdot 65$)	expansive	5.983	0.6%	3 min.
9995 ($100 \cdot 100$)	equidistant	5.883	2.3%	6 min.
9700 ($100 \cdot 100$)	expansive	6.012	0.1%	15 min.
15607 ($125 \cdot 125$)	equidistant	5.940	1.3%	15 min.
15025 ($125 \cdot 125$)	expansive	6.021	-	30 min.

Table 6.8: Results for two-dimensional steady-state calculations.

The expansive mesh containing 1565 cells takes half a minute to simulate and gives an error of 0.9% compared to the last case with 15025 cells. An equidistant mesh containing 15607 cells gives a flow with an error of 1.3%. This simulation takes 15 minutes. Figure 6.10 shows the calculated isotherms near the cavity. The ground surface is at z=560 m.
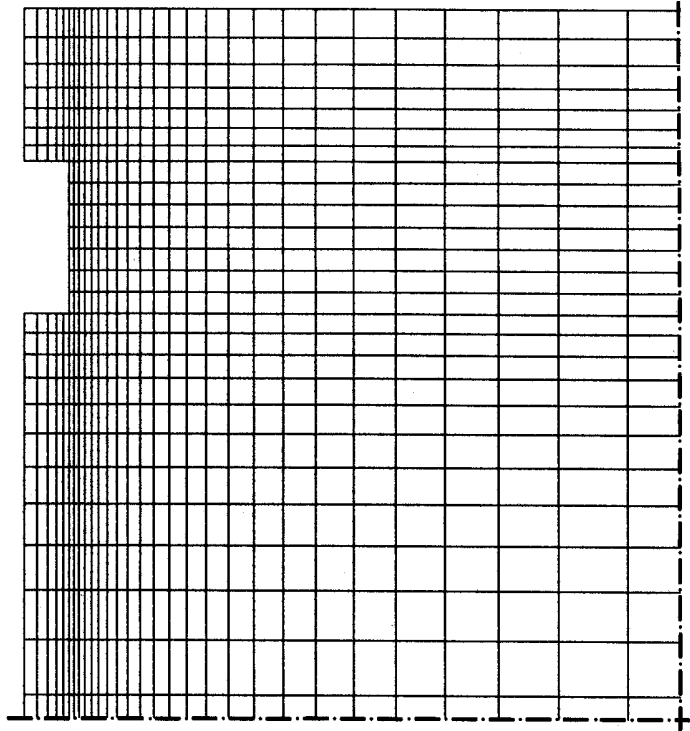
Figure 6.9: Expansive mesh near the cavern with 1565 cells.
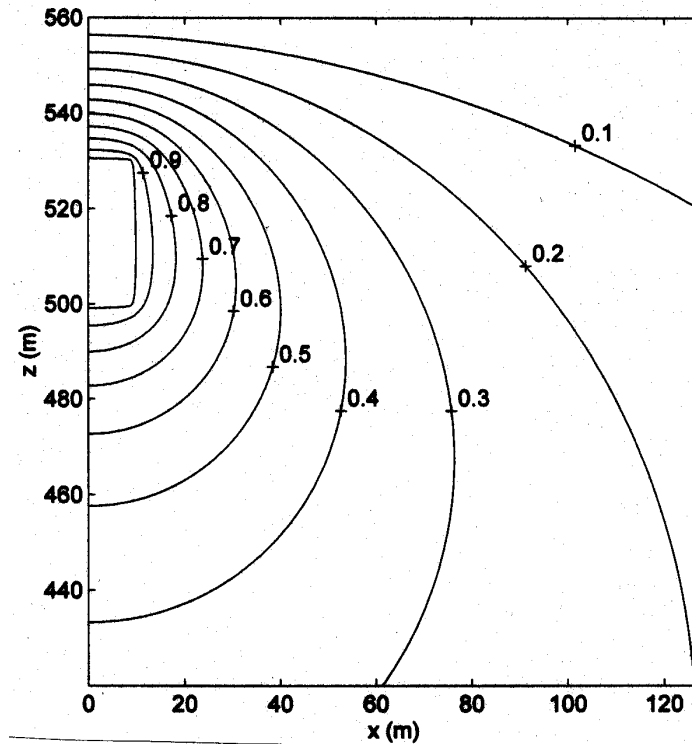
Figure 6.10: Isotherms near the cavern.

6.4.4   Transient calculations in two dimensions

In this case, the initial temperature at time $t=0$ is zero for the whole area. Figure 6.11 shows the calculated heat flows upwards through the ground surface during the first 100 years. The curve shows the heat flows for the somewhat coarse expansive mesh with 1565 (40·40) computational cells, see Table 6.8.
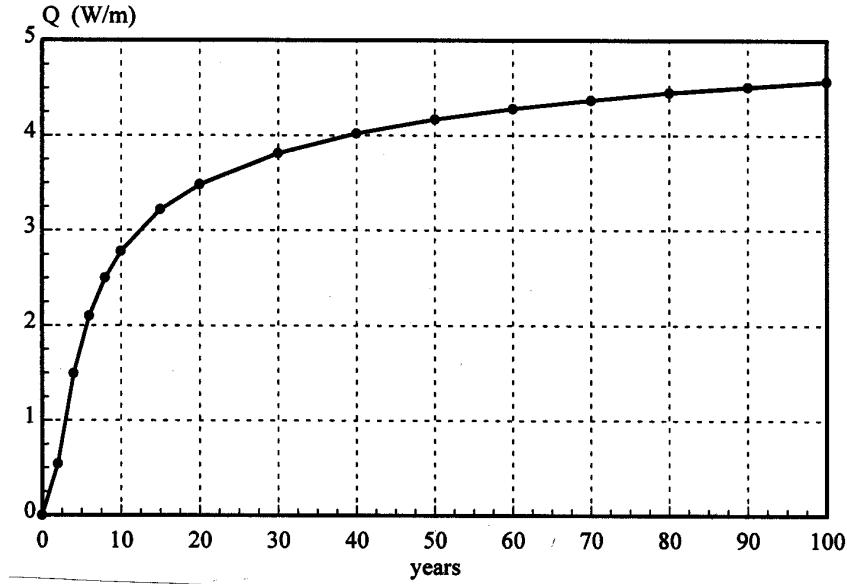
Figure 6.11: The heat flow through the ground surface during a 100 year period.

The transient calculation shows the long time needed to reach steady-state conditions. After 10 years the heat flow is 2.8 W/m. According to Table 6.8, the steady-state heat loss is 6.0 W/m. If there is a temperature change on the surfaces inside the cavern, it takes about 12 years before half of the steady-state heat flow (3.0 W/m) through the ground surface (caused by the step change in temperature) has appeared.

Table 6.9 shows the time-step for various numerical expansive meshes, the run-time to simulate 100 years, and the heat flow after 100 years. The last column shows the error compared to the case with 15025 cells. The error is almost the same compared to the steady-state calculations, see Table 6.8.

number of cells	time-step Δt	required CPU-time to simulate 100 years	Q_{ground} (W/m) after 100 years	error
48 (7 · 7)	4168 hours	1 sec.	3.777	18%
608 (22 · 28)	690 hours	5 sec.	4.486	2.7%
1565 (40 · 40)	48 hours	2.7 min.	4.567	0.9%
9700 (100 · 100)	9 hours	1.8 hours	4.603	0.1%
15025 (125 · 125)	6 hours	4.0 hours	4.610	-

Table 6.9: Time-step and required CPU-time to simulate 100 years for a few meshes.

6.4.5 Optimal mesh in two dimensions

What is the best numerical mesh, and how small is the error, using less than 1000 cells? The discretized problem is conservative. This means that the calculated heat flow is less than the true heat flow. The better the choice of the numerical mesh is, the closer are the calculated heat flow to the true one. Various calculations with different meshes have been made. By changing the number of cells in both directions, and the expansion coefficients, one can obtain an optimal mesh that gives the largest heat flow.

Figure 6.12 shows the area around the cavern with one of the best numerical meshes which has 983 cells (an expansive mesh with 39 cells in the horizontal direction, and 27 cells in the vertical direction). The figure shows 590 of the 983 cells. This mesh was obtained after about one hundred calculations with various meshes. The smallest cells are located around the corners of the cavern where the temperature gradients are large. The steady-state heat flow through the ground is Q_{ground}=5.976 W/m, which gives an error of 0.7% compared to Q_{ground}=6.021 W/m, see Table 6.8. The CPU-time is about 30 seconds. This mesh gives a smaller error compared to the mesh with 1565 cells (0.9%) in Table 6.8. Note however that the calculation time is the same in both cases with 1565 and 983 cells, respectively. More iterations are required in the case of 983 cells to reach steady-state.
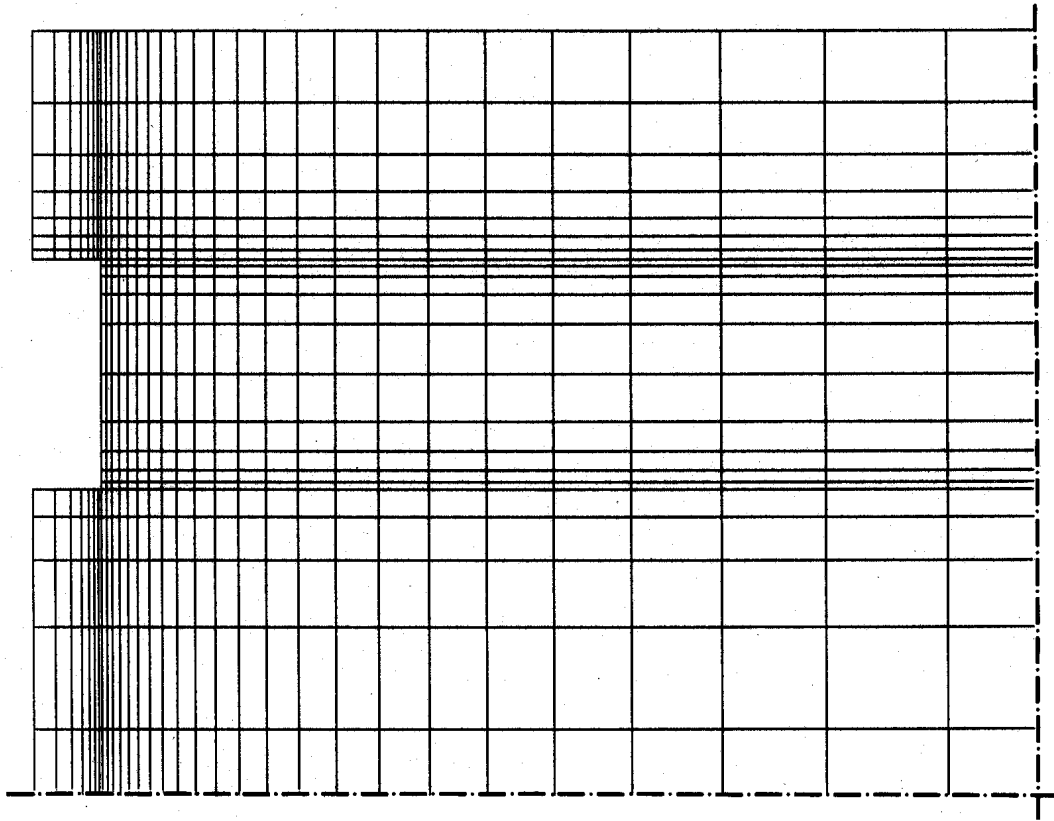
Figure 6.12: Optimal mesh using less than 1000 numerical cells. The figure shows 590 cells near the cavern. The whole computational area has 983 cells.

6.4.6 Choice of distance to outer boundaries

The calculations involve a computational area that extends 500 m outwards and 500 m downwards from the cavern. The boundary conditions are adiabatic at the boundary segments that restrict the area at these distances. This assumption leads to a calculated heat flow that is smaller compared to the true one. Table 6.10 shows the calculated heat flows for distances between 100 and 10000 m outwards and downwards to the outer boundaries. The error compared to the last case (10000 m) is shown in the right column. Expansive meshes with 15025 cells are used. Numerical tests show that the numerical error (discretization error) is less than 0.1% in the case with an extension of 10000 m.

extension (m)	Q_{ground} (W/m)	error
100	5.384	11%
500	6.021	0.6%
800	6.038	0.3%
1000	6.049	0.1%
2000	6.056	0%
5000	6.057	0%
10000	6.057	-

Table 6.10: Heat flow for different distances to the outer boundaries.

A distance of 500 m gives an error for the heat flow Q_{ground} of 0.6%. This means that the absolute error for the results in previous sections is at least 0.6% larger.

If the vertical extension is 1000 m, and the horizontal extension is 500 m, the flow becomes 6.023 W/m, i.e. an error of 0.6%. If the horizontal extension is 1000 m, and the vertical extension is 500 m, the flow becomes 6.042 W/m, i.e. an error of 0.2%. It is therefore better to use a larger horizontal extension compared to a vertical one. A rule of thumb should in this case be to extend ten times the depth of the cavern (60 m) horizontally (600 m), and eight times vertically (480 m). There should be about 1.5 as many cells horizontally compared to the number of cells vertically in an expansive mesh. The expansion coefficient should be about 1.2 horizontally, and about 1.5 vertically. The total number of cells should be at least 5000. With these proposals, the error should be less than one per cent.

6.4.7 Steady-state calculations in three dimensions

Table 6.11 shows the results for eight different meshes. Due to symmetry, only one quarter of the problem needs to be taken into account. The values for Q_{ground} shown i Table 6.11 represent here the total flow (i.e. the calculated values have been multiplied by 4). The number of computational cells ranges from 342 to 999925. The error for the heat flows is calculated relatively the last case using 991000 cells in an expansive mesh.

The case with 15968 cells gives a heat flow from the cavern of 2720 W. The calculation takes about 3 minutes on a Pentium/90. The error compared to a calculation with 910000 cells (Q=2808) is 3%. This calculation takes about 30 hours. The smallest cell outside

the corners of the cavern in the case with 910000 cells is 0.4·0.8·1.1 m^3 (compared to 3.0·4.8·5.6 m^3 for the case with 15968 cells). Figure 6.13 shows the numerical mesh near the cavern in a three-dimensional perspective in the case with 15968 cells. In this figure, 5120 of the 15968 cells are shown. Figure 6.14 shows the same numerical mesh projected on the (x, z)-, (x, y)-, and (y, z)-plane, respectively. Figure 6.15 shows the isotherms near the cavern in the (y, z)-plane at x=0.

number of cells	type of mesh	Q_{ground} (W)	error	CPU-time
342 $(7 \cdot 7 \cdot 7)$	equidistant	1474	48%	5 sec.
342 $(7 \cdot 7 \cdot 7)$	expansive	2175	23%	5 sec.
16013 $(22 \cdot 26 \cdot 28)$	equidistant	2261	19%	2.5 min.
15968 $(22 \cdot 26 \cdot 28)$	expansive	2720	3.1%	3 min.
274585 $(65 \cdot 65 \cdot 65)$	equidistant	2677	4.7%	1.8 hours
274125 $(65 \cdot 65 \cdot 65)$	expansive	2782	0.9%	1.8 hours
999925 $(100 \cdot 100 \cdot 100)$	equidistant	2722	3.1%	12.5 hours
991000 $(100 \cdot 100 \cdot 100)$	expansive	2808	-	30.5 hours

Table 6.11: Results from three-dimensional steady-state calculations.
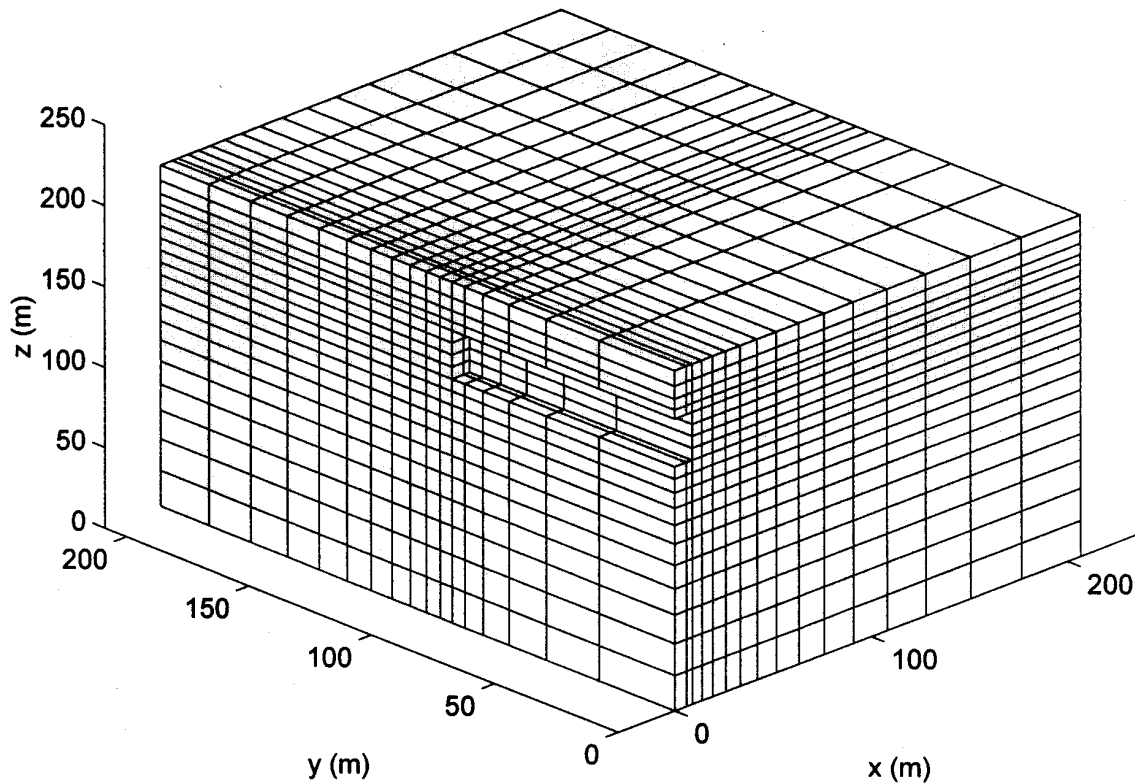
Figure 6.13: Numerical mesh around the cavern. The figure shows 5120 of the 15968 cells.
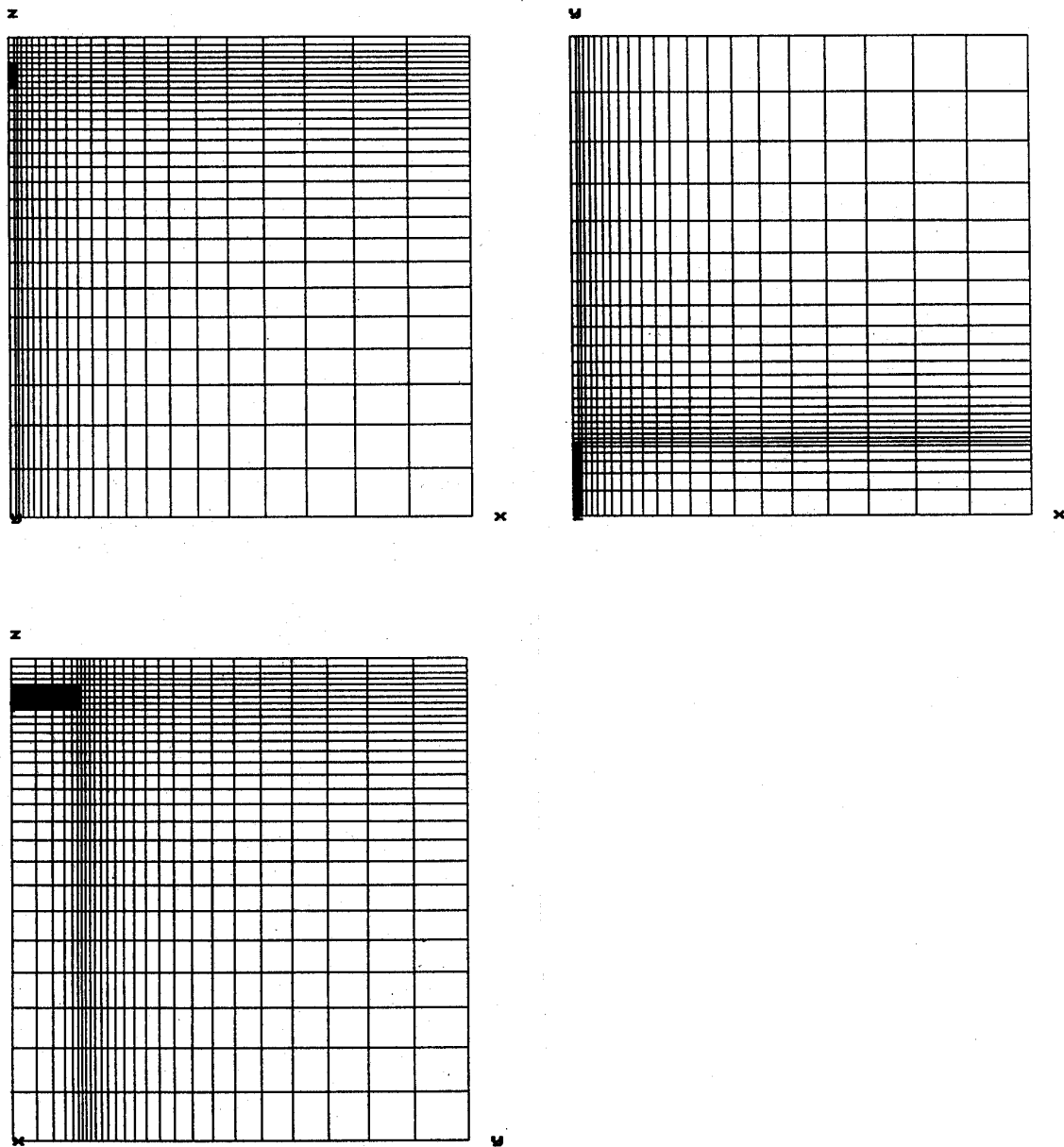
Figure 6.14: Numerical mesh with 15968 cells in the (x, z)-, (x, y)-, and (y, z)-planes.

An expansive mesh containing 15968 cells requires a simulation time of 3 minutes and gives an error of 3.1%. An equidistant mesh containing 999925 cells gives a heat flow with the same error. This simulation takes 12 hours.
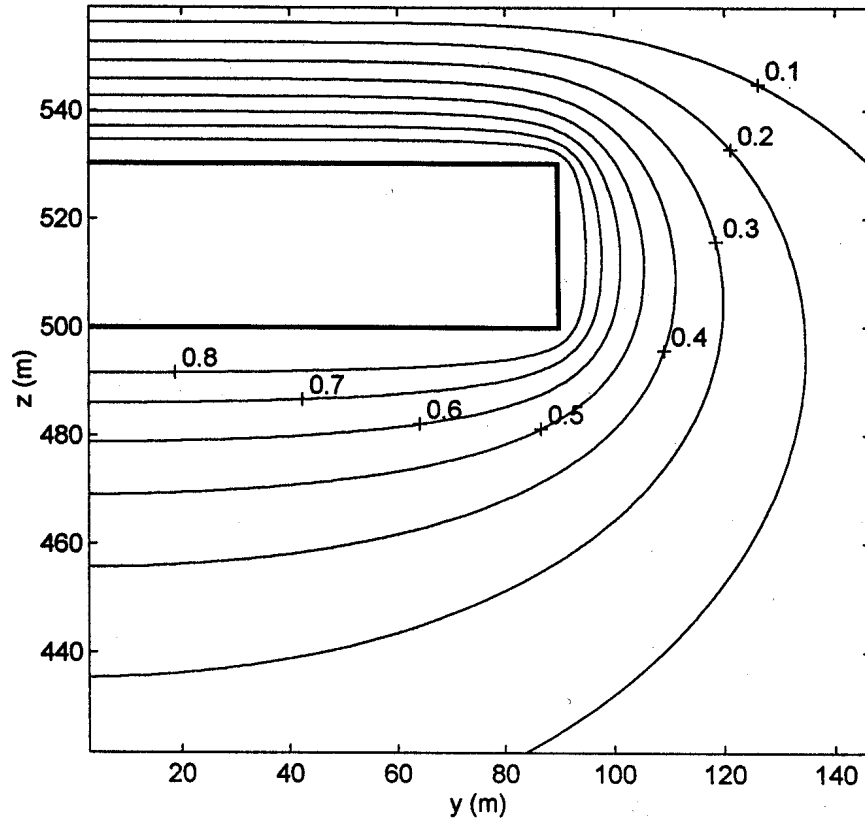
Figure 6.15: Isotherms near the cavern in the (y, z)-plane at $x{=}0$.

The three-dimensional solution may be approximated by two-dimensional calculations. Consider the case of an expansive mesh with 65 cells in each direction. According to Table 6.8, the heat flow upwards through the ground is 5.983 W/m (per meter in the y-direction). Another calculation made for $B{=}180$ gave the heat flow 16.41 W/m. The total flow becomes $2{\cdot}(5.983{\cdot}180+16.41{\cdot}18){=}2745$ W. The three-dimensional calculations gave 2782 W, see Table 6.11. The approximate value is about 1% higher than the result from the genuine three-dimensional calculation. This approximation is quite arbitrary, but it happens to give a good result here.

The problems of heat losses from rock caverns are further studied in (Hellström, 1991) and in (Claesson, 1980). Insulation on the ground decreases the heat losses from the caverns used for heat storage.

6.4.8 Conclusions

Two-dimensional calculations require an expansive mesh with about 1500 cells or an equidistant mesh with about 15000 cells for an error of 1%. The CPU-time is much less using the expansive mesh compared to using the equidistant mesh (half a minute compared with 15 minutes on a Pentium/90). An optimal mesh with less than 1000 cells gave an error of 0.7%. This calculation took about half a minute.

Three-dimensional calculations give the following results. An error of 3% for the heat flow through the ground requires an expansive mesh with about 16000 computational cells or an equidistant mesh with one million cells. The computer run-time is considerably shorter for the expansive mesh (3 minutes) than for the equidistant mesh (12 hours).

The transient calculations show the large time-scale to reach steady-state conditions. If there is a temperature change inside the cavern, it will take about 12 years before half of the steady-state surface heat flow (caused by the step change in temperature) has been reached. The CPU-time to simulate 100 years with an error smaller than 1% is typically a few minutes.

6.5 Thermal shielding of rock caverns

6.5.1 Introduction

When liquid natural gas, LNG, is stored in a rock cavern, a proper insulation to protect the surrounding rock against the cold medium (-162 °C) is required. Figure 6.16 presents the problem in schematic terms. There are three layers: rock, concrete and insulation. The corresponding thermal conductivities are λ_r, λ_c and λ_i, (W/(m·K)). The length of each layer is denoted by L_r, L_c and L_i, (m), respectively. The undisturbed temperature in the rock at $x=0$ is denoted by T_0, and the temperature in the LNG by T_-. A row of heating pipes is placed in the concrete at a distance of L_p from the rock. The distance between the pipes is denoted by B.
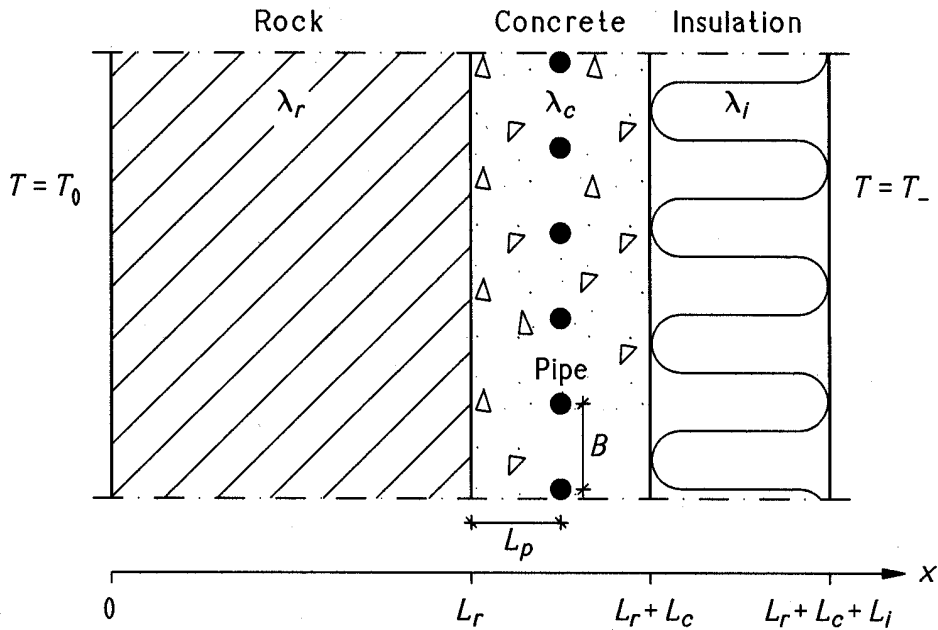
Figure 6.16: Thermal shielding with heating pipes.

The temperature in the concrete must be above the freezing point. There are drain-pipes in the concrete that would not function at a temperature below 0 °C. The coldest point in the concrete lies in the insulation at a point midway between the pipes. The task is to determine what effect the heating pipes must emit to maintain a positive temperature at this critical point, for an arbitrary spacing B between the heating pipes.

6.5.2 Mathematical formulation

The temperature at the periphery of the heating pipes is T_p and they emit an effect of q_p^B (W/m). The super-index B indicates that the heat flow refers to a width B between the pipes. The effect per unit area perpendicular to the x-axis is denoted by $q_p = q_p^B / B$ (W/m²). To find the two-dimensional steady-state solution of the problem, it suffices to

71

consider a strip with a single pipe. Figure 6.17 shows the cut-out strip and the conditions valid for the area. The heat flow through the upper and lower boundaries is zero due to symmetry midway between the pipes. The temperature at point P_0 must be above the freezing point, $T(P_0) > 0$.
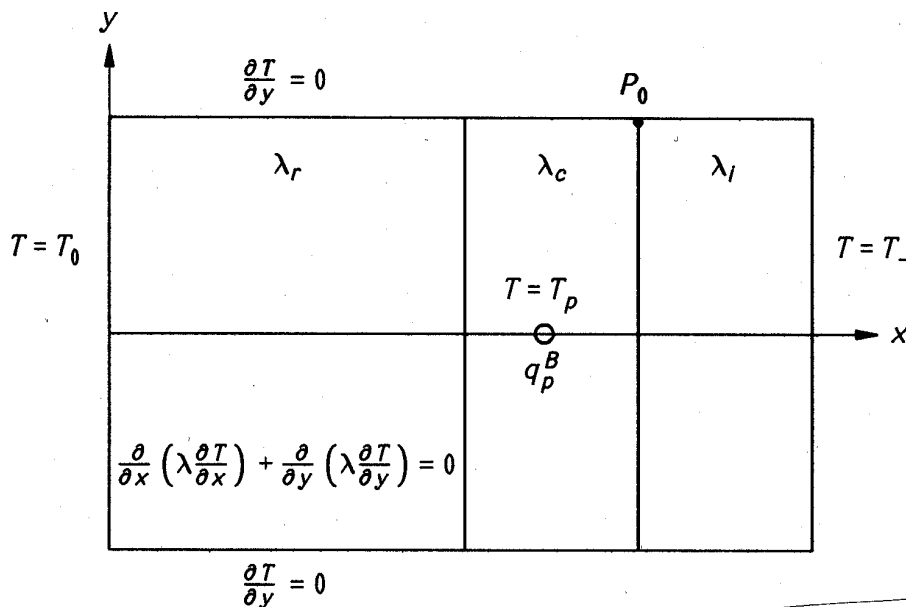
Figure 6.17: Mathematical conditions for the temperature $T(x, y)$.

6.5.3 Superposition

The problem can be solved by using superposition of an undisturbed problem and a remaining problem involving a superimposed heat source. The undisturbed problem is shown in Fig. 6.18. This is just a problem with a one-dimensional steady-state flow through the three layers. The solution is denoted by $T^0(x)$. The conditions for the remaining problem are shown in Fig. 6.19. The solutions to these two problems are given in the two sections that follow.
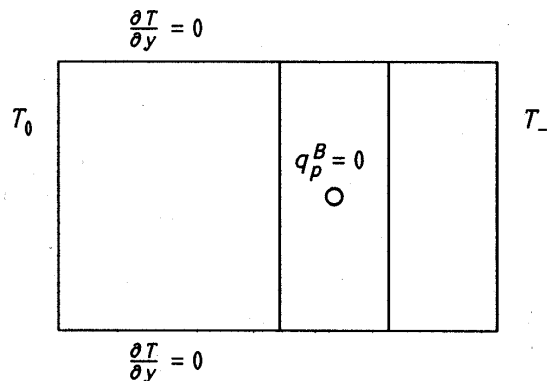
Figure 6.18: The undisturbed problem with the solution $T^0(x)$.

72
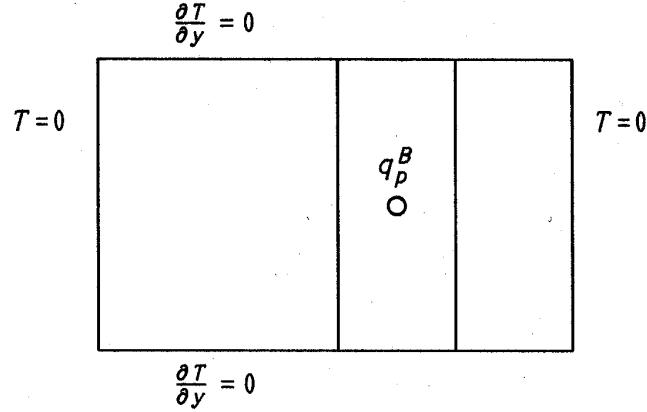
Figure 6.19: The superimposed problem with the solution $T^q(x, y)$.

6.5.4 The solution to the undisturbed problem

The solution $T^0(x)$ for the one-dimensional problem is obtained from the one-dimensional steady-state heat conduction equation:

$$\frac{d}{dx}\left(\lambda(x)\frac{dT^0(x)}{dx}\right) = 0 \qquad \begin{array}{l} T^0(0) = T_0 \\ T^0(L_r + L_c + L_i) = T_- \end{array} \tag{6.4}$$

Integration gives

$$\lambda(x)\frac{dT^0(x)}{dx} = -q^0 \tag{6.5}$$

or

$$\frac{dT^0(x)}{dx} = \frac{-q^0}{\lambda(x)} \tag{6.6}$$

Integration gives

$$T^0(0) - T^0(x) = T_0 - T^0(x) = q^0 \int_0^x \frac{dx}{\lambda(x)} \tag{6.7}$$

Inserting $x = L_r + L_c + L_i$ gives

$$T_0 - T_- = q^0 \int_0^{L_r+L_c+L_i} \frac{dx}{\lambda(x)} = q^0 \left(\frac{L_r}{\lambda_r} + \frac{L_c}{\lambda_c} + \frac{L_i}{\lambda_i}\right) \tag{6.8}$$

The heat flow q^0 per unit area (W/m^2) is

$$q^0 = \frac{T_0 - T_-}{\frac{L_r}{\lambda_r} + \frac{L_c}{\lambda_c} + \frac{L_i}{\lambda_i}} \tag{6.9}$$

73

Substituting q^0 into Eq. (6.7) gives an expression for $T^0(x)$:

$$T_0 - T^0(x) = \frac{T_0 - T_-}{\frac{L_r}{\lambda_r} + \frac{L_c}{\lambda_c} + \frac{L_i}{\lambda_i}} \cdot \int_0^x \frac{dx}{\lambda(x)} \tag{6.10}$$

Hence, the undisturbed temperature distribution in the concrete is

$$T^0(x) = T_0 - \frac{T_0 - T_-}{\frac{L_r}{\lambda_r} + \frac{L_c}{\lambda_c} + \frac{L_i}{\lambda_i}} \cdot \left(\frac{L_r}{\lambda_r} + \frac{x - L_r}{\lambda_c} \right) \qquad L_r \leq x \leq L_r + L_c \tag{6.11}$$

The temperature at the pipe T_p^0 $(x = L_r + L_p)$ is

$$T_p^0 = T^0(L_r + L_p) = \frac{T_0 \cdot \left(\frac{L_i}{\lambda_i} + \frac{L_c - L_p}{\lambda_c} \right) + T_- \cdot \left(\frac{L_r}{\lambda_r} + \frac{L_p}{\lambda_c} \right)}{\frac{L_r}{\lambda_r} + \frac{L_c}{\lambda_c} + \frac{L_i}{\lambda_i}} \tag{6.12}$$

The temperature at point P_0 at $x = L_r + L_c$ is

$$T^0(P_0) = \frac{T_0 \cdot \frac{L_i}{\lambda_i} + T_- \cdot \left(\frac{L_c}{\lambda_c} + \frac{L_r}{\lambda_r} \right)}{\frac{L_r}{\lambda_r} + \frac{L_c}{\lambda_c} + \frac{L_i}{\lambda_i}} \tag{6.13}$$

The heat flow through the layers can be represented by a thermal resistance network with resistances in series, as shown in Fig. 6.20. The following resistances (m^{2}K/W) are introduced:

$$\frac{L_r}{\lambda_r} = R_r \qquad \frac{L_p}{\lambda_c} = R_{c1} \qquad \frac{L_c - L_p}{\lambda_c} = R_{c2} \qquad \frac{L_i}{\lambda_i} = R_i \tag{6.14}$$

Here R_{c1} is the resistance of the layer between the pipe and the boundary of the rock and the concrete. R_{c2} is the resistance of the remaining concrete layer between the pipe and the critical point P_0.
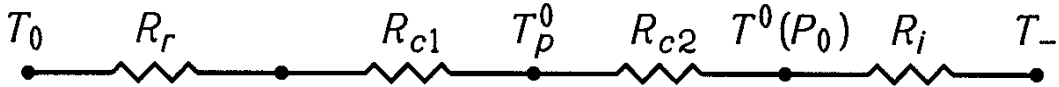
Figure 6.20: Thermal resistance network.

Equation (6.12) can be rewritten as

$$T_p^0 = \frac{T_0 \cdot (R_i + R_{c2}) + T_- \cdot (R_r + R_{c1})}{R_{tot}} \tag{6.15}$$

where

$$R_{tot} = R_r + R_{c1} + R_{c2} + R_i \tag{6.16}$$

Equation (6.13) becomes

$$T^0(P_0) = \frac{T_0 \cdot R_i + T_- \cdot (R_c + R_r)}{R_{tot}} \qquad (6.17)$$

and Eq. (6.9):

$$q^0 = \frac{T_0 - T_-}{R_{tot}} \qquad (6.18)$$

6.5.5   The solution to the remaining problem

The temperature at the pipe T_p^q for the remaining problem becomes $T_p - T_p^0$. The problem is solved for the temperature $+1$ at the periphery of the pipe. The temperature T_p^q can be adjusted so that any effect q_p is obtained.

$$T^q(x, y) = (T_p - T_p^0) \cdot T'(x, y) \qquad (6.19)$$

Here $T'(x, y)$ is the dimensionless solution to the problem shown in Fig. 6.21. This symmetric problem is solved numerically.
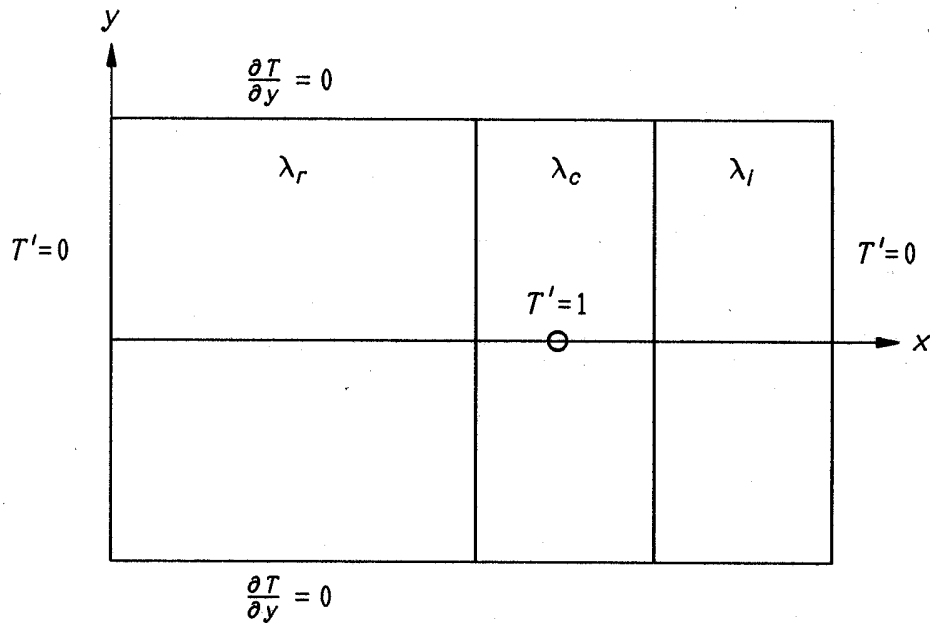
Figure 6.21: Conditions for the dimensionless problem with the solution $T'(x, y)$.

6.5.6   The complete solution

The general solution $T(x, y)$ is now:

$$T(x, y) = T^0(x) + (T_p - T_p^0) \cdot T'(x, y) \qquad (6.20)$$

The temperature T_p at the pipe is chosen so that the temperature at point P_0 becomes zero:

$$T(P_0) = T^0(P_0) + (T_p - T_p^0) \cdot T'(P_0) = 0 \tag{6.21}$$

Solving for T_p gives:

$$T_p = T_p^0 - \frac{T^0(P_0)}{T'(P_0)} \tag{6.22}$$

where

T_p^0 : temperature at the pipe from the undisturbed solution according to (6.15)
$T^0(P_0)$: temperature at point P_0 from the undisturbed solution according to (6.17)
$T'(P_0)$: temperature at point P_0 from the numerical solution $T'(x, y)$

6.5.7   Heat flows

It is of interested to know the heat flow q_p^B from the pipe and the flow over the outer boundaries. Heat balance, according to Fig. 6.22, implies that:

$$q_0^B + q_p^B = q_-^B \qquad \text{(W/m)} \tag{6.23}$$
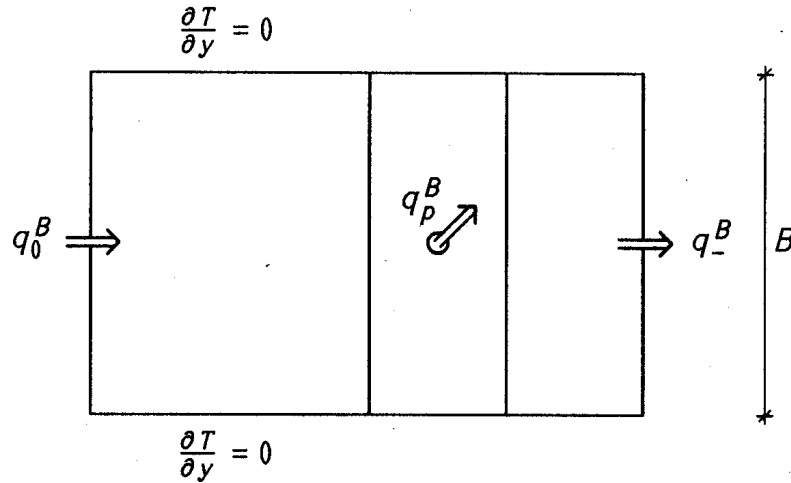
Figure 6.22: Heat flows for the problem.

Let q_0 and q_- be the corresponding heat flows per m^2:

$$q_0 = \frac{q_0^B}{B} \qquad q_- = \frac{q_-^B}{B} \qquad \text{(W/m}^2\text{)} \tag{6.24}$$

With $q_p = q_p^B / B$, (W/m^2), Eq. (6.23) yields:

$$q_0 + q_p = q_- \qquad \text{(W/m}^2\text{)} \tag{6.25}$$

Let $q(x)$ denote the *mean* heat flow in the x-direction:

$$q(x) = -\frac{1}{B} \int_{-B/2}^{B/2} \lambda \frac{\partial T(x,y)}{\partial x} dy \qquad (\text{W/m}^2) \tag{6.26}$$

Inserting (6.20) gives:

$$q(x) = -\lambda \cdot \left(\frac{dT^0}{dx} + (T_p - T_p^0) \cdot \frac{1}{B} \int_{-B/2}^{B/2} \frac{\partial T'(x,y)}{\partial x} dy \right) \tag{6.27}$$

and with (6.5):

$$q(x) = q^0 + (T_p - T_p^0) \cdot (-\lambda(x)) \cdot \frac{1}{B} \int_{-B/2}^{B/2} \frac{\partial T'(x,y)}{\partial x} dy \tag{6.28}$$

Let q_0' and q_-' denote the flow per Kelvin, (W/m²K), over the outer boundaries of the numerical problem with the dimensionless solution $T'(x,y)$, see Fig. 6.23. The corresponding heat flow from the pipe given by the numerical solution is denoted by q_p'.
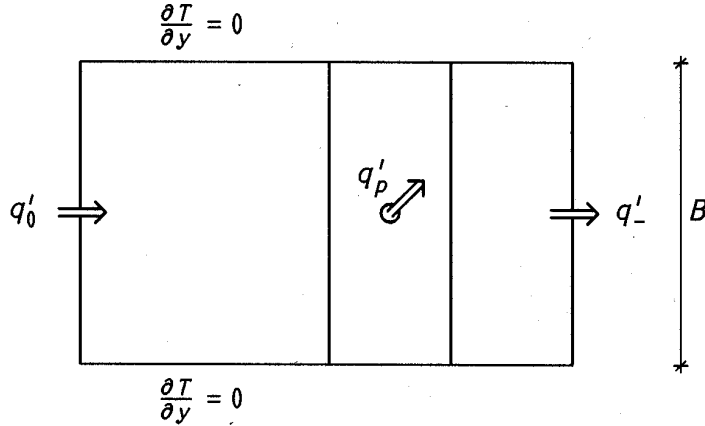
Figure 6.23: The numerical problem with flows.

The heat flow over the left boundary, q_0', is

$$q_0' = (-\lambda_r) \cdot \frac{1}{B} \int_{-B/2}^{B/2} \frac{\partial T'(0,y)}{\partial x} dy \qquad (\text{W/(m}^2\text{K)}) \tag{6.29}$$

The heat flow over the right boundary, q_-', is

$$q_-' = (-\lambda_i) \cdot \frac{1}{B} \int_{-B/2}^{B/2} \frac{\partial T'(L_r + L_c + L_i, y)}{\partial x} dy \qquad (\text{W/(m}^2\text{K)}) \tag{6.30}$$

and:

$$q_0' + q_p' = q_-' \qquad (\text{W/(m}^2\text{K)}) \tag{6.31}$$

The total mean flow over the boundaries, as obtained from (6.28) is then:

$$\begin{cases} q_0 = q^0 + (T_p - T_p^0) \cdot q_0' \\ q_- = q^0 + (T_p - T_p^0) \cdot q_-' \end{cases} \tag{6.32}$$

Finally, according to (6.25), the effect emitted from the pipe is

$$q_p = q_- - q_0 = (T_p - T_p^0) \cdot (q_-' - q_0') = (T_p - T_p^0) \cdot q_p' \qquad \text{(W/m}^2\text{)} \qquad (6.33)$$

or per meter:

$$q_p^B = B \cdot q_p \qquad \text{(W/m)} \qquad (6.34)$$

6.5.8   Summary

The numerical solution is denoted by $T'(x, y)$ for the problem shown in Fig. 6.21. From this solution, heat flows according to Fig. 6.22 also can be obtained with Eq. (6.31):

$$q_0' + q_p' = q_-' \qquad \text{(W/(m}^2\text{K))} \qquad (6.35)$$

The undisturbed solution without the pipe is denoted by $T^0(x)$, see Fig. 6.18. With the resistances defined as in (6.14) and (6.16), this gives

$$q^0 = \frac{T_0 - T_-}{R_{tot}} \qquad \text{(W/m}^2\text{)} \qquad (6.36)$$

The temperature at the pipe, according to (6.15) is

$$T_p^0 = \frac{T_0 \cdot (R_i + R_{c2}) + T_- \cdot (R_r + R_{c1})}{R_{tot}} \qquad (6.37)$$

The temperature at point P_0, according to (6.17) is:

$$T^0(P_0) = \frac{T_0 \cdot R_i + T_- \cdot (R_c + R_r)}{R_{tot}} \qquad (6.38)$$

The general solution $T(x, y)$, according to (6.20) is:

$$T(x, y) = T^0(x) + (T_p - T_p^0) \cdot T'(x, y) \qquad (6.39)$$

Here T^0 is the solution to the undisturbed problem and $T'(x, y)$ is the dimensionless numerical solution. The condition $T(P_0)=0$ gives according to (6.22):

$$T_p = T_p^0 - \frac{T^0(P_0)}{T'(P_0)} \qquad (6.40)$$

The flows are obtained according to (6.32):

$$\begin{cases} q_0 = q^0 + (T_p - T_p^0) \cdot q_0' \\ q_- = q^0 + (T_p - T_p^0) \cdot q_-' \end{cases} \qquad (6.41)$$

where q_0' and q_-' are given from (6.29) and (6.30). Finally, according to (6.33), the effect emitted from the pipe is

$$q_p = (T_p - T_p^0) \cdot q_p' \qquad \text{(W/m)}^2 \qquad (6.42)$$

or per meter of pipe (6.34):

$$q_p^B = B \cdot q_p' \qquad \text{(W/m)} \qquad (6.43)$$

6.5.9   A numerical example

The following data are used in the following example:

λ_r=3.4 λ_c=1.0 λ_i=0.025   W/(m·K)
T_0=8 T_-=−162 °C
L_r=10.0 L_c=0.6 L_i=0.25 L_p=0.4 m

The radius of the pipe, r_p, is 0.02 m. The problem is solved for B=0.60, 1.0 and 2.0 m. Resistances are calculated according to Eqs (6.14) and (6.16):

$$R_r = \frac{L_r}{\lambda_r} = 10/3.4 = 2.941 \quad \text{m}^2\text{K/W}$$

$$R_{c1} = \frac{L_p}{\lambda_c} = \frac{0.4}{1.0} = 0.4$$

$$R_{c2} = \frac{L_c - L_p}{\lambda_c} = \frac{0.6 - 0.4}{1.0} = 0.2 \tag{6.44}$$

$$R_i = \frac{L_i}{\lambda_i} = \frac{0.25}{0.025} = 10.0$$

$$R_{tot} = 2.941 + 0.4 + 0.2 + 10.0 = 13.541$$

The flow q^0 according to (6.18) is

$$q^0 = \frac{T_0 - T_-}{R_{tot}} = \frac{8.0 - (-162.0)}{13.541} = 12.55 \quad \text{W/m}^2 \tag{6.45}$$

The temperature at the pipe T_p^0 is according to (6.15):

$$T_p^0 = \frac{8.0 \cdot (10.0 + 0.2) + (-162.0) \cdot (2.941 + 0.4)}{13.541} = -33.9 \quad \text{°C} \tag{6.46}$$

For the temperature at point P_0 , see (6.17):

$$T^0(P_0) = \frac{8.0 \cdot 10.0 + (-162) \cdot (0.6 + 2.941)}{13.541} = -36.5 \quad \text{°C} \tag{6.47}$$

The thermal resistance network is shown in Fig. 6.24:
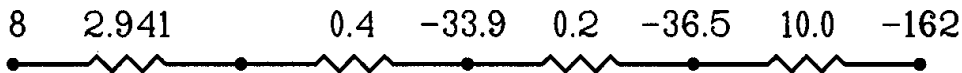
Figure 6.24: Thermal resistance network.

The dimensionless problem T' has been solved for a few values of B. The numerical solution gave the following results:

B (m)	$T'(P_0)$ (-)	q'_0 (W/m²K)	q'_- (W/m²K)	q'_p (W/m²K)
0.60	0.913	-0.281	0.092	0.373
1.0	0.830	-0.261	0.086	0.347
2.0	0.633	-0.215	0.070	0.285

From this the following results are obtained:

B (m)	T_p (°C)	q_0 (W/m²)	q_- (W/m²)	q_p (W/m²)	q_p^B (W/m)
0.60	6.04	1.33	16.23	14.9	9.0
1.0	10.0	1.10	16.33	15.3	15.3
2.0	23.7	0.17	16.60	16.4	32.8

where T_p, q_0, q_-, q_p and q_p^B are given by Eqs (6.40)-(6.43). In order to get positive temperatures in the concrete, the temperature at the pipe must be 6.0 °C for a distance $B=0.6$ m, or 23.7 °C for a distance of $B=2.0$ m.

6.5.10 Conclusions

When liquid natural gas, LNG, is stored in a rock cavern, proper insulation to protect the surrounding rock against the cold medium is needed. The temperature of the liquid natural gas is -162 °C. The temperature in the concrete must also be above the freezing point. This study shows how heating pipes may be used. The results are based on the principle of superposition.

6.6   U-value for a window accounting for the wall

6.6.1   Introduction

When a window's U-value is measured in a hotbox, the window's frame is surrounded by polystyrene or another insulation material. This provides an almost perfectly adiabatic boundary condition around the specimen.

When the window is mounted in a wall, however, there are additional heat losses due to thermal bridges around the window. The better the insulation is between the frame and the wall, the better the window's true heat losses agree with those that are measured.

Numerical calculations have been performed for estimating this effect. Both well insulated walls, and non-insulated walls, have been investigated. It is shown in this study that the U-value for a window of a normal size mounted in a wall is typically more than 10% greater than that measured in a hotbox.

6.6.2   Data for window and wall

Geometry of the window and frame

Figure 6.25 shows the frame and the window. The window has three panes, each 4 mm thick. The spacing between any two panes is 13 mm. The size of the window, including the frame, is $1.085 \cdot 1.185$ m^2. Table 6.12 shows the thermal conductivities used in the simulations. Three different cases are considered:

Case with a well insulated wall

Figure 6.26 depicts a well insulated wall, in which a window is placed close to the outer side of the wall. The thermal bridge effect between the frame and the wall is relatively small.

Case with a non-insulated wall

It is of interest to estimate the maximum flow that can arise when the window is mounted in a non-insulated wall. This is done by replacing the insulation material (4), the wood (5), and the gypsum board (7) in Fig. 6.26 with concrete (λ=1.7 W/(m·K)).

Case with no flow occurring between the frame and the wall

In this case, there is an adiabatic boundary condition between the frame and the wall. This corresponds to the case of the window being tested in a hotbox. The calculated heat flow through the window and frame should therefore be equal to the measured one.
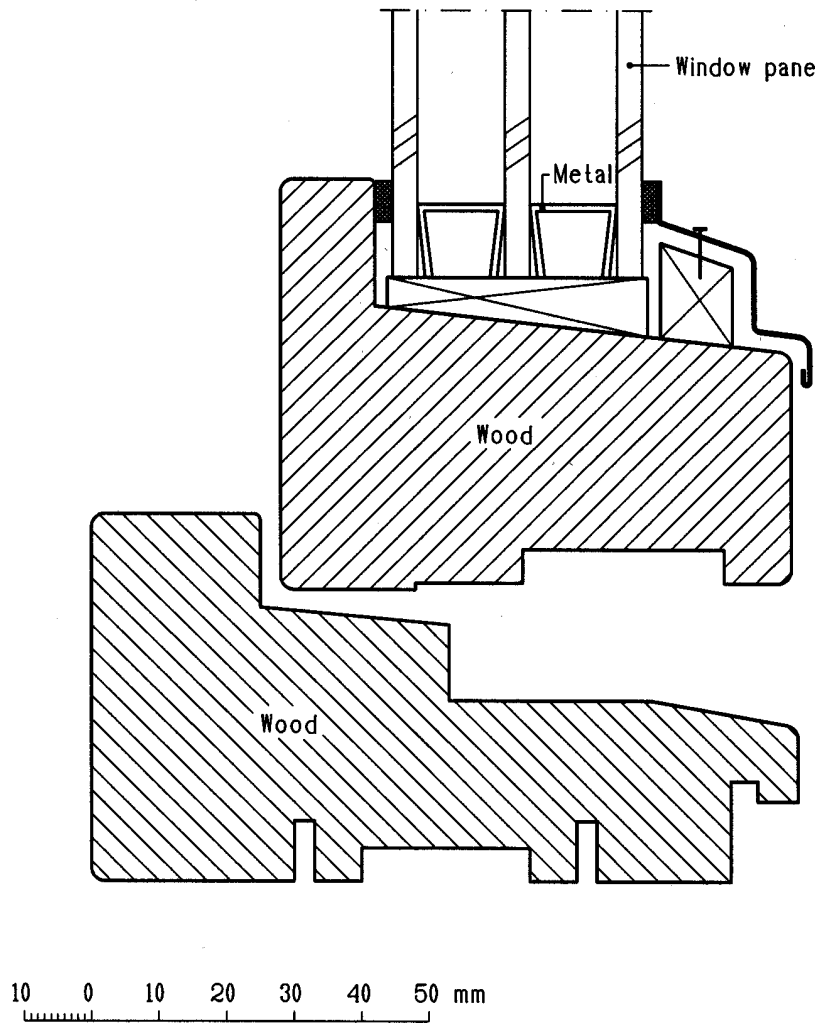
Figure 6.25: Geometry for the window and its frame.

material	λ (W/(m·K))
insulation	0.039
concrete	1.7
wood	0.14
gypsum	0.22
metal	160
glass	0.81

Table 6.12: Thermal conductivities used in the calculations.

1. Cover boarding, 22+16 mm

2. Air gap, 25 mm

3. Wind shield

4. Insulation, 245 mm

5. Wooden crossbar, $45 \cdot 45$ mm^2

6. Plastic sheeting, 0.2 mm

7. Gypsum wallboard, 13 mm
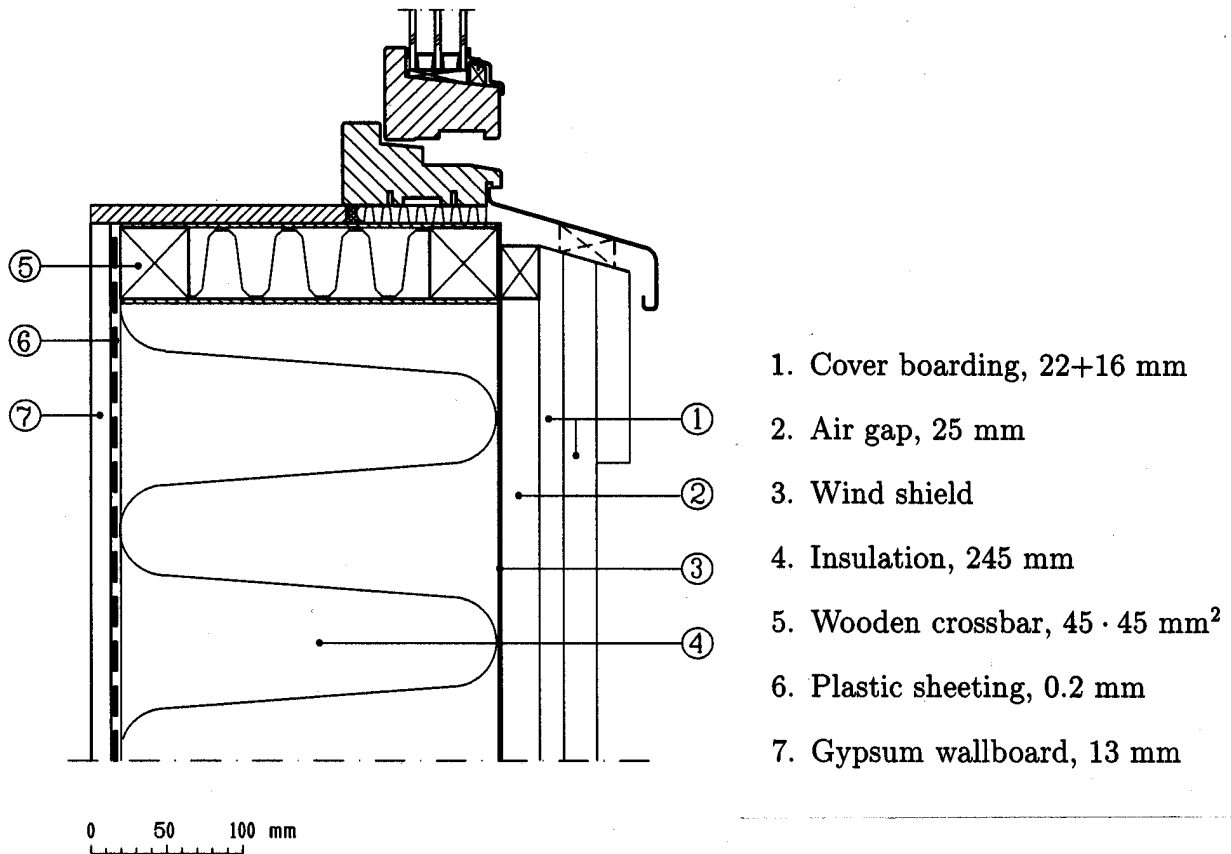
Figure 6.26: A well insulated wall with a window attached to it.

6.6.3 Equivalent U-value for the window

The heat flow is calculated using the two-dimensional heat transfer PC-program HEAT2, (Blomberg, 1990, 1991). The three-dimensional problem is approximated by considering a horizontal and a vertical cut through the window and a part of the wall. See Fig. 6.27.

The calculated flows for the vertical and horizontal cuts are denoted by q_V^{cal} and q_H^{cal}, respectively. Numerical tests have shown it to be sufficient to choose Δ=0.3 m. The flow outside this region is one-dimensional. A well-known method for calculating an equivalent U-value is to take into account the extra heat losses due to the thermal bridges between the frame and the wall. These extra heat losses are divided by the area of the window, and added to the window's one-dimensional U-value. The extra heat flow for the vertical cut becomes:
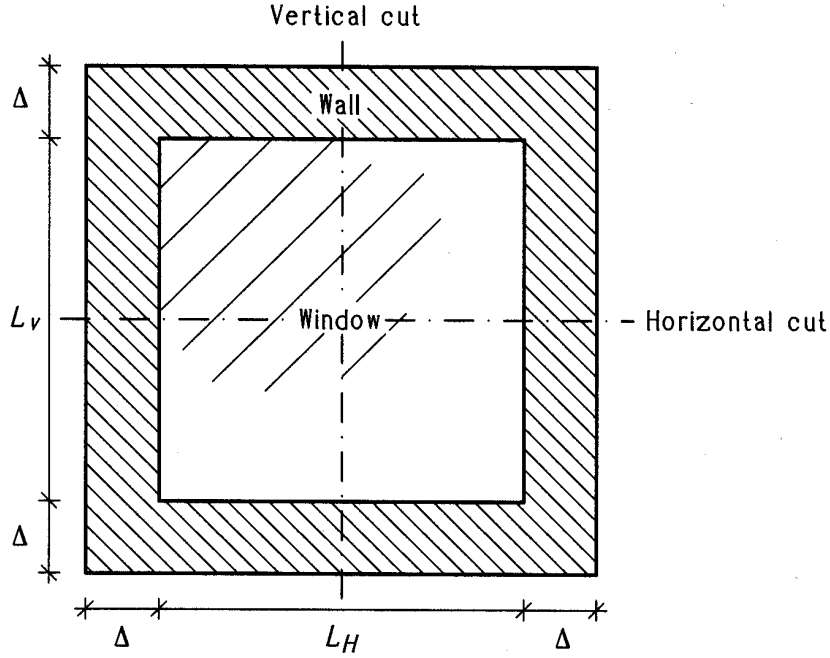
Figure 6.27: Window and the part of the wall belonging to the computational area.

$$q_V^{extra} = q_V^{cal} - (U_{win} \cdot L_V + U_{wall} \cdot 2\Delta) \quad \text{(W/(m·K))} \tag{6.48}$$

where U_{win} and U_{wall} are the one-dimensional U-values for the window and the wall, respectively. Similarly, the extra heat flow for the horizontal cut becomes

$$q_H^{extra} = q_H^{cal} - (U_{win} \cdot L_H + U_{wall} \cdot 2\Delta) \quad \text{(W/(m·K))} \tag{6.49}$$

The three-dimensional extra heat flow Q^{extra} (W/K) is approximated by:

$$Q^{extra} = q_V^{extra} \cdot L_H + q_H^{extra} \cdot L_V \quad \text{(W/K)} \tag{6.50}$$

If this extra heat flow is assigned to the window, the equivalent U-value for the window is

$$U_e = Q^{extra}/A_{win} + U_{win} \quad \text{(W/(m}^2\text{K))} \tag{6.51}$$

where A_{win} is the area for the window with the frame included.

6.6.4 Heat transfer in the window

The program HEAT2 models heat conduction in solid materials[1]. It is therefore necessary to use an equivalent thermal conductivity, λ_e, for the air layers in the window. This value takes into account the one-dimensional flow due to long-wave radiation and convection (including conduction).

---

[1]When this paper was written, HEAT2 was a pure heat conduction program. Radiation inside cavities can be modelled in newer versions.

The heat flow through an air layer may be approximated by a radiative term, q_r, and a convective term, q_c. See Fig. 6.28 and Eq. (6.52). The convective term also includes heat transfer by conduction. The radiative and convective heat transfer coefficients are denoted by α_r and α_c, respectively.
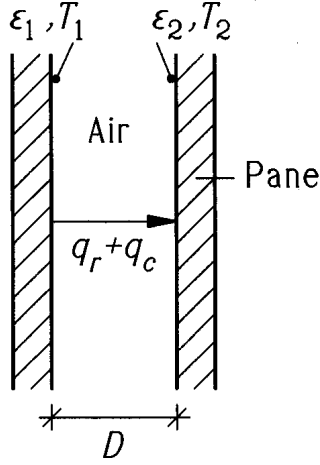
Figure 6.28: Radiative and convective heat flow inside a window.

$$q = q_r + q_c = (\alpha_r + \alpha_c) \cdot (T_1 - T_2) = \frac{\lambda_e}{D} \cdot (T_1 - T_2) \tag{6.52}$$

The radiative coefficient, α_r, is approximated, (Siegel et al, 1992), by

$$\alpha_r = 4 \cdot \epsilon_{12} \cdot \sigma_s \cdot T_m^3$$

where

$$\frac{1}{\epsilon_{12}} = \frac{1}{\epsilon_1} + \frac{1}{\epsilon_2} - 1, \quad \sigma_s = 5.67 \cdot 10^{-8} \quad \text{W}/(\text{m}^2\text{K}^4)$$

The emissivity of the surfaces, ϵ_1 and ϵ_2, is put to 0.9, which gives ϵ_{12}=0.82. The mean temperature T_m is put to 273 K. This gives α_r =3.79 W/(m²K).

The convective heat flow is due mainly to conduction, (Holman, 1986), the coefficient becoming

$$\alpha_c = \lambda_{air}/D = 0.025/0.013 = 1.92 \quad \text{W}/(\text{m}^2\text{K})$$

The equivalent thermal conductivity, according to Eq. (6.52), is

$$\lambda_e = (\alpha_r + \alpha_c) \cdot D = 0.074 \quad \text{W}/(\text{m·K})$$

6.6.5 One-dimensional U-values

The U-value for the window with its three panes and two air-layers, an internal surface resistance of 0.13 m²K/W, and an external surface resistance of 0.04 m²K/W, is

$$U_{win} = 1/(0.04 + 3 \cdot 0.004/0.81 + 2 \cdot 0.013/0.074 + 0.13) = 1.865 \quad \text{W}/(\text{m}^2\text{K})$$

The U-value for the well insulated wall becomes:

$$U_{ins.\,wall} = 1/(0.04 + 0.245/0.039 + 0.013/0.22 + 0.2 + 0.13) = 0.149 \quad \text{W/(m}^2\text{K)}$$

where the cover boarding and the air-layer have a resistance of 0.2 m²K/W. The concrete wall has the U-value

$$U_{non-ins.\,wall} = 1/(0.04 + 0.258/1.7 + 0.2 + 0.13) = 1.917 \quad \text{W/(m}^2\text{K)}$$

6.6.6 Results

The following data are used: L_H=1.085, L_V=1.185, Δ=0.3. This gives A_{win}=1.286 m².

Case with a well insulated wall

For the well insulated wall, the numerical simulations yield q_V^{cal}=2.518 and q_H^{cal}=2.330. Eq. (6.48) and (6.49) give

$$q_V^{extra} = 2.518 - (1.865 \cdot 1.185 + 0.149 \cdot 0.6) = 0.219 \quad \text{W/(m·K)}$$

$$q_H^{extra} = 2.330 - (1.865 \cdot 1.085 + 0.149 \cdot 0.6) = 0.217 \quad \text{W/(m·K)}$$

The extra heat loss, according to Eq. (6.50), becomes:

$$Q^{extra} = 0.219 \cdot 1.085 + 0.217 \cdot 1.185 = 0.495 \quad \text{W/K}$$

Equation (6.51) gives the equivalent U-value for the window:

$$U_e = 0.495/1.286 + 1.865 = 2.25 \quad \text{W/(m}^2\text{K)}$$

Figure 6.29 shows the numerical mesh for the frame and the nearest part of the wall. Figure 6.30 shows the isotherms for the same area. The temperatures indoors and outdoors are 20 °C and 0 °C, respectively.

Case with a non-insulated wall

Here, the numerical simulations give q_V^{cal}=3.908 and q_H^{cal}=3.722. The equivalent U-value for the window becomes:

$$U_e = 1.244/1.286 + 1.865 = 2.83 \quad \text{W/(m}^2\text{K)}$$

Case with no flow occurring between the frame and the wall

In this case, only the heat flow through the window and the frame is taken into account. The calculations give q_V^{cal}=2.382 and q_H^{cal}=2.196. Equations (6.48) and (6.49) are modified by omitting the terms for the wall. The equivalent U-value becomes:

$$U_e = 0.221/1.286 + 1.865 = 2.04 \quad \text{W/(m}^2\text{K)}$$
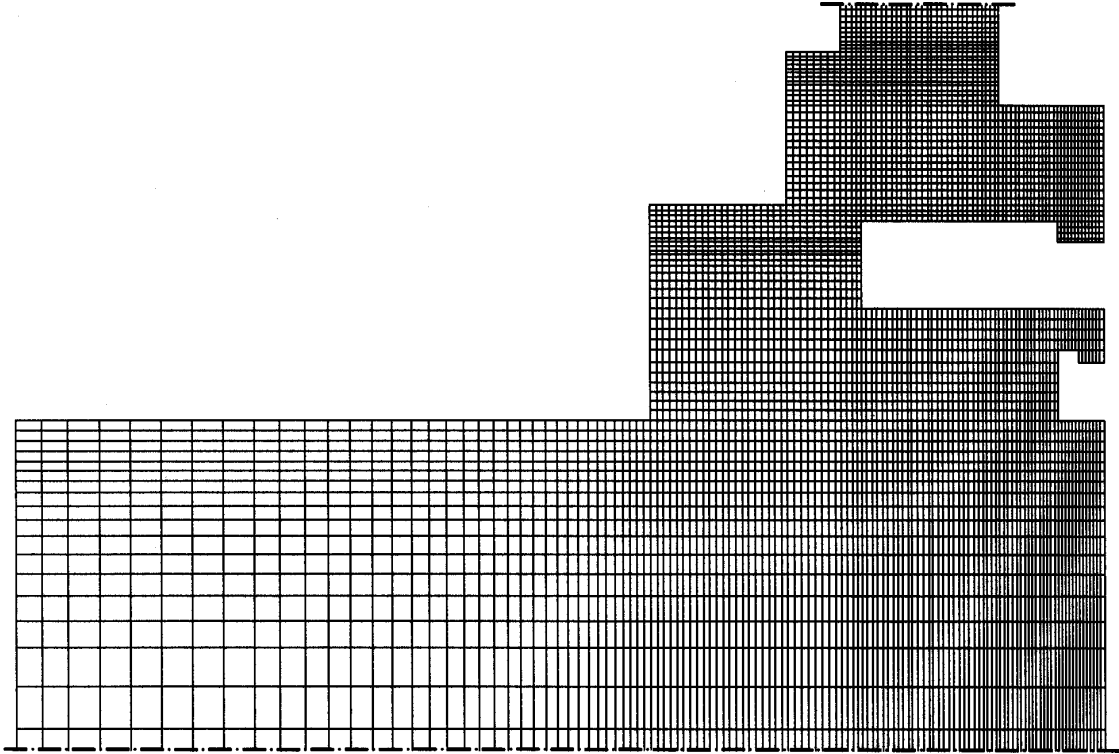
Figure 6.29: Numerical mesh for the frame and the nearest part of the wall.
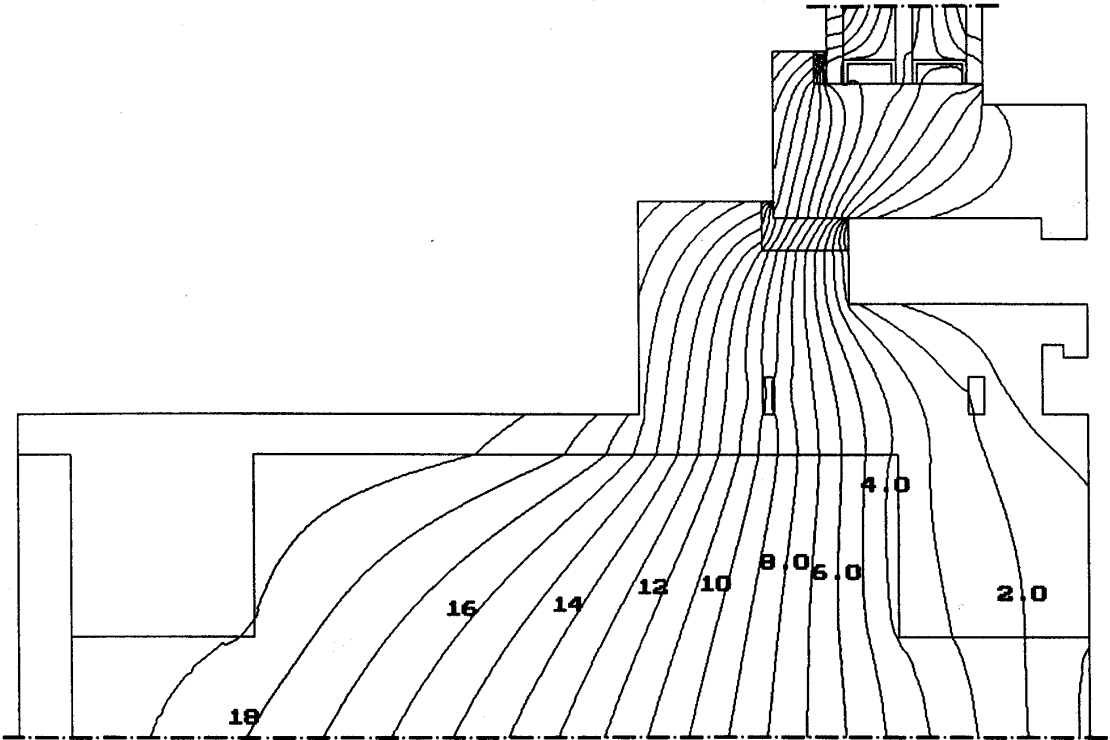
Figure 6.30: Calculated isotherms for the frame and the nearest part of the wall.

6.6.7 Conclusions

Table 6.13 shows the equivalent overall U-values in the three cases. When a window with a measured overall U-value of 2.04 W/(m^{2}K) is mounted in a relatively well insulated wall, one can expect an increase of the U-value of about 10%. This is true if the extra heat losses due to the thermal bridge between the frame and the wall are assigned to the window's U-value. If the window is installed in a non-insulated concrete wall, the U-value increases by 39%.

case	U-value (W/(m^{2}K))	increase
no flow between frame and wall	2.04	
well insulated wall	2.25	10%
non-insulated concrete wall	2.83	39%

Table 6.13: Equivalent U-values.

6.7   Temperature and moisture conditions in attics

6.7.1   Introduction

An unheated attic above a well-insulated ceiling structure is vulnerable to moisture-related damage. The better the standard of thermal insulation, the greater the risk and the smaller the margin of error due to the lower attic temperature and, thus, higher relative humidity. Even minor breaks in the ceiling barrier and small quantities of moist air from inside the house can result in severe problems. There is a risk that moisture will collect in the attic space, giving rise to the growth of mildew, discoloration and, in serious cases, rot, particularly on the inner surface of the roof. In addition, materials stored in the attic space, such as suitcases, cartons, etc. often develop mildew under such conditions and are damaged.

The measurements presented here were performed on a research attic with thermal insulation located under the floor of the attic space (Samuelsson, 1992).

The roof was constructed by mounting a 1 m high "frame" around the edge of the existing roof, which is 30 m long and 10 m wide. New roof trusses were then mounted on this frame, insulation being laid between the ceiling joists, thus producing a cold attic space. This cold space was then divided into eight sections, separated from each other by means of insulation and airtight internal walls at distances of 3.60 m. The ceiling structure above the heated space and below the cold attic consists of 500 mm of loose-fill fibre insulation on plastic film, together with secondary spaced boarding and gypsum planks. There were almost no penetrations through the plastic film.

The exhaust air from the ventilation in the offices in the hut below was discharged to the 1 m high space beneath the joist structure, thus raising its temperature to a range of 20 °C to 28 °C. Two exhaust air fans extracted air from the space, thus preventing a differential pressure across the ceiling structure between the heated area beneath and the cold attic space. Externally, the sloping roof was clad with concrete tiles.

If the outside of the roof is insulated, see Fig. 6.31, the roof itself and the attic space will become somewhat warmer and dryer. If, in addition, attic ventilation is reduced or stopped entirely, there will no longer be the adverse effects that can arise from ventilation, particularly during cold, clear nights. However, stopping the ventilation entirely involves a risk of damage if moisture finds its way into the attic.
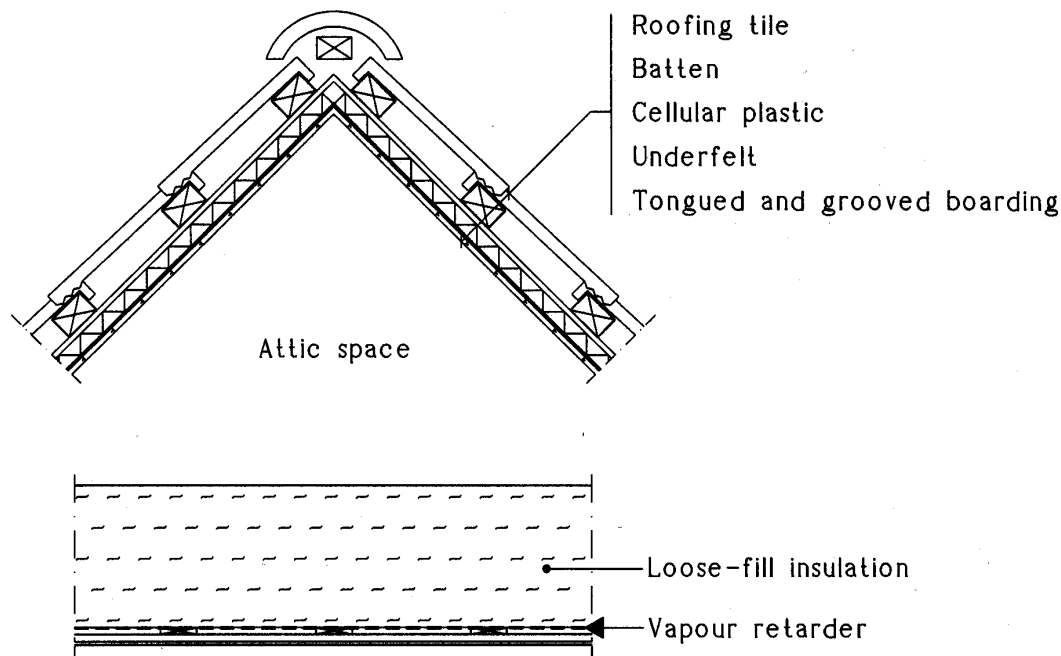
Figure 6.31: Attic with the roof construction as described below for case C.

Along half its length, the hut building adjoins a higher laboratory building. In order to ensure that ventilation was the same for the various sections, mechanical ventilation was installed. Where a particular section was to be ventilated, outdoor air was blown in on the west side by means of a fan and allowed to exit through a conventional air gap beneath the eaves on the east side. Apart from the two air supply ducts entering each section, ventilation at the eaves on the west side was completely blocked. The ridge was non-ventilated, and the air change rate was adjusted to about 2 (h^{-1}).

Of the eight sections, five were used for performance measurements of different designs, see Fig. 6.32. The gable end sections were used as protective buffer zones. The five different attic spaces that were investigated had the following features:

A. Ventilated roof space with a ceiling layer of plastic film.
B. Ventilated roof space with a ceiling consisting of 12 mm plywood with 30 mm of foamed plastic insulation on top of it directly beneath the tiles.
C. Ventilated roof space with a ceiling consisting of 12 mm plywood with 10 mm of foamed plastic insulation on top of it directly beneath the tiles.
D. Reference roof space, of conventional design, i.e. ventilated roof space with a ceiling of 12 mm roofing-grade plywood beneath the tiles. No building paper was used.
E. Unventilated roof space with a ceiling consisting of 12 mm plywood with 30 mm of foamed plastic insulation on top of it directly beneath the tiles.
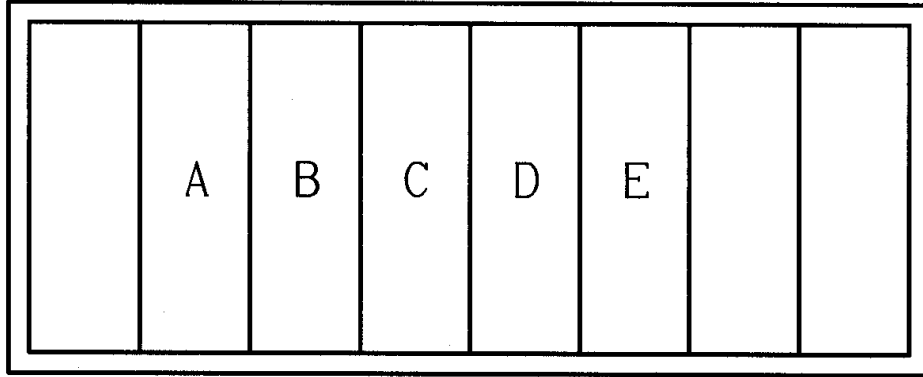
Figure 6.32: Plan of the attic spaces.

The temperature and the relative humidity in the air of the attic spaces were measured and recorded, as were temperatures and RH outdoors and in the space beneath the ceiling joists. Measurements in the air space within the attic were made at a distance of 0.5 m below the ridge. Measurements in the outdoor air were made beneath the east side of the eaves. The sensor positions are shown in Fig. 6.33.

Measurements were also made of the surface temperature and moisture ratio on the underside of the ceiling at three points in each attic space. The moisture ratio was measured as the electric resistance in the wood.

The moisture ratio in the attic space having a ceiling layer of plastic film was measured in the roof truss, about 1 cm from its upper edge. Thus, these values cannot be compared with the moisture ratios and temperatures for the other attics.

6.7.2 Measured results

Measurements were made between July 1991 and January 1992. The values shown in Figs 6.34 and 6.35 are for the week of September 9-16, 1991, with varying temperatures between day and night. The relative humidity is lowest in all cases in the attic section E, i.e. in the unventilated section having thermal insulation in the ceiling. The microclimate in this section of the attic does not change as rapidly in response to rapid changes of the outdoor climate as it does in the other attic sections. This means that, generally speaking, the relative humidity in the unventilated attic space is lower than that in the ventilated attic space, although for brief periods of time it can be at a higher level than that in the other attic spaces. However, averaged over a week, the mean value of relative humidity was always lower than that in the other attic spaces as well as outdoors. This can be seen most clearly in Fig. 6.34. Evaluation of measured values for the autumn week of September 10-16 and for the week of November 19-26 (which is not shown here), gives the weekly mean values for the air temperature and the relative humidity in the different attic spaces shown in Table 6.14. These figures should be compared with those shown in Figs 6.34 and 6.35.
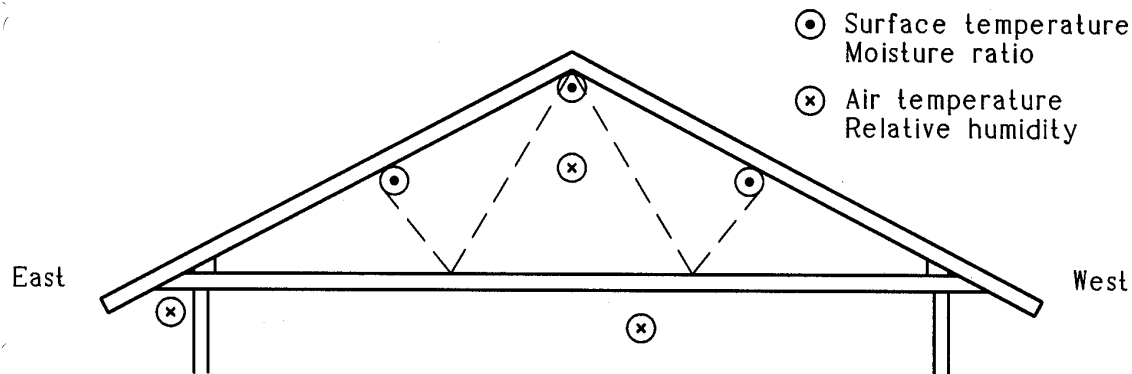
Figure 6.33: Schematic arrangement of sensor positions.

It can be concluded that additional thermal insulation of the upper side of the roof results in a slight improvement of the moisture conditions in the attic space. The thickness of this additional roof insulation is of less importance: no major differences between the sections with 10 mm and with 30 mm of insulation were observed.

measurement point	ventilation	inner surface of the roof	additional insulation	10-16th Sept. temp. (°C)	10-16th Sept. RH (%)	19-26th Nov. temp. (°C)	19-26th Nov. RH (%)
outdoors				11.6	68	2.4	87
A	yes	plastic		12.2	64	2.6	85
D	yes	plywood		12.5	63	3.0	82
C	yes	plywood	10 mm	12.8	60	3.5	78
B	yes	plywood	30 mm	13.0	59	3.7	78
E	no	plywood	30 mm	13.9	55	4.4	74

Table 6.14: Mean values of temperatures and RH in the five attic sections.

More important for the moisture conditions in the attic is the ventilation. An unventilated attic space to which there are no external inputs of moisture will have a mean microclimate that is considerably better than the microclimate in other attic spaces. This applies in particular during periods in which the outdoor climate varies between cold, damp nights and warm days.

It should be pointed out that what is studied here is an attic with no air leakage from the house. Most Swedish houses are built and ventilated in this way. Such buildings are very airtight and the room ventilation system normally creates an underpressure indoors. No potential disadvantages such as workmanship problems, overheating, or reduction in lifetime or strength of the tile roof due to the extra insulation beneath the tiles, have been studied.

RH (%)
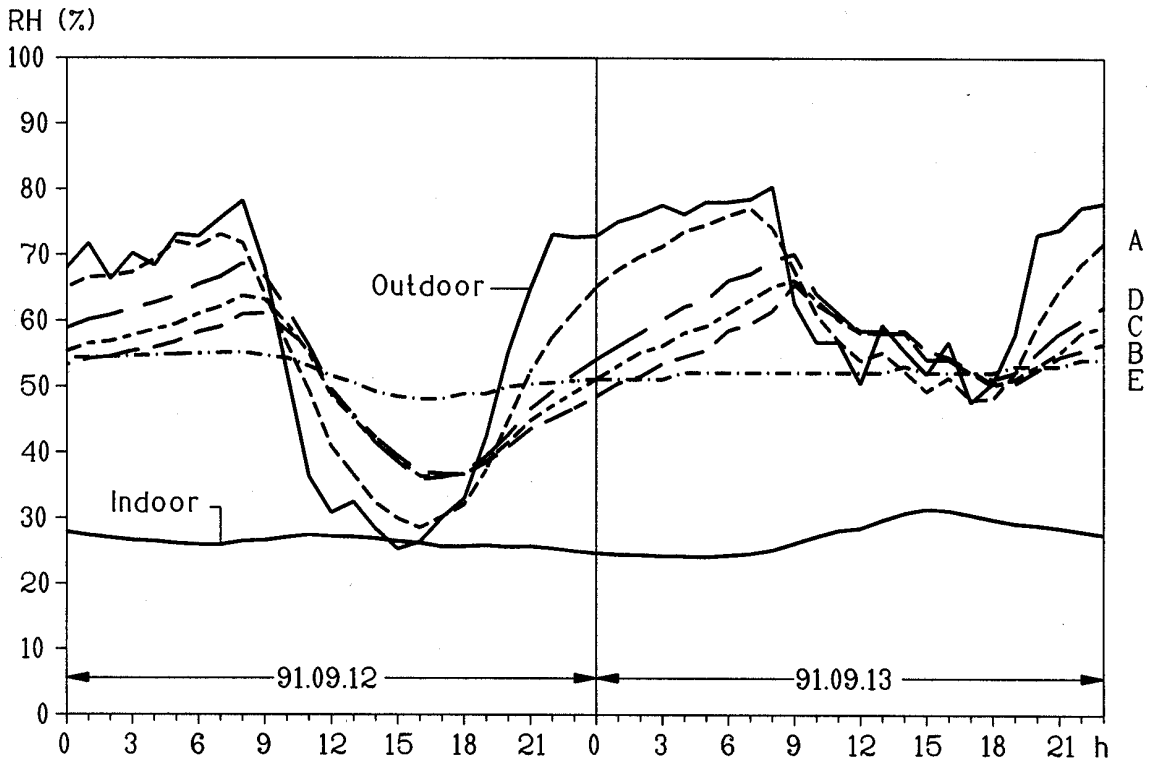
Figure 6.34: Relative humidities in the five attic spaces, September 9-16, 1991.
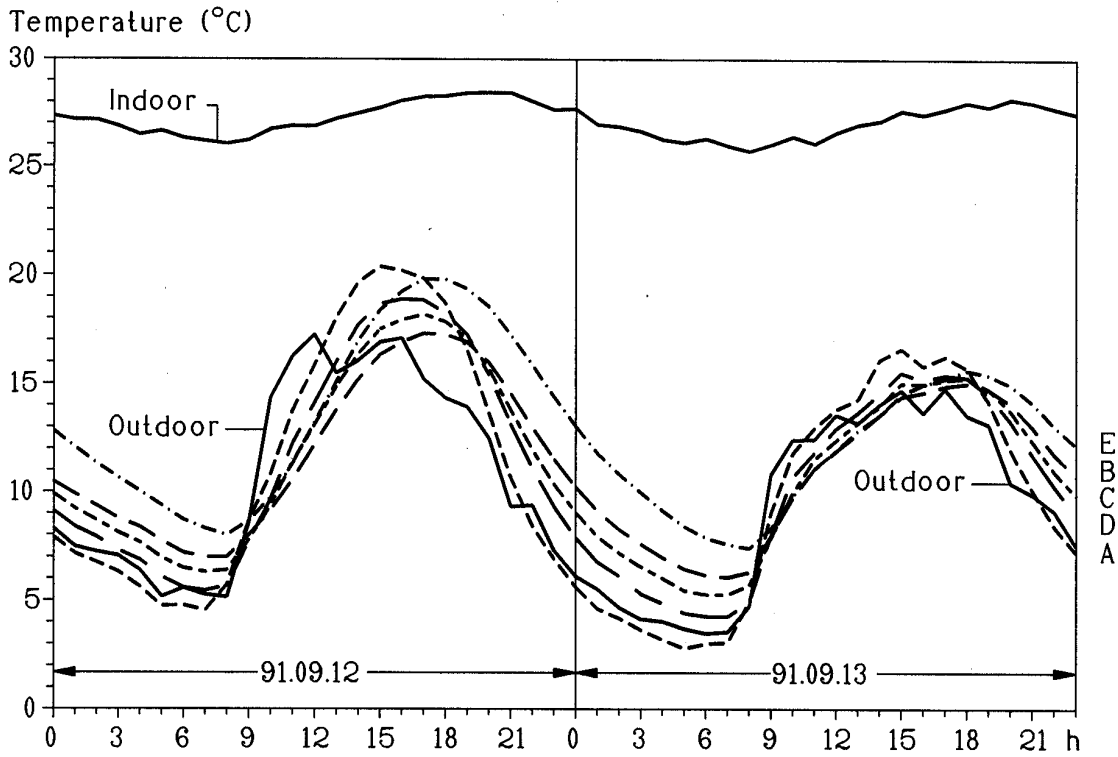
Temperature (°C)

Figure 6.35: Air temperatures in the five attic spaces, September 9-16, 1991.

6.7.3 Calculation model for temperatures

Thermal response factor method

Transient heat flow through the saddle roof and ceiling can be described in terms of response factors. This takes the heat capacity of each part into account. The thermal response factor method was introduced by D.G. Stephenson and G.P. Mitalas (Stephenson et al, 1967a, 1967b, 1971). The response factors for the simulations in this paper were calculated by the computer program TR2, (Blomberg, 1992).

Heat balance in attic

Figure 6.36 shows the symbols used in the equations for the heat balance in the attic. The heat flows through the internal boundaries of the attic depend on the outdoor air temperature T_{air}, the indoor temperature T_{in}, the temperature in the attic T_A, and the thermal response of each part. Solar and long-wave radiation on the roof can be taken into account by introducing an equivalent outdoor temperature T_e. This is further discussed later. Radiation between the inner surfaces of the attic, and between the surfaces indoors, is here neglected. This seems reasonable in light of the intention of this work to study not surface temperatures inside the attic, but only average air temperatures there.
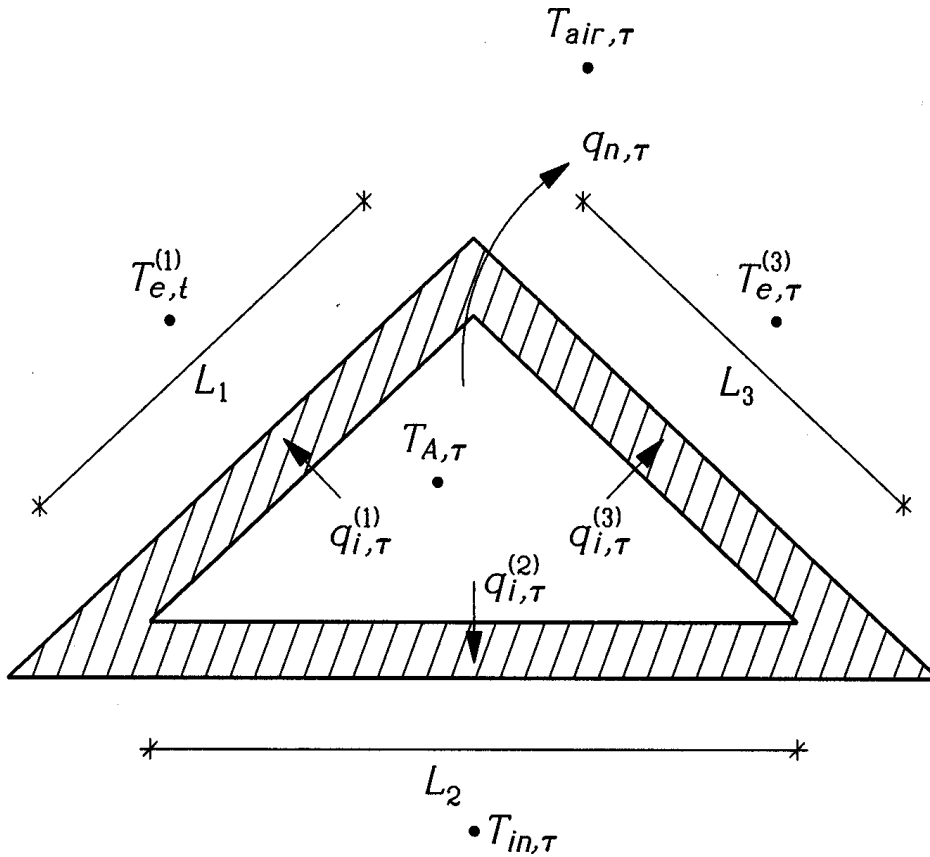
Figure 6.36: Symbols used in the equations.

The heat flow through the internal boundary on the left side of the roof at the time $t=\tau$, see Fig. 6.36, can be written as

$$q_{i,\tau}^{(1)} = \sum_{j=0}^{N} A_j^{(1)} \cdot T_{A,\tau-j} - \sum_{j=0}^{N} B_j^{(1)} \cdot T_{e,\tau-j}^{(1)} + R_1 \cdot q_{i,\tau-1}^{(1)} \quad (W/m^2) \tag{6.53}$$

Here, $T_{e,\tau-j}^{(1)}$ is the equivalent outdoor temperature at the left side at time $\tau - j$, and R_1 is a reduction factor, (Agnoletto, 1976). The response factors $A_j^{(1)}$ give the internal flow due to an internal excitation, and $B_j^{(1)}$ the internal flow due to an external excitation. The summation is to N number of terms, typically between 10 and 50. The flow through the internal boundary on the right side of the roof is dealt with in the same way:

$$q_{i,\tau}^{(3)} = \sum_{j=0}^{N} A_j^{(3)} \cdot T_{A,\tau-j} - \sum_{j=0}^{N} B_j^{(3)} \cdot T_{e,\tau-j}^{(3)} + R_3 \cdot q_{i,\tau-1}^{(3)} \quad (W/m^2) \tag{6.54}$$

The flow through the floor surface in the attic is

$$q_{i,\tau}^{(2)} = \sum_{j=0}^{N} A_j^{(2)} \cdot T_{A,\tau-j} - \sum_{j=0}^{N} B_j^{(2)} \cdot T_{in,\tau-j} + R_2 \cdot q_{e,\tau-1}^{(2)} \quad (W/m^2) \tag{6.55}$$

The heat loss due to air ventilation $q_{n,\tau}$, (W/m), is

$$q_{n,\tau} = 0.33 n V (T_{A,\tau} - T_{air,\tau}) \quad (W/m) \tag{6.56}$$

where n (h^{-1}) is the ventilation rate, V (m^3/m) is the volume of the attic per unit length. An energy balance at $t=\tau$ gives:

$$q_{i,\tau}^{(1)} \cdot L_1 + q_{i,\tau}^{(3)} \cdot L_3 + q_{i,\tau}^{(2)} \cdot L_2 + q_{n,\tau} = 0 \quad (W/m) \tag{6.57}$$

where L_1 and L_3 is the length of each side of the saddle roof and L_2 is the width of the roof. The heat capacity of the air is neglected. This equation is solved iteratively. The calculation takes typically a few seconds on a PC.

6.7.4   Calculated temperatures

Data used in simulations

Table 6.15 shows the first set of data used in the numerical simulations. The width and height of the attic are 9.3 m and 2 m, respectively. The indoor temperature ranges from about 26 °C in the night to 28 °C in the day. The outside surface resistance is put to 0.04 m^{2}K/W. The surface resistance indoors and on the inside surfaces of the attic are 0.13 m^{2}K/W. In case E, the attic is unventilated. For all other cases, the ventilation rate is $n=2$ h^{-1}. The response factors are calculated based on hourly values. Calculated and measured temperatures are compared during a period of 24 hours for September 13, 1991. The calculations were actually performed for 36 hours, the last 12 hours of the day before being included in order to account for the previous history.

material	appearing in cases	thickness (m)	thermal cond. (W/(m·K))	volumetric heat cap. (J/(m^{3}K))
roof clay brick	A,B,C,D,E	0.020	0.6	1200000
polyethylene film	A	-	-	-
plywood	B,C,D,E	0.012	0.14	700000
cellular plastic	B,E	0.030	0.036	30000
cellular plastic	C	0.010	0.036	30000
attic floor insulation	A,B,C,D,E	0.500	0.045	30000

Table 6.15: First set of data used in the numerical simulations.

Calculated temperatures with no account for radiation

As a first approach, the solar and long-wave radiation are neglected. This is due to the fact that no data for solar radiation or surface temperatures on the roof are available. Radiation is neglected by letting $T_{air}=T_e$. Figures 6.37-6.39 show the results.
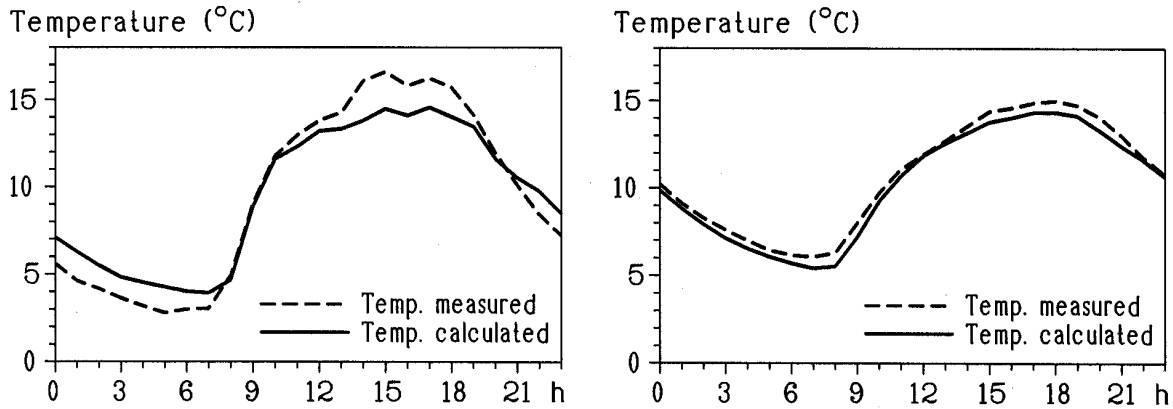
Figure 6.37: Temperature in the attic for case A (left) and case B (right).
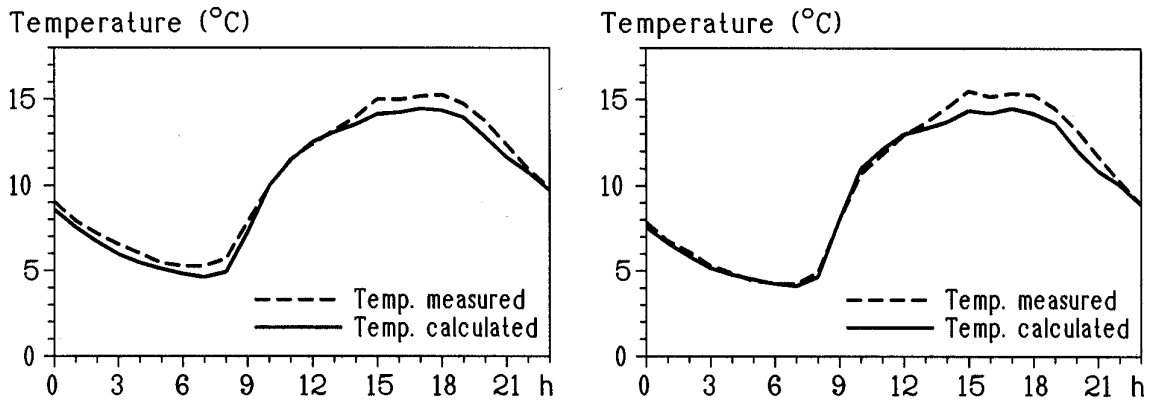
Figure 6.38: Temperature in the attic for case C (left) and case D (right).

96
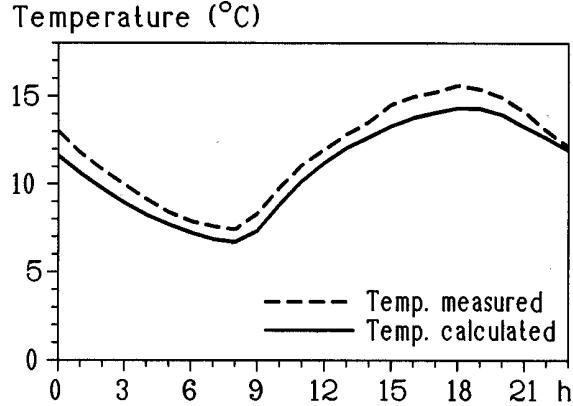
Figure 6.39: Temperature in the attic for case E (unventilated attic).

Table 6.16 shows the maximum difference between the calculated and measured temperatures. The second and third columns give the maximum positive difference between the calculated and the measured temperatures, and the hour when it occurred. The fourth and fifth columns give the maximum negative deviation.

case	max pos. dev. ($^\circ$C)	hour	max neg. dev. ($^\circ$C)	hour
A	1.7	1	2.3	14
B	(always below)	-	0.8	9
C	0.1	12	0.9	20
D	0.3	10	1.1	15
E	(always below)	-	1.4	0

Table 6.16: Maximum deviations of calculated and measured temperatures. No radiation.

During the day, the calculated temperatures for all the cases are generally below the measured ones. This is probably due to sunlight. The same is also true during nighttime, except for case A. Figure 6.35 indicates that the measured temperatures between nine o'clock in the evening and seven o'clock in the morning are below the outdoor temperatures. This is due to long-wave radiative heat loss to the sky. At night, the equivalent T_e should be smaller than T_{air}. The agreement for the other cases would be worse if T_e were lower than T_{air}.

Sensitivity analysis for case C

A sensitivity analysis was carried out for case C, see Table 6.17. No systematic variations are made, only changes of some data that reflects the uncertainty of the input. The calculated temperatures for every variation are compared with the temperatures calculated with the previous set of data according to Table 6.15. Maximum positive and negative deviations are shown here. The results indicate a small sensitivity for the changes made.

97

case	max pos. dev. (°C)	hour	max neg. dev. (°C)	hour
ventilation n=1	0.4	0	0.2	10
ventilation n=3	0.2	10	0.3	0
volume 20% larger	0.0	-	0.0	-
Roof (cellular plastic)				
λ=0.045 (+25%)	0.1	10	0.2	0
C=0.060 (+100%)	0.0	-	0.0	-
d=12.5mm (+25%)	0.2	0	0.0	10
Attic floor insulation				
λ=0.050 (+25%)	0.1	0	-	-
C=0.080 (+270%)	0.3	3	0.2	15

Table 6.17: Sensitivity analysis for case C.

Approximate formulas for radiation

An equivalent outdoor temperature models the effect of solar radiation, net long-wave radiation heat exchange, and the convective heat transfer. Approximate formulas for horizontal and vertical surfaces are given in (Höglund, 1973). The following two equations describe the equivalent temperature during day and night:

$$T_{e,day} = T_{air} + \frac{aI}{\alpha} - \frac{(9-m)}{9}(3.47 - 0.053 \cdot T_{air}) \tag{6.58}$$

$$T_{e,night} = T_{air} - \frac{(9-m)}{9}(4.57 - 0.07 \cdot T_{air}) \tag{6.59}$$

where a is the absorptance, and α, (W/(m²K)), the heat transfer coefficient for the surface. The outdoor air temperature is denoted by T_{air}. The solar intensity I, (W/m²), is given in (Höglund et al, 1985), (*Solinstrålningstabeller för helklara, halvklara och mulna typdagar*). The shading due to cloudiness is described by a cloudiness coefficient m, (Taesler, 1972), where m=0 refers to a completely clear sky and m=8 to a completely cloudy one. The cloudiness coefficient at 13.00 h was m=3 according to SMHI (*Swedish Meteorological and Hydrological Institute*). Table 6.18 shows the results obtained where Eq. (6.58), and (6.59) are used with solar intensity data from (Höglund et al, 1985). The absorptance coefficient is put to 0.8, and the surface heat transfer coefficient is put to 25 W/(m²K). The large deviations may be explained by these uncertain parameters and formulas.

case	max pos. dev. (°C)	hour	max neg. dev. (°C)	hour
A	10.1	12	2.5	20
B	5.7	14	2.2	4
C	8.2	13	2.8	4
D	10.0	12	3.0	21
E	7.8	14	3.5	3

Table 6.18: Deviations in temperature taking radiation into account.

6.7.5 Moisture conditions in the attics

Figures 6.40-6.44 show the relative humidities (RH) in the five attics (910913). Comparisons are made with calculated values, computed in the following way. Measured RH and temperature outdoors give the outdoor vapour concentration. This is assumed to be the same inside the attic, since there is no extra moisture transport through the floor from the indoor side. The calculated relative humidity inside the attic is based on the calculated temperatures (radiation being neglected).

The calculated RH is in most cases slightly higher than the measured one. This may reflect that the calculation model does not take any account of the moisture capacity.
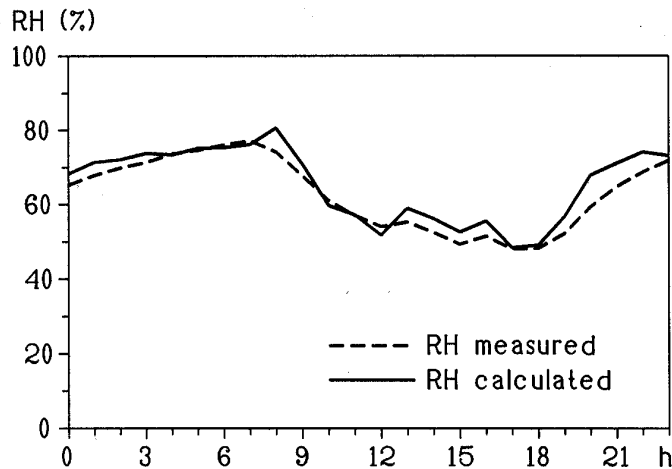
Figure 6.40: Relative humidity in the attic for case A.
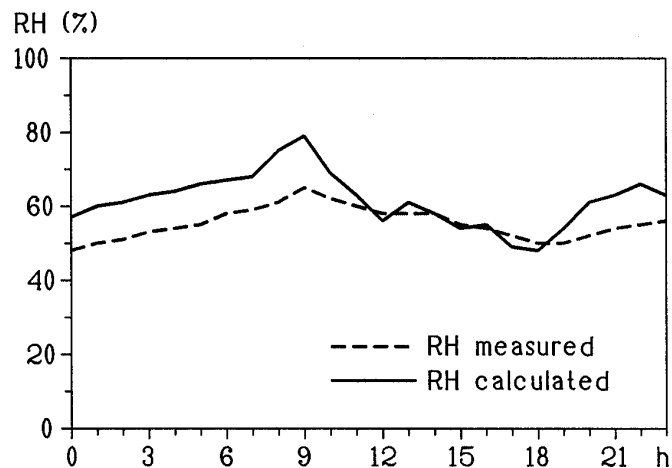
Figure 6.41: Relative humidity in the attic for case B.
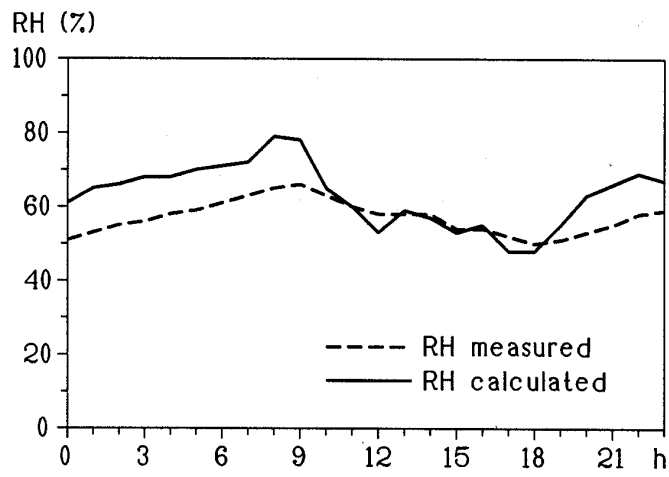
Figure 6.42: Relative humidity in the attic for case C.
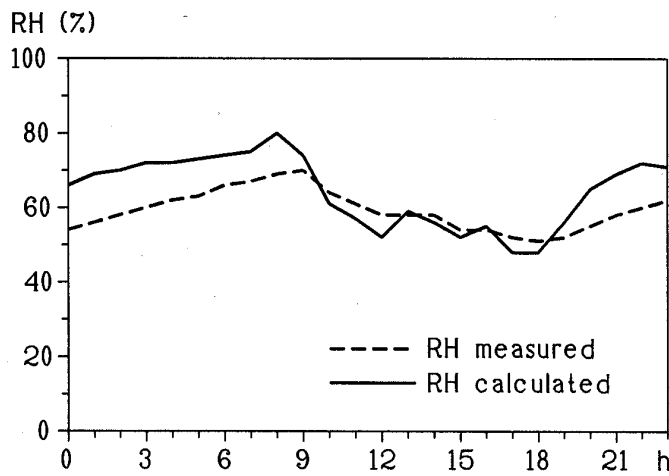
Figure 6.43: Relative humidity in the attic for case D.
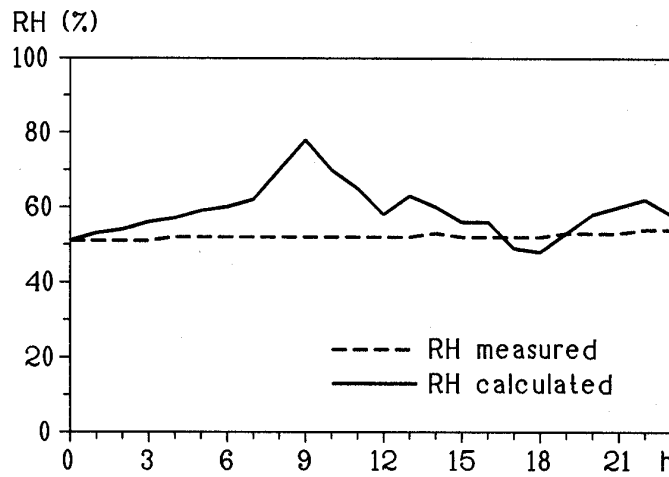
Figure 6.44: Relative humidities in the attic for case E (unventilated attic).

100

6.7.6 Conclusions

Calculations of temperature and moisture conditions in different types of attics were compared with experimental data provided by the Swedish National Testing and Research Institute, (Samuelsson, 1992).

There was relatively good agreement between measured and calculated temperatures, typically within two degrees °C when radiation was neglected. The agreement for the relative humidities was sometimes not as good, probably because the calculation model does not take any account of the moisture capacity.

The measurements and calculations indicate that an attic with an insulated top roof has a warmer and drier climate than a conventional cold attic. This allows the attic to function satisfactorily with only a small degree of ventilation. Variations in temperature and RH are also smaller under such conditions. This makes it a safer place for storing furniture and other possessions.

6.8 Insulated wall with slotted steel U-girders

6.8.1 Introduction

An insulated wall may be supported internally by thin steel girders. Calculation of the heat transmittance is a difficult numerical problem due to the high ratio of thermal conductivity between the insulation and the steel. The study that follows presents three-dimensional numerical calculations for a particular problem of this type. The proper choice of a numerical mesh is discussed. The dependence of the obtained U-value on a number of different parameters is dealt with.

Figure 6.45 shows the structure of a wall in which insulation is contained between two gypsum boards of 13 mm thickness each. The distance between the metal U-girders is denoted by L_g. There is an extra heat loss caused by the metal U-girders. This heat loss can be reduced by slitting the web of the U-girders perpendicular to the heat flow direction, as shown in Fig. 6.46. The thickness of the girder is denoted by t. The considered girder is manufactured by the Swedish firm Lindab Profil AB.
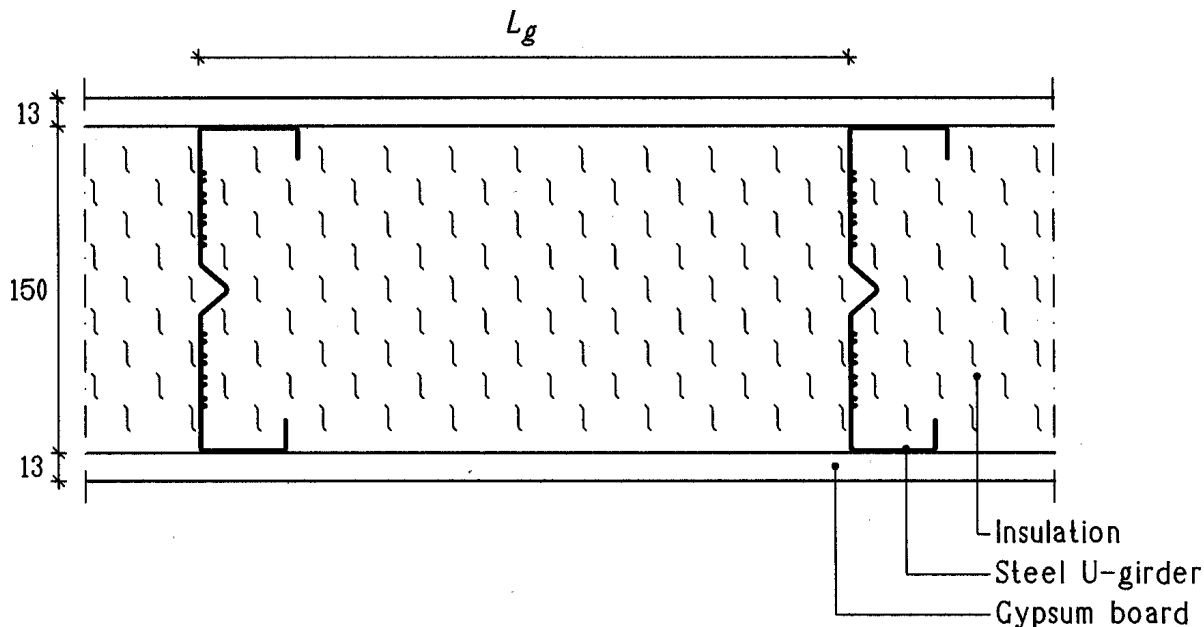
Figure 6.45: Principle sketch of a wall with metal U-girders between two gypsum boards.

6.8.2 Data for the numerical simulation

The problem is not perfectly symmetric due to different flange lengths (40 and 46 mm, see Fig. 6.46). However, this is neglected in the calculations, and the left flange length (46 mm) is used for both sides. The Swedish standards normally prescribe that the sum of the inner and outer surface resistances is 0.17 m^{2}K/W for U-value calculations. The inner and the outer surface resistances are put to half this value (0.085 m^{2}K/W) in the calculations that follow. The elevated part in the middle of the web is neglected, the web being modelled as being straight, as shown in Fig. 6.46 by the dashed lines. This will give

103

a slightly overestimated value for the heat flow through the wall (probably overestimated by less than 1%). The slitting process causes small elevated rims, as shown in Fig. 6.46. These rims are neglected in the calculations, and the effect of this is discussed later.
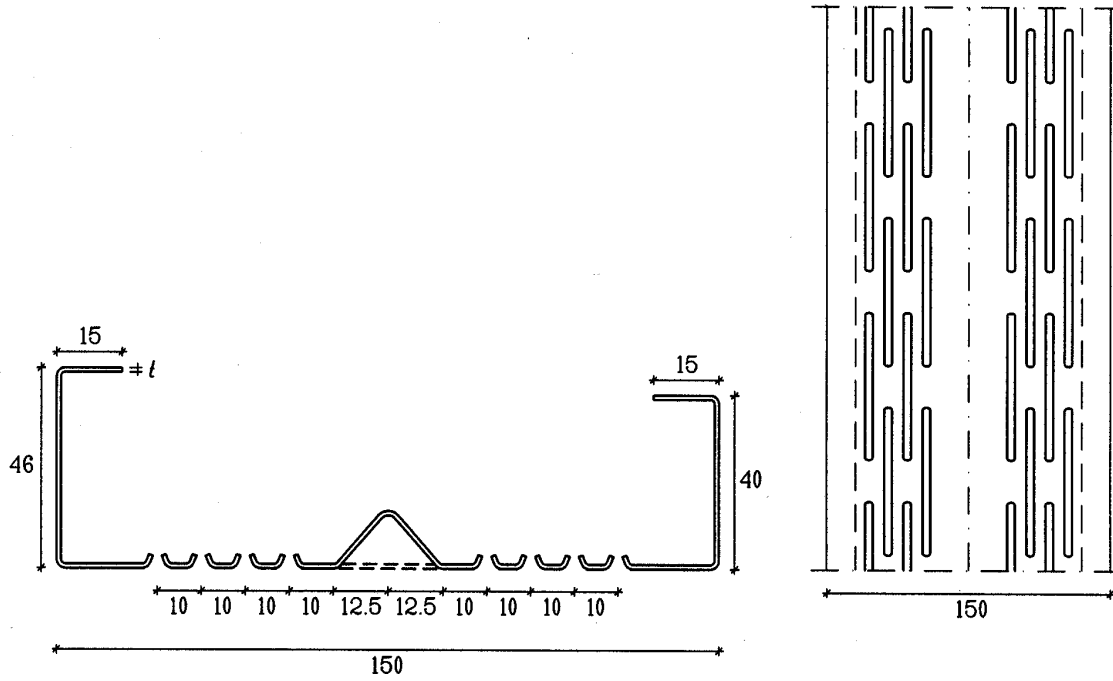
Figure 6.46: Slotted steel girders (cross-section to the left) decreases the heat conduction.

The calculations have been made for the shaded volume shown in Fig. 6.47. The height (perpendicular to the plane in Fig. 6.45) is denoted by s. The temperature in the air is 0 °C on one side of the wall and 0.5 °C at the symmetry line. The thermal conductivity is 0.036 W/(m·K) and 0.22 W/(m·K) for the insulation and the gypsum, respectively.

The number of cells required to obtain satisfactory numerical accuracy depends on various parameters, such as geometry, materials, and boundary conditions. The following criterion has been recommended as a European standard (CEN, 1995). The sum of the absolute values for all the heat flows entering the object is calculated twice, once for n cells and once for $2n$ cells. The relative difference between the flows needs to be smaller than 2%. If not, further division of the mesh is required. Since this requirement may in many cases be too lenient, however, the relative difference is taken here to be ten times smaller, i.e. 0.2%. Having about 30000 cells placed in an expansive mesh satisfied this criterion for the case considered. In this case, the numerical error becomes less than 1%, compared to the result from a calculation using 250000 cells. Simulations with 30000 and 250000 cells took 10 minutes and 2 hours, respectively, on a Pentium/90. Figure 6.48 shows the projection of the numerical mesh on the (x, y)-plane and the (x, z)-plane in the case involving 30000 cells. The position of the steel girder is shown by the thicker lines. The over-relaxation coefficient was put to $\omega = 1.95$.

104
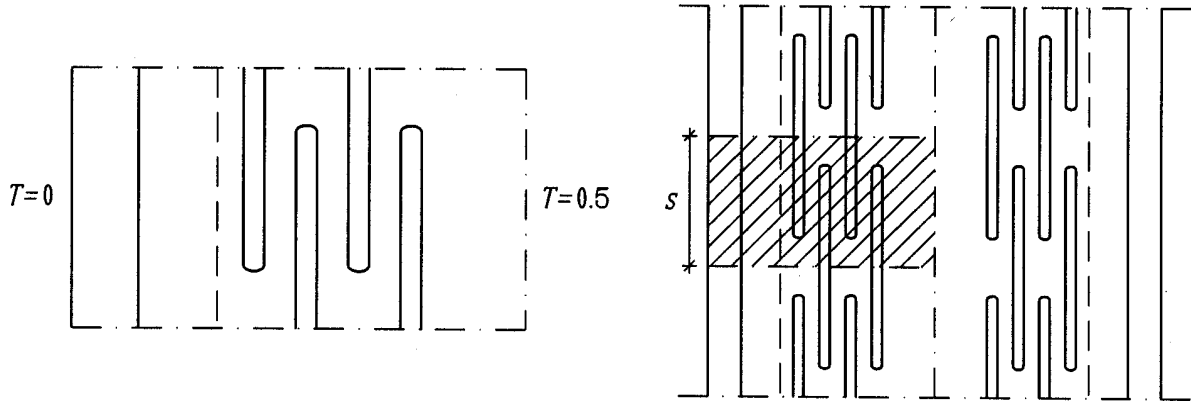
Figure 6.47: The part of girder used in the simulations.

6.8.3 Reference case

An initial numerical simulation is presented for a reference case involving the following data. The thermal conductivity of the steel is put to λ_s=60 W/(m·K). The distance between the girders is L_g=0.6 m and the thickness of the steel is t=0.7 mm, see Figs 6.45 and 6.46. The calculated heat flow through the wall becomes Q_{calc}=0.00787 W/K. The extra heat loss Q_{extra} due to the steel is

$$Q_{extra} = Q_{calc} - U_{1d} \cdot L_g \cdot s = \tag{6.60}$$

$$= 0.00787 - 0.225 \cdot 0.6 \cdot 0.05 = 0.00112 \quad \text{W/K}$$

Here U_{1d} is the U-value of the wall without a girder. The total thermal resistance is $0.17+2\cdot0.013/0.22+0.150/0.036=4.44$ m^{2}K/W, and U_{1d} becomes $1/4.44=0.225$ W/(m^{2}K).

6.8.4 Varying the distance between the girders

The U-value of the wall varies with the distance between the girders L_g. As L_g increases the U-value will approach the U-value of the wall without the girders U_{1d}. It is reasonable to assume that the extra heat loss for each girder is the same as in the reference case, Q_{extra}. This allows the following approximation of the U-value as a function of L_g:

$$U = \frac{Q_{extra}}{L_g \cdot s} + U_{1d} = \frac{0.00112}{L_g \cdot 0.05} + 0.225 = \tag{6.61}$$

$$= 0.0224/L_g + 0.225 \quad \text{W/(m}^2\text{K)}$$

Equation (6.61) is valid for center-to-center distances large enough that the heat flows due to any two girders that are adjacent to each other have negligible influence on each other. Numerical tests show that a center-to-center distance of 0.1 m gives an error of 2% as compared to Eq. (6.61). The error increases with decreasing distance. However, the distances are in reality much larger than 0.1 m.
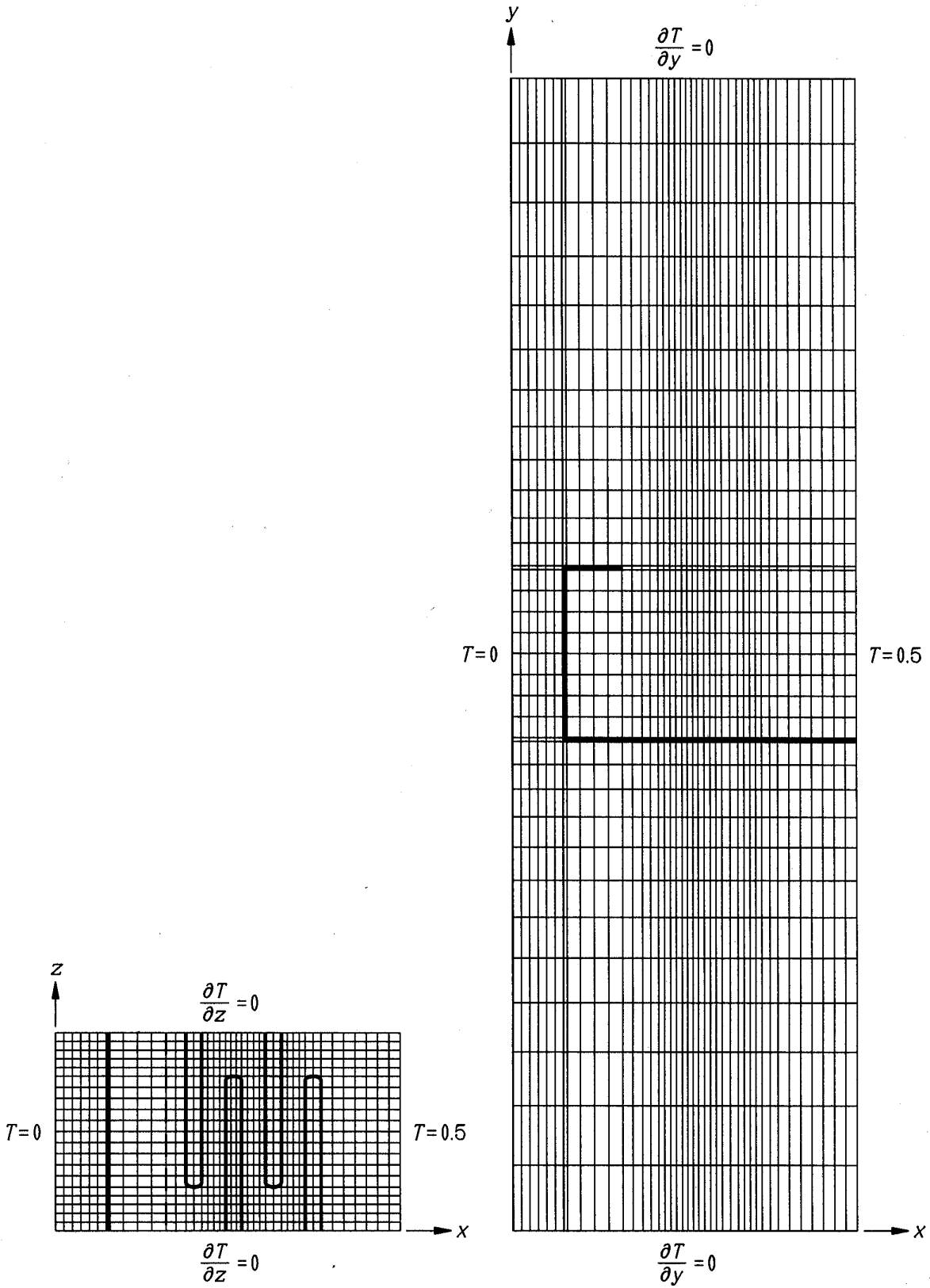
Figure 6.48: Projection of numerical mesh on the (x, y)-plane and the (x, z)-plane in the case involving about 30000 computational cells.

6.8.5 Varying the thermal conductivity of the steel

The thermal conductivity of the steel is much greater than the thermal conductivity of the insulation. Therefore, the heat flow between the steel and the insulation should be relatively small compared with the flow along the steel. Separating the problem into two cases and adding the two flows turns out to provide a rather good approximation.

In the first case, the steel is not taken into account. The one-dimensional flow with a temperature difference of 1 is $U_{1d} \cdot L_g \cdot s = 0.225 \cdot 0.6 \cdot 0.05 = 0.00675$ W/K.

The second case considers the flow in the steel and the gypsum only. The boundary condition between the steel and the insulation, and between the gypsum and the insulation, is adiabatic. Numerical simulation gives for λ_s=60 a heat flow of 0.00105 W/K. The flow is essentially proportional to the thermal conductivity of the steel. Thus, heat flow as a function of λ_s, becomes $0.00105 \cdot (\lambda_s/60) = 17.5 \cdot 10^{-6} \cdot \lambda_s$. Adding the two contributions gives the following approximate formula:

$$Q_{calc} = 0.00675 + 17.5 \cdot 10^{-6} \cdot \lambda_s \quad \text{W/K} \tag{6.62}$$

This equation is shown in Fig. 6.49 as *Fitted curve 1*. The black triangles show Q_{calc} from direct numerical calculations for different λ_s. It is clear from the figure that a better approximation can be achieved for thermal conductivities when a limited range is considered. A straight line between values for λ_s=10 and λ_s=60 gives

$$Q_{calc} = 0.00696 + 15 \cdot 10^{-6} \cdot \lambda_s \quad \text{W/K} \tag{6.63}$$

This equation is shown in Fig. 6.49 as *Fitted curve 2*.

At this point one can provide an approximate expression for the U-value as a function of L_g and λ_s. On the basis on Eqs (6.60) and (6.61), the fitted curve 2 according to Eq. (6.63) gives with s=0.05 m:

$$U = \frac{0.00696 + 15 \cdot 10^{-6} \cdot \lambda_s - 0.225 \cdot L_g \cdot s}{L_g \cdot s} + 0.225 = \tag{6.64}$$

$$= \frac{0.0042 + 0.0003 \cdot \lambda_s}{L_g} + 0.225 \quad \text{W/(m}^2\text{K)}$$

Table 6.19 shows U-values based on Eq. (6.64). The U-values obtained from direct numerical calculations are given in brackets. The error is less than 2%.

λ_s	L_g=0.3 m	L_g=0.6 m	L_g=1.0 m	L_g=0.1 m
60	0.299 (0.300)	0.262 (0.262)	0.247 (0.246)	0.447 (0.456)
40	0.279 (0.282)	0.252 (0.253)	0.241 (0.241)	
20	0.259 (0.263)	0.242 (0.243)	0.235 (0.235)	
10	0.249 (0.252)	0.237 (0.237)	0.232 (0.232)	

Table 6.19: U-values based on Eq. (6.64) and on numerical calculations (in brackets).
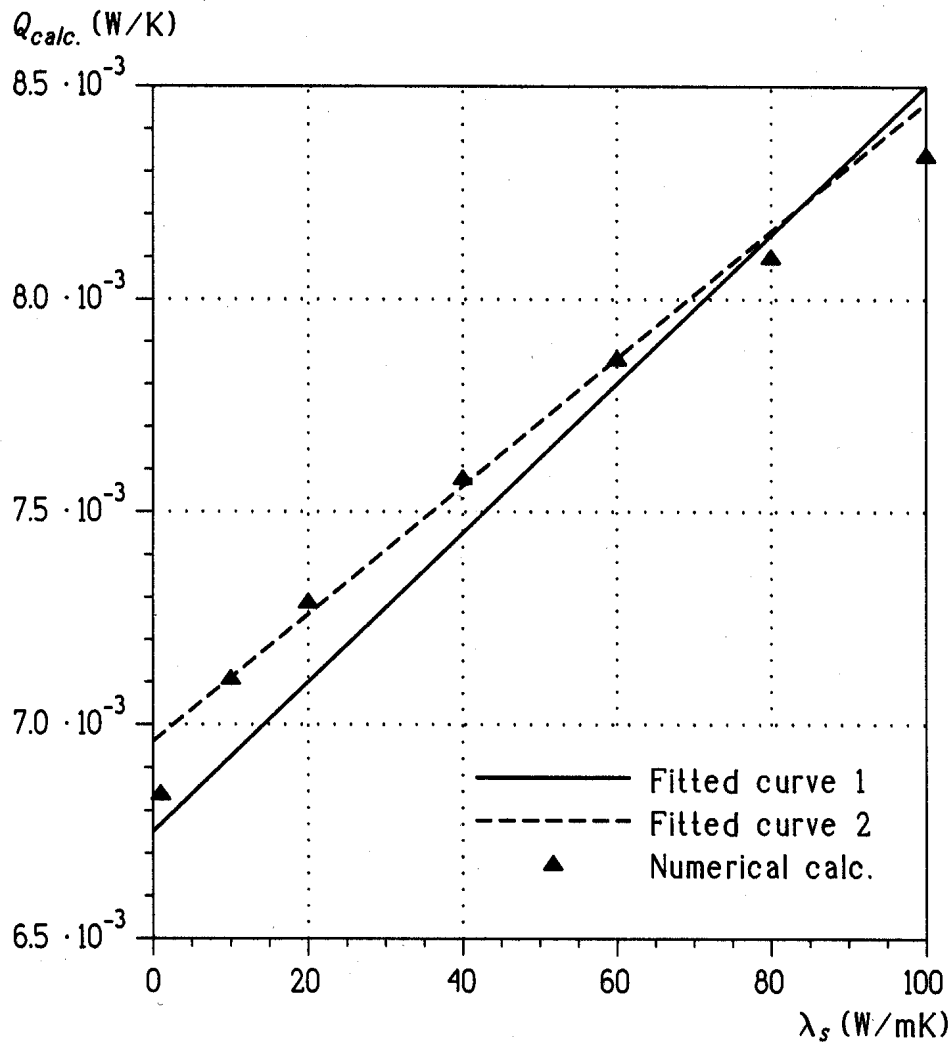
Figure 6.49: Heat flows as a function of λ_s based on the calculations.

6.8.6 Varying the thickness of the steel

Since the heat flow in the steel is approximately proportional to λ_s, one can assume that it is also proportional to the thickness of the steel t. Equation (6.64) is then modified to

$$U = \frac{0.0042 + 0.0003 \cdot \lambda_s \cdot t/0.0007}{L_g} + 0.225 =$$

or, as in the final formula for different L_g, λ_s, and t:

$$U = \frac{0.0042 + 0.43 \cdot \lambda_s \cdot t}{L_g} + 0.225 \qquad \text{W/(m}^2\text{K)} \tag{6.65}$$

$$L_g > 0.1\,\text{m} \qquad \lambda_s \geq 10\,\text{W/(m·K)} \qquad t \geq 0.0001\,\text{m}$$

Table 6.20 shows U-values for various values of t, L_g, and λ_s based on Eq. (6.65). The results obtained from the numerical calculations are in brackets. The maximum error is 2%. It may be noted that it is possible to establish an equation that also takes into account the wall thickness H and the thermal conductivity of the insulation λ_{insul}. Thus, the U-value could easily be calculated as a function of $U=f(\lambda_s, L_g, t, \lambda_{insul}, H)$.

t	λ_s	L_g	U
1	60	0.6	0.275 (0.272)
1.5	60	0.6	0.296 (0.289)
1	10	1.0	0.233 (0.233)
1.5	10	0.3	0.260 (0.265)

Table 6.20: U-values based on Eq. (6.65) and on numerical calculations (in brackets).

6.8.7 Girders without slots

Numerical calculations have also been made for a wall with girders without slots (λ_s=60, t=0.7 mm, and L_g=0.6 m). The U-value becomes U=0.413 W/(m^{2}K), which is 83% larger than the U-value for the wall alone (0.413/0.225=1.83). A wall with slotted girders, according to Table 6.19, has only 16% greater heat flow than a wall without any girder (0.262/0.225=1.16). If λ_s=20 W/(m·K), the U-value becomes 6% larger (0.242/0.225=1.06).

Another way to express this is to compare the wall above (U=0.413 W/(m^{2}K)) with a wall containing slotted girders of the steel possessing higher thermal conductivity. According to Eq. (6.65), a wall with a slotted girder in which λ_s=360 W/(m·K), or t=4.2 mm, has the same U-value 0.413 W/(m^{2}K). This shows that either the thermal conductivity or the thickness has to be decreased by a factor of six to make up for the slots. The heat flow through a girder will decrease even more with an increase in the number of narrow slots.

This underlines again the importance of an efficient slitting of the steel. Figure 6.50 illustrates this further. The temperature field along the steel web is shown here for the reference case. The path for the heat flow is increased several times.

6.8.8 Slitting the flanges

The flanges act as collectors of heat. If the flange length L_{flange} in Fig. 6.51 is decreased, the U-value will also decrease. Table 6.21 shows U-values for λ_s=60 W/(m·K), t=0.7 mm, and L_g=0.6 m obtained from two-dimensional calculations for a wall with girders without slots.
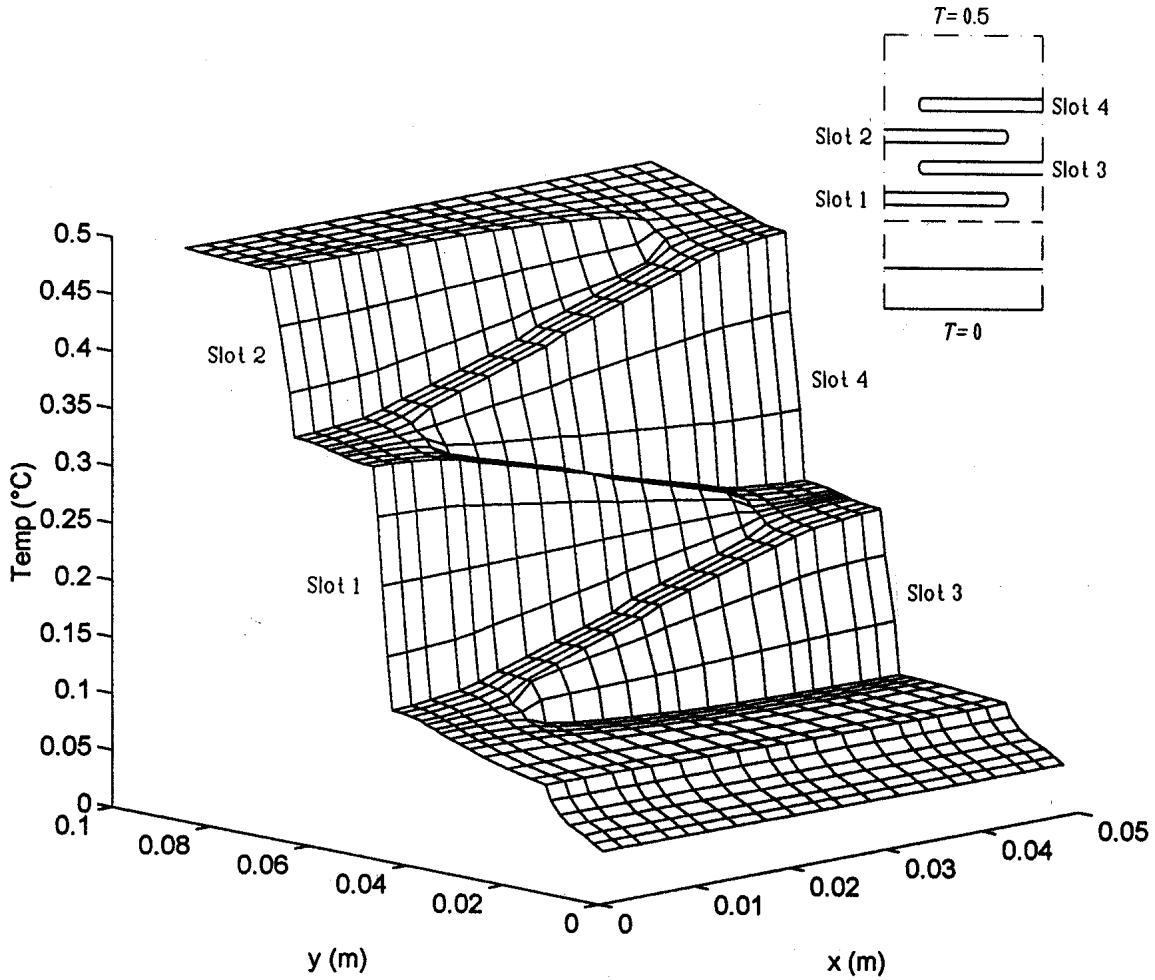
Figure 6.50: Temperature field along the steel (with slots).

It is clearly better to use shorter flanges. This may be difficult due to structural constraints. However, the flanges could instead be slotted. This would decrease the U-value for the same reason as in the case of the shorter flanges.

L_{flange}	U (W/(m²K))	lowered U-value
0.046	0.413	-
0.020	0.389	6%
0.005	0.347	16%

Table 6.21: U-values for different flange lengths.
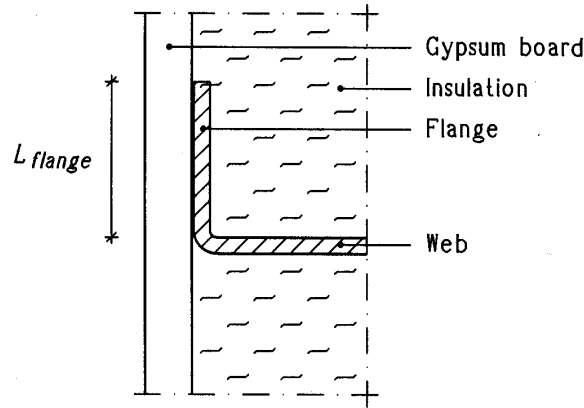
Figure 6.51: The heat flow along the web decreases as L_{flange} decreases.

6.8.9 Heat transfer within the slots

The cavities formed by the slots will probably be filled with air instead of insulation. In the numerical computations this space is assumed to be filled with insulation material. The following discussion concerns an estimate of the amount of heat transferred by radiation and convection inside these air gaps.
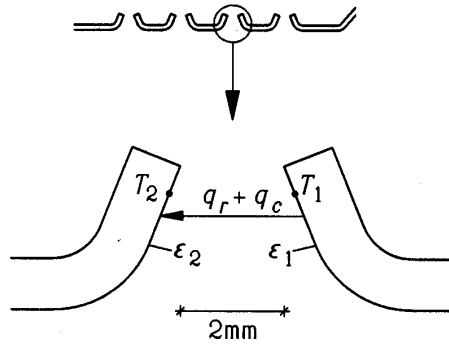
Figure 6.52: Heat transferred by radiation and convection in air gaps in slots.

The size of a gap is $D=2$ mm according to Fig. 6.52. One is on the safe side in assuming that the two opposite sides represent infinite and parallel surfaces. The heat flow between two parallel surfaces may be approximated by a radiative term, q_r, and a convective term, q_c. The convective term also includes heat transfer by conduction. The radiative and convective heat transfer coefficients are denoted by α_r and α_c, respectively. This gives

$$q = q_r + q_c = (\alpha_r + \alpha_c) \cdot (T_1 - T_2) = \frac{\lambda_e}{D} \cdot (T_1 - T_2) \quad (\text{W/m}^2) \tag{6.66}$$

The radiative coefficient, α_r, is according to (Siegel et al, 1992)

$$\alpha_r = 4 \cdot \epsilon_{12} \cdot \sigma_s \cdot T_m^3$$

where

$$\frac{1}{\epsilon_{12}} = \frac{1}{\epsilon_1} + \frac{1}{\epsilon_2} - 1, \quad \sigma_s = 5.67 \cdot 10^{-8} \quad \text{W/(m}^2\text{K}^4)$$

The emissivity of the surfaces, ϵ_1 and ϵ_2, is put to 0.2, which gives ϵ_{12}=0.1. The mean temperature T_m is put to 283 K. This gives α_r =0.52 W/(m^{2}K). The convective heat flow is due mainly to conduction, (Holman, 1986), the coefficient α_c becoming:

$$\alpha_c = \lambda_{air}/D = 0.025/0.002 = 12.5 \quad \text{W/(m}^2\text{K)}$$

The equivalent thermal conductivity λ_e, using Eq. (6.66), is then:

$$\lambda_e = (\alpha_r + \alpha_c) \cdot D = 0.026 \quad \text{W/(m·K)}$$

If ϵ_1 and ϵ_2 are put to 0.9 the equivalent thermal conductivity becomes 0.033 W/(m·K).

We see that the heat transferred by radiation and convection inside the gaps is about the same as that transferred by pure conduction in the insulation. Thus, the heat flow between the gaps is negligible compared with the flow along the steel.

6.8.10 Steel U-girders compared with wooden cross bars

It is interesting to compare the U-value for a wall having steel U-girders with that of a wall having wooden girders placed in the same position. Calculations show that, for λ_s=60, t=0.7 mm, and L_g=0.6 m, the reference wall containing slotted steel girders has the same U-value as a wall with 0.04 m thick wooden girders with thermal conductivity of 0.14 W/(m·K). A wall with 0.22 m thick wooden girders would have the same heat loss as a wall with non-slotted girders.

6.8.11 Conclusions

Using slotted steel girders is an efficient way of decreasing the heat flow. One example showed that either the thermal conductivity or the thickness of the steel had to be decreased by a factor of six to make up for the slitting. The heat flow through a girder decreases as the number of narrow slots increases.

Equation (6.65) gives a U-value that depends on the thermal conductivity of the steel λ_s, the center-to-center distance between the girders L_g, and the steel thickness t. The error is less than 2% compared with direct three-dimensional numerical calculations.

As a third conclusion it has been shown that a rather complex, genuinely three-dimensional problem can be solved on a PC. Some 30000 nodal points are sufficient to give a numerical error of less than 1%. The CPU-time is about 10 minutes on a Pentium/90. The simulation time for the case with 250000 cells was about 2 hours.

Further studies of thermal bridge effects due to steel can be found in (Elmroth, 1985) and (Jóhannesson, 1981).

6.9 Heat flow through a corner

6.9.1 Introduction

The next example is a test reference case in the European standards (CEN, 1995). Figure 6.53 shows the problem from two different viewpoints. There are two walls that meet in a corner, and a floor element. Of interest is the heat loss and the surface temperatures at the six points U to Z. Figure 6.54 shows the horizontal and vertical sections. The boundary conditions are labeled with Greek letters α, β, γ, and δ, and the materials are labeled with numbers 1-5, see Table 6.22, and Fig. 6.54.

Figure 6.55 shows the projection of the numerical mesh on the (x, y)-plane and the (y, z)-plane involving 7600 cells. Figure 6.56 shows the numerical mesh in perspective. The surface temperatures are shown on the front cover.
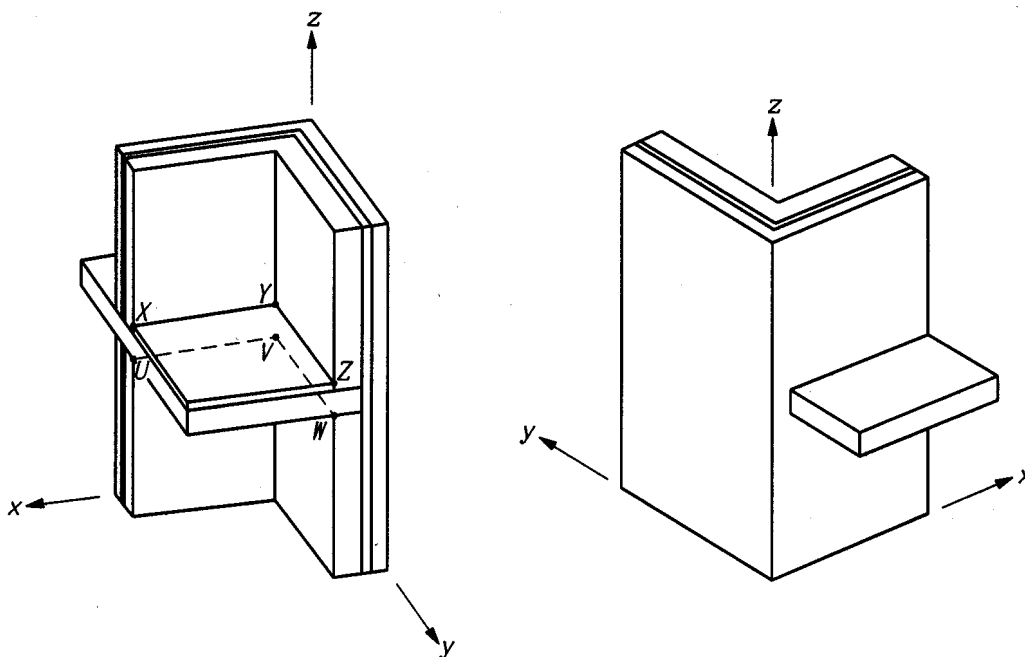
Figure 6.53: Test reference case.

material	λ, (W/(m·K))	boundary condition	T, (°C)	R, (m²K/W)
1	0.7	α	20	0.2
2	0.04	β	15	0.2
3	1.0	γ	0	0.05
4	2.5	(δ=adiabatic)		
5	1.0			

Table 6.22: Thermal conductivities and boundary conditions.
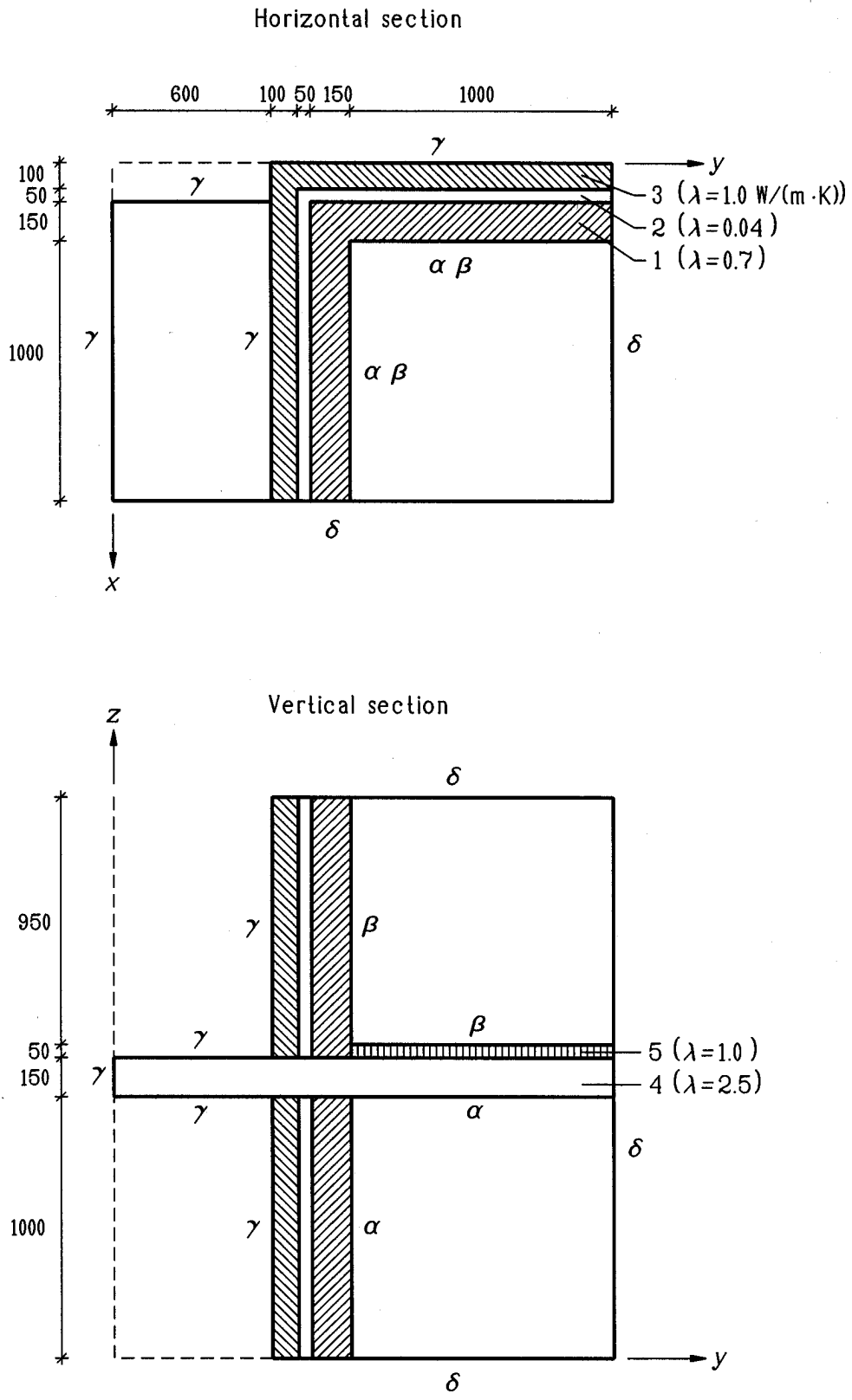
Figure 6.54: Horizontal and vertical sections of the problem.

114
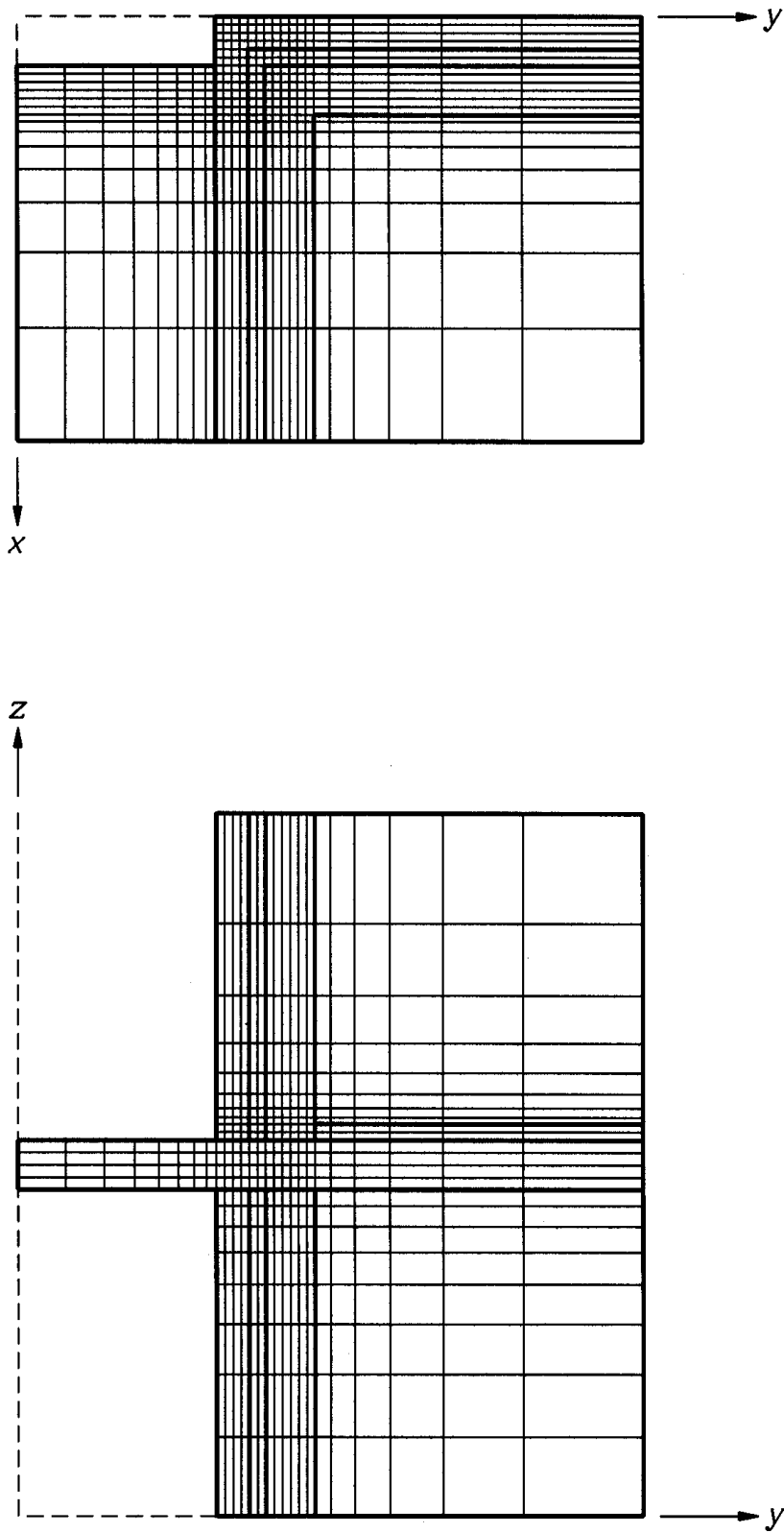
Figure 6.55: Projection of the numerical mesh on the (x, y)-plane and the (y, z)-plane involving 7600 cells.
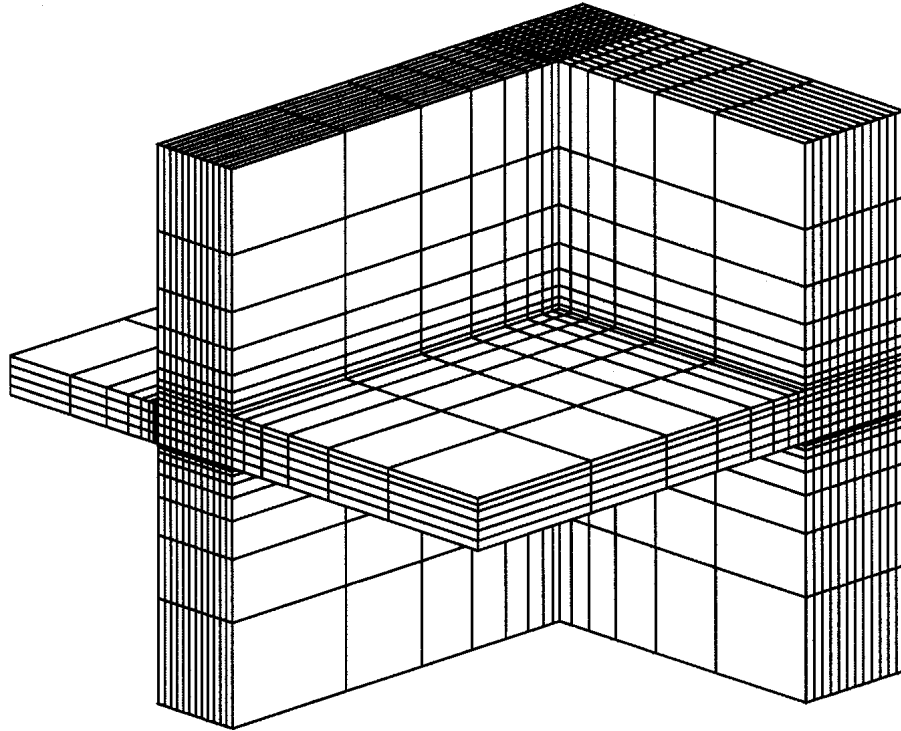
Figure 6.56: The numerical mesh in the case with 7600 cells.

6.9.2 Calculations

Table 6.23 shows the calculated heat flows as a function of number of computational nodes, and the values listed in (CEN, 1995) for this test reference case. According to (CEN, 1995) the difference between the heat flows calculated by the method being validated, in this case HEAT3, and the listed values should not differ of more than 2% from the listed values. Consider the case with 7600 cells. The relative error of the heat flows turns out to be 2-3% (if the listed values from CEN are correct). If one compares the results from HEAT3 with 7600 cells and 720900 cells, the error is about 1%. The calculation took 22 seconds (Pentium/90) using 7600 cells, 13 minutes with 246000 cells, and 44 minutes using 720900 cells, see Section 4.3.2.

surfaces	$N=7600$	$N=246000$	$N=720900$	CEN
α	45.62	46.03	46.06	46.3
β	13.64	13.86	13.87	14.0
γ	59.26	59.89	59.93	60.3

Table 6.23: Calculated heat flows (W).

Table 6.24 shows the surface temperatures obtained in HEAT3. According to (CEN, 1995) the difference between the temperatures calculated by the method being validated and the listed values should not exceed 0.1 °C.

116

point	x, y, z	N=7600	N=246000	N=720900	CEN
U	1.3, 0.9, 1.0	13.2	13.0	12.9	12.9
V	0.3, 0.9, 1.0	11.5	11.4	11.3	11.3
W	0.3, 1.9, 1.0	16.5	16.5	16.4	16.4
X	1.3, 0.9, 1.2	12.7	12.6	12.6	12.6
Y	0.3, 0.9, 1.2	11.1	11.1	11.1	11.1
Z	0.3, 1.9, 1.2	15.2	15.3	15.3	15.3

Table 6.24: Calculated surface temperatures (°C).

6.9.3 Conclusions

This three-dimensional heat conduction problem is a test reference case in the European standards (CEN, 1995). Heat flows and surface temperatures are given for different numerical meshes. It is sufficient with about 10000 numerical cells in an expansive mesh to meet the criterion for heat flows. This calculation takes 22 seconds on a Pentium/90. To fulfill the much harder requirement of surface temperatures, HEAT3 needs about one quarter of a million cells. This calculation takes 44 minutes.

6.10 Slab on the ground

6.10.1 Introduction

The following example concerns calculations in three dimensions for a slab on the ground. See Figure 6.57. The simplification in Fig. 6.58 is a typical example of how to deal with sloping boundaries. We are interested to know the heat flow from the building to the ground during one year. A steady-state calculation is made with an indoor temperature of 20 °C, and an average annual outdoor temperature of 9.4 °C. Table 6.25 shows the material properties. The internal and external surface resistances are 0.13 m²K/W and 0.04 m²K/W, respectively. A study dealing with frost penetration under a building is presented in (Harderup et al, 1994).
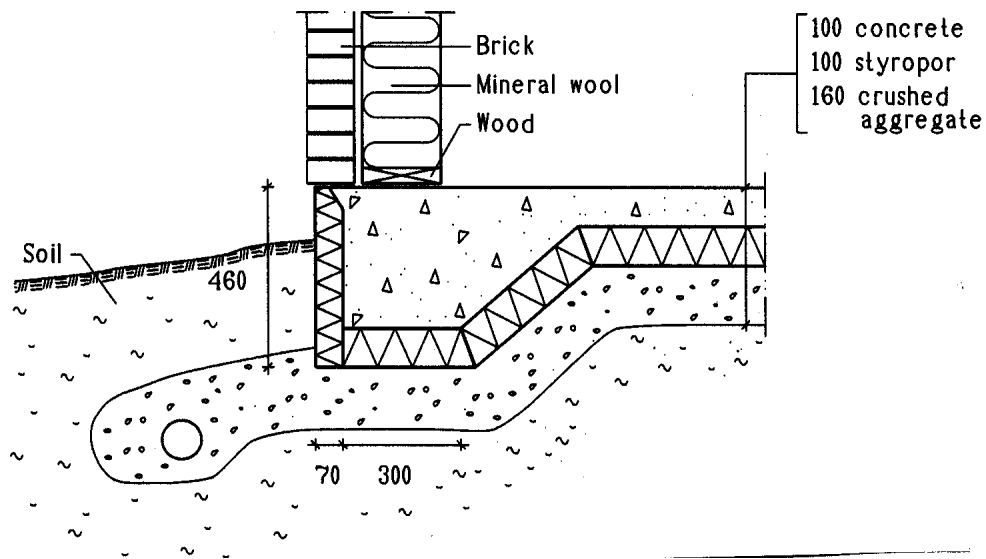
Figure 6.57: Slab on the ground.
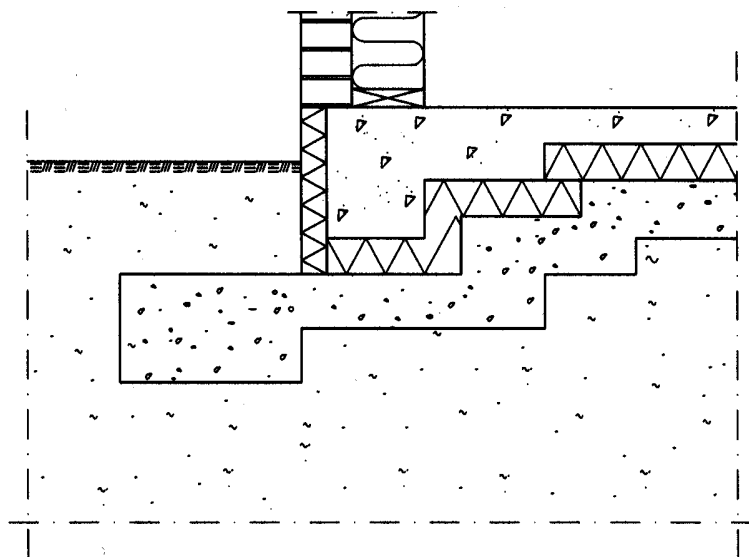
Figure 6.58: Simplified geometry for the calculations.

119

material	λ, (W/(m·K))
soil	2.2
crushed aggregate	2.0
brick	0.44 (0.60)
wood	0.14
concrete	1.7
styropor	0.039
mineral wool	0.036

Table 6.25: Thermal conductivities.

The resistance of the air gap in the wall is taken into account in such way that an effective thermal conductivity 0.44 W/(m·K) for the brick is used.

The size of the house, measured between the interior sides of the walls, is $10 \cdot 8$ m^2. Due to symmetry, only one quarter of the house is considered.

Figure 6.59 shows the numerical mesh around the slab projected on the vertical and horizontal sections as displayed by H3VIEW. The walls are indicated by thicker lines in the horizontal section. The whole computational volume has 25221 cells. Figure 6.60 shows the mesh around the slab in two perspectives as drawn by MATLAB. The figures show a part of the computational volume with 15834 of the 25221 cells. Note the expansive mesh with smaller cells concentrated to the corner of the edge where the temperature gradients are high.

The calculations are made for an area extending 20 m outwards and 20 m downwards from the house. A rule of thumb is to extend at least twice the width of the house (or the length if this is larger), in this case about 20 meters. If 40 m (65426 cells) would be used instead of 20 m (25221 cells), the difference of the heat flows would be less than 0.1% for this particular case.

For a two-dimensional calculation, the heat flows would differ with 0.9%, for this particular case, comparing extensions of 40 m and 20 m, respectively. A two-dimensional calculation requires about 30 m extension to establish a numerical error less than 0.1-0.2%. The rule of thumb is to use an extension three times the width of the house for a two-dimensional calculation. It may be noted that the horizontal extension from the house is more important than the vertical one. More recipes for slab on the ground calculations are given in (Hagentoft, 1988).
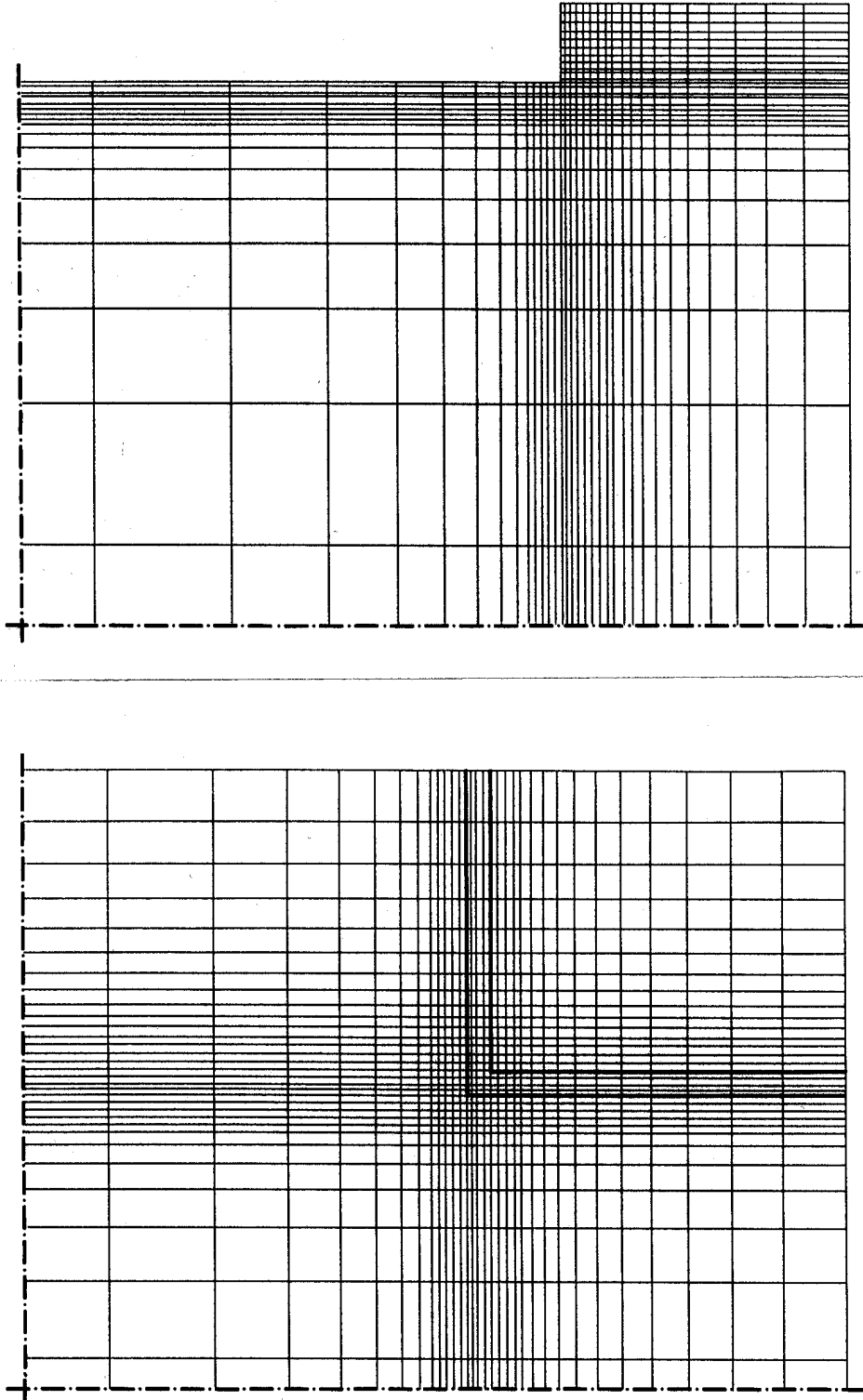
Figure 6.59: Numerical mesh around the slab projected on the vertical and horizontal sections as displayed by H3VIEW. The whole computational volume has 25221 cells. The walls are indicated by thicker lines in the horizontal section. Note the expansive mesh with smaller cells concentrated to the corner of the edge where the temperature gradients are high.
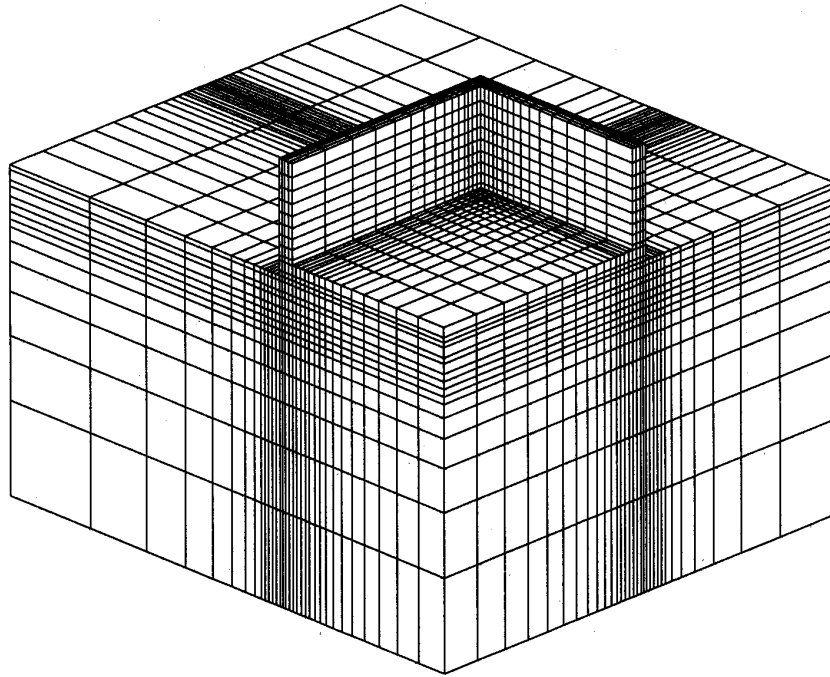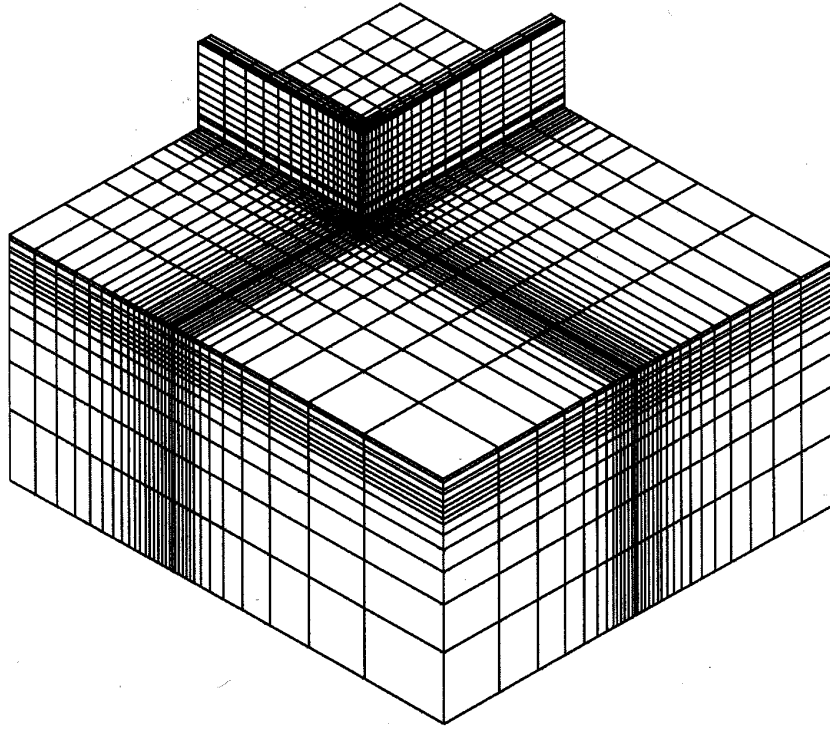
Figure 6.60: The mesh around the slab in two perspectives as drawn by MATLAB. The figures show a part of the computational volume with 15834 of the 25221 cells.

6.10.2 Results

Table 6.26 shows the heat flow through the floor, through the walls, to the ground, and the minimum and maximum surface temperatures. The criterion $\delta=1\cdot10^{-4}$ is used, see Eq. (6.1) in Section 6.2.4. With $\delta=1\cdot10^{-5}$, the results will be the same but this calculation takes about half an hour instead of three minutes.

The heat flow to the ground from the house during one year becomes $61.1\cdot4\cdot24\cdot365 = 2.1$ MWh. Note that the calculated heat flows represent one quarter of the house, so we multiply by 4.

A calculation using 200000 cells shows that the numerical error is less than 2% compared to using 25221 cells. The calculation using 200000 cells takes about one hour.

	heat flow (W)	min. T (°C)	max. T (°C)
floor	78.6	15.5	19.7
interior sides of walls	17.4	15.4	19.8
exterior sides of walls	35.0	9.4	9.9
ground	61.1	9.4	9.7

Table 6.26: Calculated heat flows and surface temperatures, (N=25221).

6.10.3 Conclusions

A three-dimensional calculation of the heat loss to the ground is shown. Figures 6.57 and 6.58 show how to deal with sloped boundaries. Using 25000 cells in an expansive mesh should give a numerical error of less than 2%. The calculation takes about three minutes on a Pentium/90. A rule of thumb is to extend the calculation volume in the ground at least twice the width of the house (or the length if this is larger).

6.11 House with a floor heating system

6.11.1 Introduction

This section deals with houses partially heated by a floor heating system. Figure 6.61 shows a foundation[1] with a cavity under the slab in which there is a given input Q_{fh} (floor heating). Most of the heat will flow upwards to the room above, but there will also be a certain heat loss to the ground due to the floor heating. The problem is how to represent this floor heating by an appropriate U-value for the floor. Formulas are given below for the heat loss to the ground. Only the steady-state problem is considered here.
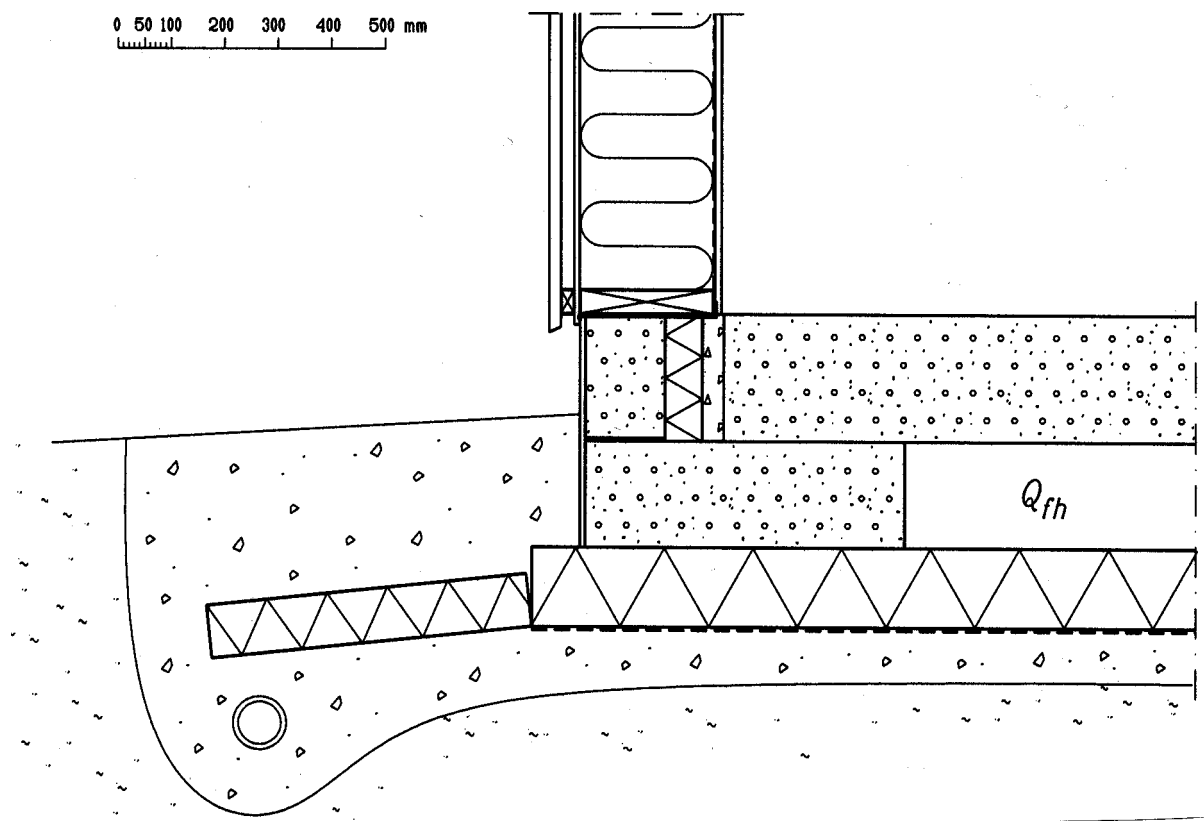
Figure 6.61: Foundation with a floor heating system.

Figure 6.62 shows a schematic representation of the involved heat flows and temperatures for the basic case (case I). The indoor temperature is denoted by T_i, and the outdoor temperature by T_o. The effect of the floor heating is denoted by Q_{fh}, (W), and the heat flow through the floor is denoted by Q_f, (W).

The heat flow from the floor heating system Q_{fh} may be zero, see Fig. 6.63 (case II). The heat flow to the ground is in this case denoted by Q_f^0. A numerical simulation gives Q_f^0 for the temperature difference $T_i - T_0$.

---

[1]The foundation is called Termogrund (patent no. 8900698-5). It is made by Lättklinkerbetong AB, Box 27, S-444 21, Stenungsund, Sweden.
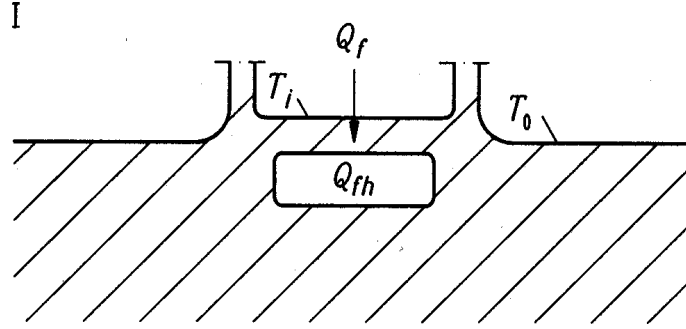
Figure 6.62: Schematic figure of involved heat flows and temperatures. Case I.
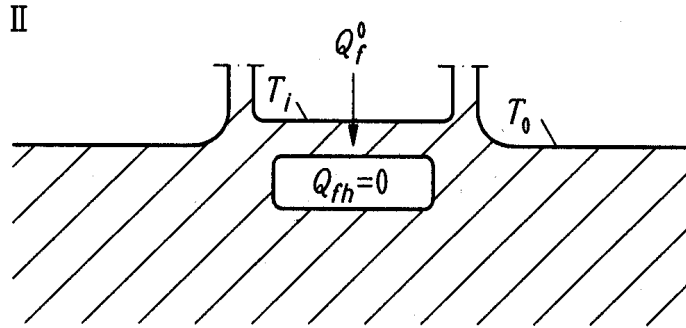
Figure 6.63: Heat flows for zero floor heating (Q_{fh}=0). Case II.

The two considered heat flow problems (case I and II) are linear. This means that the principle of superposition may be used. In order to analyze the situation we consider the difference between case I and II, see Fig. 6.64. Subtracting case II from case I gives a situation where the indoor and outdoor temperatures are zero. The heat flow through the floor becomes $Q_f - Q_f^0$.

Consider now this difference between I and II, see Fig. 6.64. The heat flow rate Q_{fh} is supplied in the floor cavity, and the temperature is zero on *both* the indoor and outdoor boundaries. A numerical calculation gives the fraction f_{loss} of the provided heat to the ground, i.e. the heat flow through the outer boundary $f_{loss} \cdot Q_{fh}$, see Fig. 6.65. The rest, $(1 - f_{loss}) \cdot Q_{fh}$, flows into the house.

It should be noted that f_{loss} does not depend on the boundary temperatures. It depends only on the geometry, the thermal conductivities, and the surface heat resistances. In general, the fraction f_{loss} decreases when the slab size increases. The thermal resistance above the cavity should be low, and the cavity should be well insulated underneath and on the sides in order to decrease the heat loss to the ground.

I–II
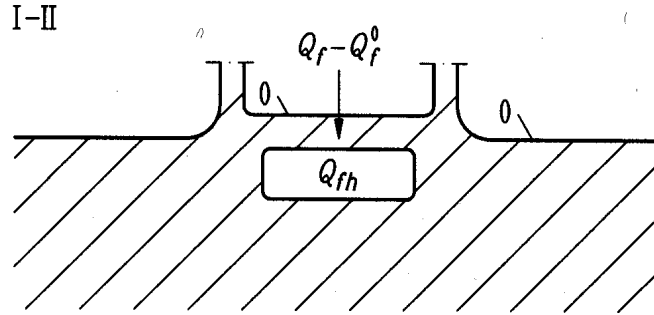
Figure 6.64: Heat flows for case II subtracted from case I.
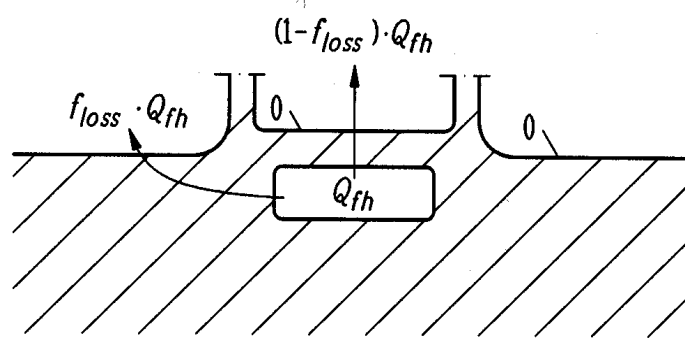
Figure 6.65: Calculation that gives the fraction f_{loss}.

The heat flow through the floor $Q_f - Q_f^0$ in Fig. 6.64 is the same as the calculated heat flow $-(1 - f_{loss}) \cdot Q_{fh}$, see Fig. 6.65. Thus we have

$$(1 - f_{loss}) \cdot Q_{fh} + Q_f - Q_f^0 = 0 \qquad (6.67)$$

The total effect to the ground is $Q_f + Q_{fh}$, see Fig. 6.62. Equation (6.67) may be written

$$Q_f + Q_{fh} = Q_f^0 + f_{loss} \cdot Q_{fh} \qquad (6.68)$$

This is the basic equation. Two numerical calculations are required as described above. The first one gives Q_f^0, see Fig. 6.63 (case II), and the second one gives f_{loss}, see Fig. 6.65.

6.11.2   Heat balance including heat losses above ground

We now take into account the net heat loss above ground for the house. This net loss above ground is denoted by Q_{env}, see Fig. 6.66. It includes heat transmission through the walls, the roof, the windows and the doors. It may also include heat loss by ventilation, and other terms that give a heat loss or a heat supply.
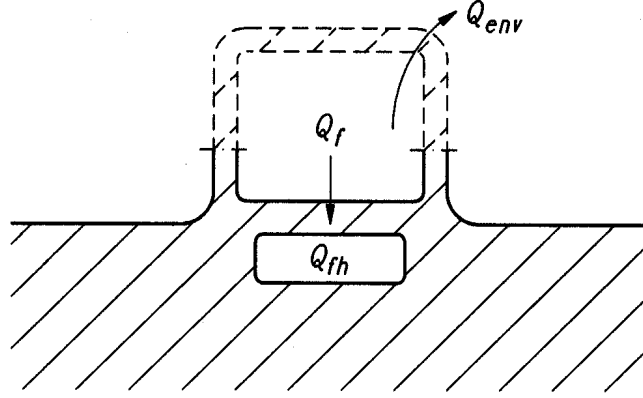
Figure 6.66: Heat balance including heat losses above ground

Consider Fig. 6.66. The total effect Q_{tot} given in the room and in the floor heating system is

$$Q_{tot} = Q_{env} + Q_f + Q_{fh} \qquad (6.69)$$

Using Eq. (6.68) gives

$$Q_{tot} = Q_{env} + Q_f^0 + f_{loss} \cdot Q_{fh} \qquad (6.70)$$

The total heat loss consists of the heat loss above ground, Q_{env}, the heat loss to the ground without floor heating, Q_f^0, and finally the extra heat loss due to floor heating, $f_{loss} \cdot Q_{fh}$.

Let η denote the fraction of the total input Q_{tot} that is supplied by the floor heating system Q_{fh}:

$$\eta = \frac{Q_{fh}}{Q_{tot}} \qquad 0 \le \eta \le 1 \qquad (6.71)$$

Equation (6.70) becomes

$$Q_{tot} = Q_{env} + Q_f^0 + \eta \cdot f_{loss} \cdot Q_{tot} \qquad (6.72)$$

This gives an expression for the total effect as a function of η

$$Q_{tot} = \frac{1}{1 - \eta \cdot f_{loss}} \cdot (Q_{env} + Q_f^0) \qquad (6.73)$$

For the floor heating we have

$$Q_{fh} = \frac{\eta}{1 - \eta \cdot f_{loss}} \cdot (Q_{env} + Q_f^0) \qquad (6.74)$$

If no floor heating is used ($\eta=0$), the total input in the house is $Q_{env}+Q_f^0$. If all the effect is supplied via the floor heating system ($\eta=1$), the needed effect is

$$Q_{tot} = Q_{fh} = \frac{1}{1 - f_{loss}} \cdot (Q_{env} + Q_f^0) \qquad (6.75)$$

It should be noted that the energy demand in this case increases by a factor $1/(1\text{-}f_{loss})$.

128

6.11.3 Effective U-value for the floor

The U-value for the floor in the case when no floor heating is used (Q_{fh}=0) is denoted by U_f^0, (W/(m²K)). It is defined by

$$U_f^0 = \frac{Q_f^0}{(T_i - T_0) \cdot A_f} \qquad \text{(W/(m²K))} \tag{6.76}$$

where A_f, (m²), is the floor area. An effective U-value for the floor U_f^{eff}, (W/(m²K)), is now defined as the heat flow through the floor, plus the effect from the floor heating system, per square meter floor area and degree Kelvin. Equation (6.68) gives

$$U_f^{eff} = \frac{Q_f + Q_{fh}}{(T_i - T_0) \cdot A_f} = \frac{Q_f^0 + f_{loss} \cdot Q_{fh}}{(T_i - T_0) \cdot A_f} \tag{6.77}$$

Equation (6.76) gives

$$U_f^{eff} = U_f^0 + f_{loss} \cdot \frac{Q_{fh}}{(T_i - T_0) \cdot A_f} \tag{6.78}$$

6.11.4 A numerical example

As an example we consider the construction in Figure 6.67. For simplification, the problem is analyzed in two dimensions with HEAT2. Thus, the calculated heat flows are per unit length perpendicular to the section shown in Figure 6.67.
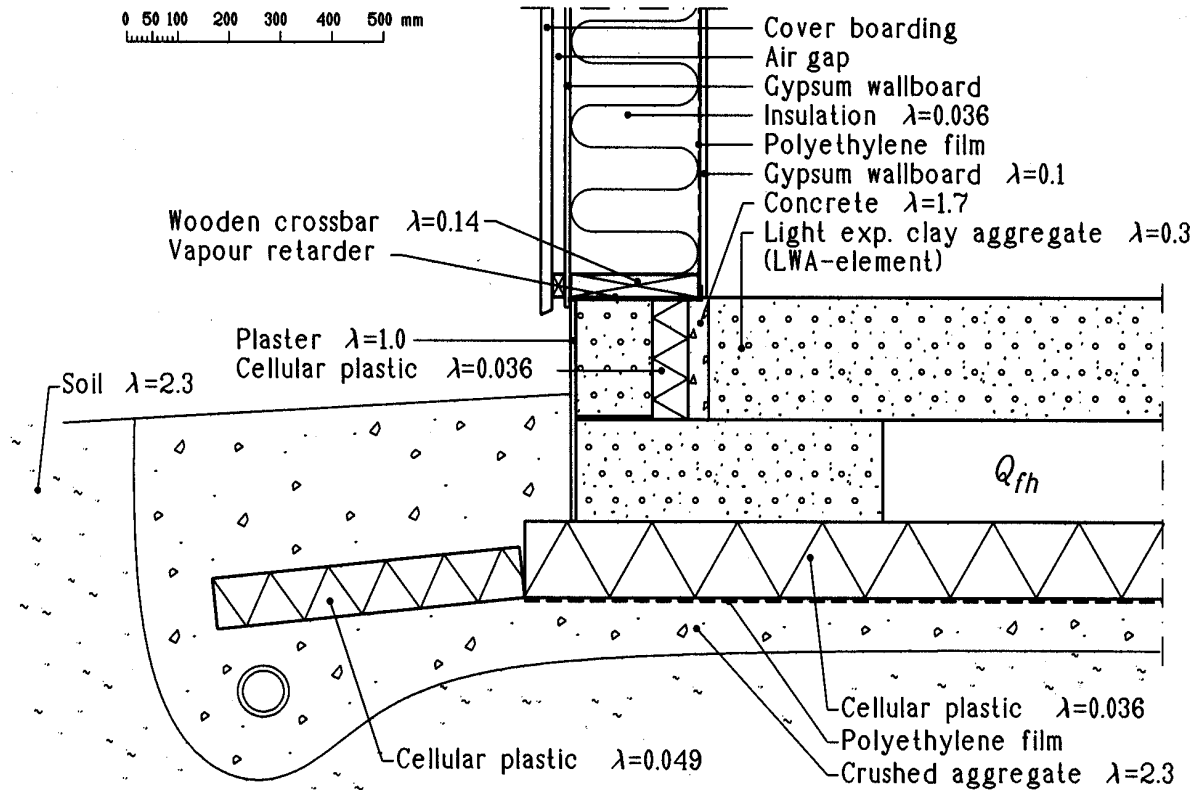
Figure 6.67: Foundation with a floor heating system for the numerical example.

The width of the house is 10 m. Due to symmetry, only half of the house is considered. The calculation area involves 25 meters of the ground below and outwards from the house. The temperatures indoors and outdoors are 20 °C and 0 °C, respectively. About 5000 numerical nodes in an expansive mesh are used.

Two independent calculations are made. The first one gives the heat flow Q_f^0=18.7 W/m (half of the house) when the floor heating is zero, see Fig. 6.63. Equation (6.76) gives U_f^0=0.187 W/(m²K). For the second calculation, consider Fig. 6.65. Here is the indoor and outdoor temperature 0 °C. A constant effect Q_{fh}, which may be arbitrarily chosen, gives the fraction f_{loss}=0.147. A smaller slab width gives larger values of U_f^0 and f_{loss}. Numerical simulations using a width of 5 m instead of 10 m give an increase of about 40% for U_f^0, and about 25% for f_{loss}.

Assume that the small and well insulated house has a net heat loss above ground of Q_{env}=16.7 W/m (half of the house). Three cases are studied: no floor heating, only floor heating, and partial heating by the floor heating system.

In the first case, no effect is given in the floor heating system (Q_{fh}=0, $\eta = 0$), i.e. the house is heated internally. The total effect needed is, Eq. (6.73),

$$Q_{tot} = \frac{1}{1 - \eta \cdot f_{loss}} \cdot (Q_{env} + Q_f^0) = Q_{env} + Q_f^0 = 16.7 + 18.7 = 35.4 \quad \text{W/m} \quad (6.79)$$

The U-value for the floor becomes U_f^{eff}=U_f^0=0.187 W/(m²K).

In the second case, the house is completely heated by the floor heating system ($\eta = 1$). The total effect becomes

$$Q_{tot} = Q_{fh} = \frac{1}{1 - \eta \cdot f_{loss}} \cdot (Q_{env} + Q_f^0) = \quad (6.80)$$

$$\frac{1}{1 - 1 \cdot 0.147} \cdot (16.7 + 18.7) = 41.5 \quad \text{W/m}$$

The effective U-value for the floor becomes, Eq. (6.78),

$$U_f^{eff} = U_f^0 + f_{loss} \cdot \frac{Q_{fh}}{(T_i - T_0) \cdot A_f} = \quad (6.81)$$

$$0.187 + 0.147 \cdot \frac{41.5}{20 \cdot 5} = 0.248 \quad \text{W/(m²K)}$$

The direction for the heat flow through the floor Q_f is downwards in the first case, and upwards in the second case. When is this heat flow zero? In this third case, Eq. (6.68) gives with Q_f=0 the effect of the floor heating system

$$Q_{fh} = \frac{Q_f^0}{1 - f_{loss}} = \frac{18.7}{1 - 0.147} = 21.9 \quad \text{W/m} \quad (6.82)$$

The total effect needed is, Eq. (6.69),

$$Q_{tot} = Q_{env} + Q_f + Q_{fh} = 16.7 + 0 + 21.9 = 38.6 \quad \text{W/m} \quad (6.83)$$

The effective U-value for the floor is in this case, Eq. (6.78),

$$U_f^{eff} = U_f^0 + f_{loss} \cdot \frac{Q_{fh}}{(T_i - T_0) \cdot A_f} = \tag{6.84}$$

$$0.187 + 0.147 \cdot \frac{21.9}{20 \cdot 5} = 0.219 \quad \text{W/(m}^2\text{K)}$$

Figures 6.68-6.70 show the isotherms around the edge of the slab for the three cases. Figure 6.68 shows the case without floor heating with temperatures falling from the floor downwards and outwards. The second case, with only floor heating, gives a temperature inside the cavity for the floor heating of about 23 °C, see Fig. 6.69. In the third case, see Fig. 6.70, the average heat flow through the floor, including thermal bridge effects on the sides, is zero.

The more of the total heating demand that is supplied by the floor heating system, the more does the heat loss to the ground (and the effective U-value for the floor) increase. If no heat is provided by the floor heating system, the U-value becomes 0.187 W/(m²K). The value increases with 33% to 0.248 in the case where the whole house is heated by the floor system. If half of the energy demand were supplied by the floor heating system (η=0.5), the U-value would be 0.215 W/(m²K), i.e. an increase of 15%.

A house with a larger heat loss above ground will have a larger effective U-value for the floor, for a given $\eta > 0$. Also, the temperature inside the cavity with the floor heating system will increase. As an example consider the next two cases where the net heat loss above ground is doubled to Q_{env}=33.4 W/m (half of the house).

In the first case, no effect is given in the floor heating system (Q_{fh}=0, $\eta = 0$), i.e. the house is heated internally. The total effect needed is, Eq. (6.73),

$$Q_{tot} = \frac{1}{1 - \eta \cdot f_{loss}} \cdot (Q_{env} + Q_f^0) = (Q_{env} + Q_f^0) = 33.4 + 18.7 = 52.1 \text{ W/m} \tag{6.85}$$

The U-value for the floor becomes U_f^{eff}=U_f^0=0.187 W/(m²K).

In the second case, the house is completely heated by the floor heating system ($\eta = 1$), and the total effect becomes

$$Q_{tot} = Q_{fh} = \frac{1}{1 - \eta \cdot f_{loss}} \cdot (Q_{env} + Q_f^0) = \tag{6.86}$$

$$\frac{1}{1 - 0.147} \cdot (33.4 + 18.7) = 61.1 \quad \text{W/m}$$

The effective U-value for the floor is, Eq. (6.78),

$$U_f^{eff} = U_f^0 + f_{loss} \cdot \frac{Q_{fh}}{(T_i - T_0) \cdot A_f} = \tag{6.87}$$

$$0.187 + 0.147 \cdot \frac{61.1}{20 \cdot 5} = 0.277 \quad \text{W/(m}^2\text{K)}$$

which is 48% larger than 0.187 W/(m²K). Figure 6.71 shows the isotherms around the edge of the slab for this case. The temperature inside the cavity for the floor heating is about 27 °C.

The effective U-values for the floor are shown in Table 6.27 with additional results for Q_{env}=100 W/m.

η	Q_{env}=16.7 W/m	Q_{env}=33.4 W/m	Q_{env}=100 W/m
0	0.187	0.187	0.187
0.5	0.215	0.228	0.281
1	0.248	0.277	0.392

Table 6.27: Effective U-value for the floor U_f^{eff} as a function of η and Q_{env}.
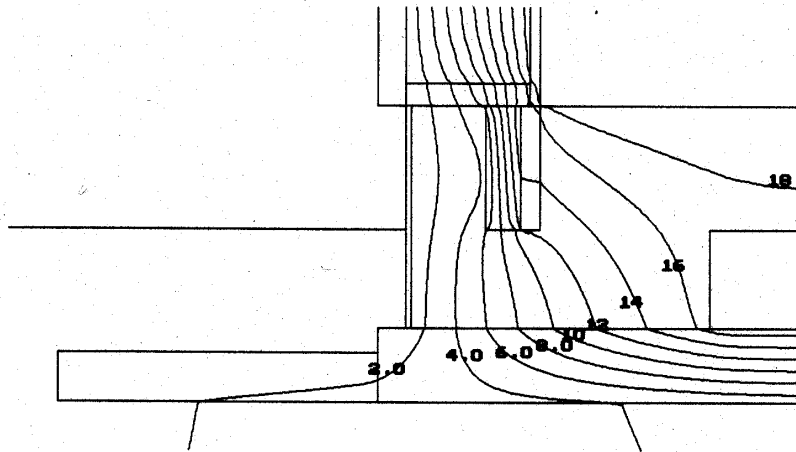
Figure 6.68: House heated internally (no floor heating).
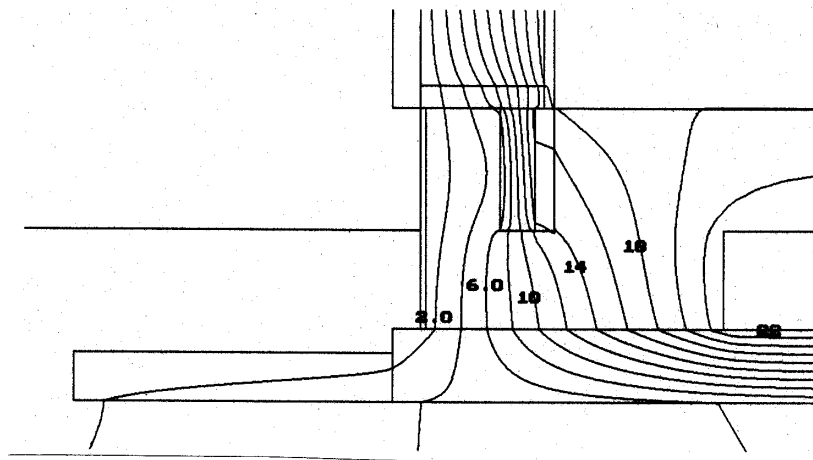
Figure 6.69: House heated completely by floor heating.

132
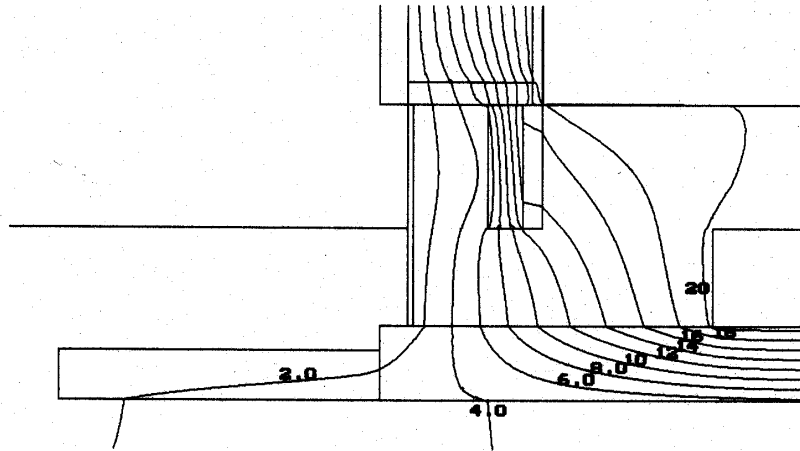
Figure 6.70: House heated partially by floor heating. The flow through the floor is zero.
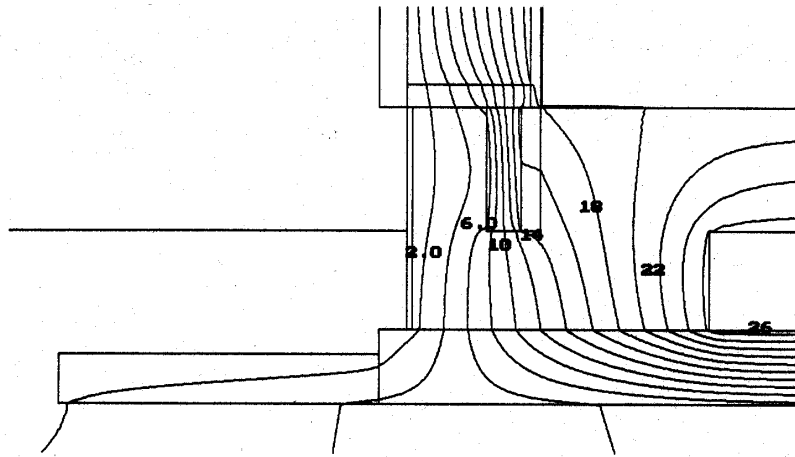
Figure 6.71: House heated completely by floor heating (Q_{env}=33.4 W/m).

6.11.5 Conclusions

Formulas are given for the heat loss to the ground and for the effective U-value for the floor. The more of the total heating demand that is supplied by the floor heating system, the more does the heat loss to the ground (and the effective U-value for the floor) increase. An effective U-value for the floor U_f^{eff}, (W/(m²K)), is calculated as

$$U_f^{eff} = U_f^0 + f_{loss} \cdot \frac{Q_{fh}}{(T_i - T_0) \cdot A_f} \tag{6.88}$$

where two independent numerical simulations give U_f^0 and f_{loss}. Table 6.27 shows the effective U-value U_f^{eff} for the floor construction shown in Fig. 6.67 for some values of η and Q_{env}. Note that Q_{env} refers to the net heat loss above ground for half of the house.

6.12   Construction block filled with insulation

6.12.1   Introduction

Figure 6.72 shows a hollow light expanded clay aggregate block filled with polystyrene. The polystyrene decreases the heat flow through the block. Figure 6.73 shows a wall of these blocks. The blocks are fitted closely together with a relatively thick horizontal layer of mortar between them. There are no vertical layers of mortar. The path of the heat flow is mainly in the y-direction. The mortar between the blocks gives a thermal bridge effect. The heat flow may be reduced by a mineral wool strip in the mortar, see Fig. 6.74. Figures 6.73, 6.75, and 6.76 show the wall in three orthogonal cross-sections.

This study presents three-dimensional numerical calculations of the heat flow through the wall using HEAT3. The proper choice of the numerical mesh is discussed. The dependence of the obtained U-value on a few parameters is dealt with.
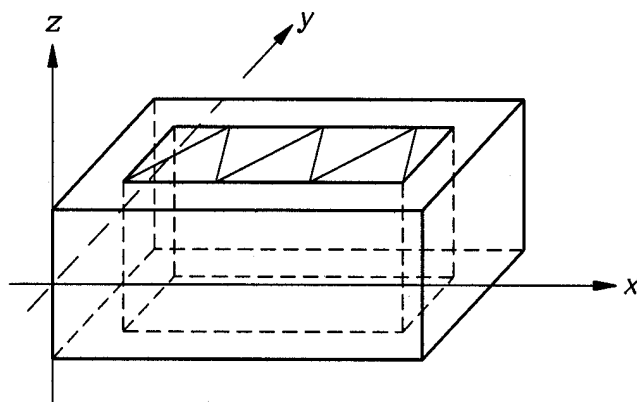
Figure 6.72: Hollow light expanded clay aggregate block filled with polystyrene.
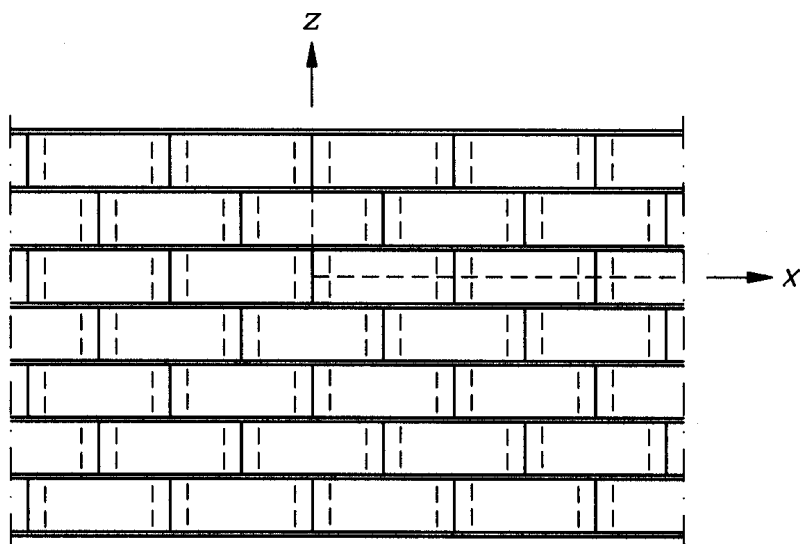
Figure 6.73: (x, z)-section of a wall containing the blocks.

135
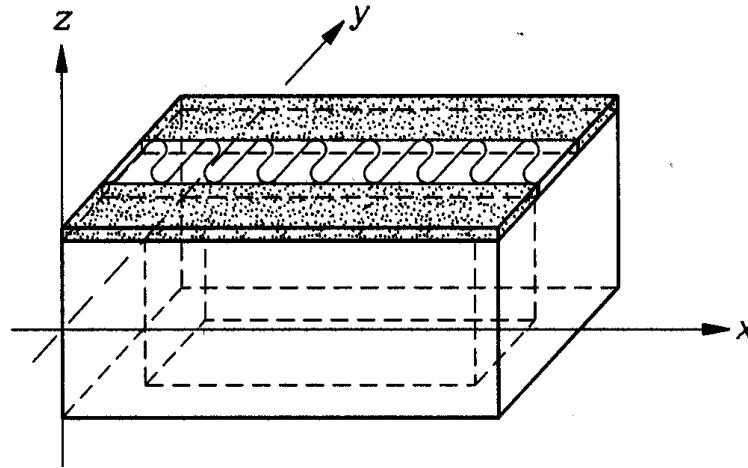
Figure 6.74: A mineral wool strip reduces the thermal bridge effect in the mortar.
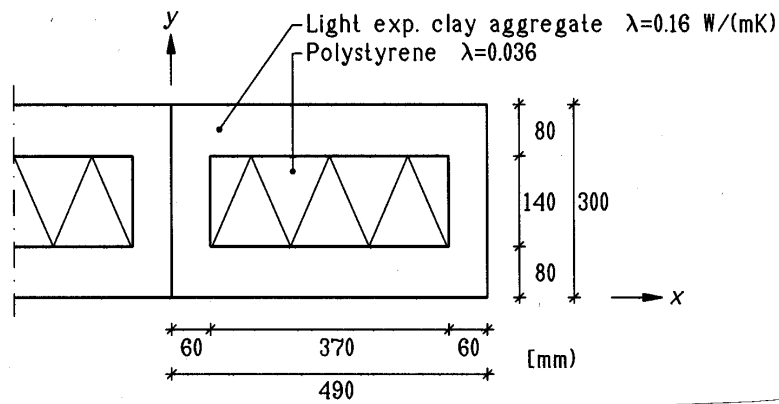
Figure 6.75: (x, y)-section of an expanded clay aggregate block filled with polystyrene.
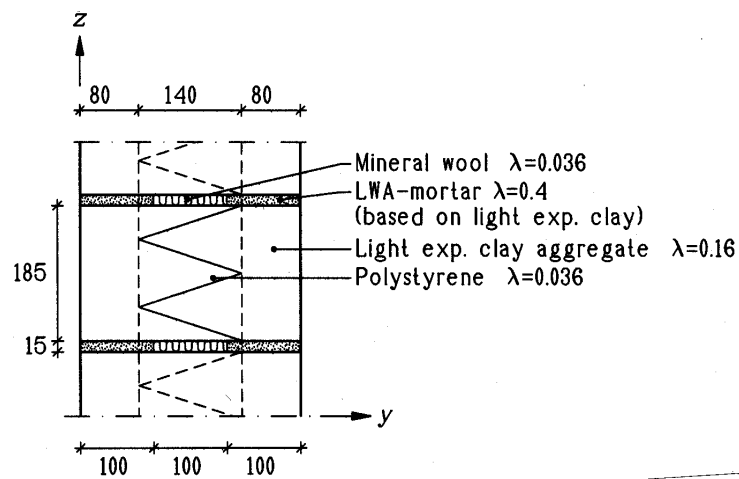
Figure 6.76: (y, z)-section of the blocks with a layer of mineral wool in the mortar.

136

6.12.2 Data for numerical simulation

The calculations have been made for the shaded part shown in Fig. 6.77. This part is enlarged in Fig. 6.78. There are symmetry planes at $x=0$ mm and $x=245$ mm, and at $z=0$ mm and $z=200$ mm. The boundary condition at these planes is adiabatic.
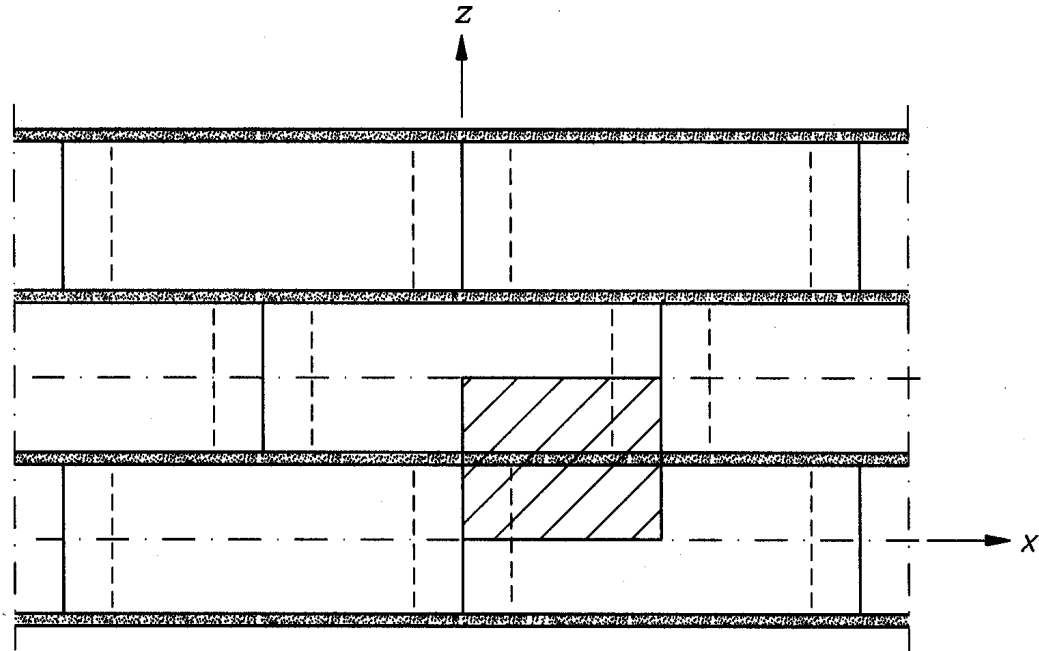
Figure 6.77: The shaded part is used in the simulations.
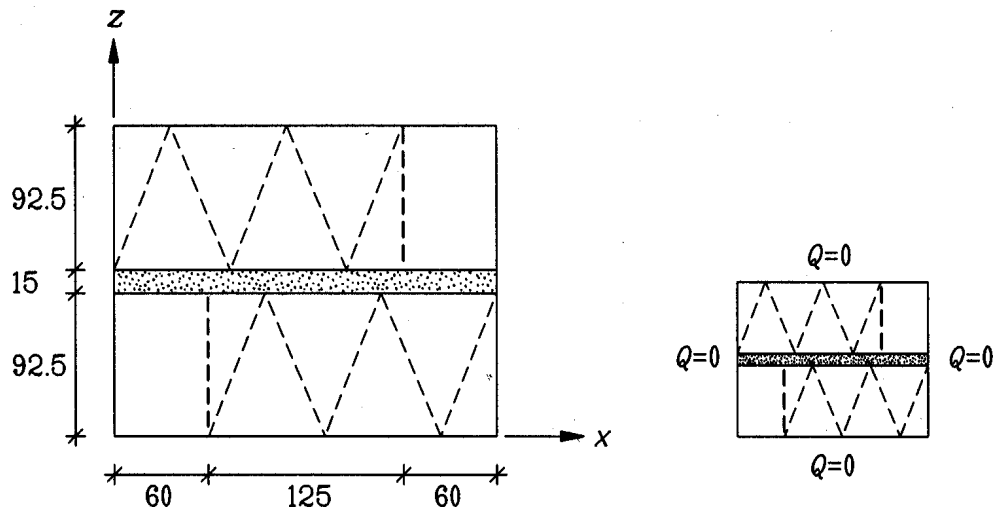
Figure 6.78: (x, z)-section of the computational volume. The boundary conditions are shown to the right.

The inner and outer surface resistances are 0.13 m^{2}K/W and 0.04 m^{2}K/W, respectively. If the inner and the outer surface resistances are put to the average value 0.085 m^{2}K/W, there will be a symmetry plane at $y=0.150$, see Fig. 6.76. Numerical tests

show that this simplification gives an error of less than 0.05%. This is discussed further in Section 6.12.4. The boundary temperature at y=0.150 is put to 0.5 °C (no surface resistance), and 0 °C at y=0 (with a surface resistance of 0.085 m^{2}K/W). This gives a calculated heat flow directly in (W/K), and the U-value in (W/(m^{2}K)). Figure 6.79 shows the volume in a three-dimensional perspective as drawn by H3VIEW. Figures 6.80 and 6.81 show the computational volume in sections (x, y) and (y, z), respectively.
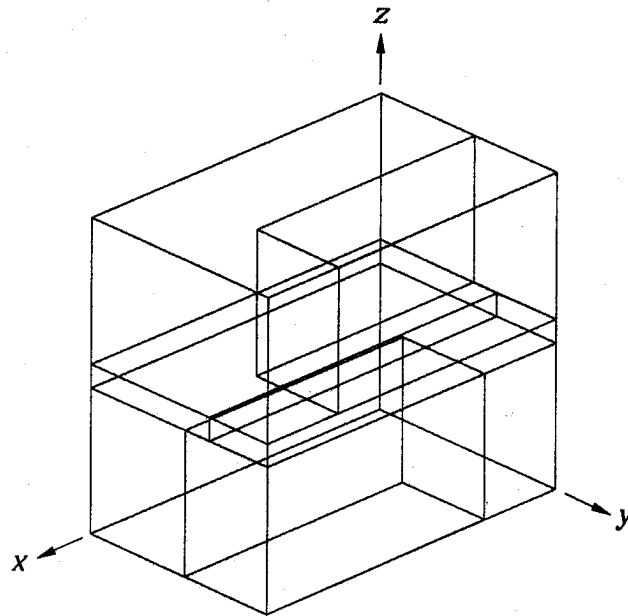
Figure 6.79: The computational volume shown in perspective by H3VIEW.
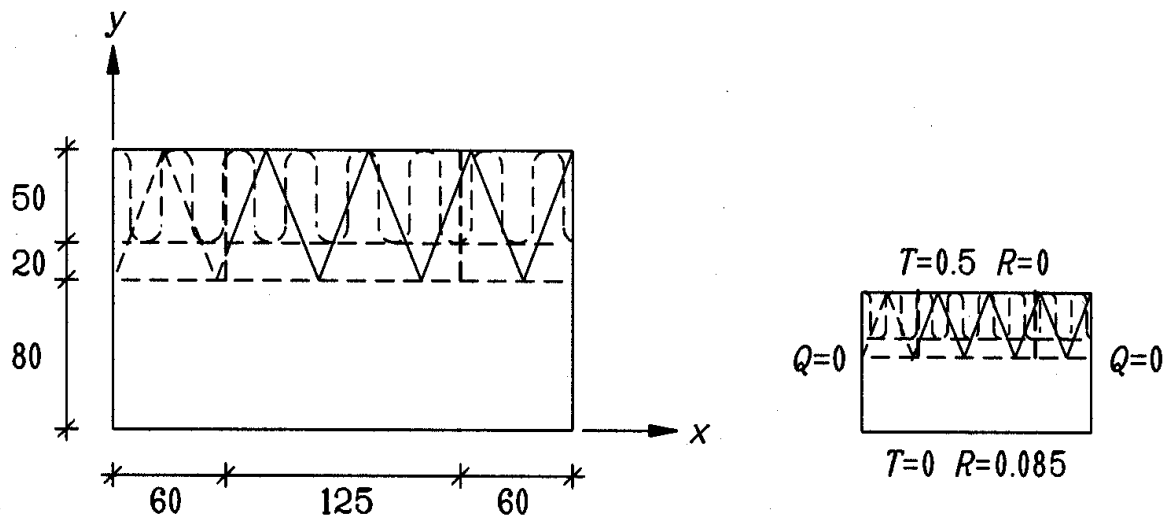
Figure 6.80: (x, y)-section of the computational volume. The boundary conditions are shown to the right.
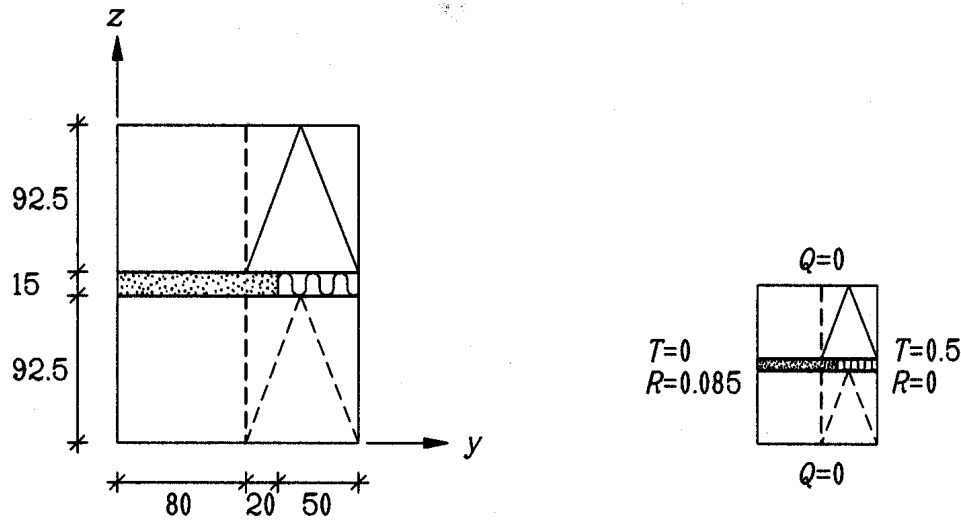
Figure 6.81: (y, z)-section of the computational volume. The boundary conditions are shown to the right.

6.12.3 Calculations

Table 6.28 shows the U-values for the wall obtained for seven different numerical meshes and the required computation time for a Pentium/90. The error is relative to the last case with one million cells. It is sufficient with about 1000 cells to have an error of one per cent. The calculation time is only a few seconds. Fig. 6.82 shows the numerical mesh projected on the (y, z)-, (x, z)-, and the (x, y)-planes in the case with 56160 computational cells.

The U-value is 0.301 W/(m²K). Calculations by hand using a simplified method described in the European standard (CEN, 1996) give a U-value of 0.296, i.e. an error of about 2%.

number of cells	$(N_x \cdot N_y \cdot N_z)$	U (W/(m²K))	ε (%)	CPU-time
27	$(3 \cdot 3 \cdot 3)$	0.2873	4.8	3s
175	$(7 \cdot 3 \cdot 5)$	0.2950	2.1	3s
1080	$(12 \cdot 10 \cdot 9)$	0.2975	1.2	5s
7200	$(24 \cdot 15 \cdot 20)$	0.2999	0.43	14s
56160	$(48 \cdot 30 \cdot 39)$	0.3007	0.17	2.3m
421875	$(75 \cdot 75 \cdot 75)$	0.3011	0.03	51m
1000000	$(100 \cdot 100 \cdot 100)$	0.3012	-	3h 26m

Table 6.28: Calculated U-values for different numerical meshes.

139
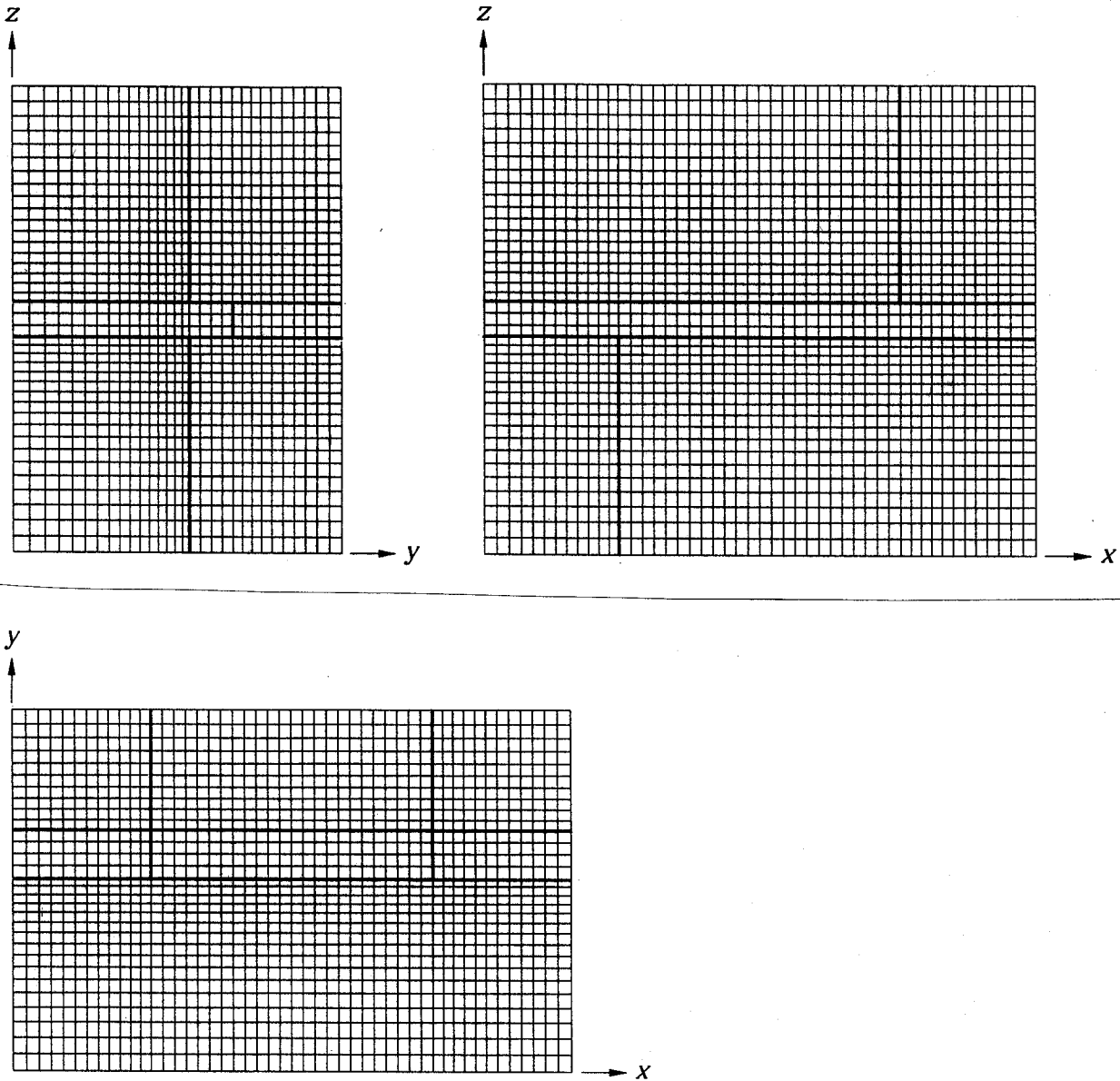
Figure 6.82: Numerical mesh projected on the (y, z)-, (x, z)-, and the (x, y)-planes in the case with 56160 computational cells.

6.12.4 Calculations without symmetry in the y-direction

In order to obtain symmetry in the y-direction, the inner and the outer surface resistances were put to the average value 0.085 m^{2}K/W. Numerical simulations without this symmetry in the y-direction have also been made. The inner and outer surface resistances were here put to 0.13 m^{2}K/W and 0.04 m^{2}K/W, respectively. The results show that the heat flows will differ with less than 0.05%. Figure 6.83 shows the temperatures at a cut in the (x, y)-plane along the middle of the mortar and the mineral wool strip (z=0.1 m). The numerical mesh has in this case 112320 cells ($48 \cdot 60 \cdot 39$). The mesh is the same as the case with 56160 cells in Table 6.28, but the number of cells is doubled in the y-direction

from 30 to 60. Fig. 6.84 shows the isotherms for the same section. The isotherm of 0.5 °C is slightly displaced from the center ($y=0.15$) towards the boundary with the higher surface resistance of 0.13 m²K/W at $y=0.3$ m.
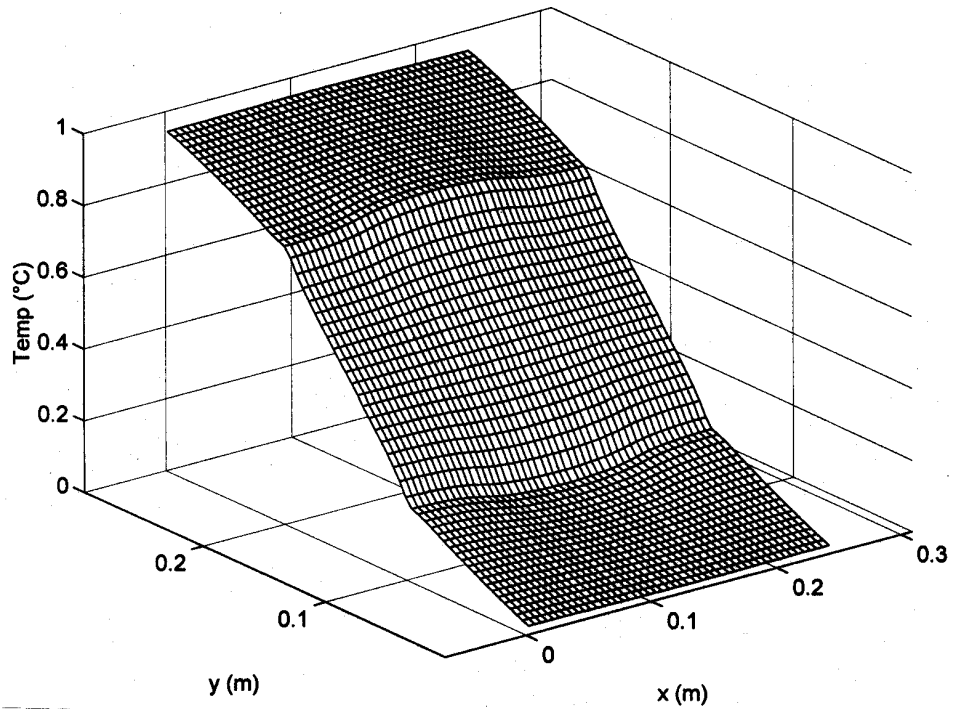
Figure 6.83: Temperatures in the (x, y)-plane at $z=0.1$ m.
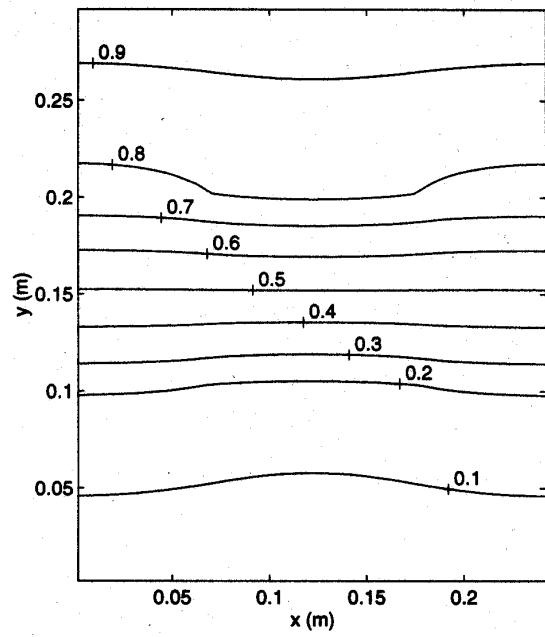
Figure 6.84: Isotherms in the (x, y)-plane at $z=0.1$ m.

6.12.5   A few parametric variations

The U-value for the basic case is 0.301 W/(m²K), see Table 6.28. If the mineral wool strip is replaced by mortar, the U-value becomes 0.366 W/(m²K), i.e. 22% larger. Calculations by hand using a simplified method described in the European standard (CEN, 1996) gives in this case a U-value of 0.355, i.e. an error of 3%.

If the thermal conductivity of the mortar is 1.0 W/(m·K) instead of 0.4, and the mineral wool strip is replaced by mortar, the U-value becomes 0.488 W/(m²K), i.e. 62% larger than the U-value for the basic case.

If the blocks are homogeneous without any polystyrene, and the mineral wool strip is replaced by mortar (λ=0.4), the U-value becomes 0.537 W/(m²K) which is 78% larger than the basic case.

6.12.6   Conclusions

It is sufficient to have about 1000 cells in order to obtain a numerical error of 1% for this well-behaved problem. A few seconds are enough for simulating the problem on a PC.

The polystyrene inside the blocks and the mineral wool strip reduce the thermal bridge effect considerably. The U-value for the wall without any insulation decreases from 0.537 to 0.301 W/(m²K), i.e. 44%.

6.13 Heat flow through a wall with metal studs

6.13.1 Introduction

Heat conduction in constructions with both insulation and metal parts often causes particular computational problems because of the wide difference in thermal conductivities.

An example is a test reference case in the European standards (CEN, 1995) for heat conduction in two dimensions. Fig. 6.85 shows a cross-section of the wall. The width and height is 0.5 m and 0.0475 m, respectively. There are four different materials with thermal conductivities between 0.029 W/(m·K) and 230 W/(m·K). It is a difficult numerical problem due to the high ratio of the maximum and minimum thermal conductivity. In this case the ratio becomes almost 8000 (230/0.029=7900).

The boundary conditions are shown in Fig. 6.85. The temperature is 20 °C and the surface resistance is 0.11 m²K/W at the bottom. The temperature is 0 °C and the surface resistance is 0.06 m²K/W at the top. The heat flow is zero through the two vertical boundaries due to symmetry.
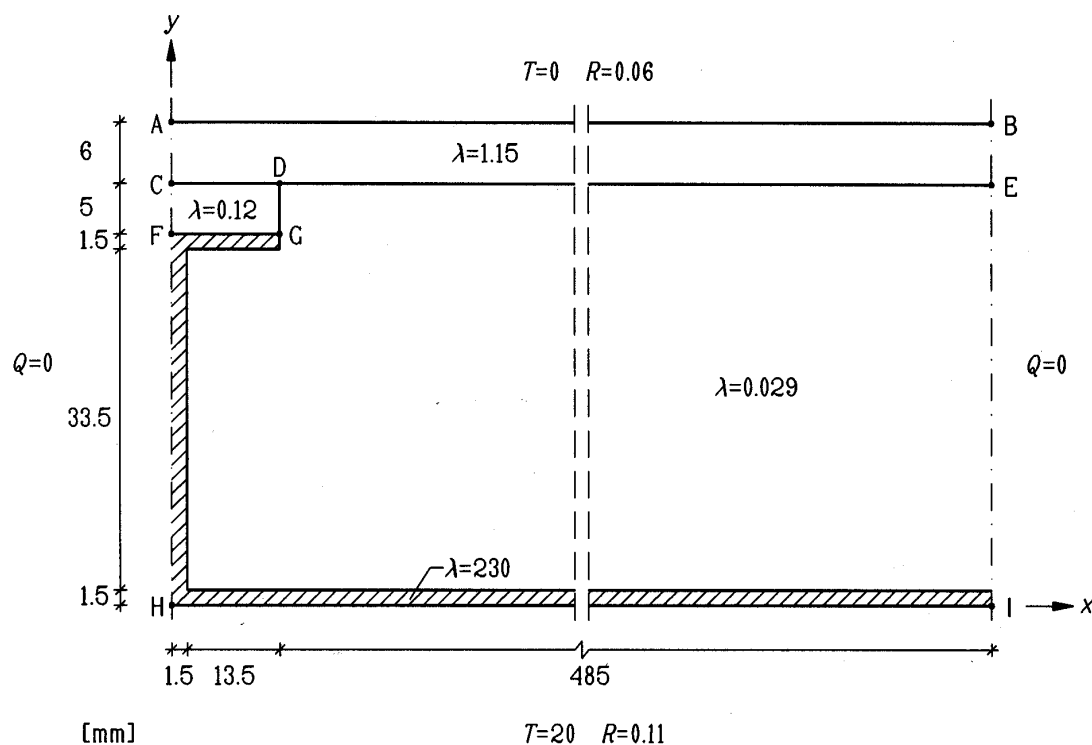
Figure 6.85: Test reference case in the European standards.

6.13.2 Calculations for different meshes

Table 6.29 shows the calculated heat flows through the wall for six different expansive numerical meshes and the required computation time on a Pentium/90. The error ε for

the heat flow is relative to the last case with 15625 cells. It is sufficient with about 1200 cells to have an error of 0.1%. The calculation time in this case is less than a minute (about 2000 iterations).

The last column shows the best choices of the relaxation coefficient, see Section 4.3.2. The calculation time depends largely on this choice. Consider the case with 1254 cells. Using $\omega=1.995$ gives a calculation time of about half a minute. If $\omega=1.9$ is used, a calculation time of about 10 minutes is required. Using $\omega=1.95$ gives a calculation time of about 6 minutes. A good choice of the relaxation coefficient may be made as follows. Look at the difference between the heat flows at the surfaces after a few hundred iterations for some different values of ω. Choose the coefficient that gives the smallest difference. Note that the optimum ω normally becomes larger with a denser grid.

cells	Q (W/m)	ε (%)	CPU-time	ω
32	8.541	11	1 sec.	-
72	9.382	1.2	1 sec.	-
374	9.456	0.4	5 sec.	-
1254	9.479	0.1	30 sec.	1.995
4550	9.490	0.01	4 min.	1.996
15625	9.491	-	10 min.	1.998

Table 6.29: Calculated heat flows for different meshes.
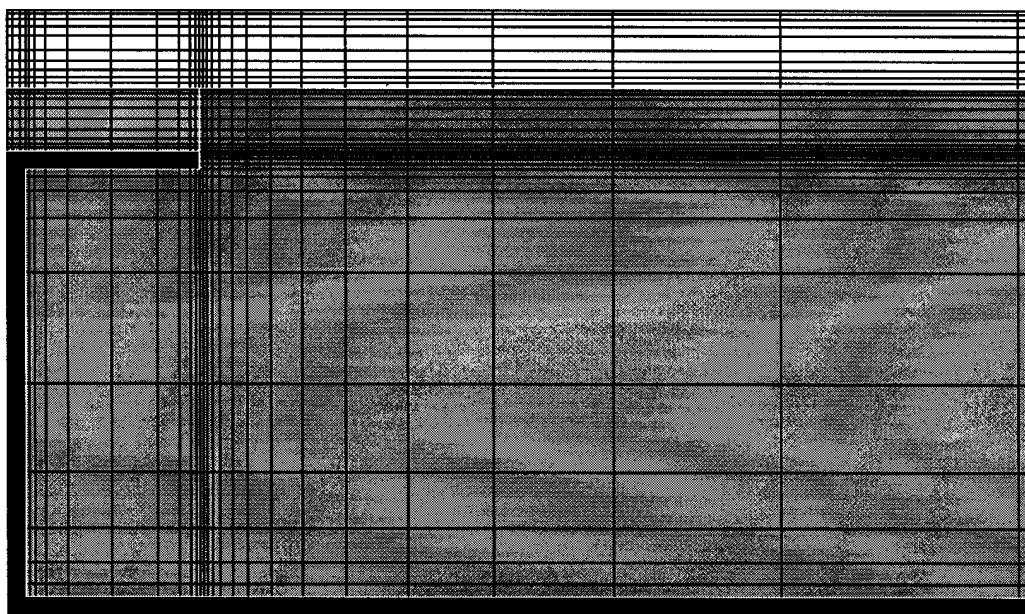
Figure 6.86: Numerical mesh for the left-most part of the problem (1254 cells).

144

Fig. 6.86 shows the numerical mesh for the critical left-hand part of the problem in the case with 1254 computational cells. The remaining 5/6 of the wall contains about 200 of the 1254 cells.

The heat flow through the wall is 9.5 W/m according to (CEN, 1995). The heat flow calculated by the method to be validated, in this case HEAT2, should not differ by more than 0.1 W/m. About 100 numerical cells suffice to fulfill this requirement.

Table 6.30 shows the surface temperatures obtained by HEAT2 for the last three cases with 1254, 4550, and 15625 cells, respectively. According to (CEN, 1995) the difference between the temperatures calculated by the method to be validated and the listed values shown in the last column should not exceed 0.1 °C. All temperatures are the same, except at location G, see Fig. 6.85. The temperature gradients are large at this location. This makes the interpolation difficult. About 4000 cells are needed to meet the CEN requirement.

location	(x, y)	N=1254	N=4550	N=15625	CEN
A	(0, 0.0475)	7.1	7.1	7.1	7.1
B	(0.5, 0.0475)	0.8	0.8	0.8	0.8
C	(0, 0.0415)	7.9	7.9	7.9	7.9
D	(0.015, 0.0415)	6.3	6.3	6.3	6.3
E	(0.5, 0.0415)	0.8	0.8	0.8	0.8
F	(0, 0.0365)	16.4	16.4	16.4	16.4
G	(0.015, 0.0365)	16.1	16.2	16.3	16.3
H	(0, 0)	16.8	16.8	16.8	16.8
I	(0.5, 0)	18.3	18.3	18.3	18.3

Table 6.30: Calculated surface temperatures (°C).

Figure 6.87 shows the temperature field for the case with 1254 cells. The temperature field is viewed from the upper right corner in Fig. 6.85. Note that the length scale is about 10 times larger in the x-direction compared to the y-direction. Figure 6.88 shows the isotherms for the left-hand part of the problem (the same area as in Fig. 6.86).
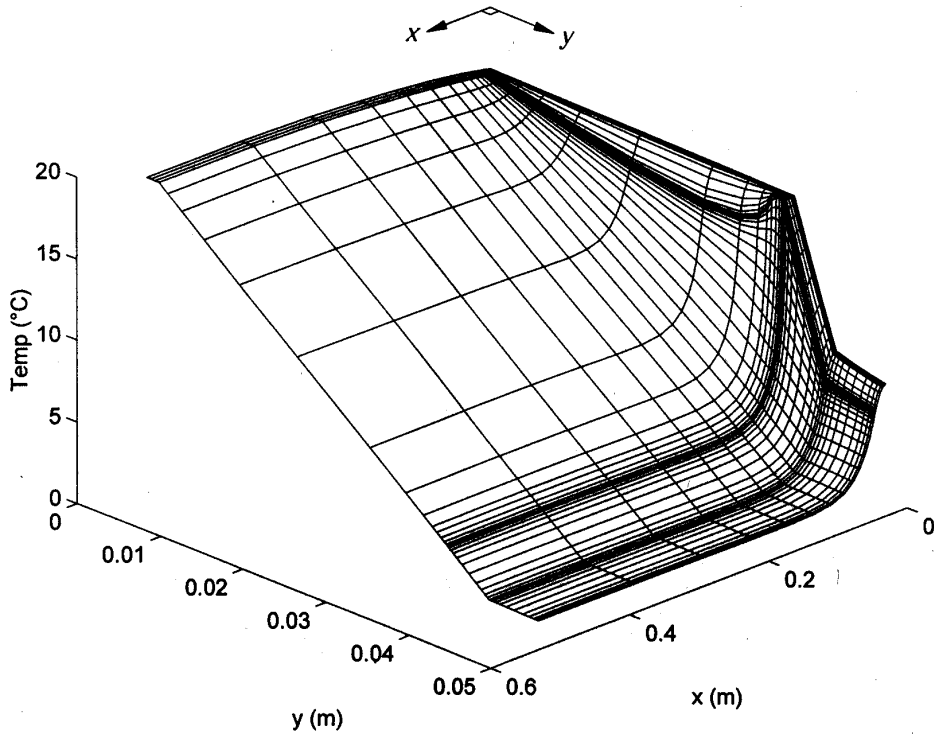
Figure 6.87: Calculated temperatures for the case with 1254 cells.
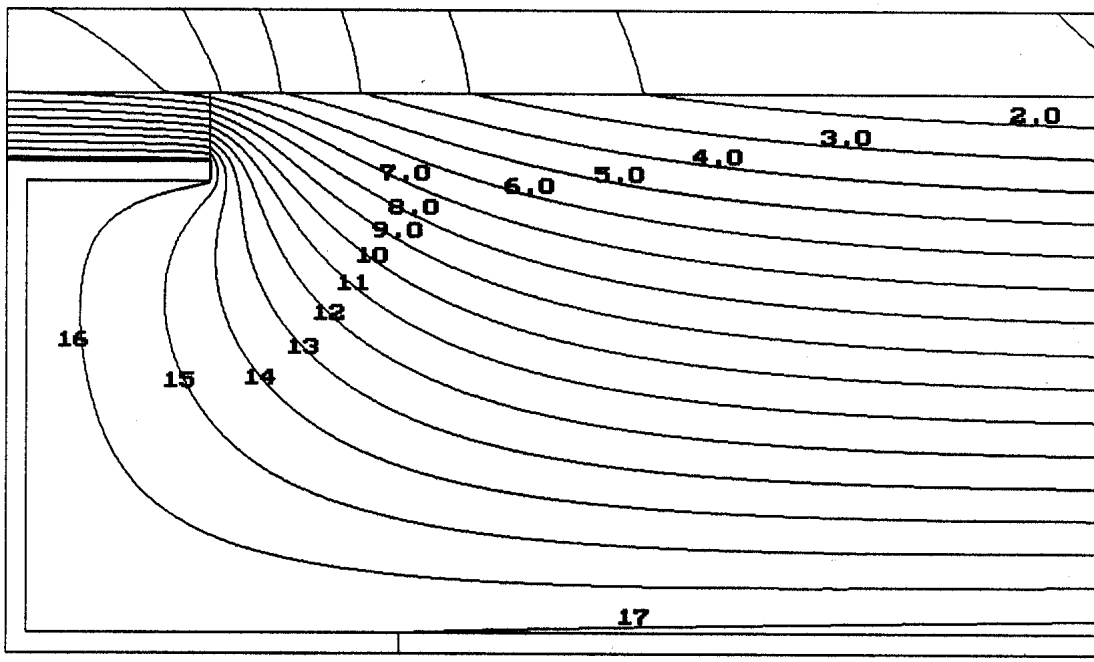
Figure 6.88: Isotherms for the left part of the problem.

6.13.3 Conclusions

This reference case is a relatively difficult numerical problem due to the high ratio of the maximum and minimum thermal conductivity (almost 8000). About 1000 cells are needed to give an error of 0.1% for the heat flows through the wall. This calculation took less than a minute on Pentium/90. The rate of convergence for this steady-state problem depends largely of the chosen successive over-relaxation coefficient. Using ω=1.995 gives a calculation time of about half a minute using 1254 cells. If ω=1.9 is used, a calculation time of about 10 minutes is required. Using ω=1.95 gives a calculation time of about 6 minutes.

The large temperature gradients, especially at location G, makes the interpolation of temperatures difficult. About 4000 cells is needed using HEAT2 to fulfill the requirement for temperatures in (CEN, 1995). About 100 numerical cells suffice to fulfill the requirement for heat flows.

Chapter 7

Heat conduction coupled to radiation in a cavity

The problem of thermal radiation in a cavity coupled to heat conduction and ventilation is analyzed in detail. There are $2N + 1$ coupled nonlinear equations to solve for a cavity with N subsurfaces. The corresponding thermal flow network with a new component for the nonlinear radiation shows in a lucid way the various interacting processes between radiation, conduction and ventilation. After direct elimination of $N + 1$ unknowns, an exact matrix equation for the N surface temperatures remains to be solved. This equation is well suited for an iterative computer solution procedure, which turns out to be robust and very rapid. An abridged description of the presented method is given in (Blomberg et al, 1995a).

A calculation for a brick roof section with 16 cavities using some 1700 nodes for heat conduction and 8 subsurfaces in each cavity, gave a numerical accuracy on the one per cent level (and one minute CPU-time).

This chapter, dealing with radiation, uses some special symbols. Therefore, a separate nomenclature is given.

Nomenclature

Symbol   Quantity, (Units)

Symbol	Quantity, (Units)
A_i	area of surface element i, (m^2)
c	heat capacity, (J/(kg·K))
F	view factor, (-)
G	incident radiation, (W/m^2)
J	radiosity, (W/m^2)
K	thermal conductance, (W/K)
$\mathbf{M}_{sb}$	coupling matrix between surface and boundary temperatures
$\mathbf{M}_\Theta$	coupling matrix between surface and excess radiation temperatures
$\dot{m}_a$	ventilation mass flow rate, (kg/s)
N	number of surface elements of the cavity
Q	heat flow, (W)
T	temperature, (°C)
T_{so}	linearization temperature level, (°C)
T_r	radiosity temperature, (°C)
$\tilde{T}$	temperature, (K)
$\mathbf{T}_s$	column matrix for surface temperatures, (°C)
$\dot{V}_a$	volume flow rate, (m^3/s)
$\mathbf{X}_{sv}$	coupling matrix between surface and ventilation temperatures

Greek letters

α_c	convective heat transfer coefficient, (W/(m^{2}K))
ϵ	emissivity, (-)
ρ	density, (kg/m^3)
σ	Stefan-Boltzmann constant, (5.67·10^{-8} W/(m^{2}K^4))
Θ_r	excess radiation temperature, (°C)
ε	relative error, (-)

Subscripts and superscripts

a	air
b	boundary of the cavity
i	surface element i
r	radiation
s	surface
v	ventilation

7.1 Introduction

Heat conduction in solid building parts coupled to long-wave thermal radiation in air cavities is a frequently occurring and studied type of process in building physics. The cavity, which may be ventilated, may be an attic, a room, a crawl-space, the space between glass panels in a window, closed air volumes in brick, and cracks and other voids in building thermal envelopes.
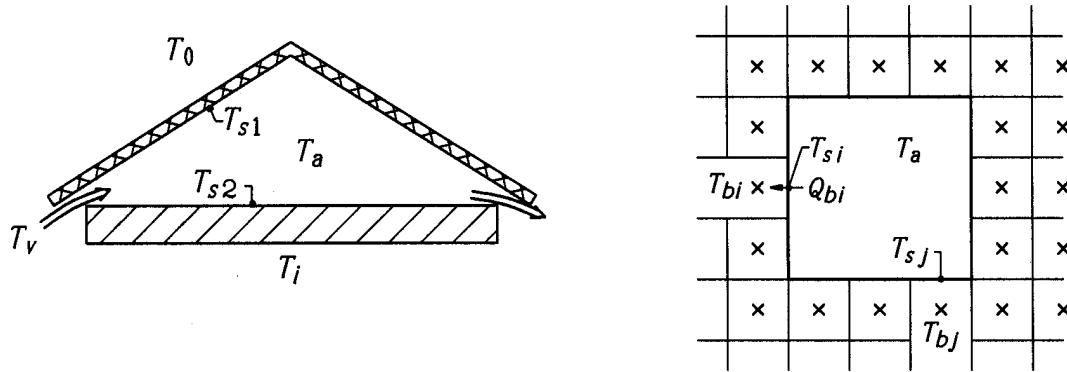
Figure 7.1: Heat conduction coupled to radiation in a cavity. Left: attic, right: numerical simulation.

This coupling between conduction and radiation occurs in many discrete models, in which the thermal process is represented by a few temperatures. Figure 7.1 shows as two examples an attic (left) and a cavity in a solid material (right). The attic air, roof surface and floor surface temperatures T_a, T_{s1} and T_{s2}, respectively, are to be determined. The ambient temperatures (T_0 and T_i for the attic) outside the enclosing walls of the cavity are prescribed. There is an interaction between heat conduction through attic roof and floor, long-wave radiation between the attic surfaces, convective heat exchange between air and surfaces. There may be ventilation with a prescribed inlet air temperature T_v and a prescribed ventilation rate.

Figure 7.1, right, illustrates the coupling problem for a numerical calculation using finite differences or finite elements. The temperatures in the nodes of the numerical mesh inside the solid material are calculated step by step. At each iteration step, there are given temperatures T_{bi} in internal nodes bordering on the cavity. The problem is to calculate the surface temperatures T_{si} and the heat flow rates Q_{bi} (W) into the boundary cells.

The steady-state case with long-wave radiation in the diffuse-gray approximation is considered. The cavity may be ventilated. The problem how to represent and solve, in a handy and lucid way, the heat and radiation balance equations is dealt with in this chapter. A particular aim is to minimize the required computational work. This is important for numerical simulations, in which the cavity balance equations are to be solved at each iteration step.

The equation system is nonlinear because of the fourth-power radiation law. This problem is specifically addressed, and a rapidly converging iteration process is proposed.

7.2 Considered problem

Figure 7.2 shows the problem considered. The air in the cavity has a single bulk temperature T_a. The cavity is surrounded by an envelope of solid material. The temperatures outside the envelope, T_{bi}, are prescribed. The surface temperatures T_{si} are to be determined. There is long-wave radiative heat exchange at the surface of the cavity. The cavity is ventilated with prescribed ventilation rate $\dot{m}_a$ (kg/s) and inlet air temperature T_v.
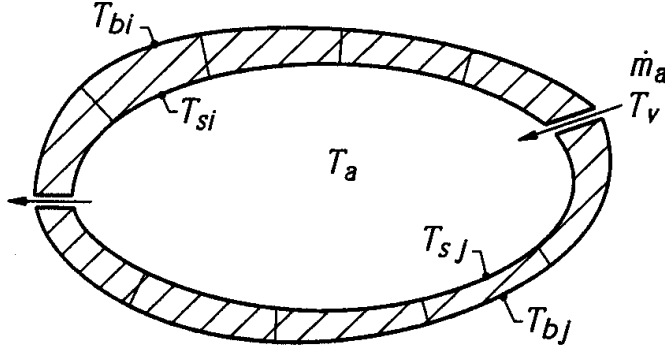
Figure 7.2: Ventilated air cavity with heat conduction through a solid envelope and radiation exchange between surface elements i.

The cavity surface is divided into N elements. Surface element i has the area A_i and the temperature T_{si}. The problem is to determine $T_{s1}, ... T_{sN}$ and T_a for prescribed boundary temperatures $T_{b1}, ... T_{bN}$ and inlet ventilation temperature T_v.

7.3 Heat balance equations

There are heat balance equations for the air in the cavity and for the N surface elements. There are also N radiation balance equations, which are coupled to the surface balances.

The heat balance equation for the air in the cavity is:

$$K_v(T_v - T_a) + \sum_{i=1}^{N} K_{ai}(T_{si} - T_a) = 0 \tag{7.1}$$

The ventilation conductance (or convectance) K_v (W/K) and the air-to-surface conductances K_{ai} (W/K) are defined by

$$K_v = c_a \dot{m}_a = c_a \rho_a \dot{V}_a \qquad K_{ai} = A_i \alpha_{ci} \tag{7.2}$$

Here, $c_a \simeq 1000$ J/(kg·K) is the heat capacity of air (at constant pressure), and $\dot{m}_a$ (kg/s) the air mass flow rate. The volume flow rate (m^3/s) becomes $\dot{V}_a = \dot{m}_a/\rho_a$. The convective heat transfer coefficients α_{ci}, (W/(m^{2}K)), may be different for different surface elements i. The difficult question of proper choice of α_{ci} will not be discussed here.

The heat balance for surface element i is:

$$K_{ai}(T_a - T_{si}) + K_{bi}(T_{bi} - T_{si}) = Q_{ri} \qquad i = 1, ... N \tag{7.3}$$

The first left-hand term is the convective heat transfer from air to surface. The other term is the steady-state heat conduction through envelope element i. The total thermal conductance of element i with the surface area A_i for one-dimensional heat flow through the envelope is denoted K_{bi} (W/K). The heat flow rates are balanced by the radiation Q_{ri} (W), which is the net radiation from surface i.

We use throughout this section thermal conductances K (W/K) and not thermal resistances $R = 1/K$ (K/W), since the formulas become somewhat handier using conductances.

The heat balance equations (7.1) and (7.3) may be represented graphically by a thermal network. Figure 7.3 shows the conductance network for $N = 3$. The $N + 1 = 4$ nodes with the temperatures T_{s1}, T_{s2}, T_{s3} and T_a represent the balance equations. There are prescribed temperatures $T_{bi}, i = 1, 2, 3$, at the boundary nodes. The inlet air temperature T_v is also represented by a boundary node.
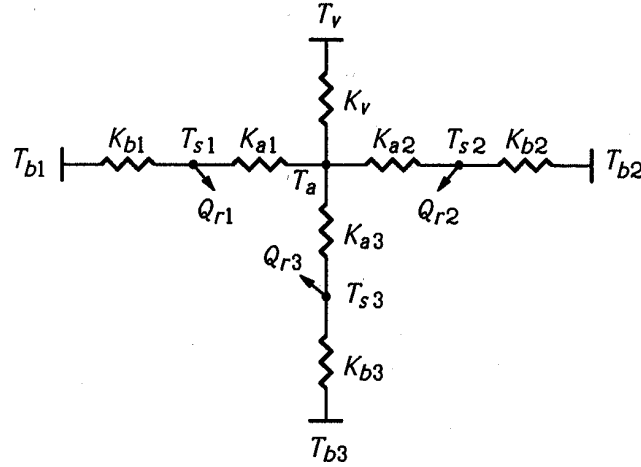
Figure 7.3: Thermal conductance network to represent the heat balance equations for air and cavity surface elements ($N = 3$).

7.4 Radiation balance equations

Only long-wave radiation in the diffuse-gray approximation is considered. See for example (Siegel et al, 1992), or (Holman, 1986). The radiation energy balance equations are, (Holman, 1986):

$$J_i = \epsilon_i \sigma \tilde{T}_{si}^4 + (1 - \epsilon_i) G_i$$

$$Q_{ri} = A_i (J_i - G_i)$$

$$A_i G_i = \sum_{j=1}^{N} A_j J_j F_{ji} \qquad i = 1, ...N \qquad (7.4)$$

Here, J_i (W/m^2) is the radiosity of surface element i, i.e. the total radiation which leaves surface i per unit area and unit time. The emissivity of the gray and diffuse surface i is

denoted ϵ_i, and σ is the Stefan-Boltzmann constant. The tilde sign ˜ denotes temperature in Kelvin:

$$\tilde{T}_{si} = T_{si} + 273.15 \quad (T_{si} \text{ in } {}^\circ\text{C}, \quad \tilde{T}_{si} \text{ in } \text{K}) \tag{7.5}$$

The radiation incident on surface i per unit area is G_i. The reflectivity is equal to $1 - \epsilon_i$, since total absorptivity and emissivity are equal in the gray-diffuse approximation. The net radiation that leaves surface i is Q_{ri} (W). The view factors F_{ij} satisfy the equations

$$A_i F_{ij} = A_j F_{ji} \qquad \sum_{j=1}^{N} F_{ij} = 1 \tag{7.6}$$

The first equation of (7.4) states that the total radiation J_i that leaves surface i is equal to the emission and the reflected part of the incident radiation G_i. The second equation defines the net radiation Q_{ri} that leaves surface i. The third equation of (7.4) gives the incident radiation on surface i involving view factors and radiation J_j from all surface elements. There is radiation from i on itself when F_{ii} is larger than zero.

Elimination of G_i between the first two equations of (7.4) gives:

$$Q_{ri} = \frac{\epsilon_i A_i}{1 - \epsilon_i} \left(\sigma \tilde{T}_{si}^4 - J_i \right) \qquad i = 1, ... N \tag{7.7}$$

Elimination of G_i between the first and third equations of (7.4) gives equations for the radiosities J_i:

$$\frac{\epsilon_i A_i}{1 - \epsilon_i} \left(\sigma \tilde{T}_{si}^4 - J_i \right) = \sum_{j=1}^{N} A_i F_{ij} (J_i - J_j) \qquad i = 1, ... N \tag{7.8}$$

Equations (7.6) are used to obtain the sum with its difference $J_i - J_j$ on the right hand side of (7.8).

The considered problem involves $2N+1$ unknowns: the air temperature T_a, the surface temperatures $T_{s1}, ... T_{sN}$, and the radiosities $J_1, ... J_N$. The $2N + 1$ balance equations are (7.1) for air, (7.3) combined with (7.7) for the surface elements, and (7.8) for the radiation exchange. A particular problem is the fourth-power $(T_{si} + 273.15)^4$, which makes the equation system nonlinear.

7.5 Radiation equations in temperature form

The radiation balance equations (7.8) are linear relations between the unknown radiosities J_i. For problems with given surface temperatures T_{si}, there is certainly no need to reformulate the equations. They should be used directly. In the considered case, however, the heat balance equations involving temperatures are coupled to the radiation equations and other formulations should be considered.

A common approach is to linearize the equations by expansion of the terms involving $\tilde{T}_{si}^4$ around a suitable temperature level $\tilde{T} = \tilde{T}_{so}$. In building physics applications (except fire), the surface temperatures T_{si} vary within a rather limited interval. The differences

$T_{si} - T_{so}$ (and $T_{si} - T_{sj}$) are small compared to $\tilde{T}_{so}$, and the error in the linearization becomes rather small. The linearization procedure is used here, but the remaining terms are retained, so that the equations remain exact.

A direct (or a Taylor) expansion of the fourth power x^4 near a point $x = x_0$ is:

$$x^4 = x_0^4 + 4x_0^3(x - x_0) + 6x_0^2(x - x_0)^2 + 4x_0(x - x_0)^3 + (x - x_0)^4 \tag{7.9}$$

or

$$x^4 = x_0^4 + 4x_0^3 \cdot (x - x_0) + (x - x_0)^2(x^2 + 2xx_0 + 3x_0^3) \tag{7.10}$$

These two expressions are exact. The first two terms give the linear approximation. The remaining part is proportional to $(x - x_0)^2$.

Now, let T_{so} (°C) be a suitable, but freely chosen, temperature level for the cavity surface temperatures:

$$\tilde{T}_{so} = T_{so} + 273.15 \tag{7.11}$$

With $x = \tilde{T}_{si}$ and $x_0 = \tilde{T}_{so}$, Eq. (7.9) or (7.10) may be written in the following way:

$$\tilde{T}_{si}^4 = \tilde{T}_{so}^4 + 4\tilde{T}_{so}^3 \cdot [T_{si} - T_{so} + \Theta_r(T_{si})] \tag{7.12}$$

In the last factor, $T_{si} - T_{so}$ is used instead of $\tilde{T}_{si} - \tilde{T}_{so}$. The nonlinear terms are contained in the function $\Theta_r(T_{si})$. We will called it the *excess radiation temperature*. The excess radiation temperature is from (7.10) and (7.12) defined by:

$$\Theta_r(T) = \Theta_r(T, T_{so}) = \frac{(T - T_{so})^2 \left(\tilde{T}^2 + 2\tilde{T}\tilde{T}_{so} + 3\tilde{T}_{so}^2\right)}{4\tilde{T}_{so}^3}$$

$$\left(\tilde{T} = T + 273.15 \, , \, \tilde{T}_{so} = T_{so} + 273.15\right) \tag{7.13}$$

The function Θ_r depends on T and on the chosen temperature level T_{so}. The following alternative expression is obtained from (7.12) and (7.9):

$$\Theta_r(T) = \frac{3}{2\tilde{T}_{so}}(T - T_{so})^2 + \frac{1}{\tilde{T}_{so}^2}(T - T_{so})^3 + \frac{1}{4\tilde{T}_{so}^3}(T - T_{so})^4 \tag{7.14}$$

The separation of $\tilde{T}^4$ into a linear part and a nonlinear correction, Eq. (7.12), is illustrated in Figure 7.4. The linear part is the tangent to $\tilde{T}^4$ at the point $\tilde{T} = \tilde{T}_{so}$. The nonlinear part is, as indicated in Figure 7.4, left, equal to $4\tilde{T}_{so}^3 \cdot \Theta_r(T)$. Eq. (7.12) may be written in the following way:

$$\frac{\tilde{T}^4 - \tilde{T}_{so}^4}{4\tilde{T}_{so}^3} = T - T_{so} + \Theta_r(T) \tag{7.15}$$

This relation is shown in Figure 7.4, right (for $T_{so} = 17$°C). It should be noted that $\Theta_r(T)$ is positive (and zero for $T = T_{so}$). The adjective in the denomination *excess* radiation temperature associates to this fact.
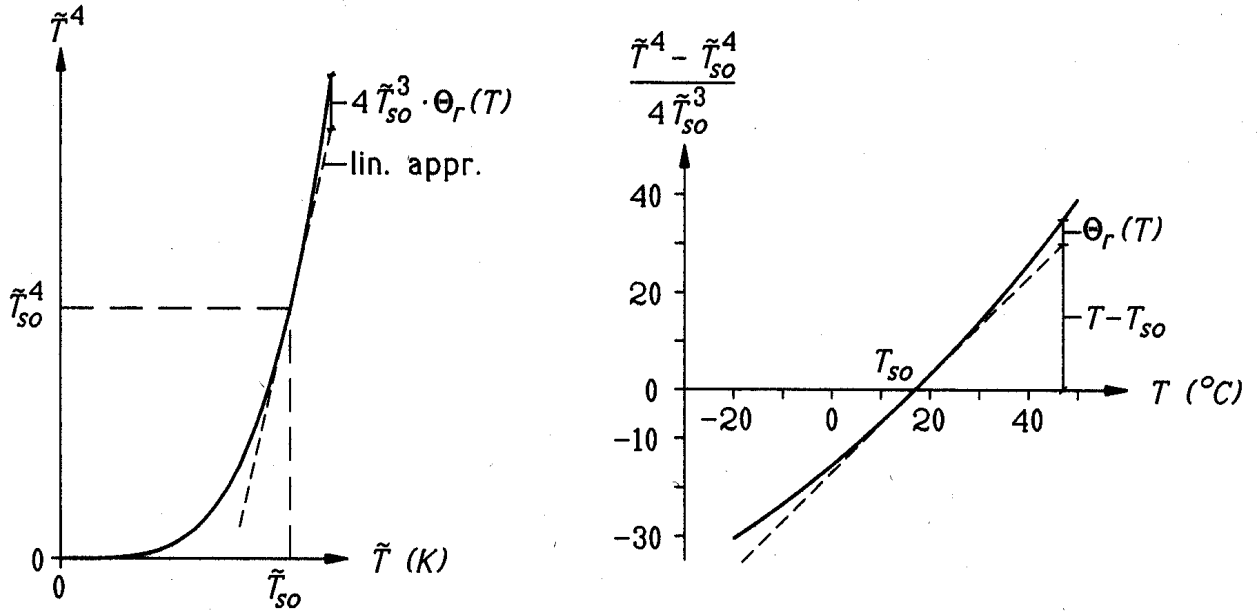
Figure 7.4: Linear and nonlinear part of $\tilde{T}^4$ according to Eq. (7.12), left, or (7.15), right, (for $T_{so} = 17°C$).

In the linear or first-order approximation, $\Theta_r(T_{si})$ is neglected. The relative error $\varepsilon_{(1)}$ is essentially given by the first term of $\Theta_r(T_{si})$ in (7.14):

$$\frac{\tilde{T}_{si}^4 - \tilde{T}_{so}^4}{4\tilde{T}_{so}^3} \simeq T_{si} - T_{so} \qquad \varepsilon_{(1)} = \frac{\Theta_r(T_{si})}{T_{si} - T_{so}} \simeq \frac{3}{2} \cdot \frac{T_{si} - T_{so}}{\tilde{T}_{so}} \tag{7.16}$$

In the second-order approximation, the first term in (7.14) is retained. The relative error $\varepsilon_{(2)}$ is then essentially given by the second term of $\Theta_r(T_{si})$ in (7.14) (divided by $T_{si} - T_{so}$):

$$\frac{\tilde{T}_{si}^4 - \tilde{T}_{so}^4}{4\tilde{T}_{so}^3} \simeq T_{si} - T_{so} + \frac{3}{2} \cdot \frac{(T_{si} - T_{so})^2}{\tilde{T}_{so}} \qquad \varepsilon_{(2)} \simeq 1 \cdot \left(\frac{T_{si} - T_{so}}{\tilde{T}_{so}}\right)^2 \tag{7.17}$$

Consider the example $T_{so} = 17°C$ ($\tilde{T}_{so} = 290$ K) and $T_{si} - T_{so} = 10°C$. The error in temperature in the linear approximation is given by the first term of (7.14): $1.5 \cdot 10^2/290 = 0.5°C$, which should be compared to the linear value $10°C$. The relative error $\varepsilon_{(1)}$ becomes $0.5/10$ or 5%. In the second-order approximation, the temperature error according to the second term of (7.14) becomes $10^3/290^2 = 0.012°C$, which should be compared to $10 + 0.5°C$. The relative error $\varepsilon_{(2)}$ becomes $0.01/10.5$ or 0.1%.

All excess radiation temperatures $\Theta_r(T_{si})$ are positive. Only the differences occur in the radiation balance equations. The errors in radiative heat flows are therefore smaller than the above errors. This is illustrated in the example in Section 7.12.

We now define the *"radiosity" temperature* T_{ri}, (°C), of surface i by

$$T_{ri} = \frac{J_i - \sigma\tilde{T}_{so}^4}{4\sigma\tilde{T}_{so}^3} + T_{so} \quad \text{or} \quad J_i = \sigma\tilde{T}_{so}^4 + 4\sigma\tilde{T}_{so}^3 \cdot (T_{ri} - T_{so}) \tag{7.18}$$

156

These expressions for J_i and Eq. (7.12) for $\tilde{T}_{si}^4$ are inserted in the radiation balance equations (7.8). With these deliberate choices, the radiation balance equations become:

$$K_{ri}\left[T_{si} + \Theta_r(T_{si}) - T_{ri}\right] = \sum_{j=1, j \neq i}^{N} K_{ij}^r (T_{ri} - T_{rj}) \qquad i = 1, ...N \tag{7.19}$$

The introduced radiation conductances (W/K) are:

$$K_{ri} = 4\sigma \tilde{T}_{so}^3 \cdot \frac{\epsilon_i A_i}{1 - \epsilon_i} \qquad K_{ij}^r = 4\sigma \tilde{T}_{so}^3 \cdot A_i F_{ij} \qquad (i \neq j) \tag{7.20}$$

The net radiation Q_{ri}, Eq. (7.7), becomes:

$$Q_{ri} = K_{ri}(T_{si} + \Theta_r(T_{si}) - T_{ri}) \qquad i = 1, ...N \tag{7.21}$$

The radiation balance equations (7.19) involve the temperatures T_{ri}. The nonlinear part is contained in the excess radiation temperature $\Theta_r(T_{si})$. We have a *temperature representation* of the radiation equations. Equations (7.19) with the net radiation (7.21) may be represented graphically by a thermal radiation network with unknown radiosity temperatures T_{ri} in N nodes. The case $N = 3$ is shown in Figure 7.6, right. A particular problem is the nonlinear part in (7.21). This part may be represented by an extra heat flow rate $I_{ri} = K_{ri}\Theta_r(T_{si})$ (W) from node T_{si} to node T_{ri}. See Figure 7.5. The arrow, which is wavelike to associate to radiation, shows the direction of the nonlinear contribution.

$$Q_{ri} = K_{ri} \cdot (T_{si} - T_{ri}) + I_{ri}$$

$$I_{ri} = K_{ri}\Theta_r(T_{si})$$
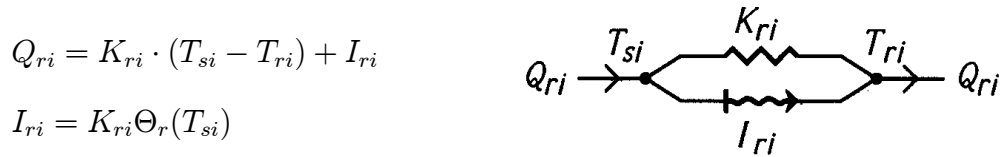
Figure 7.5: Equation (7.21) for the net radiation Q_{ri} and its graphical representation with an extra heat transfer I_{ri} due to the nonlinear part.

7.6   Thermal network

The final balance equations for heat and radiation in temperature form are now from (7.1), (7.3) inserting (7.21), and (7.19):

$$K_v(T_v - T_a) + \sum_{i=1}^{N} K_{ai}(T_{si} - T_a) = 0 \qquad \text{(for } T_a)$$

$$K_{ai}(T_a - T_{si}) + K_{bi}(T_{bi} - T_{si}) + K_{ri}(T_{ri} - T_{si} - \Theta_r(T_{si})) = 0 \qquad \text{(for } T_{si}, \, i = 1, ...N)$$

$$K_{ri}(T_{si} + \Theta_r(T_{si}) - T_{ri}) + \sum_{j=1, j \neq i}^{N} K_{ij}^r(T_{rj} - T_{ri}) = 0 \qquad \text{(for } T_{ri}, \, i = 1, ...N) \tag{7.22}$$

These equations express energy balances for T_a, T_{si} and T_{ri}, respectively. The radiation conductances K_{ri} and K_{ij}^r $(i \neq j)$ are defined by (7.20). The nonlinear part of the radiation is accounted for by the excess radiation temperature $\Theta_r(T_{si})$ defined by (7.13).

The equation system may be represented graphically by a thermal network with $2N+1$ nodes with the temperatures $T_a, T_{s1}, ...T_{sN}, T_{r1}, ...T_{rN}$. There are conductances K (or resistances $R = 1/K$) between the nodes. The solution is determined by the prescribed boundary temperatures $T_{b1}, ...T_{bN}$ and T_v.

Figure 7.6 shows the complete thermal network for $N = 3$. The heat balance part (left) and radiation part (right) are superimposed on each other. The connections between the two parts are indicated by double lines at the nodes $T_{si}, i = 1, 2, 3$.

The surface temperature T_{si} is used in the conductive-convective part of the thermal network to calculate the heat flow to T_{bi} and T_a. See Fig. 7.6, left. The excess radiation temperature $\Theta_r(T_{si})$ must be added to T_{si} when the radiative heat flow to T_{ri} is calculated, Eq. (7.21). The nonlinear radiation is represented by a conductance K_{ri} and the extra heat transfer $I_{ri} = K_{ri}\Theta_r(T_{si})$ from T_{si} to T_{ri}. See Fig. 7.5 and Fig. 7.6, right. The linear approximation is obtained by neglecting I_{ri}.
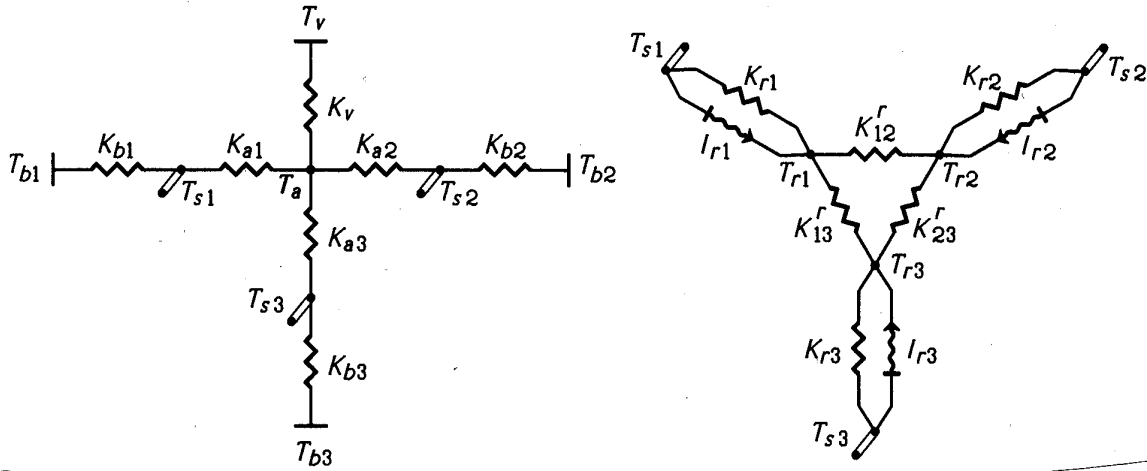
Figure 7.6: Thermal network for $N = 3$. The radiation part (right) is connected to the heat flow part (left) at the nodes T_{si}. The linear part of the radiation is accounted for by the conductance K_{ri}, and the nonlinear correction by the extra heat transfer $I_{ri} = K_{ri}\Theta_r(T_{si})$.

7.7 Equations in matrix form

The thermal network, Figure 7.6, and the corresponding balance equations in the form (7.22) provide a very clear way to represent the physical process with its various interactions. The following form of the equations is more convenient to use when the equations

are to be solved:

$$K_a T_a = K_v T_v + \sum_{j=1}^{N} K_{aj} T_{sj}$$

$$K_{si} T_{si} + K_{ri} \Theta_r(T_{si}) = K_{ai} T_a + K_{bi} T_{bi} + K_{ri} T_{ri} \qquad i = 1, ...N$$

$$K_{ri}(T_{si} + \Theta_r(T_{si})) + \sum_{j=1}^{N} K_{ij}^r T_{rj} = 0 \qquad i = 1, ...N \tag{7.23}$$

The following conductances are introduced:

$$K_a = K_v + \sum_{j=1}^{N} K_{aj} \tag{7.24}$$

$$K_{si} = K_{ai} + K_{bi} + K_{ri} \qquad i = 1, ...N \tag{7.25}$$

The conductance K_a is the sum of all conductances to the air node T_a, and K_{si} is the sum of the three conductances to surface node T_{si}. See Figure 7.6. It is notationally convenient to introduce the "conductances" K_{ii}^r:

$$K_{ii}^r = -K_{ri} - \sum_{j=1, j \neq i}^{N} K_{ij}^r \qquad i = 1, ...N \tag{7.26}$$

The quantity $-K_{ii}^r$ is equal to the sum of the conductances to the radiosity node T_{ri}. The negative sign should be noted. Eqs. (7.20) using (7.6) give:

$$K_{ii}^r = -4\sigma \tilde{T}_{so}^3 \cdot A_i \left(\frac{1}{1 - \epsilon_i} - F_{ii} \right) \qquad i = 1, ...N \tag{7.27}$$

The solution of the equation system (7.23) presented below involves direct elimination of $N+1$ unknowns to a reduced system, which has to be inverted by, for example, Gaussian elimination. The most clear way to describe the procedure is to use matrices. Equations (7.23) may in matrix form be written in the following way:

$$K_a T_a = K_v T_v + \mathbf{X}_a^\dagger \mathbf{T}_s$$

$$\mathbf{D}_s \mathbf{T}_s + \mathbf{D}_r \Theta_r(\mathbf{T}_s) = \mathbf{X}_a T_a + \mathbf{D}_b \mathbf{T}_b + \mathbf{D}_r \mathbf{T}_r$$

$$\mathbf{D}_r \left[\mathbf{T}_s + \Theta_r(\mathbf{T}_s) \right] + \mathbf{K}_r \mathbf{T}_r = \mathbf{0} \tag{7.28}$$

Boldfaced letters denote matrices. Diagonal matrices are denoted by $\mathbf{D}$, while $\mathbf{X}$, $\mathbf{T}$ and Θ_r denote column matrices.

The radiation conductance matrix $\mathbf{K}_r$ has $N \times N$ elements $K_{ij}^r, i, j = 1, ...N$, defined by (7.20) for $i \neq j$ and by (7.27) for $i = j$. The column matrix $\mathbf{X}_a$ has the conductances K_{ai} as elements, and the transposed matrix $\mathbf{X}_a^\dagger$ is the corresponding single row matrix with N elements:

$$\mathbf{X}_a = \begin{pmatrix} K_{a1} \\ \vdots \\ K_{aN} \end{pmatrix} \qquad \mathbf{X}_a^\dagger = (K_{a1}, ..., K_{aN}) \tag{7.29}$$

159

The surface temperatures T_{si} and the excess radiation temperatures $\Theta_r(T_{si})$, $i = 1, ...N$, are represented by the column matrices $\mathbf{T_s}$ and $\mathbf{\Theta}_r$:

$$\mathbf{T}_s = \begin{pmatrix} T_{s1} \\ \vdots \\ T_{sN} \end{pmatrix} \qquad \mathbf{\Theta}_r(\mathbf{T}_s) = \begin{pmatrix} \Theta_r(T_{s1}) \\ \vdots \\ \Theta_r(T_{sN}) \end{pmatrix} \tag{7.30}$$

The column matrices $\mathbf{T}_r$ and $\mathbf{T}_b$ have T_{ri} and $T_{bi}, i = 1, ...N$, as elements. The diagonal matrices $\mathbf{D}_s$, $\mathbf{D}_r$ and $\mathbf{D}_b$ have the conductances K_{si}, K_{ri}, and K_{bi}, respectively, in the diagonal, while all other elements are zero. We have for example:

$$\mathbf{D}_r = \begin{pmatrix} K_{r1} & & 0 \\ & \ddots & \\ 0 & & K_{rN} \end{pmatrix} \qquad \mathbf{D}_r^{-1} = \begin{pmatrix} 1/K_{r1} & & 0 \\ & \ddots & \\ 0 & & 1/K_{rN} \end{pmatrix} \tag{7.31}$$

The inverse of a diagonal matrix is readily obtained. The diagonal elements are just inverted. The matrix $\mathbf{D}_r^{-1}$ has the components $1/K_{ri}$ in the diagonal.

7.8 Equations for surface temperatures

The $2N + 1$ equations (7.23) or (7.28) may be reduced to N equations by rather straightforward eliminations. The first equation in (7.28) relates T_a to $\mathbf{T}_s$. Elimination of T_a gives two matrix equations which contain $\mathbf{T}_s$ and $\mathbf{T}_r$:

$$\left(\mathbf{D}_s - \mathbf{X}_a \mathbf{X}_a^\dagger / K_a \right) \mathbf{T}_s + \mathbf{D}_r \mathbf{\Theta}_r(\mathbf{T}_s) = \mathbf{X}_a K_v T_v / K_a + \mathbf{D}_b \mathbf{T}_b + \mathbf{D}_r \mathbf{T}_r$$

$$\mathbf{T}_r = -\mathbf{K}_r^{-1} \mathbf{D}_r \left[\mathbf{T}_s + \mathbf{\Theta}_r(\mathbf{T}_s) \right] \tag{7.32}$$

Here, $\mathbf{K}_r^{-1}$ is the inverse matrix to $\mathbf{K}_r$. The matrix $\mathbf{X}_a \mathbf{X}_a^\dagger / K_a$ has the $N \times N$ elements $K_{ai} K_{aj} / K_a$.

Insertion of the second equation for $\mathbf{T}_r$ in the first one gives an equation involving $\mathbf{T}_s$ only. The equations involve the inverse $\mathbf{K}_r^{-1}$. The need to calculate this inverse is avoided by multiplying the second equation by $\mathbf{K}_r$ and the first one by $\mathbf{K}_r \mathbf{D}_r^{-1}$, and eliminating $\mathbf{K}_r \mathbf{T}_r$. This gives a final equation involving the N unknown surface temperatures $\mathbf{T}_s$ only:

$$\mathbf{M} \mathbf{T}_s + (\mathbf{D}_r + \mathbf{K}_r) \mathbf{\Theta}_r(\mathbf{T}_s) = \mathbf{K}_r \mathbf{D}_r^{-1} \left(\mathbf{D}_b \mathbf{T}_b + \mathbf{X}_a K_v T_v / K_a \right) \tag{7.33}$$

It should be noted that the original system contains $2N + 1$ unknowns. After the above eliminations, an equation system with N unknowns only is to be solved.

The matrix $\mathbf{M}$ is given by:

$$\mathbf{M} = \mathbf{D}_r + \mathbf{K}_r \mathbf{D}_r^{-1} \left(\mathbf{D}_s - \mathbf{X}_a \mathbf{X}_a^\dagger / K_a \right) \tag{7.34}$$

Multiplication by a diagonal matrix is quite simple to perform. The explicit components M_{ij} of $\mathbf{M}$ become:

$$M_{ij} = K_{ri}\delta_{ij} + K_{ij}^r \frac{K_{sj}}{K_{rj}} - \frac{K_{aj}}{K_a} \sum_{k=1}^{N} K_{ik}^r \frac{K_{ak}}{K_{rk}} \tag{7.35}$$

Here, δ_{ij} denotes Kronecker's function: $\delta_{ii} = 1$ and $\delta_{ij} = 0$ for $i \neq j$.

Let $\mathbf{M}^{-1}$ be the inverse matrix to $\mathbf{M}$. In general, it must be computed numerically. The final matrix equation for the surface temperatures $\mathbf{T}_s$ is now:

$$\mathbf{T}_s = \mathbf{M}_{sb}\mathbf{T}_b + \mathbf{X}_{sv}T_v + \mathbf{M}_\Theta\mathbf{\Theta}_r(\mathbf{T}_s) \tag{7.36}$$

The new matrices, with explicit expressions for the components given to the right, are:

$$\mathbf{M}_{sb} = \mathbf{M}^{-1}\mathbf{K}_r\mathbf{D}_r^{-1}\mathbf{D}_b \qquad M_{ij}^{sb} = \frac{K_{bj}}{K_{rj}} \sum_{k=1}^{N} M_{ik}^{-1}K_{kj}^r \tag{7.37}$$

$$\mathbf{X}_{sv} = \mathbf{M}^{-1}\mathbf{K}_r\mathbf{D}_r^{-1}\mathbf{X}_aK_v/K_a \qquad X_i^{sv} = \frac{K_v}{K_a} \sum_{k=1}^{N} \left[\frac{K_{ak}}{K_{rk}} \sum_{j=1}^{N} M_{ij}^{-1}K_{jk}^r \right] \tag{7.38}$$

$$\mathbf{M}_\Theta = -\mathbf{M}^{-1}(\mathbf{D}_r + \mathbf{K}_r) \qquad M_{ij}^\Theta = -M_{ij}^{-1}K_{rj} - \sum_{k=1}^{N} M_{ik}^{-1}K_{kj}^r \tag{7.39}$$

The matrix $\mathbf{M}_{sb}$ represents the coupling between $\mathbf{T}_s$ and $\mathbf{T}_b$, and the column matrix $\mathbf{X}_{sv}$ the coupling between $\mathbf{T}_s$ and the inlet ventilation temperature T_v. The matrix $\mathbf{M}_\Theta$ couples $\mathbf{T}_s$ to the nonlinear terms in $\mathbf{\Theta}(\mathbf{T}_s)$.

7.9 Iterative solution

The nonlinear equation system (7.36) for $\mathbf{T}_s$ must be solved iteratively. The first tentative solution $\mathbf{T}_s^{(1)}$ is obtained by neglecting the excess radiation temperatures $\mathbf{\Theta}_r(\mathbf{T}_s)$:

$$\mathbf{T}_s^{(1)} = \mathbf{M}_{sb}\mathbf{T}_b + \mathbf{X}_{sv}T_v \tag{7.40}$$

This is the solution in the conventional linear approximation. The exact solution is readily obtained by successive substitutions:

$$\mathbf{T}_s^{(n)} = \mathbf{T}_s^{(1)} + \mathbf{M}_\Theta\mathbf{\Theta}_r(\mathbf{T}_s^{(n-1)}) \qquad (n = 2, 3, ...) \tag{7.41}$$

This substitution technique is well suited for computer solution. Each step involves the calculation of $\Theta_r(T_{si}^{(n-1)})$, $i = 1, ...N$, and a matrix multiplication $\mathbf{M}_\Theta\mathbf{\Theta}_r(\mathbf{T}_s^{(n-1)})$. The iterations are repeated until all differences $|T_{si}^{(n)} - T_{si}^{(n-1)}|$, $i = 1, ...N$, are sufficiently small. The iterative procedure converges rapidly in building physics applications for which $|T_{si} - T_{so}|/\tilde{T}_{so}$ is of the order 1/10th.

The choice of T_{so} influences the convergence rate, which is determined by $(T_{si} - T_{so})/\tilde{T}_{so}$, $i = 1, ...N$. The denominator $\tilde{T}_{so}$ is not sensitive to the choice of T_{so}, while

the numerator $T_{si} - T_{so}$ changes more. But the choice should not be too critical. See Section 7.12.

7.10   Other quantities

The other unknown quantities are readily obtained, when $T_{si}, i = 1, ...N$, are known. The air temperature T_a is given by the first equation in (7.23):

$$T_a = (K_v T_v + \sum_{i=1}^{N} K_{ai} T_{si})/K_a \qquad (7.42)$$

The radiosity temperatures $T_{ri}, i = 1, ...N$, are obtained from the second equation of (7.23) $(K_{ri} \neq 0)$:

$$T_{ri} = (K_{si} T_{si} - K_{ai} T_a - K_{bi} T_{bi})/K_{ri} + \Theta_r(T_{si}) \qquad (7.43)$$

The radiosities J_i are then obtained from (7.18).

The heat flow rates to the boundary nodes and via ventilation are of particular interest, since they give the response of the whole system. Let Q_{bi} (W) denote the heat flow to the boundary node T_{bi}:

$$Q_{bi} = K_{bi}(T_{si} - T_{bi}) \qquad i = 1, ...N \qquad (7.44)$$

The heat flow rate from the cavity due to ventilation, Q_v (W), is:

$$Q_v = K_v(T_a - T_v) \qquad (7.45)$$

7.11   Final formulas

Let us summarize the final formulas for the solution of the problem shown in Fig. 7.2. The original $2N+1$ equations to solve are (7.1), (7.3) with Q_{ri} given by (7.7), and (7.8). The same equation system in temperature form, using the concept of an excess radiation temperature $\Theta_r(T_{si})$, is given by (7.22). After elimination of T_a and the radiosity temperatures T_{ri}, the equation system (7.33) or (7.36) for the N surface temperatures T_{si} remains to be solved.

The N surface temperatures $T_{s1}, ...T_{sN}$ are the solution of (7.36):

$$\mathbf{T}_s = \mathbf{M}_{sb}\mathbf{T}_b + \mathbf{X}_{sv}T_v + \mathbf{M}_\Theta\Theta_r(\mathbf{T}_s) \qquad (7.46)$$

The square matrices $\mathbf{M}_{sb}$ and $\mathbf{M}_\Theta$, and the column matrix $\mathbf{X}_{sv}$ are given by (7.37-7.39). Here, $\mathbf{M}^{-1}$ is the inverse matrix to (7.34). The various conductances that appear in the expressions for the matrix components (7.35) and (7.37-7.39) are defined by (7.24), (7.25), (7.27), (7.20) and (7.2).

162

The first order linear solution is obtained by neglecting the excess radiation temperatures $\Theta_r(T_{si})$ in Eq. (7.46):

$$\mathbf{T}_s \simeq \mathbf{T}_s^{(1)} = \mathbf{M}_{sb}\mathbf{T}_b + \mathbf{X}_{sv}T_v \tag{7.47}$$

The exact solution is determined iteratively from (7.41).

The air temperature T_a is then obtained from (7.42), and the radiosity temperatures T_{ri} by (7.43). The heat flows Q_{bi} and Q_v are given by (7.44) and (7.45).

7.12   Numerical example

The presented method of solution will here be illustrated by a single application concerning an Italian brick roof. Each large lightweight brick contains 16 cavities in a rectangular pattern. See Figure 7.7. The thermal conductivities (W/(m·K)) of different areas are shown. The steady-state process in the two-dimensional section is to be simulated.
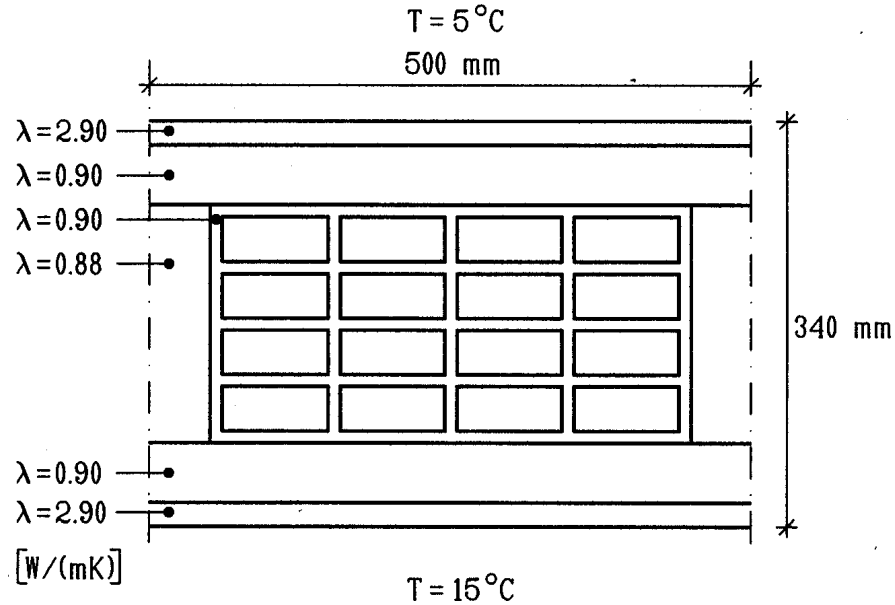
Figure 7.7: Considered section of a brick roof with 16 cavities.

The outside temperature is 5 °C, and the temperature below the roof is 15 °C. The surface resistances inside and outside are both 0.1 m²K/W. The vertical sides are considered adiabatic. The cavities are not ventilated ($K_v=0$). The convective heat transfer coefficients α_{ci} are put to 1.0 W/(m²K), which is the expected order of magnitude from empirical relations (Kreith et al, 1986). The emissivity ϵ_i of all surfaces is 0.9.

The process has been simulated for different meshes. Figure 7.8 shows one of the finer meshes. The number of computational cells N_c is 3860. Each cavity has $N=40$ surface elements. The coarsest mesh has $N_c=127$, and $N=4$, i.e. one surface temperature on each side of the rectangular cavities.

The temperatures lie between 5 and 15 °C. The temperature level T_{so} is therefore put to 10 °C for all 16 cavities.

The above procedure for cavity balances has been incorporated in the PC-program HEAT2. This program for two-dimensional transient and steady-state heat transfer contains the above procedure to account for radiation in cavities. The maximum number of computational cells N_c is 15625, the maximum number of cavities is 20, and the maximum number of radiative elements N in each cavity is 125 in the standard version.
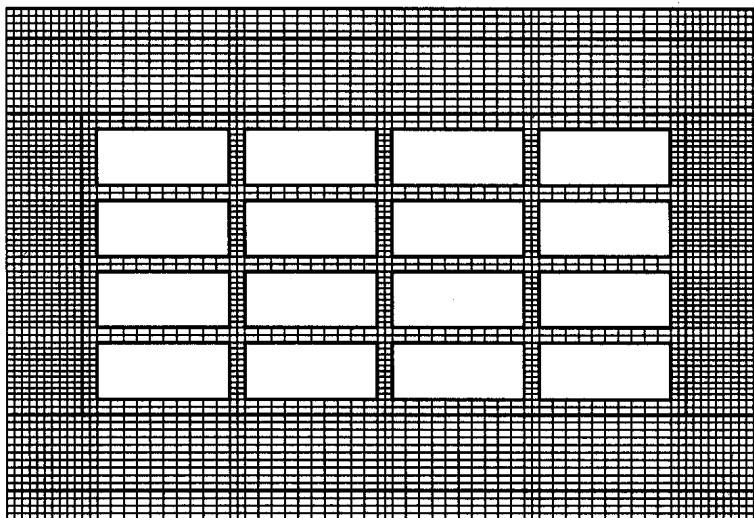
Figure 7.8: The numerical mesh with N_c=3860 and N=40.

Table 7.1 shows the calculated heat flow (W/m) through the brick roof section for different computational meshes. A second order of approximation is used. The results will in these cases be the same if higher orders of approximation are used. The finest mesh with 9225 cells and 80 radiative elements in each cavity is judged to have a very small numerical error. The error relative to the value for this finest mesh is 2.1% with 1412 cells, and 0.2% with 3860 cells. Even in the case with 127 cells and 4 radiative elements, the error turns out to be relatively small (2.6%). The last column shows the approximate calculation time on a Pentium/90. Figure 7.9 shows the calculated isotherms.

N_C	N	Heat flow (W/m)	error (%)	CPU time
127	4	5.823	2.6	5 sec.
1412	4	5.849	2.1	20 sec.
1684	8	5.915	1.0	1 min.
3860	40	5.960	0.2	5 min.
9225	80	5.973	-	20 min.

Table 7.1: Heat flow, error, and CPU-time for four different meshes.
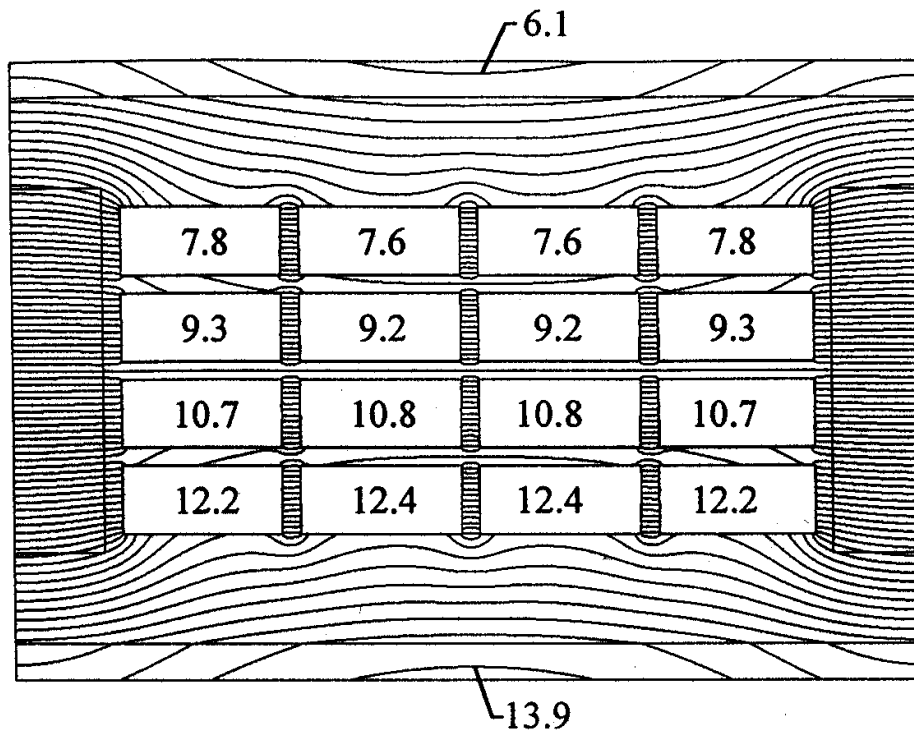
Figure 7.9: Calculated isotherms with an interval of 0.1 °C. The horizontal isotherm in the middle has the temperature 10 °C. The air temperatures are written in the cavities.

7.13 Choice of T_{so} and rate of convergence

The temperature level T_{so} for the linearization procedure may be chosen at will. The choice will influence the rate of convergence in the iteration (7.41). Table 7.2 shows the calculated heat flow $Q^{(n)}$ for different iteration steps for the mesh with N_c=3860 and N=40.

Iteration step	T_{so} (°C)					
	10	5	15	0	-80	100
1	5.959	5.897	5.898	5.836	5.030	7.192
2	5.960	5.960	5.960	5.960	5.970	5.996
3					5.959	5.961
4					5.960	5.960

Table 7.2: Heat flows (W/m) with N_C=3860 and N=40.

Table 7.2 shows that the choice of T_{so} is not particularly critical, especially with higher orders of approximation. If T_{so} is put to the same value as one of the prescribed boundary temperatures, 5 °C or 15 °C, the error in the case with linear (first order) approximation turns out to be about one per cent. Even extreme choices such as $T_{so} = -80$ °C or $T_{so} = 100$ °C require only three iterations to obtain four digit accuracy.

The considered problem is well-behaved with small temperature differences in the cavities. We have used the iterative solution procedure in many other problems without any difficulties.

The calculations take somewhat longer time with higher orders of approximation. For most building physics applications, the linear approximation should be sufficient. One iteration in Eq. (7.41) may be performed to check this in case of doubts.

7.14 Conclusions

The problem of thermal radiation in a cavity coupled to heat conduction and ventilation has been analyzed. A particular complication is the nonlinearity due to the fourth-power radiation law. There are $2N + 1$ coupled nonlinear equations to solve for a cavity with N subsurfaces.

The radiation balance equations are formulated in a particular form, where the nonlinear radiative part is represented by a so-called excess radiation temperature. The $2N + 1$ equations may be represented graphically in a thermal flow network, where a new component is introduced to represent in an exact way the effect of the nonlinear radiative part. This graphical representation shows in a lucid way the various interacting processes between radiation, conduction and ventilation.

The second step in the analysis was to formulate the equations in matrix form and to reduce the number of equations by direct elimination of $N + 1$ unknowns. The elimination involved a single inversion of a $N \cdot N$ matrix. The remaining matrix equation for the N surface temperatures with its linear and nonlinear parts, Eq. (7.46), is well suited for an iterative solution procedure, which is readily implemented on a computer. Each iterative step involves the calculation of the excess radiation temperatures and a matrix multiplication.

The solution procedure was illustrated by an example concerning a brick roof section with 16 cavities. A calculation with some 1700 nodes for the heat conduction and 8 subsurfaces in each cavity gave a numerical accuracy on the one per cent level and required one minute of CPU-time (Pentium/90). The linear approximation, or one iteration step only, was shown to be sufficient in the considered case.

The choice of linearization temperature influences the required number of iteration steps. However, it was shown that more than one iteration was necessary only for quite extreme choices.

Chapter 8

Concluding survey

Conclusions have been presented directly in the different studies. Here, a brief survey and reiteration of conclusions are given.

8.1 Computer programs

Computer programs for transient and steady-state heat conduction in two and three dimensions have been developed. These are called HEAT2 (Blomberg, 1990, 1991) and HEAT3 (Blomberg, 1993a, 1994a). The programs are part of a library (Arfvidsson et al, 1993), developed by *Lund Group for Computational Building Physics*, containing about 30 programs within the fields of building physics and ground heat.

The robust method of explicit finite differences is used. This method closely follows the physical equations. The mathematical equations for two- and three-dimensional heat conduction and the numerical formulation are presented in Chapter 3.

HEAT2 and HEAT3 can be used for analyses of thermal bridge effects, heat transfer through corners of a window, heat loss from a house to the ground, to mention but a few applications.

HEAT2W (Blomberg, 1994b) is a drawing program that makes it simple to describe a large range of heat transfer problems. The user builds up the geometry by using rectangles of different materials. The current version of HEAT2W serves as a preprocessor to the DOS-version HEAT2. A generated input file is read into HEAT2 where boundary conditions have to be specified before the problem can be simulated. The numerical mesh is automatically generated, but can easily be changed. HEAT2W gives many advantages being a program under the Microsoft Windows environment, such as exporting (or importing) objects (e.g. pictures or text) via the clipboard to other programs for drawing or editing. It is also possible to scan a building design drawing and import it via the clipboard into HEAT2W. The actual heat transfer problem could easily be described just by drawing rectangles "on" the imported design drawing.

HEAT2R (Blomberg, 1994c) is a computer program for transient and steady-state heat conduction in cylindrical coordinates r and z.

TR2 (Blomberg, 1992) is a PC-program for calculation of surface heat flows in one and two dimensions for building components under transient conditions according to the thermal response factor method.

8.2   Numerical studies

In chapter 4 a few numerical studies are reported. The first topic involves accuracy considerations for different computational meshes. Generally, the smaller the computational cells are, the better is the agreement with the "true" temperature distribution. The accuracy using an expansive mesh is often considerably higher than that using an equidistant mesh with the same number of cells.

Different numerical techniques can be used to decrease CPU-time. It has been shown that the successive over-relaxation method in the steady-state case is simple to use and that it is very efficient. An optimized ω may give calculation times between 1/50th and 1/10th of that required for a calculation not using over-relaxation (ω=1.0). The optimized ω lies typically in the range 1.8-2.

Another technique is the method of subdivision, which means that the mesh is gradually refined. The analyses show that this method decreases CPU-time in some cases. However, if one succeeds in finding an optimized relaxation factor ω, either by use of analytical equations or by numerical tests, subdivision should be of minor importance.

Results from two or three calculations using different meshes may be used to estimate more accurate results. Consider the example in Section 6.2 entitled *Metal thermal bridges in thermal insulation*. This is a problem in three dimensions with a quite irregular mesh. The error was lowered from 3.8% to 0.3% by combining results from three calculations with 128, 1215, and 2736 cells, respectively. These three calculations take together less than a minute. A single numerical simulation requires 110000 cells to give an error of 0.3%. This calculation will take about 15 minutes. The method of combining results from two calculations with 1215 and 2736 cells lowered the error from 3.8% to 1.1%. The gain using this technique can be quite substantial.

8.3   Applications

With our numerical technique and computer programs, it is quite easy to solve ordinary heat conduction problems. A problem using 15000 computational nodes may require a few minutes of CPU-time on a modern PC. The difficult case of steel girders in thermal insulation, using one million computational cells, was solved in about five hours on a Pentium (90 MHz).

The programs have been used to solve many thermal problems. A number of examples are reported in order to provide the user with help and guidelines concerning choice of numerical mesh, accuracy, etc. One example deals with certain low-conductivity panels placed in foam. This problem with its intricate geometry is solved without difficulty with the three-dimensional program HEAT3. Another example deals with the thermal bridge

of a wall with steel girders in mineral wool. The thermal conductivity of steel is about 1700 times higher than that of mineral wool. This may cause numerical accuracy problems. The use of one million computational cells made it possible to establish a numerical error of about 0.1%.

One study deals with a house with a floor heating system, see Section 6.11. Formulas are given for the heat loss to the ground and for the effective U-value for the floor. The more of the total heating demand that is supplied by the floor heating system, the more does the heat loss to the ground (and the effective U-value for the floor) increase.

The problem of thermal radiation in a cavity coupled to heat conduction and ventilation is analyzed in detail. There are $2N + 1$ coupled nonlinear equations to solve for a cavity with N subsurfaces. The corresponding thermal flow network with a new component for the nonlinear radiation shows in a lucid way the various interacting processes between radiation, conduction and ventilation. After direct elimination of $N + 1$ unknowns, an exact matrix equation for the N surface temperatures remains to be solved. This equation is well suited for an iterative computer solution procedure, which turns out to be robust and very rapid. Newer versions of HEAT2 may account for thermal radiation in cavities. Figure 5.1 shows calculated isotherms for a window frame with 20 cavities. See also the figures on the back cover. This calculation took a few minutes on a PC (about 2500 numerical cells). Another calculation for a brick roof section with 16 cavities, using some 1700 nodes for heat conduction and 8 subsurfaces in each cavity, gave a numerical accuracy on the one per cent level (and one minute CPU-time).

Appendix A

Analytical solution for a parallelepiped

The analytical solution to the problem described in Section 4.1 is presented below. Figure 4.1 shows a homogeneous parallelepiped with a thermal conductivity of 1.0. The temperature at the surface $z=L_z$ is 1. On the other five sides the temperature is zero. The domain V of the parallelepiped is limited by

$$0 \leq x \leq L_x, \quad 0 \leq y \leq L_y, \quad 0 \leq z \leq L_z$$

For the steady-state case, the Laplacian operator is zero

$$\nabla^2 T = 0 \text{ inside V} \qquad 0 \leq x \leq L_x, \quad 0 \leq y \leq L_y, \quad 0 \leq z \leq L_z$$

The boundary conditions are

$$T = 0 \text{ at all boundaries except } z = L_z$$

A solution is presented for two different boundary conditions on the surface $z=L_z$

I. $\qquad T(x, y, L_z) = 1 \qquad 0 < x < L_x, \quad 0 < y < L_y$

II. $\qquad \left. \dfrac{\partial T}{\partial z} \right|_{(x,y,L_z)} = 1 \qquad 0 < x < L_x, \quad 0 < y < L_y$

Solution for case I

The general solution that satisfies the Laplace equation and the five boundary conditions of zero temperature is

$$T(x,y,z) = \sum_{m=1}^{\infty} \sum_{n=1}^{\infty} a_{mn} \sin\left(\frac{m\pi x}{L_x}\right) \sin\left(\frac{n\pi y}{L_y}\right) \sinh\left(\sqrt{\left(\frac{m^2}{L_x^2} + \frac{n^2}{L_y^2}\right)} \pi z\right)$$

The coefficients a_{mn} are determined by the remaining boundary condition for case I:

$$\sum_{m=1}^{\infty} \sum_{n=1}^{\infty} a_{mn} \sin\left(\frac{m\pi x}{L_x}\right) \sin\left(\frac{n\pi y}{L_y}\right) \sinh\left(\sqrt{\left(\frac{m^2}{L_x^2} + \frac{n^2}{L_y^2}\right)} \pi L_z\right) = 1$$

The coefficients a_{mn} are determined in the following way. A well-known one-dimensional Fourier expansion of 1 in the interval $0 < x < L_x$ is (Stroud, 1986):

$$\frac{4}{\pi}\left[\frac{1}{1}\sin\left(\frac{\pi x}{L_x}\right) + \frac{1}{3}\sin\left(\frac{3\pi x}{L_x}\right) + ...\right] = 1 \qquad 0 < x < L_x$$

or

$$\frac{4}{\pi}\sum_{m=0}^{\infty}\frac{1}{2m+1}\sin\left(\frac{(2m+1)\pi x}{L_x}\right) = 1 \qquad 0 < x < L_x$$

In the same way, we have in y-direction:

$$\frac{4}{\pi}\sum_{n=0}^{\infty}\frac{1}{2n+1}\sin\left(\frac{(2n+1)\pi y}{L_y}\right) = 1 \qquad 0 < y < L_y$$

The product of these two series is

$$\frac{16}{\pi^2}\sum_{m=0}^{\infty}\sum_{n=0}^{\infty}\frac{1}{(2m+1)(2n+1)}\sin\left(\frac{(2m+1)\pi x}{L_x}\right)\sin\left(\frac{(2n+1)\pi y}{L_y}\right) = 1 \cdot 1 \qquad \text{(A.1)}$$

Identification of the terms gives the odd coefficients:

$$\frac{16}{\pi^2}\frac{1}{(2m+1)(2n+1)} = a_{2m+1,2n+1}\sinh\left(\pi L_z\sqrt{\frac{(2m+1)^2}{L_x^2} + \frac{(2n+1)^2}{L_y^2}}\right)$$

The coefficients $a_{2m,2n}$ are zero. The solution is

$$T(x,y,z) = \frac{16}{\pi^2}\sum_{m=0}^{\infty}\sum_{n=0}^{\infty}\frac{\sin\left(\frac{(2m+1)\pi x}{L_x}\right)}{2m+1}\frac{\sin\left(\frac{(2n+1)\pi y}{L_y}\right)}{2n+1}\frac{\sinh\left[\pi z\sqrt{\frac{(2m+1)^2}{L_x^2} + \frac{(2n+1)^2}{L_y^2}}\right]}{\sinh\left[\pi L_z\sqrt{\frac{(2m+1)^2}{L_x^2} + \frac{(2n+1)^2}{L_y^2}}\right]}$$

The flow through the bottom side $z = 0$ is

$$Q_0 = \int_0^{L_x}dx\int_0^{L_y}dy\left.\frac{\partial T}{\partial z}\right|_{(x,y,0)} \qquad \text{(A.2)}$$

The derivative becomes

$$\left.\frac{\partial T}{\partial z}\right|_{(x,y,0)} = \frac{16}{\pi^2}\sum_{m=0}^{\infty}\sum_{n=0}^{\infty}\frac{\sin\left(\frac{(2m+1)\pi x}{L_x}\right)}{2m+1}\frac{\sin\left(\frac{(2n+1)\pi y}{L_y}\right)}{2n+1}\frac{\pi\sqrt{\frac{(2m+1)^2}{L_x^2} + \frac{(2n+1)^2}{L_y^2}}\cdot 1}{\sinh\left(\pi L_z\sqrt{\frac{(2m+1)^2}{L_x^2} + \frac{(2n+1)^2}{L_y^2}}\right)}$$

The essential integral in x is

$$\int_0^{L_x}\sin\left(\frac{(2m+1)\pi x}{L_x}\right)dx = \left[-\frac{L_x}{(2m+1)\pi}\cos\left(\frac{(2m+1)\pi x}{L_x}\right)\right]_{x=0}^{x=L_x}$$

$$= \frac{L_x}{\pi(2m+1)}\left(1 - \underbrace{\cos\left((2m+1)\pi\right)}_{-1}\right) = \frac{2L_x}{\pi(2m+1)}$$

There is a similar expression in y. The total flow Q_0 is then

$$Q_0 = \frac{64}{\pi^3} L_x L_y \sum_{m=0}^{\infty} \sum_{n=0}^{\infty} \frac{1}{(2m+1)^2} \frac{1}{(2n+1)^2} \frac{\sqrt{\frac{(2m+1)^2}{L_x^2} + \frac{(2n+1)^2}{L_y^2}}}{\sinh\left(\pi L_z \sqrt{\frac{(2m+1)^2}{L_x^2} + \frac{(2n+1)^2}{L_y^2}}\right)} \quad \text{(A.3)}$$

Solution for case II

The boundary condition at $z=L_z$ is now:

$$\sum_{m=1}^{\infty} \sum_{n=1}^{\infty} a_{mn} \sin\left(\frac{m\pi x}{L_x}\right) \sin\left(\frac{n\pi y}{L_y}\right) \pi \sqrt{\frac{m^2}{L_y^2} + \frac{n^2}{L_y^2}} \cosh\left[\pi L_z \sqrt{\frac{m^2}{L_x^2} + \frac{n^2}{L_z^2}}\right] = 1$$

Identification in (A.1) gives

$$\frac{16}{\pi^2} \frac{1}{(2m+1)(2n+1)} =$$

$$a_{2m+1,2n+1} \pi \sqrt{\frac{(2m+1)^2}{L_x^2} + \frac{(2n+1)^2}{L_x^2}} \cosh\left[\pi L_z \sqrt{\frac{2m+1)^2}{L_x^2} + \frac{(2n+1)^2}{L_x^2}}\right]$$

The temperature field becomes

$$T(x,y,z) = \frac{16}{\pi^3} \sum_{m=0}^{\infty} \sum_{n=0}^{\infty} \frac{\sin\left(\frac{(2m+1)\pi x}{L_x}\right)}{2m+1} \frac{\sin\left(\frac{(2n+1)\pi y}{L_y}\right)}{2n+1} \cdot$$

$$\frac{\sinh\left(\pi z \sqrt{\frac{(2m+1)^2}{L_x^2} + \frac{(2n+1)^2}{L_y^2}}\right)}{\sqrt{\frac{(2m+1)^2}{L_x^2} + \frac{(2n+1)^2}{L_y^2}} \cdot \cosh(\pi L_z \sqrt{\frac{(2m+1)^2}{L_x^2} + \frac{(2n+1)^2}{L_y^2}})}$$

The flow Q_0 according to Eq. (A.2) through $z = 0$ is obtained by integration in x and y. This gives

$$Q_0 = \frac{64}{\pi^4} L_x L_y \sum_{m=0}^{\infty} \sum_{n=0}^{\infty} \frac{1}{(2m+1)^2} \frac{1}{(2n+1)^2} \frac{1}{\cosh\left[\pi L_z \sqrt{\frac{(2m+1)^2}{L_x^2} + \frac{(2n+1)^2}{L_y^2}}\right]} \quad \text{(A.4)}$$

Appendix B
List of heat conduction programs

The following list shows a selection of computer programs that can be used for solving heat conduction problems. The list is not complete, it shows only a few of the most common programs. The information is taken from product catalogues, the Internet, and (Thyholt et al, 1994). See next page for addresses.

Name	2D	3D	Cylindrical coordinates	Steady-state	Transient	Finite differences	Finite elements
ABAQUS	x	x	x	x	x		FEM
ALGOR	x	x		x	x		FEM
ANSYS	x	x	x	x	x		FEM
CALFEM	x	x		x	x		FEM
FIDAP	x	x	x	x	x		FEM
FLOTRAN	x	x	x	x	x		FEM
FLUENT	x	x	x	x	x		FEM
FRAME	x			x		FDM	
GF2DIM	x			x		FDM	
HCONP	x			x		FDM	
HEAT2	x			x	x	FDM	
HEAT2R			x	x	x	FDM	
HEAT3		x		x	x	FDM	
I-DEAS	x	x	x	x	x		FEM
ISOTHERM	x			x			FEM
ISO-2	x			x		FDM	
KOBRU86	x			x		FDM	
MARC	x	x	x	x	x		FEM
MATLAB	x	x	x	x	x		FEM
NACHOS2	x		x	x	x		FEM
NASTRAN	x	x	x	x	x		FEM
PLAN	x	x		x		FDM	
PLAN3D	x	x		x		FDM	
PC3D	x	x		x	x	FDM	
RAMPANT	x	x	x	x	x		FEM
SECTRA	x				x	FDM	
THAFEM	x		x	x	x		FEM
TOPAZ	x		x	x	x		FEM
TRISCO		x		x		FDM	
VOLTRA		x			x	FDM	
WAEBRU	x	x		x	x	FDM	

Table B.1: A selection of common computer programs for heat conduction.

ABAQUS. FEM-Tech AB. Pilgatan. 8, S-721 30 Västerås, Sweden.

ALGOR. Algor Inc. 150 Beta Drive, Pittsburgh, PA 15238-2932, USA.

ANSYS/FLOTRAN. Swanson Analysis System Inc. Johnson road, P.O. Box 65, Houston, PA 15342-0065, USA.

CALFEM. Division of Structural Mechanics, Lund University. P.O. Box 118, S-221 00 Lund, Sweden.

FIDAP. Fluid Dynamics International. 500 Davis Street, Suite 600, Evanston, IL 60201, USA.

FLUENT/RAMPANT. Fluent Europe Ltd. Hutton's Buildings, 146 West Street, Sheffield, S1 4ES, UK.

FRAME. Enermodal Engineering Limited. 368 Phillip Street, Waterloo, Ontario, N2L 5J1, Canada.

GF2DIM. Gullfiber AB. S-260 50 Billesholm, Sweden.

HCONP. Carl-Eric Hagentoft. Kärnvedsgatan 16, S-416 80 Göteborg, Sweden.

HEAT2/HEAT2R/HEAT3. Department of Building Physics, Lund University. P.O. Box 118, S-221 00 Lund, Sweden.

I-DEAS. SDRC UK Ltd, Software Products Marketing Division. Milford House, Priory End, Hitchin, Hertfordshire, SG4 9AL, UK.

ISOTHERM. Institut für Fenstertechnik e.V. Theodor-Giessl-Strasse 9, D-8200 Rosenheim, Germany.

ISO-2. W. Schmidli. Bodenackerstrasse 52, CH-5200, Brugg, Switzerland.

KOBRU86/SECTRA/TRISCO/VOLTRA. Physibel C.V. Heirweg 21, B-9990 Maldegem, Belgium.

MARC. MARC Analysis Research Corporation. Bredewater 26, 2715 CA Zoetermeer, The Netherlands.

MATLAB. MathWorks Inc. Cochituate Place, 24 Prime Park Way, Natick, Massachusetts, 01760, USA.

NACHOS2. Sandia National Labs. Albuquerque, NM, USA.

NASTRAN. MSC. 815 Colorado Blvd., CA 9004, USA.

PLAN/PLAN3D. GWJ. Berlinerstrasse 62, D-03046 Cottbus, Germany.

PC3D. Harvard Thermal. P.O. Box 508, Harvard Massachusetts, 01451-0508, USA.

THAFEM. Department of Mechanical Engineering. Linköpings Universitet, S-581 83 Linköping, Sweden.

TOPAZ. Lawrence Livermore National Lab. Livermore, CA, USA.

WAEBRU. Institut F. Bauphysik F. Architekten, Technische Universität Wien, Karlsplatz, A-1040 Wien, Austria.

References

Agnoletto, L. 1976. *Comportamento termico delle pareti multistrato in regime variabile.* Istituto di Fisica Tecnica. Universita' di Padova, Via F. Marzolo 9, 35131 Padova, Italy.

Agnoletto, L.; T. Blomberg; P. Romagnoni. 1993. *Two-dimensional transient heat conduction through building components.* Proceedings of *CLIMA 2000*, page 218. CLIMA 2000 Secretariat, CIBSE, Delta House, 222 Balham High Road, London SW12 9BS, UK.

Arfvidsson, J.; T. Blomberg; J. Claesson; C-E. Hagentoft. 1993. *Lund library of computer models in building physics.* Proceedings of the 3rd conference on *Building Physics in the Nordic Countries*, Building Physics '93 (Bjarne Saxhof, editor), page 271. Thermal Insulation Laboratory, Lyngby, Denmark, 1993. ISBN 87-984610-0-1 Volume 1.

Blomberg, T. 1990. *HEAT2 - A heat transfer PC-program.* Proceedings of the 2nd conference on *Building Physics in the Nordic Countries*. Division of Building Technology, Department of Civil Engineering, The Norwegian Institute of Technology, The University of Trondheim, Alfr. Getz vei 3, N-7034 Trondheim, Norway.

Blomberg, T. 1991. *HEAT2 - A heat transfer PC-program. Manual for HEAT2.* Department of Building Physics, Lund University. P.O. Box 118, S-221 00 Lund, Sweden. CODEN:LUTVDG/(TVBH-7122).

Blomberg, T. 1992. *TR2 - Thermal response factors in one and two dimensions.* Department of Building Physics, Lund University. P.O. Box 118, S-221 00 Lund, Sweden. CODEN:LUTVDG/TVBH-7138.

Blomberg, T. 1993a. *HEAT3 - A three-dimensional heat transfer computer program.* Proceedings of the 3rd conference on *Building Physics in the Nordic Countries*, Building Physics '93 (Bjarne Saxhof, editor), page 339. Thermal Insulation Laboratory, Lyngby, Denmark, 1993. ISBN 87-984610-0-1 Volume 1.

Blomberg, T.; J. Claesson. 1993b. *Metal thermal bridges in thermal insulation.* Proceedings of the 3rd conference on *Building Physics in the Nordic Countries*, Building Physics '93 (Bjarne Saxhof, editor), page 91. Thermal Insulation Laboratory, Lyngby, Denmark, 1993. ISBN 87-984610-0-1 Volume 1.

Blomberg, T. 1993c. *U-value for a window accounting for the wall.* Proceedings of the 3rd conference on *Building Physics in the Nordic Countries*, Building Physics '93 (Bjarne Saxhof, editor), page 73. Thermal Insulation Laboratory, Lyngby, Denmark, 1993. ISBN 87-984610-0-1 Volume 1.

Blomberg, T.; I. Samuelsson. 1993d. *Temperature and moisture conditions in attics.* Proceedings of the 3rd conference on *Building Physics in the Nordic Countries*, Building Physics '93 (Bjarne Saxhof, editor), page 547. Thermal Insulation Laboratory, Lyngby, Denmark, 1993. ISBN 87-984610-2-8 Volume 2.

Blomberg, T. 1994a. *HEAT3 - A three-dimensional heat transfer computer program. Manual for HEAT3.* Department of Building Physics, Lund University. P.O. Box 118, S-221 00 Lund, Sweden. CODEN:LUTVDG/(TVBH-7169).

Blomberg, T. 1994b. *HEAT2W - HEAT2 for Windows.* Department of Building Physics, Lund University. P.O. Box 118, S-221 00 Lund, Sweden. CODEN:LUTVDG/(TVBH-7168).

Blomberg, T. 1994c. *HEAT2R - A PC-program for heat conduction in cylindrical coordinates r and z.* Department of Building Physics, Lund University. P.O. Box 118, S-221 00 Lund, Sweden. CODEN:LUTVDG/(TVBH-7178).

Blomberg, T. 1994d. *Heat conduction in two and three dimensions. Computer modelling of Building Physics Applications.* Department of Building Physics, Lund University. P.O. Box 118, S-221 00 Lund, Sweden. Report TVBH-1006. ISRN LUTVDG/TVBH--94/1006--SE/(1-114). ISBN 91-628-1311-0.

Blomberg, T.; J. Claesson. 1995a. *Heat conduction coupled to radiation in cavity walls.* Proceedings of *International Symposium on Moisture Problems in Building Walls.* Departamento de Engenharia Civil, Faculdade de Engenharia da Universidade do Porto. Rua dos Bragas, 4099 Porto Codex, Portugal.

Blomberg, T. 1995b. *Stålbyggnadsdagen 1995.* Stålbyggnadsinstitutet. Swedish Institute of Steel Construction. Drottning Kristinas väg 48, S-114 28 Stockholm, Sweden. Publikation 154.

Borland. 1993. *Borland Pascal.* Borland International, Inc., 1800 Green Hills Road P.O. Box 660001, Scotts Valley, CA 95067-0001, USA.

Borland. 1995. *Delphi.* Borland International, Inc., 1800 Green Hills Road P.O. Box 660001, Scotts Valley, CA 95067-0001, USA.

Chapra, S. C., R. P. Canale. 1985. *Numerical Methods for Engineers.* McGraw-Hill Book Company. New York.

Claesson, J., B. Eftring. 1980. *Optimal distribution of thermal insulation and ground heat losses.* Byggforskningsrådet. The Swedish Council for Building Research. Report D33:1980.

Claesson, J., B. Eftring, P. Eskilson, G.Hellström. 1985. *Markvärme - En handbok om termiska analyser.* Written in Swedish. The Swedish Council for Building Research. Reports T16-T17:1985.

Claesson, J., T. Blomberg, P. Wallentén. 1989a. *Korttidsvärmelagring i bergrum.* Department of Building Physics, Lund University. P.O. Box 118, S-221 00 Lund, Sweden.

Claesson, J.; T. Blomberg. 1989b. *Thermal shielding of rock caverns with heating pipes.* Department of Building Physics, Lund University. P.O. Box 118, S-221 00 Lund, Sweden. CODEN:LUTVDG/(TVBH-7114).

Claesson, J. C-E. Hagentoft. 1994. *Basic Building Physics. Preliminary version.* Department of Building Physics, Lund University. P.O. Box 118, S-221 00 Lund, Sweden.

CEN. 1995. *Thermal bridges in building construction - Heat flows and surface temperatures - Part1: General calculation methods.* European Committee for Standardization, rue de Stassart 36, B-1050 Brussels, Belgium. Ref. No. EN ISO 10211-1.

CEN. 1996. *Building components and building elements - Thermal resistance and thermal transmittance - Calculation method.* European Committee for Standardization, rue de Stassart 36, B-1050 Brussels, Belgium. Ref. No. EN ISO 6946:1996.

Glicksman, L.R. 1991. *Two-dimensional heat transfer effects on vacuum and reflective insulations.* Depts of Building Technology and Mechanical Engineering, Massachusetts Institute of Technology, Cambridge, USA.

Gullfiber AB. 1989. *GFSTEEL.* Gullfiber AB, S-260 50 Billesholm, Sweden.

Eftring, B. 1990. *Numerisk beräkning av temperaturförlopp. Numerical calculations of thermal processes.* (Written in Swedish). Byggforskningsrådet. The Swedish Council for Building Research. Report R81:1990.

Elmroth, A. 1985. *Energisnåla stålhallar. Byggnadstekniska lösningar för god lufttäthet och effektiv värmeisolering.* Stålbyggnadsinstitutet. Swedish Institute of Steel Construction. Drottning Kristinas väg 48, S-114 28 Stockholm, Sweden. ISBN No. 91-85644-40-4.

Hagentoft, C-E. 1988. *Heat loss to the ground from a building.* Department of Building Physics, Lund University. P.O. Box 118, S-221 00 Lund, Sweden. CODEN:LUTVDG/ TVBH-1004.

Harderup, L-E, Blomberg T, Elmroth A. 1994. *Die Frosteindringung bei der Grundlegung für Gebäude ohne Unterkellerung* (Frost penetration under the foundation of a building without cellar, written in German). Department of Building Physics, Lund University. P.O. Box 118, S-221 00 Lund, Sweden. Report TVBH-7174.

Hellström, G. 1991. *Ground heat storage. Thermal analyses of duct storage systems. I Theory.* Dept. of Mathematical Physics, Lund University, P.O. Box 118, S-221 00 Lund, Sweden.

Hirsch, C. 1992. *Numerical computation of internal and external flows.* John Wiley & Sons Ltd. ISBN 0-471-92385-0.

Holman, J.P. 1986. *Heat transfer.* McGraw-Hill Book Company. New York.

Höglund, I. 1973. *Metod för beräkning av extrema yttemperaturer hos isolerade ytterkonstruktioner.* Byggforskningsrådet. The Swedish Council for Building Research. Report R6:1973.

Höglund, I.; V. Girdo; C.G. Troedsson. 1985. *Solinstrålningstabeller för helklara, halvklara och mulna typdagar.* Inst. för Byggnadsteknik, Kungliga Tekniska Högskolan, Stockholm, Sweden.

Jóhannesson, G. 1981. *Köldbryggor i plåtkonstruktioner.* Department of Building Physics, Lund University. P.O. Box 118, S-221 00 Lund, Sweden. CODEN:LUTVDG/ TVBH-3006.

Kakaç, S.; Y. Yener. 1985. *Thermal radiation heat transfer.* Hemisphere Publishing Corporation. Washington DC, USA. ISBN 0-89116-789-7.

Kreith, F.; M-S. Bohn. *Principles of heat transfer.* Fourth edition, revised edition. Harper & Row, Publishers, New York (1986).

MathWorks Inc. 1992. *MATLAB.* Cochituate Place, 24 Prime Park Way, Natick, Mass. 01760, USA.

McElroy, et al. 1984. *Development of advanced thermal insulation for appliances.* Oak Ridge National Lab, Martin Marietta Report ORNL/CON-159.

MicroWay. 1991. *NDP Pascal 486.* Research Park, Box 79, Kingston, Massachusetts 02364, USA.

Samuelsson, I. 1992. *Fuktsäkrare byggnadsdelar.* SP, Swedish National Testing and Research Institute, Box 857, S-501 15 Borås. SP AR 1992:17.

Siegel, R.; J.R. Howell. 1992. *Thermal radiation heat transfer*. Hemisphere Publishing Corporation. Washington DC, USA.

Solomou. 1993. *Master's thesis*. Depts of Building Technology and Mechanical Engineering, Massachusetts Institute of Technology, Cambridge, USA.

Stephenson, D.G., G.P. Mitalas. 1967a. *Room thermal response factors*, ASHRAE Transactions, Vol. 77, Part III, NO. 2019.

Stephenson, D.G., G.P. Mitalas. 1967b. *Cooling load calculations by the thermal response factor method*, ASHRAE Transactions, Vol. 73, Part I.

Stephenson, D.G., G.P. Mitalas. 1971. *Calculation of heat conduction transfer functions for multi-layer slabs*, ASHRAE Transactions, Vol. 77, Part II, NO. 2202.

Stroud, K.A. 1986. *Fourier series and harmonic analysis*. Stanley Thornes Ltd. Old Station Drive, Leckhampton, Cheltenham GL53 0DN, UK.

Taesler, R. 1972. *Klimatdata för Sverige*. The Swedish Meteorological and Hydrological Institute (SMHI), D459. Box 601 76 Norrköping, Sweden.

Thyholt, M.; I. Andresen, B. Hugdal, Ö. Aschehoug. 1994. *Frame and Edge Seal Technology - A State of the Art Survey*. SINTEF Arkitektur og byggteknikk. Alfred Getz vei 3. N-7034 Trondheim. ISBN 82-595-7796-8. Report STF62 A94004.

List of figures

List of tables